Bio-integrative Polymer Surfaces

Caroline Imogen Biggs

A thesis submitted in partial fulfilment of the requirements for the degree of Doctor of Philosophy in Chemistry

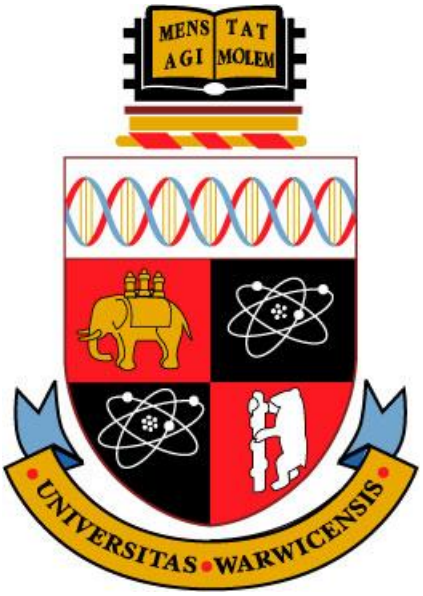

University of Warwick

Department of Chemistry

September 2015

Table of Contents

Chapter One

Chapter Two

Chapter Three

Chapter 4

Chapter 5

Appendix One

Appendix Two - Publications

List of Figures

Chapter One

Chapter Two

Chapter Three

Chapter Four

List of Tables

Chapter Two

Chapter Three

Chapter Four

Acknowledgments

Firstly, a huge thank you to Dr Matthew Gibson for not only providing me the opportunity to undertake my PhD research but also for his support, guidance and unwavering optimism. The progression of this research would not have been possible without his insight and encouragement and I am also very grateful for his support of my prolific conference attendance and my outreach activities, both of which have served to inspire my research. I must also thank the BBSRC for the funding of the project and both the Department of Chemistry and the School of Life Sciences for their support throughout. For the practical aspects of this work I am grateful to Dr Steve Edmondson for his advice regarding ellipsometry, Dr Ben Douglas for an introduction to DSA and QCM, Dr Marc Walker for running the XPS experiments, Dr Lijiang Song and Phil Aston for their help with the MS and Dr Andrew Hook at the University of Nottingham for the microcontact printing.

Thank you to all of the members of the Gibson Group for providing such an enjoyable daily environment, it has been a real pleasure to watch the group grow and I have greatly enjoyed working with you all. To Dan, Tom and Sarah-Jane, your contributions to the completion of thesis, both though scientific discussion and through your friendship, have been invaluable and I will be forever grateful. I am also very grateful to all of my family and friends for enriching my life outside of the lab. In particular, thank you to my parents for installing my love of learning, and always supporting my choice to continue studying. Finally, thank you to my husband, Rich, who has so patiently lived through the ups and downs of this project. A decade of your love and encouragement has made me who I am today and I couldn't have done this without your support.

Declaration

This thesis is submitted to the University of Warwick in support of my application for degree of Doctor of Philosophy. It has been composed by myself and has not been submitted in any previous form for any degree at any other university. The work presented was carried out by the author except for the XPS experiments in Chapters Two and Three, which were carried out by Dr Marc Walker at the University of Warwick and the direct microcontact printing in Chapter Four, which was carried out by Dr Andrew Hook at the University of Nottingham.

Aspects of Chapter Two have been published: Caroline I. Biggs, Steve Edmondson and Matthew I. Gibson, Thiol–ene immobilisation of carbohydrates onto glass slides as a simple alternative to gold–thiol monolayers, amines or lipid binding *Biomaterials Science*, 2014, **3**, 175–181

Abstract

Protein-carbohydrate interactions mediate a diverse range of biological responses including pathogen-cell adhesion. In this age of decreased antibiotic discovery and increased antibiotic resistance, the study of protein-carbohydrate interactions is crucial to improve our understanding of pathogen-host interactions and surface bound carbohydrates, glycoarrays, offer a powerful tool towards furthering knowledge in this area. These concepts and current glycoarray methodologies are described in **Chapter One**. This thesis aims to develop glycan immobilisation techniques both directly and using polymeric tethers. Acrylate silane linkers are used to immobilise thiol-terminated monosaccharides by thiol-ene "click", as described in **Chapter Two**. These immobilised glycans are then used to interrogate lectin-carbohydrate interactions. In **Chapter Three** the synthesis of poly(oligo(ethylene glycol)methyl ether methacrylate)s (pOEGMA)s and poly(*N*-isopropylacrylamide)s (pNIPAM)s, by reversible addition fragmentation transfer (RAFT) polymerisation is presented. The reduction of the terminal thiocarbonylthio group was explored for thiol-ene surface modifications and thiol-gold reactions. The resulting polymer coatings are characterised and a detailed Quartz Crystal Microbalance study compares their grafting. In **Chapter Four**, the concepts of glycan immobilisation and polymer grafting are combined and glycan-terminated polymers are synthesised, surface grafted and used to explore protein-carbohydrate interactions. The thesis concludes with the direct contact printing of high density arrays of glycosylated polymers, showing the potential of this technique as a screening tool to monitor these biologically relevant processes.

Abbreviations

µCP	Microcontact Printing
A.C.	Alternating current
ACVA	4,4′-Azobis(4-cyanovaleric acid)
AHMA	6-Azidohexyl methacrylate
AIBN	Azobisisobutyronitrile
APDIPES	3-Aminopropyldiisopropylethoxysilane
APDMES	3-Aminopropyldimethylethoxysilane
APTES	3-Aminopropyltriethoxysilane
ATRP	Atom-transfer radical polymerisation
AuNP	Gold nanoparticle
BSA	Bovine serum albumin
C	Mass sensitivity constant
CFG	Consortium for Functional Glycomics
Con A	Concanavalin A
CP	Cloud point
CPBD	2-Cyano-2-propyl benzodithioate
CRP	Controlled radical polymerisation
CTA	Chain transfer agent
D	Dissipation
DEG	Di(ethylene glycol)
DMAP	4-(Dimethylamino)pyridine
DMF	Dimethylformamide

DMP	2-(Dodecylthiocarbonothioylthio)-2-methylpropanoic acid
DMSO	Dimethyl sulfoxide
DNA	Deoxyribonucleic acid
DP	Degree of polymerisation
DSA	Drop shape analysis
E. coli	*Escherichia coli*
EDC	*N*-(3-Dimethylaminopropyl)-*N'*-ethylcarbodiimide hydrochloride
ESI	Electrospray ionisation
f	Frequency
FITC	Fluorescein isothiocyanate
FRP	Free radical polymerisation
Gal	Galactose
GAMA	2-Gluconamidoethyl methacrylate
Glc	Glucose
HEPES	4-(2-Hydroxyethyl)piperazine-1-ethanesulfonic acid, *N*-(2-Hydroxyethyl)piperazine-*N*′-(2-ethanesulfonic acid)
HUVEC(s)	Human umbilical vein endothelial cell(s)
IR	Infrared
LCST	Lower critical solution temperature
m	Mass
MALDI-Tof	Matrix-assisted laser desorption/ionisation time-of-flight
Man	Mannose
Min	Minute
M_n	Number average molecular weight

Mol	Moles
MRSA	Methicillin resistant *Staphylococcus aureus*
MS	Mass spectrometry
M_w	Weight average molecular weight
n	Overtone number
NCA	*N*-Carboxyanhydride
NHS	*N*-Hydroxysuccinimide
NIPAM	*N*-Isopropylacrylamide
NMP	Nitroxide-mediated polymerisation
NMR	Nuclear magnetic resonance
OEG	Oligo(ethylene glycol)
PBS	Phosphate buffered saline
PDEAEMA	Poly(2-(diethylamino)ethyl methacrylate)
PDMS	Polydimethysiloxane
PEG	Poly(ethylene glycol)
PFP	Pentafluorophenyl
PHEMA	Poly(2-hydroxyethyl methacrylate)
PMMA	Poly(methyl methacrylate)
PNA	Peanut agglutinin
PNIPAM	Poly(*N*-isopropylacrylamide)
POEGMA	Poly(oligo(ethylene glycol)methyl ether methacrylate)
PPEGMA	Poly(poly(ethylene glycol)methyl ether methacrylate)
PPFMA	Poly(pentafluorophenyl methacrylate)
QCM(-D)	Quartz-crystal microbalance (with dissipation)
RAFT	Reversible addition-fragmentation chain transfer

ROMP	Ring opening metathesis polymerisation
RT	Room temperature
SAM	Self-assembled monolayer
SBA	Soybean agglutinin
SEC	Size exclusion chromatography
SPPS	Solid phase peptide synthesis
TB	Tuberculosis
TCEP	Tris(2-carboxyethyl)phosphine
TEMPO	4-*N*-Amino-2,2,6,6-tetramethylpiperidine 1-oxyl-4-yl
THF	Tetrahydrofuran
Tris	Trisaminomethane buffer
UV	Ultraviolet
VRE	Vancomycin resistant *Enteroccus*
WGA	Wheat germ agglutinin
XPS	X-Ray photoelectron spectroscopy

Colour Code for Graphs

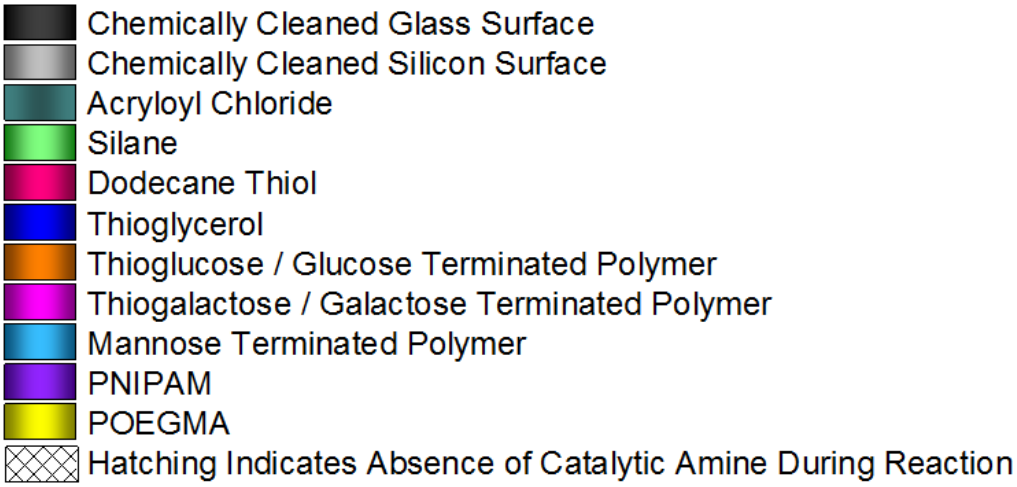

Chapter One

1. Introduction

1.1. Glycoarrays

1.1.1. The Antibiotic Problem

Globally, there has been a decrease in the discovery of new antibiotics, whilst at the same time the resistance to existing antibiotic treatments is increasing, exacerbated by the intense misuse of current antibiotic therapies.[1] This poses a major public health challenge. Taking the example of tuberculosis (TB); resurgence is being seen in both the Western world and poorer nations. This is due to the reasons stated above being combined with a decrease in vaccination compliance. Despite a mortality rate of around two million deaths per year, the diagnostic techniques for TB remain underdeveloped, requiring costly and time consuming chest X-rays, blood tests and culture of infected samples.[2] A novel technology allowing investigation into both the causative mechanisms of the bacterial infection and also a cheaper, more convenient and more rapid diagnostic tool would therefore be highly beneficial to global health.

Tuberculosis is far from the only problem; infectious diseases are the second-leading cause of death worldwide and even in economically advanced countries they remain the third-leading cause.[3] Species such as methicillin resistant *Staphlococcus aureus* (MRSA) and vancomycin resistant *Enterococcus* (VRE) are becoming prevalent, and for some infectious diseases there are no longer any effective antibiotics left.[4] Therefore, the study of infectious processes is crucial in terms of

allowing us to make the best use of our limited set of antibiotics through the development of faster and more accurate diagnostic devices.

1.1.2. Protein-Carbohydrate Interactions

Carbohydrates, one of the four major classes of biomolecules, are highly complex macromolecules fulfilling a huge range of roles within living organisms. The structural and chemical diversity of carbohydrate molecules arises due to the numerous combinations of the monosaccharide building blocks which are possible. The type and stereochemical configuration of the glycosidic linkages between the monosaccharides, branching and site specific modifications all contribute to their complex nature. As a result, carbohydrates are the most structurally diverse of the major classes of biomolecules.[5] Mammalian glycans are primarily composed from the ten most common monosaccharide units; glucose, galactose, mannose, *N*-acetyl glucosamine, *N*-acetyl galactosamine, fucose, xylose, glucuronic acid, iduronic acid and sialic acid, Figure 1.1. Although this is fewer than the number of amino acid building blocks available for protein synthesis, the number of potential glycans that can be synthesised from these ten building blocks is far greater than for the protein comparison, Figure 1.2. This extra complexity, when compared to both proteins and DNA, is a result of the assembly of the monosaccharides into linear and branched macromolecules and the possible enantiomers, diastereoisomers and anomers available. This resulting very high information density and complexity of the glycome is reflected in the wide variety of functions carried out by carbohydrates.

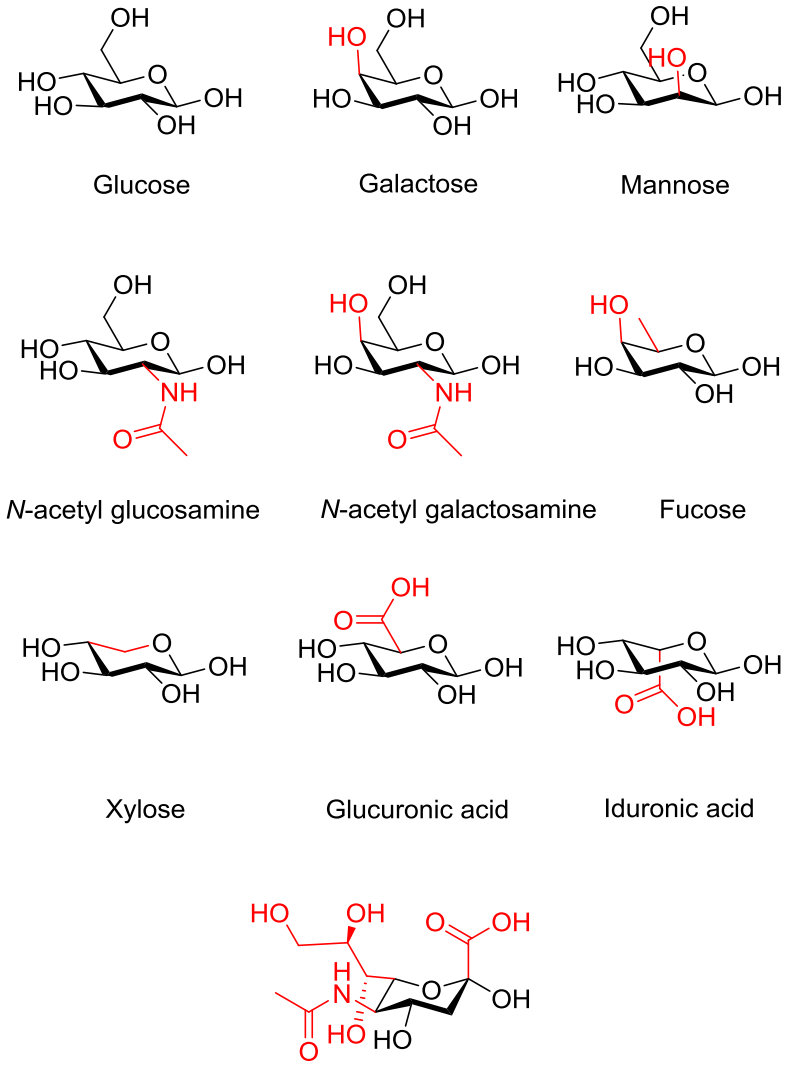

Figure 1.1: The ten most common human monosaccharide units, the red colour indicates structural features that differ from the glucose unit

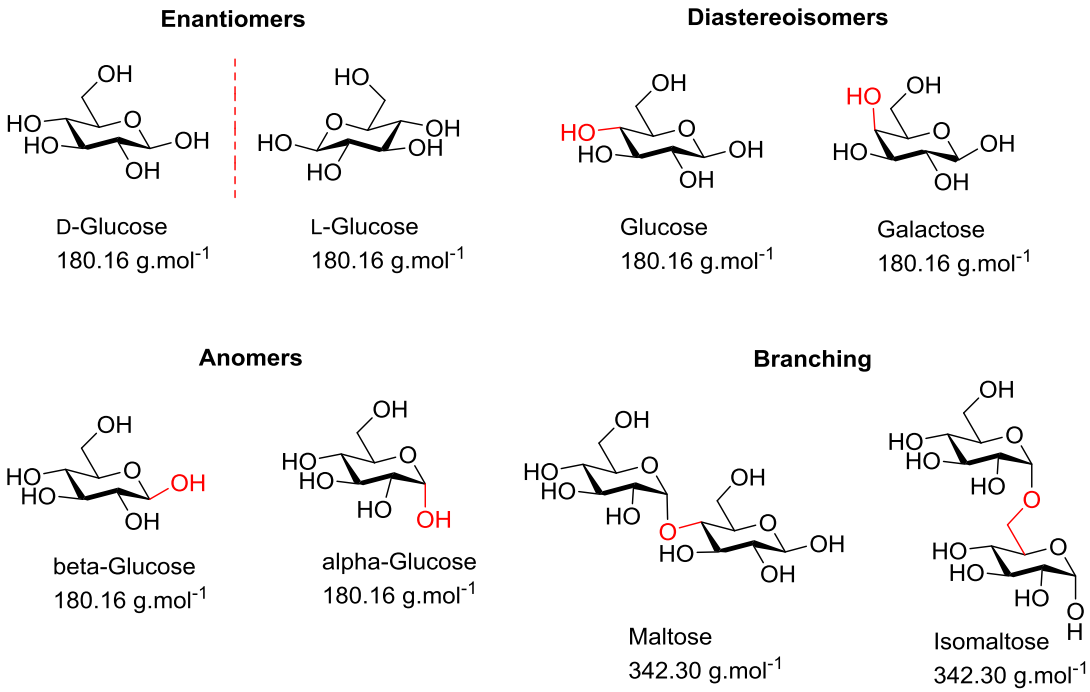

Figure 1.2: The potential complexity arising from the different enantiomers, diasteroisomers, anomers and branching for glucose

Protein-carbohydrate interactions are involved in events ranging from cell-cell and cell-matrix communications to cellular processes such as fertilisation, growth, infection and immunity, Figure 1.3. These carbohydrate binding proteins include carbohydrate-specific enzymes and lectins.[6] Lectins are defined as proteins which bind carbohydrates, but are themselves not antibodies or enzymes.[7] They specifically and non-covalently bind carbohydrates based upon their chemical and physical properties, such as branching pattern and stereochemistry. The lectins can be subdivided into two classes, the C-type and the P-type, named as such due to the C-type requiring calcium ions in order to facilitate binding and the P-type containing a phosphate functional group. There are only two members of the P-type lectin group, both involved in the delivery of newly synthesised soluble acid hydrolyses to the lysosome in eukaryotes.[8] Conversely, the C-type lectins are numerous and

include both secreted and transmembrane proteins. These proteins contain a C-type lectin fold, which is a ligand-binding motif where the carbohydrate binding can occur. However, this domain is also present in many proteins which do not bind carbohydrates and in these cases it can be used to bind other proteins, lipids, inorganic molecules and, in the case of antifreeze glycoproteins, ice.[9] These binding processes are typically reversible. Despite the significant structural homology between the lectins, their bonding specificities are usually different in terms of the types of glycan that they can recognise with high specificity.[10]

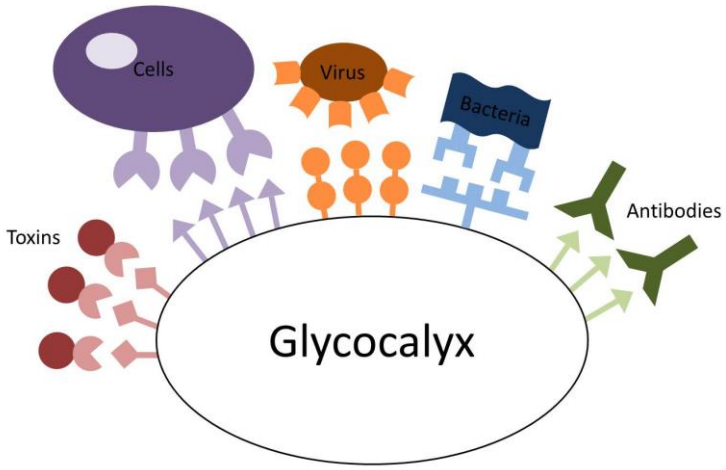

Figure 1.3: Interactions between the carbohydrates coating a cell surface and the receptors present on toxins, other cells (proteins), viruses, bacteria and antibodies

The lectin-carbohydrate interaction is non-covalent, existing through a network of hydrogen bonds and electrostatic interactions. The high avidity for multivalent ligands is a result of the frequent lectin oligomerisation. The actual binding affinity for a carbohydrate to its target lectin is typically very weak, however the presentation of multiple copies of the target carbohydrate on a cell surface significantly enhances the weak individual binding events, in a process known as the

cluster glycoside effect.[11] These multivalent assemblies enhance the binding potency by several methods; chelation, subsite binding, clustering and statistical rebinding.[12]

Lectins can be further categorised into three classes: simple, multidomain and macromolecular. Amongst the simplest class are practically all plant lectins and it is therefore unsurprising that the plant lectins, and more specifically the legume lectins, are the most thoroughly studied and can be used as model systems. Around 100 members have been characterised and they are typically isolated from the seeds of the plant in which they are present. Each legume lectin contains four invariant amino acids in the binding site; one each of asparagine, aspartic acid, glycine and either leucine or an aromatic amino acid.[10] The prototype member of the family is concavalin A (Con A) which is isolated from the jack bean. It is present as a dimer at low pH (< 5.5) and a tetramer at high pH (> 7) and the binding site in each subunit is specific for α-mannosyl and α-glucosyl residues. Another well studied lectin, peanut agglutinin (PNA), extracted from *Arachishypogaea*, exhibits specificity for the T-antigen (Galβ1-3GalNAc).

1.1.3. Bacterial Cell Adhesion

Prior to the occurrence of infection, bacteria typically require adhesion onto the host cells, a process involving protein-carbohydrate interactions. The ability to interfere with this initial interaction can provide an effective alternative to conventional antibiotics, especially in cases of antibiotic resistance. The proteins that mediate the adhesion of pathogenic organisms onto host tissues are known as adhesins and they are present on bacterial appendages (pili or fimbriae) or on the cell surface. For example type 1 fimbriated *E. coli* are involved in lower urinary tract infections, whereas those with P-fimbriae are involved in bladder infections. These

adhesions can also be used detect bacteria and provide structural information on their adhesion proteins and carbohydrate specificities.[13]

Carbohydrates have shown promise in the field of anti-adhesion therapeutics, using competitive inhibition in the prevention of infection. The bacteria bind the carbohydrate, or its analogue, rather than the carbohydrates on the host cell, and thus adhesion and infection can be prevented. Synthetic oligosaccharides covalently bound to multivalent scaffolds have been developed in order to overcome the problems associated with the low binding affinities of monovalent glycosides.[14] Synthetic glycopolymers have also been implored as multivalent inhibitors. The polymer scaffolds can be functionalised with pendant and/or terminal carbohydrates and have the advantage of straightforward and scalable synthetic routes, however inherent size dispersity is unavoidable. [15]

There are several advantages in targeting the virulence factors rather than the bacteria themselves. Primarily, as the pathogens are not killed or stopped from growing, but rather have their pathogenicity inhibited, the selection pressure for antibiotic resistance is reduced. Additionally, normal microbiota within the organism are not disrupted.

1.1.4. Glycoarray Technology

The detection and quantification of bacterial species is thus of great importance; microarray technology can be used to probe the mechanisms of bacterial adhesion and aid both diagnostics and the development of new treatments, Figure 1.4. The facile and rapid detection of bacteria is of particular importance in this era of increasing antibiotic resistance. If a correct diagnosis of the infection can be

quickly and easily obtained then the prevalence of unnecessary antibiotic prescribing, one of the causes of increased antibiotic resistance, can be reduced.

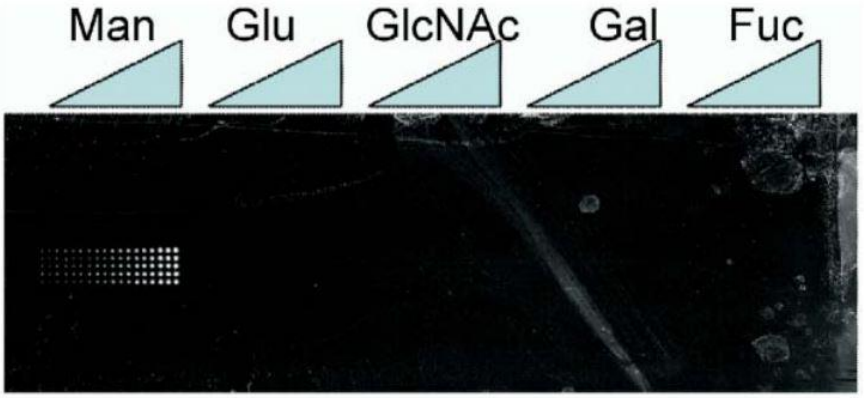

Figure 1.4: Glycoarray coated with mannose, glucose, *N*-Acetylglucosamine, galactose and fucose. Labelled *E. coli* are seen to bind only to the mannose coated regions, due to the presence of a mannose specific receptor protein (FimH) on their surface. Such systems can be used as diagnostic tools for the detection of pathogens. Taken from the work of M. D. Disney and P. H. Seeberger[16]

A microarray is a solid substrate onto which compounds of interest are immobilised; they are used to assay large amounts of biological material in a high throughput manner.[17] The field of microarray technology began with antibody microarrays and quickly became applied to DNA. Today, however, there is great interest in the potential applications of carbohydrate microarrays, sometimes termed glycoarrays, which are surfaces displaying a large number of different carbohydrates, Figure 1.5. These arrays have the potential to not only shorten the timescales involved in biochemical measurements, but also offer miniaturisation, which is as straight forward with solution studies. This is of particular importance when you consider that, despite huge improvements in their production, pure oligosaccharides and glycoconjugates are still typically produced in very small quantities.[18]

Carbohydrate arrays have transformed a number of medical and biological research areas, and can be considered as simplified biomimics of the cell glycocalyx.[19]

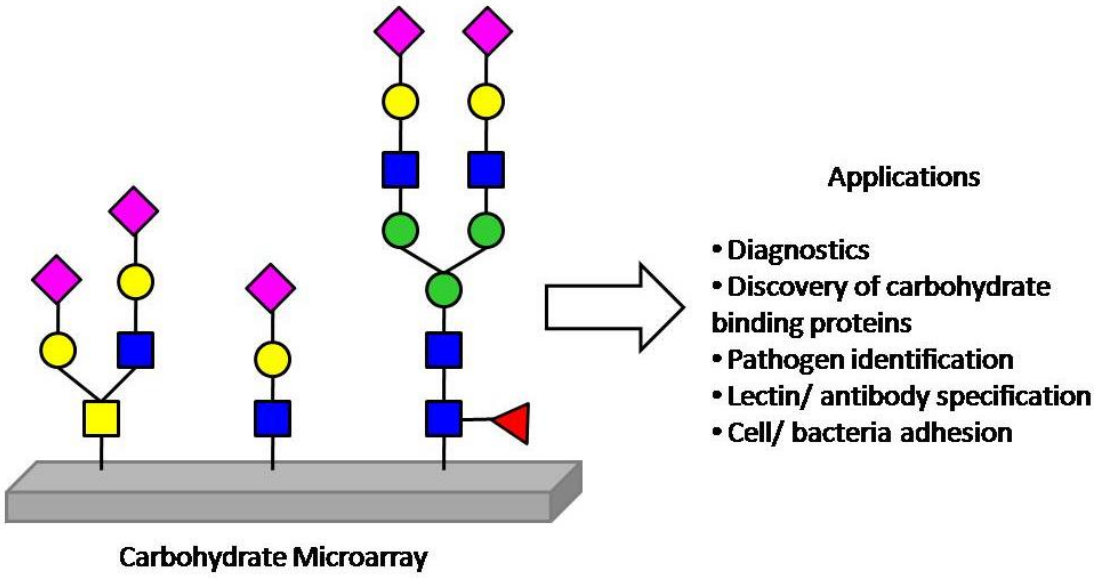

Figure 1.5: Current applications of carbohydrate microarrays, adapted from the work of N. Laurent, J. Voglmeir and S. L. Flitsch[18]

The immobilisation of the carbohydrates onto the array surface is critical to the success of the technology. Broadly speaking, the immobilisation techniques can be categorised into covalent bonding or non-covalent (physical) adsorption. Each category can be further divided into site specific (regioselective) and site non-specific, with respect to the attachment of the glycan on the surface, Figure 1.6.[18] Due to non-covalent immobilisations relying on the glycans adhering to the surfaces typically *via* hydrogen bonds, van der Waals interactions or other non-covalent interactions, a large contact area must be available. Therefore the glycans must be sufficiently large, making this technique unsuitable for adhering individual carbohydrates, which would be removed during the washing steps.[20] Non-covalent immobilisation has been seen using a nitrocellulose[21] or oxidised black polystyrene

coating[22] to adhere polysaccharides in a non-site-specific fashion, or streptavidin-coated surfaces for adhering biotin conjugated glycans.[23] The simplest covalent immobilisations involve the attachment of free glycans onto boronic acid,[24] phthalimide[25] or azidoaryl[26] coated surfaces in a non-site-specific fashion. Techniques for the site-specific covalent attachment of the glycans have been the most extensively developed and there are numerous examples within the literature. Typically, modified sugars are required to bind to the surfaces, for example homobifunctional disuccinimidyl functionalised glass requires ethanolamine functionalised sugars for binding.[16]

The use of covalent, orthogonal linkers is highly advantageous and they are widely employed,[18] including by the Consortium for Functional Glycomics (CFG),[27] which employs the amino linkers to react with succinimidyl ester glass slides. The latest version of the CFG array system (version 5.2, 2012)[28] employs 20 different spacer arms, ranging from simple Sp0 linkers, comprised of $-CH_2CH_2NH_2$, to peptide linkers, such as Sp24 and Sp25 (lysine-valine-alanine-asparagine-lysine-threonine and valine-alanine-asparagine-lysine respectively).[16] The use of linkers in protein-carbohydrate binding systems allows controlled access to the binding pocket and can be used to improve selectivity. “Click” chemistry inspired routes have also been developed, utilising alkyne or azido- sugars with their complementary surfaces. More recently, thiol-ene type click reactions have gained attention in both their radical and nucleophilic (Michael addition) formats,[29] see section 1.2.6. However, often glycans which have been synthesised *de novo* chemically or chemo-enzymatically must be subjected to further modification and/or coupling in order to react with the desired array surface. In addition to the challenges associated with generating cost-effective, reproducible arrays and minimising non-specific binding

interactions, this requirement for functionalised glycans is hindering progress towards a complete microarray technology; where in the future it may be possible to present the entire glycome on one chip or on a series of chips.

The type of surface onto which the glycans are immobilised is also important. Gold has been used to support self-assembled monolayers of alkenethiols, onto which monosaccharides can be immobilised,[30, 31] but glass is most commonly used, including amino and epoxy silanised surfaces.[32] However, the development of a carbohydrate surface attachment that is compatible with a variety of surfaces would be highly desirable, allowing more extensive characterisation techniques to be utilised and also increasing the applications for the resulting microarrays.

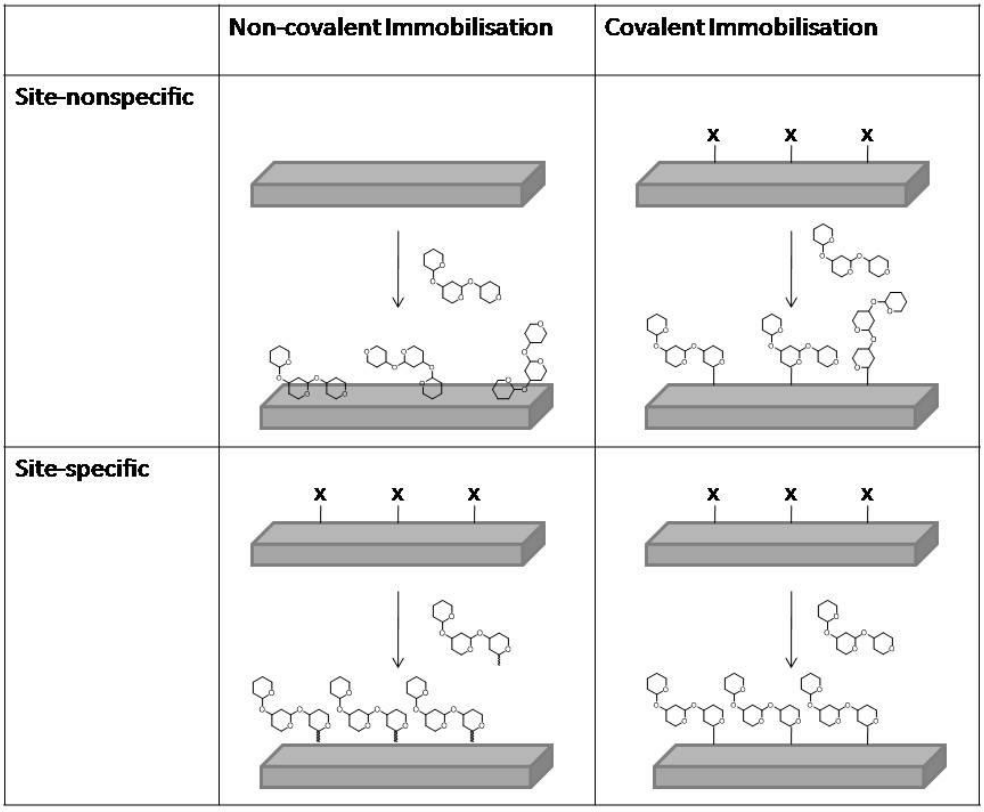

Figure 1.6: Categories for the immobilisation of carbohydrates onto solid supports. Adapted from the work of S. Park *et al.*[20]

Recent progress in microarray technology has seen the introduction of arraying robots and printers, incorporating scanning devices for efficient monitoring of detection signals. These methods can be divided into contact and non-contact printing. In contact printing, the glycans are printed onto the surface *via* the touch of a steel pin which has been immersed in a glycan solution. Typically 0.5 nL of solution is printed in each spot. In non-contact printing, a piezoelectric printer delivers approximately 0.3 nL of glycan solution *via* a glass capillary and electrical impulses, without touching the surface.[33]

As an alternative to carbohydrate microarrays, lectin microarrays have been developed as a platform for glycan analysis. Instead of functionalising the surface with carbohydrates, lectins (or carbohydrate antibodies) are immobilised and fluorescently labelled glycoproteins are added. This method is being introduced as an alternative to conventional glycan analytical techniques, such as mass spectrometry or liquid chromatography, because it does not require removal of the glycan from the core protein prior to analysing. It enables direct analysis of crude glycoprotein containing samples; however it is not quantitative and is best suited to comparative studies such as differential profiling.[34]

In addition to the immobilisation of the carbohydrates, the elucidation with biological material can also pose challenges. Typically, fluorescently-labelled proteins are added in order to assess binding, however, the isolation and labelling of proteins often proves to be challenging and it would be preferable to instead incubate the functionalised slides with whole bacteria. This can create the problem of non-specific adhesion to the slides, as bacteria adhere to and colonise all non-living surfaces. This colonisation process begins with the adhesion of a single cell or cell

aggregates and continues, if the conditions are favourable, with the growth and division of the adhered cells. The resulting micro-colonies have both advantageous applications (e.g. waste water treatment) but also pose serious disadvantages,[35] as in this case where they will reduce the resolution of the assay and give rise to false positive results. A non-fouling or hydrophilic surface could circumvent this problem, by resisting the adhesion of the proteins, bacteria and cells. The development of glass-based carbohydrate microarrays with high carbohydrate-spotting density *and* a protein-resistant surface (Figure 1.7) has the potential to significantly improve this technology. It is proposed that this can be achieved using linkers composed of polymers of oligo(ethyleneglycol) or *N*-isopropylacrylamide, which possess both protein resistant[36, 37] and stimuli-responsive[38] properties, as explained in section 1.2.5 Many polymers have been shown to exhibit attributes that are desirable for biomedical applications, such as antifouling properties,[39] making them suitable for many array applications, but the synthesis of well defined, reproducible polymers is crucial to the success of these systems, requiring precision polymerisation methods.

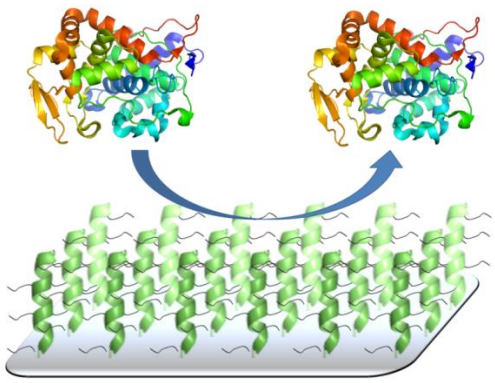

Figure 1.7: Protein resistant surfaces are used to reduce non-specific binding and give higher resolution assays, taken from the work of J. Wang *et al.* [40]

1.2. Polymerisations

1.2.1. Controlled Radical Polymerisation Techniques

In order for polymeric species to be useful in biological and analytical applications, it has been shown that it is very important to exercise control over their properties, namely the molecular weight, dispersity and architecture. This allows the fabrication of systems which are defined and reproducible.[41] Much of the recent development in the field of polymer chemistry has focused on these challenges and several innovative techniques for producing highly defined polymers, generally referred to as controlled radical polymerisations (CRP), have been developed. These techniques build on the advantages of conventional free radical polymerisation (FRP), with its benefit of not requiring stringent process conditions and its ability to be used for the (co)polymerisation of a wide range of vinyl monomers, however they offer far greater control over the resulting polymer chains.[42] Generally the CRP methods work by extending the lifetime of the propagating chains. This is achieved by establishing a dynamic equilibrium between a minimal concentration of active radicals (propagating chains) and a predominant amount of dormant chains in the system, therefore reducing the occurrence of termination processes. Due to chains remaining as dormant species, where they are capable of reactivation and chain extension, rather than terminating, CRP can be classed as a "living" system.[43] The basic mechanistic principle for this process is seen in Figure 1.8.

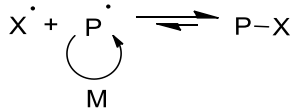

Figure 1.8: The basic mechanistic principle of CRP

Nitroxide-mediated polymerisation (NMP),[44] atom transfer radical polymerisation (ATRP)[45] and reversible addition-fragmentation chain transfer (RAFT)[46] polymerisation are the three most popular CRP processes in use today. In NMP, the control is achieved through the addition of an alkoxyamine initiator, which results in the reversible end-capping of growing polymer chains with a nitroxide species.[47, 48] ATRP is a metal-mediated polymerisation technique, where the presence of a transition metal catalyst, typically copper, determines the equilibrium between the active and dormant species.[45, 49]

1.2.2. RAFT Polymerisation

This work has made use of RAFT polymerisation, which was first reported by the CSIRO group back in 1998.[46] There are many advantages to this technique, it is considered to be one of the most versatile CRP techniques available; it can tolerate a wide range of monomers, solvents and initiators, exhibits good end group fidelity and can produce polymers and copolymers with narrow dispersity, often to high conversion.[50] The seminal RAFT polymerisation paper described the polymerisation of a variety of (meth)acrylates, styrenic and acid (salt) monomers in a free radical polymerisation process, but with the key addition of a small amount of a thiocarbonoylthio-containing compound as a chain transfer agent (CTA), Figure 1.9. The addition of the CTA allowed control over the free radical process and the production of polymers with dispersities typically less than 1.2. This is achieved through the rapid equilibrium between active and dormant forms of the propagating radical species; therefore all chains will grow and will have an equal chance of growth. The molecular weight increases linearly with conversion and the molecular weight distribution can be very narrow. The choice of chain transfer agent (CTA) is important and there are four classes, with the basic structure consisting of a central

thiocarbonylthio group attached to an R and Z group, Figure 1.9. Through modifications to the free radical leaving group (R) and the activation/deactivation of the thiocarbonyl double bonds, by altering the Z component, a wide range of monomer species can be accessed.

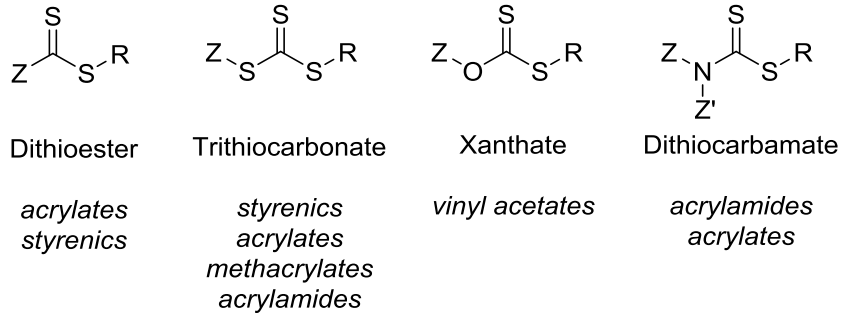

Figure 1.9: CTA structure categories with the type of monomer typically used for each listed below in italics

In a conventional radical polymerisation process, the radicals are generated (initiation), the individual chains then grow for 5-10 s (propagation) before undergoing combination or disproportionation (termination). RAFT polymerisation, Figure 1.10, possesses the characteristics of a living polymerisation. The chains all begin to grow at the start of the polymerisation and continue to grow until the monomer is consumed. The mechanism consists of five key events. The first stage (initiation) and final stage (termination) are the same as in the conventional radical process, however the stages in between differ and it is in these steps that the control over the process occurs.[51] Following initiation an initial equilibrium is established; the propagating radical ($P_n^{\cdot}$) adds to the CTA to form an intermediate radical species. This radical then fragments into a polymer adduct of the CTA and a new radical ($R^{\cdot}$), which can react with the monomer to form a new propagating radical ($P_m^{\cdot}$) in the reinitiation step. Then, in the main equilibrium step, the polymer radical

($P_m^{\cdot}$) can add to the CTA, releasing the other radical ($P_n^{\cdot}$). Due to the rapid equilibrium between the active propagating radical species ($P_n^{\cdot}$ and $P_m^{\cdot}$) and the CTA polymer adduct, there is equal probability of growth for all chains and hence control over the resulting polymer chains is possible. As it is the R group that initiates the polymer chain growth in the initial equilibrium step, this radical leaving group should be a better leaving group then the propagating radical ($P_n^{\cdot}$) and be sufficiently reactive to re-initiate the polymerisation. It is also important for the Z group to activate the C=S bond to the addition of the radical and then stabilise the resulting adduct.

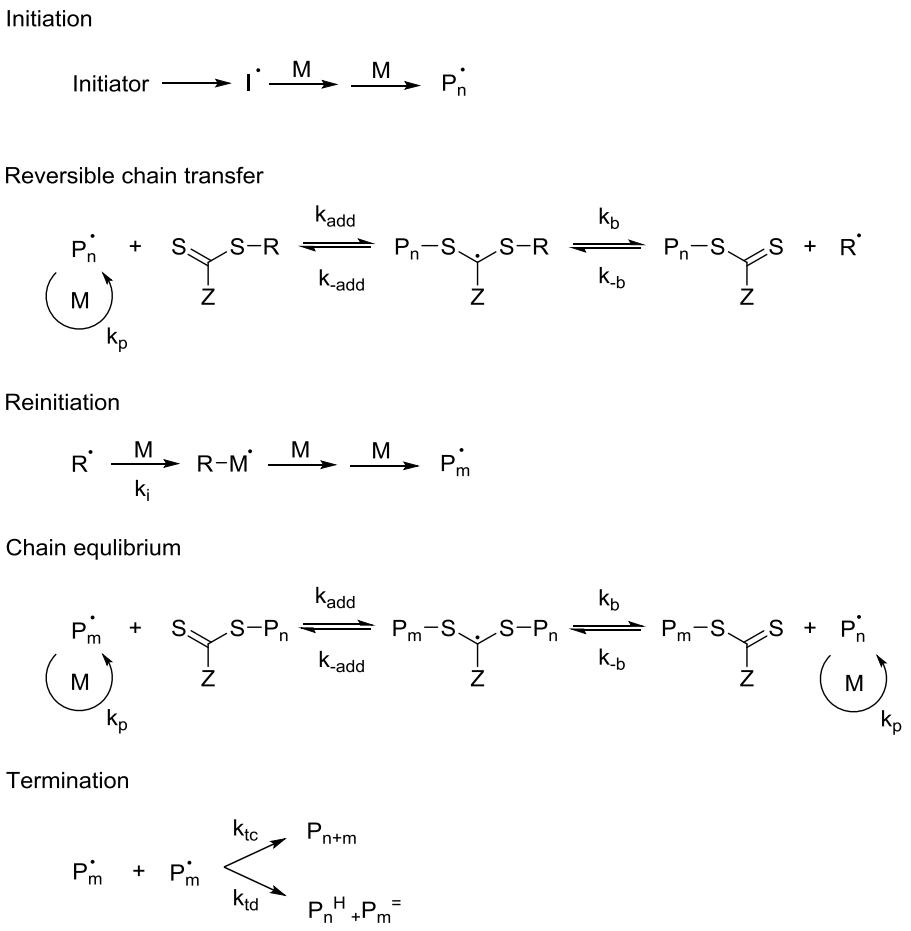

Figure 1.10: The proposed mechanism of RAFT polymerisation, adapted from the work of G. Moad, E. Rizzardo and S. H. Thang[51]

Although unrelated to the requirements of this work, it is also important to note that RAFT polymerisation has been successfully used to synthesise more complex architectures, including block copolymers, stars, hyperbranched polymers and hybrid nanoparticles, showing the high levels of control that are possible.[52]

1.2.3. End Group Modification of RAFT Polymers

A major advantage of the RAFT technique is that the nature of the CTA leads to functional groups at both ends of the polymer chain. Both the α-end and/or ω-end can be modified, without the need for further manipulation, by incorporating appropriate functionality into the RAFT agent at the R or Z position (Figure 1.11), making the technique very versatile and suitable for a wide range of applications.[50] Incorporation of functionality into the R group of the initiating species can produce, for example, carboxylic acid,[53] peptide[54] and lipid α-end-functionalised polymers.[55]

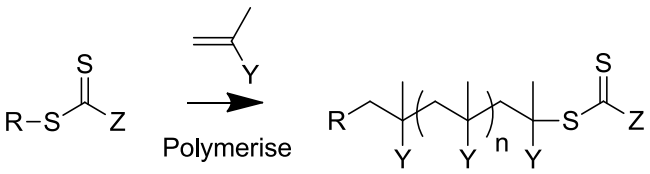

Figure 1.11: RAFT agent and resulting RAFT polymer, showing the α-end (R) and ω-end (Z)

The ability to functionalise the α-end of the polymer during RAFT polymerisation is also seen in other types of CRP, such as ring opening metathesis polymerisation (ROMP) and atom transfer radical polymerization (ATRP), but a novel feature of RAFT is the ability to also functionalise the ω-end of the chain. This is possible due to the presence of the thiocarbonate, which can be modified, or removed, post-polymerisation.[50] Although nitroxide mediated polymerization appears to allow functionality at both ends, the R_1 group is typically the benzoyl

peroxide initiator and the R_2 and R_3 are part of the TEMPO radical structure, so the options for varying the groups are limited, Figure 1.12.

Most useful to this project is the conversion of the thiocarbonylthio group to a thiol end group, which can then react with a gold surface or an alkene functional group. Literature techniques for this process involve reacting with excess amine to act as a nucleophile,[56] or addition of a reducing agent such as PBu_3[57] or tris(2-carboxyethyl)phosphine (TCEP).[58] The reaction of thiol-terminated RAFT polymers with gold has been reported, often to stabilise metal nanoparticles.[59,60]

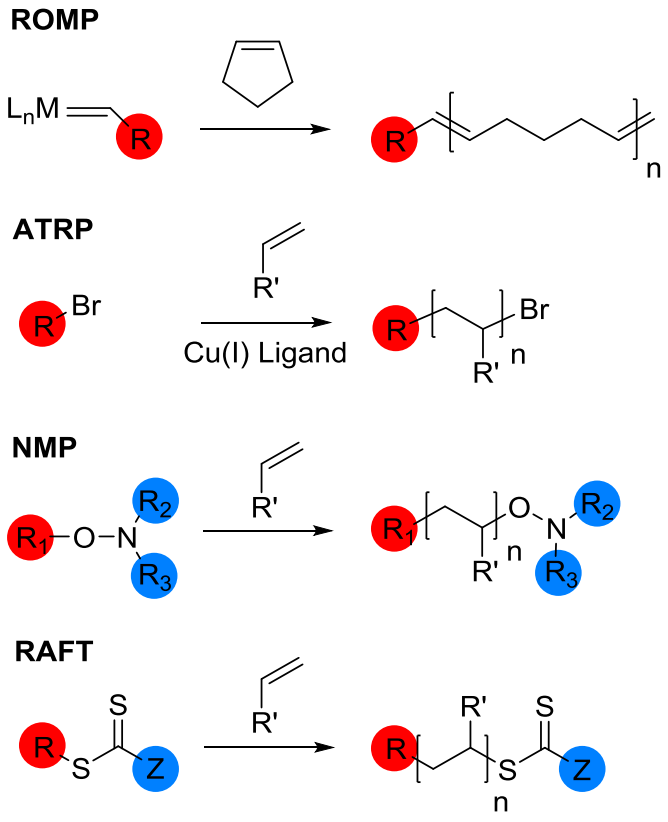

Figure 1.12: Location of functional groups introduced by the initiator/CTA in polymers produced by ROMP, ATRP, NMP and RAFT. ROMP (excluding the functionality of the double bond) and ATRP allow functionality at only one end of the polymer chain, whereas NMP and RAFT allow functionalisation at both ends

Additionally, work into the synthesis of glycopolymers has been successful through highly efficient post-polymerisation alkyne-azide cycloaddition reactions, allowing the creation of libraries of glycopolymers.[61, 62] Glycopolymers are synthetic polymers containing carbohydrate pendant or terminal groups along the backbone.[63] The presence of multiple sugar units along each polymer chain allows them to bind lectins in a multivalent fashion and therefore benefit from the cluster glycoside effect.[11] They can be synthesised using post-polymerisation modification processes, Figure 1.13. Monomers bearing functional groups of interest (chemoselective handles) are polymerised to create a library of polymer precursors, still retaining their chemoselective handles. These polymers can then be modified with bifunctional reagents to produce the desired functional polymers. This post-polymerisation modification allows access to functionality which would not have been compatible with the polymerisation process if included within the monomer. Also, due to producing a stock of polymer precursors from the same initial polymerisation process, there is the ability to create differently modified polymers with the same molecular weight and dispersity. The creation of these libraries of different glycopolymers, but with the same or very similar molecular weights and molecular weight distributions are very useful in order to probe structure-property relationships.[62]

RAFT polymerisation has been used to synthesise poly(pentafluorophenyl methacrylate) (pPFMA) backbones, which are then reactive to further modification. As a modification to this process, a tandem post-polymerisation modification method has been developed. The pPFMA scaffold can be functionalised with allylamine, resulting in pendant alkene functionality, and then subjected to thiol-ene “click” chemistry (see section 1.2.6) in order to introduce the biofunctionality.[64]

Alternatively, a 3-step tandem post-polymerisation methodology can be used to synthesise glycopolymers with secondary binding motifs, which mimic glycan branching.[65]

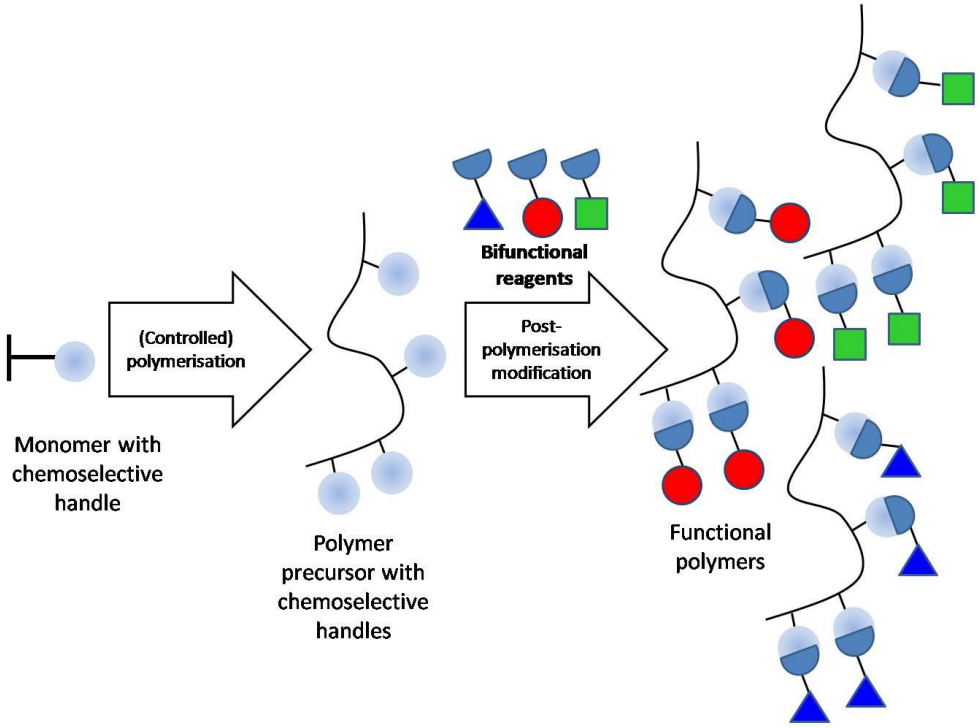

Figure 1.13: The process of creating functional polymers using a two-step post-polymerisation modification process

1.2.4. Characterisation of Polymers

Polymers, can be characterised by nuclear magnetic resonance (NMR) spectroscopy and proton NMR spectroscopy can be used to follow a polymerisation reaction through the disappearance of characteristic monomer peaks or the appearance of polymer product peaks. Size exclusion chromatography (SEC), a technique established particularly for the characterisation of polymeric species, can be used alongside NMR spectroscopic analysis. In SEC, the polymer chains are separated based upon their size (hydrodynamic volume) in solution. The polymer sample for analysis is dissolved and then pumped through a column packed with

porous cross-linked polystyrene beads. As the polymer solution travels through the column the smaller macromolecules permeate the pores in the beads and take a long time to be eluted from the end of the column. Conversely, the larger macromolecules are unable to enter the pores and thus they quickly pass through the column. The elution of the sample from the column is monitored using an ultraviolet (UV) detector or by monitoring the light scattering, viscosity or refractive index of the solution. By comparing the data to known standards, the number average molecular weight (M_n) and weight average molecular weight (M_w) for the polymer can be calculated.

1.2.5. Thermally-Responsive Materials

Polymers can be designed to change through their responsiveness to one or more stimuli, such as temperature, pH, light, electrical and magnetic fields and ionic strength. This particular class of polymers are termed "stimuli-responsive" or "smart", indicating that they undergo a significant structural change in response to an external stimulus. Typical polymer responses are changes in shape, surface characteristics or solubility. A particularly useful aspect of these materials is that a significant change can be induced through only a small stimulus, i.e. the response is non-linear.[66] The bulk response of the polymer is usually due to multiple small co-operative interactions, which when summed over the whole polymer result in a large structural change. Highly directional hydrogen bonding, although weak in nature, plays a key role in these switching processes, particularly for polymer systems where the hydrogen bonds along the polymer chains can be altered by external stimuli such as chemicals, pH and temperature.[67]

Temperature changes are the most commonly used and well-studied responsive stimuli, with poly(*N*-isopropylacrylamide) (pNIPAM), a thermally-responsive polymer, being the original and the most studied responsive material. pNIPAM undergoes a sharp coil to globule transition in water at approximately 32°C, during which it changes from a hydrophilic to hydrophobic state.[68] The pNIPAM chains, in common with other thermally-responsive polymers, undergo a phase transition arising from the entropic gain as the water molecules associated with the side-chain groups are released into the bulk solution, see Figure 1.14. The temperature at which this occurs is known as the Lower Critical Solution Temperature (LCST) and corresponds to the point at which the enthalpic contribution of the water which is hydrogen-bonded to the polymer chain becomes less than the entropic gain that can be achieved if the water is lost to the bulk aqueous phase. Polymers which exhibit LCST-type behaviour exist in flexible, extended coils when dissolved in aqueous solution due to the domination of the extensive hydrogen bonding interactions with the surrounding water molecules. Upon an increase in temperature, however, this bonding becomes disrupted and this allows the prevalence of intra- and inter-molecular hydrogen bonding between polymer molecules, causing them to hydrophobically collapse and aggregate into globules.[69]

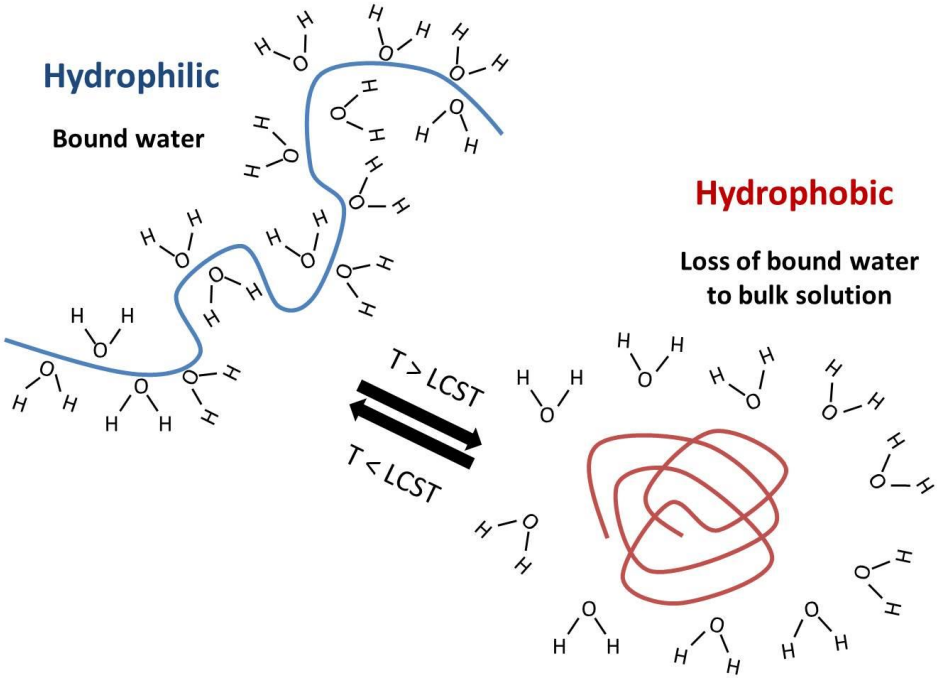

Figure 1.14: Schematic of the hydrophilic to hydrophobic change which occurs as the polymer solution passes through its LCST

Due to the dependence of the process upon water binding, it can be altered or tuned by varying the hydrogen-bonding capabilities of the constituent monomer units and varying the hydrophilic or hydrophobic co-monomer content. PNIPAM has been particularly well studied due to the fact that its LCST of 32°C is close to body temperature (37°C) and it is therefore suited to biomedical applications. It is, however, far from the only polymer to exhibit this thermal-responsive behaviour, poly (oligo ethylene glycol (meth)acrylates) have also been well investigated[70] and example structures are seen in Figure 1.15. Further examples include poly(*N*-substituted (meth)acrylamide)s, poly(*N*-vinylalkylamide)s, poly(lactam)s, poly(pyrrolidone)s, poly(alkoxide)s, poly(2-alkyl-2-oxazoline)s.[71] Although the temperature at which these polymers switch from hydrophobic to hydrophilic in solution is referred to in the literature as the LCST transition temperature, in practice the physical property which has been measured is often the "cloud point". This is the

temperature at which the solution transitions from transparent to opaque at a given solution concentration and is more experimentally accessible than the absolute LCST, which must be obtained by finding the lowest point on a temperature *vs.* composition phase diagram.[72]

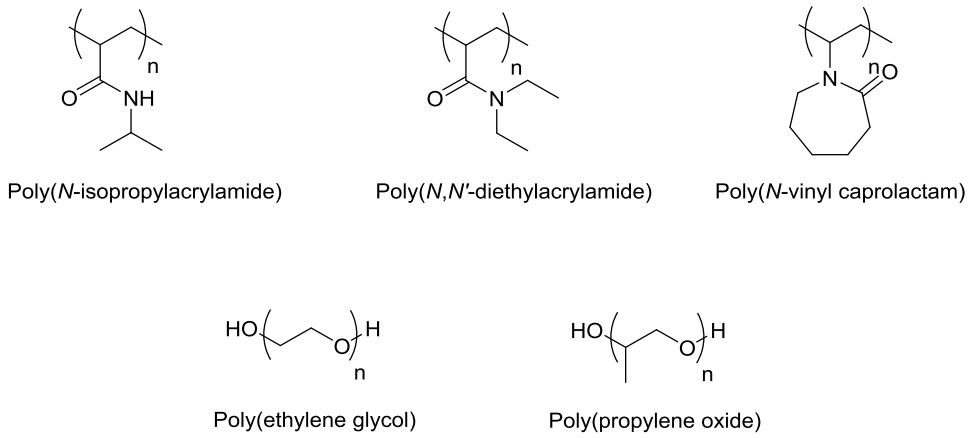

Figure 1.15: Examples of responsive polymers

These stimuli responsive polymers have many current and potential applications within the biomedical field,[73] especially for controlled drug release vehicles and enhancing the polymer's interaction with biological membranes.[74] For example, gold nanoparticles coated with thermo responsive poly(oligo(ethylene glycol) methyl ether methacrylate)s (pOEGMAs) have been seen to reversibly cross between a water/oil interface, which is used as a basic mimic of a biological surface and can suggest potential applications in crossing cell membranes.[75] Beyond the biomedical field, responsive polymers can be used to influence catalytic activity[76] or as purification tools.[77]

Thermoresponsive polymers have also been used to functionalise flat substrates, see Section 1.3. These polymer brushes can exist in the extended or collapsed form and thus switch between hydrophilic and hydrophobic surface

properties for applications such as controlling cell culture and adhesion.[78, 79] One of the challenges with these approaches is the efficient functionalisation of the grafted surfaces, a problem that can be addressed through the application of "click" chemistry.

1.2.6. Thiol-Ene "Click" Reactions and their Polymer Applications

When "click" chemistry was first termed by Kolb *et al.* in 2001, they defined a stringent set of criteria which a process must meet in order to be termed "click".[80] These criteria stated that the reaction must be modular, stereospecific, wide in scope, give very high yields and generate only inoffensive by-products which are easily removed by nonchromatographic methods. Additionally, the process is required to utilise simple reaction conditions, readily available starting materials and reagents, either no solvent or a benign or easily removed solvent and simple product isolation.[80] Initially, the most extensively researched "click" reaction was the Cu(I)-mediated Huisgen reaction between an alkyne and an azide,[81] however in recent years the thiol-ene "click" has increased in popularity.[29]

It is these thiol-ene "click" reactions that are of relevance to this work. The reactions of sulfur containing compounds with alkenes were first reported over 100 years ago in the vulcanisation of natural rubber (poly(*cis*-isoprene)) by sulfur. This hydrothiolation of a carbon-carbon double bond can be considered to be the birth of classical thiol-ene chemistry; the radical addition of thiols across a non-activated alkene bond. Today, however, the term thiol-ene is used to describe the addition of thiols to a wide variety of unsaturated functional groups including maleimides, acrylates, norbornenes and non-activated carbon-carbon double bonds.[82] The thiol-ene reaction has a number of attractive attributes that make it facile and versatile.

Primarily, it can proceed under a variety of different reaction conditions, namely the radical pathway (catalysed by nucleophiles, acids or bases), or without added catalyst (if carried out in a highly polar solvent) or *via* supramolecular catalysis (with β-cyclodextrin).[83] Secondly, a wide range of carbon-carbon double bonds and virtually any thiol can be used in the reaction, increasing its versatility.[84] Finally, the process is typically very rapid. The combination of these desirable attributes results in high efficiency and orthogonality of the reactions and are of particular interest in macromolecular synthesis and functionalised biomolecules.

The thiol-ene reaction can be conducted by a radical process, proceeding through initiation, propagation and termination steps. The initiation step generates the thiyl radical, $RS^{\cdot}$, through photoinitiation or thermal lysis of the S-H bond. The propagation can then proceed by the direct addition of the radical across the alkene, followed by chain transfer to a second thiol molecule. The thiyl radical is therefore regenerated and the thiol-ene product is formed. Termination can then occur through a radical-radical coupling process.[84] General "ene" reactivity falls with decreasing electron density of the double bond, with a few exceptions,[83] and terminal enes are more reactive than internal ones.

Alternatively, the thiol-ene reaction can occur under base catalysed additions, with no radicals required. These types of reactions can also be known as thiol-Michael or conjugate addition. In this case the alkene bond needs to bear an electron withdrawing substituent in order to activate it towards thiol addition, which can slightly reduce the versatility of the process, compared to the radical option. A weak base, such as triethylamine, is usually sufficient in order to catalyse the deprotonation of the thiol to the thiolate anion. This resulting powerful nucleophile

can then add to the activated "ene" bond at the more electrophilic β-carbon atom and form an intermediate carbon-centered anion. This anion can then abstract a proton from either the thiol or the ammonium cation and form the thiol-ene product. As with the radical process, the products are formed with anti-Markovnikov orientation and the two are compared in Figure 1.16.[84] As an alternative to base catalysis, nucleophilic catalysis is also possible using primary/secondary amines or phosphines and it has been suggested that certain tertiary phosphines are capable of catalysing more efficient additions than the typically used bases.[29]

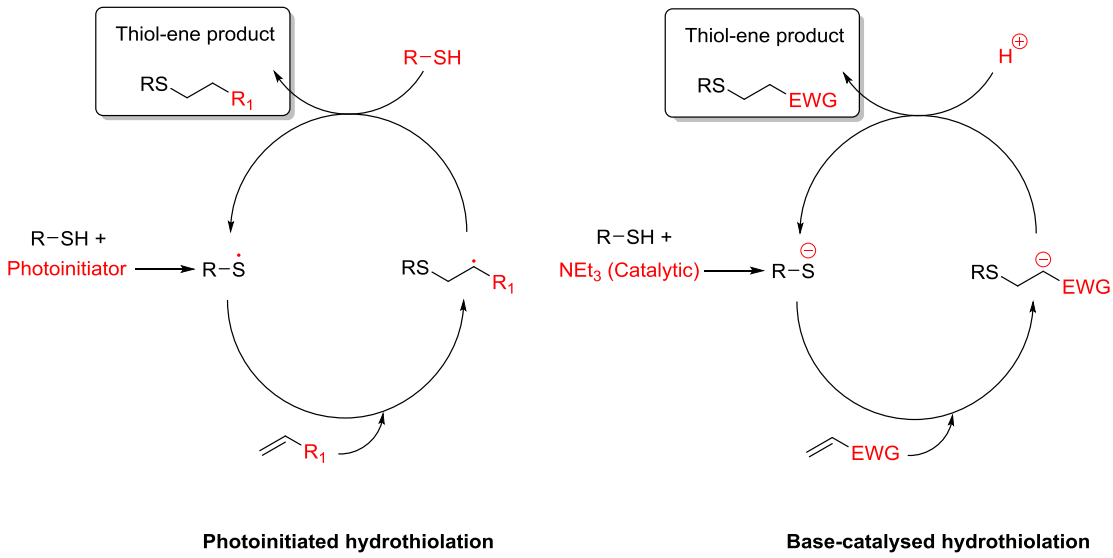

Figure 1.16: The mechanism for the hydrothiolation of a C=C bond in the presence of a photoinitiator and hv (left) and the proposed base-catalysed mechanism for the hydrothiolation of an activated C=C bond (right). The differences between the mechanisms are shown in red. Adapted from the work of A. B. Lowe[84]

Thiol-ene "click" has many applications in polymer science. In one such example, a sequence of RAFT polymerisation, aminolysis and then the Michael addition of either allyl or propargyl acrylate has been used to yield alkene and alkyne

functionalised polymers. From these polymers a second coupling reaction can then be carried out in order to add an R-SH molecule of interest onto the chains using thiol-ene or thiol-yne "click". The resulting end-functional and bis(end-functional)polymers demonstrate the versatility of the thiol chemistry.[85]

1.3. Surface Grafted Polymers

1.3.1. Techniques for Surface Grafting

To enable well-defined, stimuli responsive polymer coatings, the surface chemistry needs to be understood. The modification of surfaces can be achieved by physical adsorption of the molecules of interest; however, it can be difficult to direct the adsorption to specific parts of the surface and only certain compounds and surfaces are compatible. When chemical grafting is used instead, the functionalisation may be targeted and the technique may be used in conjunction with surface structuration techniques.[86] Within this subdivision, either self-assembled monolayers (SAMs) or polymeric/multilayers can be attached. A typical monolayer chemical grafting technique is the addition of thiols onto gold (and other lesser used metals including silver and platinum) to form a self-assembled, well orientated layer.[87] The easy of formation of the Au-S bond is highly advantageous and excellent structural control is possible, however the bond is relatively weak and, unless a polydentate ligand is used, the SAM is typically unstable to physical stress.[88] Due to the presence of the dithioester or trithiocarbonate RAFT end group on RAFT-synthesised polymers, they can undergo binding to gold surfaces. The RAFT group is often transformed into a thiol, using a nucleophile such as a primary amine, prior to gold binding. Alternatively, the polymers can bind to the surface through the RAFT group, which is particularly useful for polymers which are incompatible with

the reduction step, such as poly(acrylic acid). This process also removes the possibility of forming disulfides, rather than thiols, in the reduction process.[89]

Alternatively, should gold be an undesirable substrate, there are many possibilities when it comes to forming chemically grafted monolayers onto oxide surfaces. This opens up a greater range of modifiable substrates as the oxide surfaces include metals (e.g. Al, Fe, Cr), semiconductors (e.g. Si) or materials with surface bound hydroxyl groups. The hydroxyl groups, typically activated through wet etching, dry etching or plasma activation, act as anchoring points for the subsequent formation of dense monolayers. One of the most commonly used surface modifiers are the alkylsilanes, silicon based compounds containing alkyl group(s) and leaving group(s), such as chlorides, alkoxys or hydrides. The silane substrates can be grafted to the oxide anchoring group on the surfaces, *via* a very rapidly forming covalent linkage,[90] resulting in a generally more stable layer than the thiol-gold system, however it is typically less ordered and less dense.[91]

The choice of silane group is important, not only should the linker contain the appropriate functionality for further modification but the functionality level is also important. Monofunctional-silanes, R_3SiX, have the capability to form only one covalent grafting bond to the substrate, due to the presence of only one hydrolysable leaving group. The resulting surface structures are typically reproducible, but the surface coverage is limited due to the presence of the additional bulky R groups. In order to obtain more stable layers with greater coverage, trifunctional-silanes can be employed, $RSiX_3$ (Figure 1.17). The presence of three leaving groups in the molecule allows intra-molecular cross-linking to occur and stabilise the system. Unfortunately, the trifunctionality also allows oligomerisation of the silane in solution either before

or during the attachment process and therefore increases the disorder of the structures. Better leaving groups on the silane (e.g. X = I) result in extensive multilayers, however, poor leaving groups (e.g. X = H) may not react and therefore a balance must be sought.

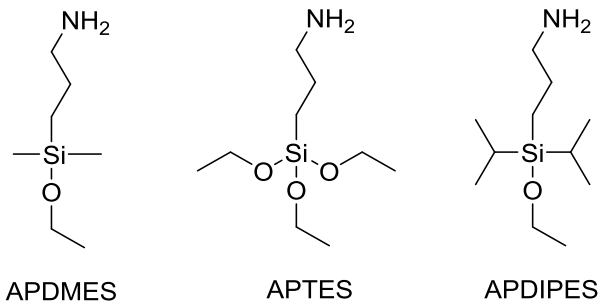

Figure 1.17: APDMES is an example of a monofunctional-silane, R_3SiX, it has only one hydrolysable leaving group and can therefore only form one bond to the substrate. APTES is a trifunctional-silane, $RSiX_3$, it can result in a more stable silane layer, due to the occurrence of intramolecular cross-linking. APDIPES has been designed to improve the monolayer stability, without multilayer build-up

The mechanism of silane SAM formation proceeds *via* three steps, as seen in Figure 1.18. Initially, the organosilanes are hydrolysed by the water molecules that are bound to the oxide surface and converted to the corresponding hydroxysilanes. The hydroxysilanes can then hydrogen bond to the oxide surface, but due to the nature of the hydrogen bonds they are still able to migrate laterally across the surface and aggregate. The aggregated molecules can then condense onto the surface to form the Si-O-Si bonds. In the case of the multifunctional silanes, these bonds can form between neighbouring silanol groups in addition to between the silane and the surface, stabilising the layer. The key role of surface bound water in the first step is very important in the SAM formation. If too much water is present, the silane may polymerise in the bulk phase and rough layers will be obtained, however, if too little water is present, the monolayers will be incomplete. The optimal water concentration

has been found to be 0.15 mg of water in 100 mL of solvent[92] and bicyclohexane, heptanes, toluene, cyclohexane, benzene and hexadecane have all been suggested as appropriate solvents to facilitate this requirement.[88] Alternatively, the silane monolayers can be formed from the vapour phase, where solvent is not required. The advantages of this technique can include decreased formation of siloxane oligomers, reduced surface contamination and denser monolayers.

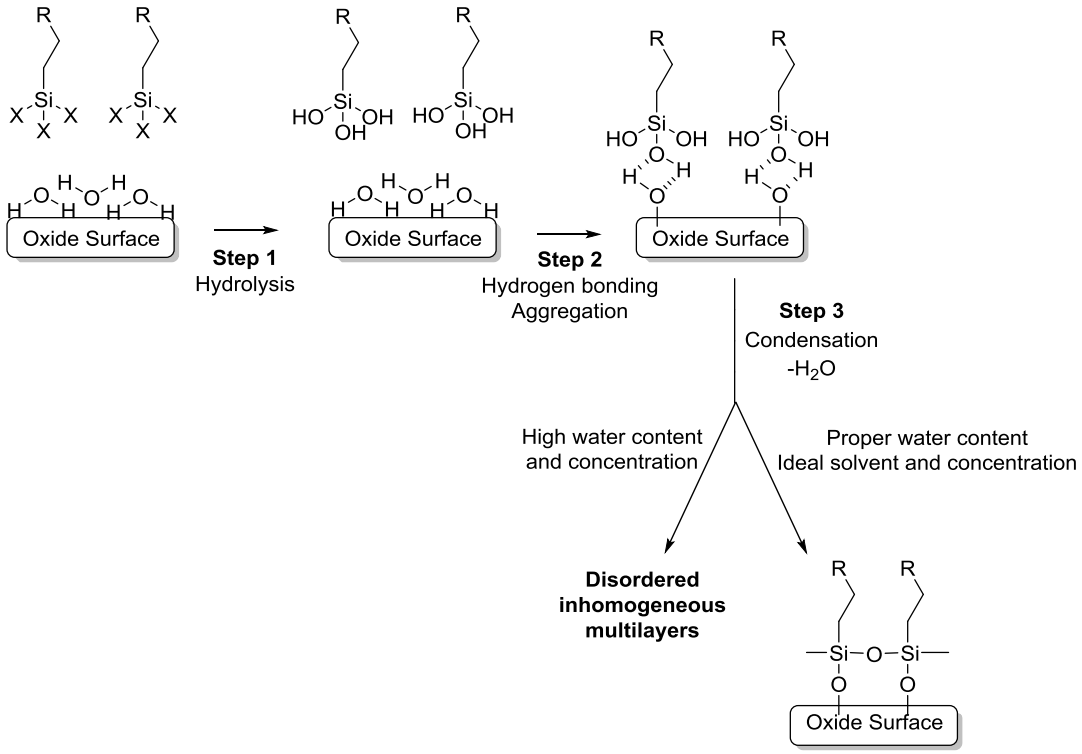

Figure 1.18: The mechanism of silane self-assembly on oxide surfaces, adapted from the work S. P. Pujari *et al.*[88] If the condensation proceeds ideally, a covalently bound and laterally cross-linked monolayer is formed (bottom right). However, if the water content and silane concentration are not controlled, disordered multilayer may be formed (bottom left)

By coating the surfaces with silane containing a relevant functional moiety, it is then possible to attach on biomolecules, such as DNA,[93] cross-linkers or other molecules of interest, including polymers. Covalently attaching organosilanes to silica and glass in order to attach antibodies or receptors, for biosensing applications,

has been seen and investigations into the glass preparatory methods have been reported.[94] Additionally, silane linked immobilisation of carbohydrates has been demonstrated, using multistep synthetic routes to attach underivitised monosaccharides for array applications.[32]

The attachment of polymers to a surface to form polymer brushes; covalently tethered polymer chains which form an ultrathin coating can proceed by one of two different methods.[40] Firstly, the *grafting to* technique involves attaching pre-synthesised polymer chains onto a prepared substrate by phys- or chem-isorption.[95] This method can therefore be combined with the silanation process, should a chemical bond be required. It is experimentally simpler and allows full polymer characterisation to be undertaken prior to the grafting. However, the density of brushes formed using the *grafting to* method is limited, due to steric repulsion between the chains. The alternative technique is *grafting from* brush formation, both examples are seen in Figure 1.19. This involves surface-initiated polymerisation and can produce much denser and more controlled brushes, although it is experimentally more complex.[96, 97]

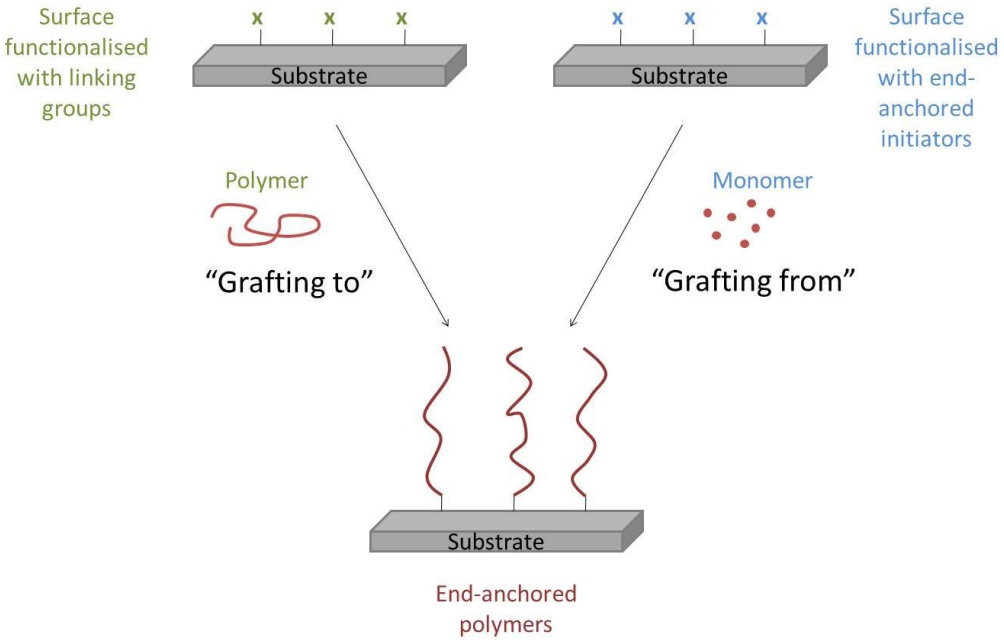

Figure 1.19: Grafting to and grafting from polymer brush formation techniques

1.3.2. Applications of Polymer Coated Surfaces

Surfaces that resist the adsorption of protein have been well studied,[36] with poly- or oligo- ethylene glycol functionality considered to be the classic example.[98] Polymer brushes can be designed to prevent non-specific protein adsorption, which can be advantageous in biosensing, healthcare and diagnostic applications.[38] For example, the infections associated with microbial adhesion and subsequent biofilm formation on intravascular catheters are a major cause of morbidity and mortality.[99] Silicone rubber, the primarily used catheter material, due to its flexibility, low toxicity and physiological inertness, is very susceptible to microbe adhesion. Coating the rubber with diblock copolymers of poly(ethylene glycol) and cationic antimicrobial polycarbonate resulted in the desired antifouling and antibacterial properties.[99] Titanium surfaces, utilised in hip, knee and dental implants, also suffer from non-specific cell adhesion. In this case, the resistance to non-specific cell

adhesion is desired alongside a controlled cell adhesion process, which is used to promote osteoblast differentiation and improve the bond between the implant and the bone. Polymer brushes synthesised from saccharide-substituted methacrylic, 2-gluconamidoethyl methacrylate (GAMA) provided resistance to cell adhesion and modification of the hydroxyl groups on the sugar residues with an adhesion peptide provided the enhanced specific cell adhesion, Figure 1.20.[100] Alternative protein-resistant surfaces are derived from the polymer brushes created from the surface initiated ring-opening polymerisation of α-amino acid *N*-carboxyanhydrides (NCAs). This polymerisation process creates covalently tethered polypeptide chains, which were shown to have an α-helical secondary structure, essentially insensitive to changes in pH, and to prevent non-specific protein adsorption.[40] For diagnostic devices, the reduction in non-specific protein adsorption means that only the specific receptor-ligand responses are observed, and the occurrence of false positive results is reduced.[101] POEGMA brushes have been seen to exhibit these desirable non-fouling properties, which can be tuned by varying the backbone molecular weight and the length of the PEG side chains,[102, 103] as have pNIPAM brushes.[104]

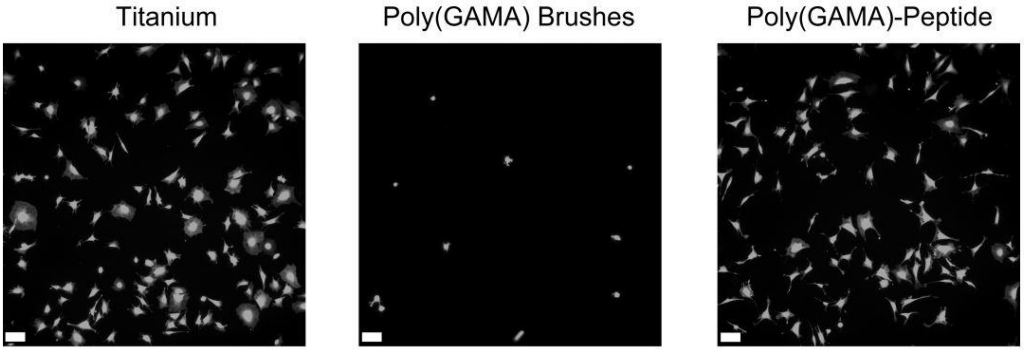

Figure 1.20: Adhesion of osteoblast like cells onto unmodified titanium, titanium coated with poly(GAMA) brushes and titanium coated with poly(GAMA) brushes with an adhesion protein tethered. Demonstrating the ability of the polymer brush to resist cell adhesion when in its native state and also promote adhesion when coupled to the appropriate peptide. Taken from the work of J.E. Raynor *et al.*[100]

Beyond the scope of biosensing and healthcare, anti-fouling coatings are highly coveted for the prevention of biofouling by marine algae onto ship hulls. As an alternative to environmentally unfavourable antifouling paints, self-assembled surface active block copolymers have shown some foul-release efficiency. The polymers are designed with perfluoro groups as the hydrophobic component and PEG chains for hydrophilicity in order to create an amphiphilic surface, which exhibits release of the problematic algae.[105]

Stimuli responsive polymer brushes, functional polymers attached at one end to a planar substrate or particle, can undergo molecular conformational changes when triggered by a change in temperature, pH, light, solvent or mechanical stress.[106, 107] When in a good solvent, the chains fully stretch away from the surface, resulting in a larger change in conformation than for the corresponding free polymer chains in solution. In order to fully exploit the responsive brush behaviour, the spacing of the grafted polymer chains should be controlled. At a low grafting density the response will be similar to that of the free polymers, but at high grafting densities there may not be sufficient free space to facilitate the conformational change. In addition to the homopolymer brushes (single-component systems where the responsive behaviour results from the conformational changes of the polymer chains), block copolymer brush and mixed polymer brush systems have also been developed. In the block copolymer systems, the brushes are synthesised with two distinct polymer blocks. The stimuli then cause phase separation, exposing one block or the other and altering the surface properties. The mixed polymer system is composed of at least two chemically different polymers grafted to the surface. Depending on which polymer is exposed at any given time, the surface properties are switched between the properties of the constituent polymers. In the case of

nanopatterned pNIPAM brushes, systems can be designed in which the temperature dependent conformational changes of the polymer can control the display of the biomolecules immobilised onto the polymer-free regions of the surface. When the polymer chain collapse above the LCST, the underlying substrate is available for protein absorption, whereas below the critical temperature the adsorption is retarded.[104] Applications of these polymer brushes and films include biomedical sensors, microfluidic devices and self-healing coatings.[67, 106]

Dense polymer brushes exhibit the desirable properties of controlled swelling and wetability, multifunctional character and adjustable macromolecular parameters. These polymer brushes can be functionalised *via* either the chain ends or side chain coupling in order to incorporate cell-cues into the structure for cell adhesion.[108] For example, thin but dense brushes, synthesised by surface-initiated ATRP, have been modified with peptide ligands to promote the endothelialisation of blood-contacting biomaterials. The brushes, composed of poly(2-hydroxyethyl methacrylate) (pHEMA) or poly(poly(ethylene glycol) methyl ether methacrylate) (pPEGMA), are themselves resistant to non-specific protein and cell adhesion, reducing the likelihood of non-specific binding away from the arginylglycylaspartic acid (RGD) containing peptide ligands. The RGD containing peptide ligands specifically bind to integrin receptors present on cells allowing the polymer brush system to promote cell adhesion (Figure 1.21).[109] The synthesis of these dense brushes is primarily achieved through controlled surface-initiated polymerisation and there has been recent progress regarding the problem of analysing the grafted polymeric species. Large areas of grafted-from polymer brush growth can be detached or etched away from the surface in order to remove enough polymer solution for characterisation.[107, 108]

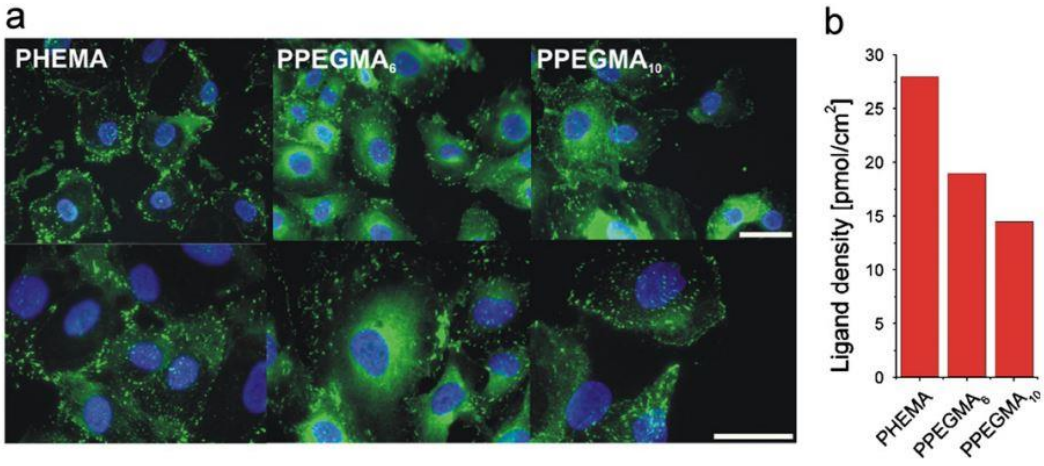

Figure 1.21: Fluorescence micrographs of human umbilical vascular endothelial cells (HUVECs) adhering to polymer brush coated surfaces functionalised to 20 nm with pHEMA and two pPEGMAs with different OEG side chain length ($pPEGMA_{10}$ and $pPEGMA_{10}$) The lower cell adhesion present on the $pPEGMA_{10}$ surface compared to the $pPEGMA_6$ surface is proposed to be due to increased brush swelling resulting in less ligand affinity and therefore lower ligand density present on the surface, as seen in the graph. Taken from the work of S. Tugulu *et al.*[109]

In addition to the use of polymer coatings for promoting or preventing cell adhesion, responsive polymer coatings can afford more precise control over these processes. Systems have been designed to bind a biological moiety under one set of conditions, but then reverse this process and become non-adhesive when the conditions change. This is particularly useful in tissue engineering; the cells need to adhere to the surface in order to grow, but must then easily detach at an appropriate time to allow harvesting. Ideally the detachment process shouldn't require biochemical or chemical reagents due to tissue contamination concerns. Thermoresponsive coatings circumvent this problem as only a small change in temperature is require for cell release and it is therefore a gentler alternative to mechanical dissociation or enzyme degredation.[74] The most widely studied systems are pNIPAM films, for both the tissue engineering/cell culture applications and the creation of "smart" biofouling microfluidic devices, with the capability to absorb

proteins from a solution and then release them on demand.[110] As an alternative to polymer coatings, manipulation of cell adhesion can also be achieved through the use of surface grafted peptides.[111]

The use of polymer brushes as a spacer molecule in the immobilisation of bioactive compounds has also been studied. The use of the polymer tether can improve the bioactivity through reduction of steric constraints and by shielding the bioactive compound from hydrophobic surface induced denaturation. Commonly used polymers substrates for bioconjugation include poly(styrene), used in antimicrobial surfaces, tissue culture and bioanalytical assays, and poly(ethylene), which is used in drug delivery, biomedical devices and biocompatible materials. Polymer microarrays, formed from the ink-jet or contact printing of monomer solutions and subsequent *in situ* polymerisation, have been used to screen large numbers of polymers for specific biological interactions. Surfaces that promote as well as those that resist the adhesion of cells are of interest and can be identified.[112] Back in 2004, an early example of this work identified polymer coatings which could promote the attachment of human embryonic stem cells and support their spreading and differentiation.[113] Further work in the area has progressed with the development of high-throughput screening techniques allowing correlation of the cell behaviour to polymer properties, concluding that high acrylate containing monomer result in the most desirable polymers for these applications,[114] Figure 1.22.

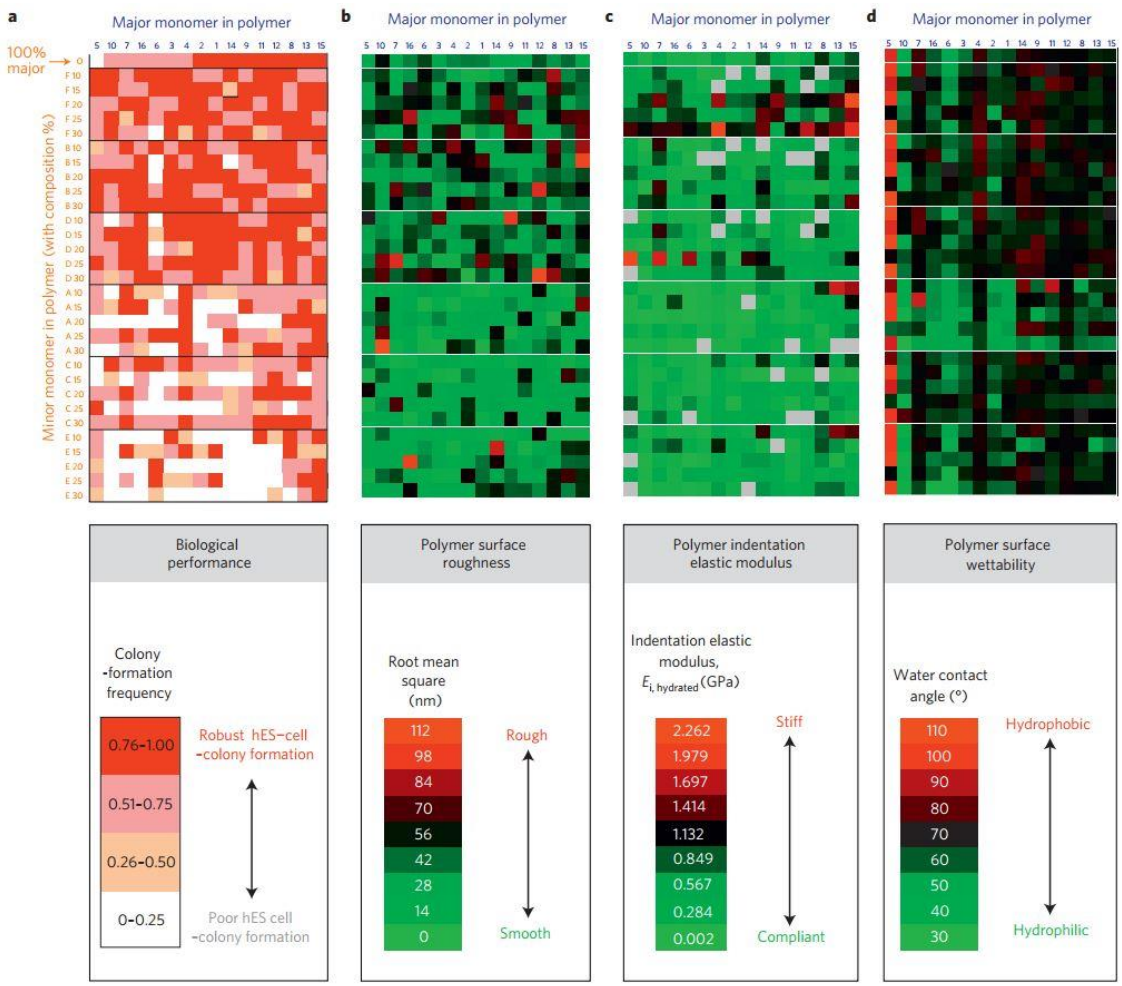

Figure 1.22: Comparison of the biological performance of the polymer surface coating, in terms of colony formation frequency, correlated with the physical properties of the coating (surface roughness, indentation elastic modulus and surface wettability) allowing the development of the structure-function relationships. Each glass array has been prepared from the copolymerisation of 16 major monomers with each of six minor monomers in six different ratios, to create 496 different combinations. It is seen that optimal human embryonic stem cell substrates are generated from monomers with high acrylate content and moderate surface wettability. From the work of Y. Mei *et al.*[114]

1.4. Surface Analysis

1.4.1. Contact Angle Analysis

Contact angle analysis, also known as drop shape analysis (DSA), is used to determine the contact angle made by a liquid on a surface, *via* an image analysis method. It can be used to measure the surface tension, from the shadow image of a sessile drop, or the interfacial tension, from the shadow image of a pendant drop.

Experimentally, the drop is either administered onto the solid substrate, in the case of sessile drops, or allowed to hang from the end of the needle, in the case of the pendant drop. The drop is then imaged and typically the image is transferred to the analysis software.[115] The contour of the drop is recognised using a grey-scale analysis of the image and a geometric model is fitted to the contour, in order to describe the drop shape. The contact angle the drop makes with the solid substrate can then be calculated by combining the information from the drop shape function and the sample baseline, Figure 1.23.

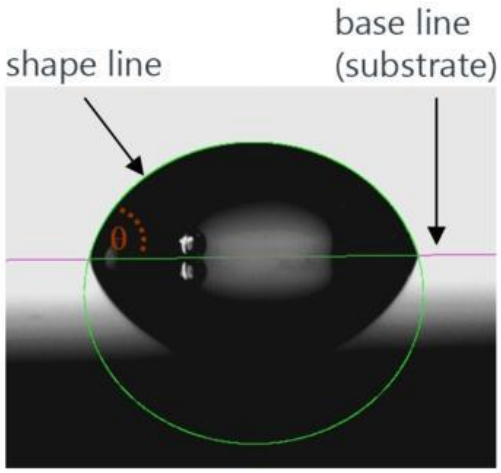

Figure 1.23: A sessile drop shown with a fitted baseline and contour (shape line), taken from the Kruss Drop Shape Analyser online reseources[115]

The contact angle that a liquid drop forms on a solid surface is defined by the mechanical equilibrium of the drop under the action of the three interfacial tensions: solid-vapour (γ_{sv}), solid-liquid (γ_{sl}) and liquid-vapour (γ_{lv}), Figure 1.24. Due to the ease with which contact angle measurements can be obtained experimentally, it is an attractive technique for estimating these interfacial tensions.[116] However, there are a number of issues which must be considered if using these angle measurements for such calculations. Firstly, the roughness or the smoothness and heterogeneity of the

surface is very important. Rough surfaces can cause contact angle hysteresis and very rough surfaces can generate contact angles which are larger than for the corresponding chemically identical, smooth surface.[117]

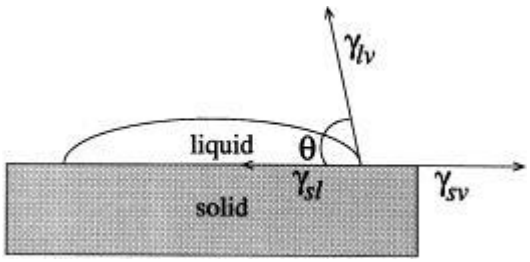

Figure 1.24: Schematic of a sessile-drop contact angle system, taken from the work of D. Y. Kwok and A. W. Neumann[116]

1.4.2. Ellipsometry

Another technique for surface analysis and characterisation is ellipsometry. This is an optical technique which can be used to investigate the thickness of thin films. An incident radiation (laser source) is reflected or absorbed by the sample and the change in polarisation of the radiation source is measured. This change is recorded as two parameters, psi (amplitude component) and delta (phase difference), which are combined with wavelength of the incident light in order to calculate the layer thickness, error and confidence interval. It has the advantages of being non-destructive, contactless and providing sub-nanometre resolution. However, you must know the optical constants for your system, which may involve using approximations if suitable literature values are not available and the data must be modelled in order to obtain useful information.[118]

1.4.3. X-Ray Photoelectron Spectroscopy (XPS)

In order to obtain information regarding the elemental composition of a surface, XPS may be used. This spectroscopic technique involves irradiating the

surface with a beam of X-rays and measuring the kinetic energy and number of electrons released from the top 10 nm of the sample. The data obtained is displayed as a graph of binding energy *vs* counts. The binding energy of each peak can then be assigned, based upon literature values, in order to identify the element, and orbital, from which the electron was released.[119]

1.4.4. Quartz-Crystal Microscopy with Dissipation (QCM-D)

A quartz-crystal microbalance with dissipation is used to study molecular interactions and molecular adsorption at surfaces by measuring the change in resonant frequency of a quartz crystal upon addition of mass to a surface.[120] It has the advantages of sub-nanogram detection capabilities, being label free and readily modifiable for a diverse range of surface chemistries. The mass of very thin surface bound layers and the binding events can be monitored in real time, allowing interface characterisation and evaluation of kinetics. The applications include detection of carbohydrates, nucleic acids, antibodies and cells and characterisation of enzyme activity.[121] The QCM-D monitors both the frequency and energy dissipation response for the crystal and can therefore provide information about the kinetics of mass changes and the structural changes simultaneously. The quartz crystal sensors utilised in these experiments are in the form of a thin quartz disc sandwiched between two electrodes and they are excited to oscillation by applying A.C. voltage. This oscillation then decays exponentially once the driving A.C. voltage is switched off. The QCM-D instrument monitors this decay and extracts two parameters resonance frequency (f) and dissipation (D). The dissipation parameter gives information about how long the crystal continues to oscillate after the driving voltage of the system is turned off, i.e. how quickly the energy is dissipated from the system. For soft and viscous films, the dissipation is high due to frictional losses within the

films causing dampening of the sensor oscillation. Conversely, for rigid films the dissipation is low.

The data can be displayed as a raw data plot ($\Delta D/\Delta f$ against time) or modelling can be carried out in order to obtain additional quantitative information. The Sauerbrey equation, (Figure 1.25) can be used to model thin, rigid films (where the frequency and dissipation harmonic do not appear to spread during the course of the experiment).[122] For soft and laterally homogenous films, viscoelastic modelling of ΔD and Δf must instead be performed. This is because the viscoelastic films will not fully couple to the oscillation of the crystal and will instead cause dampening. The Sauerbrey relation will therefore underestimate the mass at the surface and the Voigt or Maxwell model must be used instead.

$$\Delta m = \frac{-C\Delta f}{n}$$

Figure 1.25: The Sauerbrey equation for calculating the change in mass (Δm) on the surface C is ((crystal thickness x crystal density) / fundamental frequency), which is equal to 17.7 ng Hz^{-1} cm^{-2} for a 5 MHz quartz crystal. n is the overtone number (i.e 1, 3, 5 etc.). Δf is the change in frequency in Hz

The origins of QCM-D were not in polymer chemistry, however it has become a useful tool for studying polymer binding and surface ordering. The ability to monitor the binding of polymers to surfaces in real time and obtain data regarding the kinetics of these grafting processes is very desirable.[123] Through such studies, it has been seen that at a low grafting density polymer chains can exhibit a pancake-like formation (if the chains interact attractively with the surface) or a mushroom-like formation (if the chain-surface interaction is non-attractive). Once a high grafting density is reached the chains stretch away from the surface and form brushes due to the combination of chain-chain repulsion and elasticity.[124,125] A polymer chain

grafted to a surface can undergo conformational changes, which influence its interfacial properties such as hydrophobicity, hydrophilicity, adsorption and adhesion.[126] The dehydration and hydration of the chains can be observed through monitoring of the frequency shift (Δf) of the QCM-D plot whereas the collapse and swelling are related to the dissipation change (ΔD). A plot of Δf *vs.* ΔD describes the relationship between dehydration and collapse. If ΔD increases linearly with $-\Delta f$ it indicates that the conformational change involves only one kinetic process and that the dehydration and collapse must occur simultaneously.[125]

The thermoresponsive behaviour of pNIPAM brushes has been investigated using QCM-D. It is known that below its LCST (~32°C), free pNIPAM chains are swollen into a random coil, whereas above the LCST they collapse into globules.[127] The pNIPAM chains were grafted to a gold surface and therefore a low density was observed, producing mushroom type structures. The mass layer on the surface decreases with temperature, with a transition occurring at ~34°C, due to the loss of water molecules once the polymer has reached its LCST.[125] With *grafting from* polymerisation a much higher grafting density, and pancake-like structure, is achieved yet the LCST transition is still observed at ~34°C.[128] The pancake-to-brush conformational change can be observed over time.[129] Initially there is a slow decrease in Δf showing slow grafting due to steric hindrance, this then dramatically speeds up once the grafted chains move to a brush conformation to accommodate the incoming chains.[125]

Work on thio-functional oligo(ethylene glycol) (OEG) polymers has shown that using disulfide di(ethylene glycol) (DEG) polymers results in more mass adsorbed onto the gold, when compared to thiols with only one sulfur atom available

for adsorption. The disulfide DEG polymers also showed greater adsorption than di-thio and tri-thio species, despite having the same or fewer available sulfur atoms. This has been rationalised as being due to the steric effects on the sulfur atoms and the resulting differences in adsorbing bond angle, which results in a weaker dissociation of charge. It was also found that when longer OEG polymers were used, the binding was less than that for the shorter counterparts.[130] A variety of QCM chip coatings are commercially available allowing investigation of systems other than sulfur-gold binding. For example, silicon dioxide coated QCM chips have been functionalised with thiol-containing silanes to allow real-time monitoring of the addition of macromonomers of poly (ethylene glycol methyl ether acrylate) ($pEGA_{454}$) and poly (ethylene glycol methyl ether methacrylate) ($pEGMA_{1100}$).[131]

In addition to monitoring the adsorption of polymers onto the surfaces, QCM-D can also be used to monitor the interactions of a ready functionalised surface with a solution. Layer-by-layer assemblies of lectins onto glycopolymers have been produced, using the mannose/galactose glycopolymers as selective Con A/PNA lectin binders, respectively.[132] Beyond the scope of polymer systems, QCM-D can be used to monitor the protein resistance of a functionalised chip and therefore select surface-coatings that exhibit desirable bio-inert properties.[37]

1.5. "Switchable" Polymer Coatings for Microarray Applications

Through the preparation of pOEGMA and pNIPAM polymer brushes, which have been seen to exhibit biocompatibility[133, 134] and both protein resistant [36, 103] and stimuli-responsive[37, 135] properties,[110] it is proposed that "smart-switchable" microarray surfaces, as seen in Figure 1.26, can be produced. Although the exact mechanisms by which polymer surfaces resist protein adsorption, and therefore render surfaces resistant to cell adhesion, are still unclear, it is known that the adsorption behaviour is influenced by molecular parameters such as packing density, chain length and chain conformation.[110] Above the critical temperature the surface is hydrophobic, allowing the formation of small, well-defined spots of carbohydrate solution and therefore high density array generation is possible. Below the critical temperature, the surface becomes hydrophilic, exhibiting reduced protein adhesion and therefore preventing non-specific binding and false positive diagnoses.

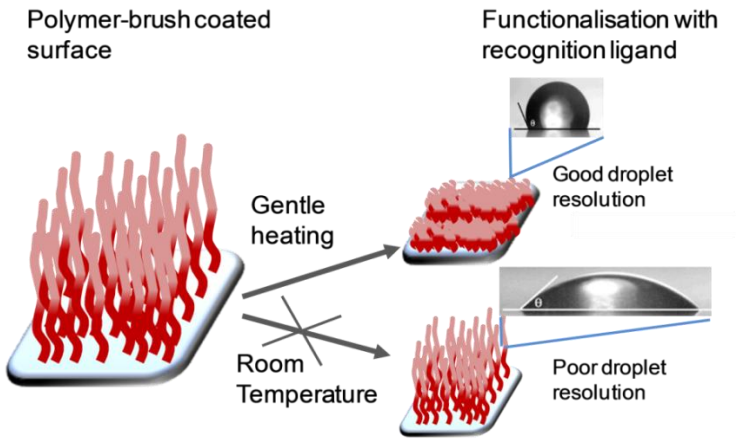

Figure 1.26: An example of "smart-switchable" polymer functionalised surface. Below the LCST the polymer chains are fully hydrates and the surface exhibits hydrophilic properties. When heated above the LCST the collapse of the chains switches the surface to amore hydrophobic state

1.6. Aims

This work aimed to investigate techniques for the functionalisation of a variety of solid supports with both pOEGMA and pNIPAM polymer brush-like systems and carry out a comparison between the two different polymer coatings. These surfaces were then to be tested for their desirable properties (protein resistance and stimuli-responsive behaviours) and their ability to integrate with current glycoarray scanning protocols. On route to the polymer immobilisation, thiolated monosaccharide arrays were to be produced and used as low density arrays in order to probe lectin-carbohydrate binding events.

The work was then to conclude with the synthesis and subsequent immobilisation of glycosylated polymers onto glass slides. The final aim was to use the silane acrylate coatings combined with the terminal-glycan functionalised polymers to generate high density glycoarray systems, through the application of direct microcontact printing and to demonstrate the potential of these systems for probing biologically relevant binding interactions.

1.7. References

1. H. C. Neu, *Science*, 1992, **257**, 1064-1073.

2. A. Koul, E. Arnoult, N. Lounis, J. Guillemont and K. Andries, *Nature*, 2011, **469**, 483-490.

3. C. Nathan, *Nature*, 2004, **431**, 899-902.

4. K. M. G. O'Connell, J. T. Hodgkinson, H. F. Sore, M. Welch, G. P. C. Salmond and D. R. Spring, *Angew. Chem. Int. Ed.*, 2013, **52**, 10706-10733.

5. A. Adibekian, P. Stallforth, M.-L. Hecht, D. B. Werz, P. Gagneux and P. H. Seeberger, *Chem. Sci.*, 2011, **2**, 337-344.

6. H. Lis and N. Sharon, *Chem. Rev.*, 1998, **98**, 637-674.

7. I. J. Goldstein, R. C. Hughes, M. Monsigny, T. Osawa and N. Sharon, *Nature*, 1980, **285**, 66-66.

8. J. M. Rini, *Annu. Rev. Biophys. Biomol. Struct*, 1995, **24**, 551-577.

9. R. Cummings and R. McEver, in *Essentials of Glycobiology*, ed. A. Varki, Cold Spring Harbor Laboratory Press, Second edn., 2008.

10. M. Ambrosi, N. R. Cameron and B. G. Davis, *Org. Biomol. Chem.*, 2005, **3**, 1593-1608.

11. J. J. Lundquist and E. J. Toone, *Chem. Rev.*, 2002, **102**, 555-578.

12. L. L. Kiessling, J. E. Gestwicki and L. E. Strong, *Angew. Chem. Int. Ed.*, 2006, **45**, 2348-2368.

13. R. J. Pieters, *Med. Res. Rev.*, 2007, **27**, 796-816.

14. M. C. Galan, P. Dumy and O. Renaudet, *Chem. Soc. Rev.*, 2013, **42**, 4599-4612.

15. G. Mulvey, P. I. Kitov, P. Marcato, D. R. Bundle and G. D. Armstrong, *Biochimie*, 2001, **83**, 841-847.

16. M. D. Disney and P. H. Seeberger, *Chem. Biol.*, 2004, **11**, 1701-1707.

17. T. Horlacher and P. H. Seeberger, *Chem. Soc. Rev.*, 2008, **37**, 1414-1422.

18. N. Laurent, J. Voglmeir and S. L. Flitsch, *Chem. Commun.*, 2008, 4400-4412.

19. P. H. Seeberger and D. B. Werz, *Nature*, 2007, **446**, 1046-1051.

20. S. Park, J. C. Gildersleeve, O. Blixt and I. Shin, *Chem. Soc. Rev.*, 2013, **42**, 4310-4326.

21. D. N. Wang, S. Y. Liu, B. J. Trummer, C. Deng and A. L. Wang, *Nat. Biotechnol.*, 2002, **20**, 275-281.

22. W. G. T. Willats, S. E. Rasmussen, T. Kristensen, J. D. Mikkelsen and J. P. Knox, *Proteomics*, 2002, **2**, 1666-1671.

23. K. Godula and C. R. Bertozzi, *J. Am. Chem. Soc.*, 2010, **132**, 9963-9965.

24. H.-Y. Hsiao, M.-L. Chen, H.-T. Wu, L.-D. Huang, W.-T. Chien, C.-C. Yu, F.-D. Jan, S. Sahabuddin, T.-C. Chang and C.-C. Lin, *Chem. Commun.*, 2011, **47**, 1187-1189.

25. D. Wang, G. T. Carroll, N. J. Turro, J. T. Koberstein, P. Kovac, R. Saksena, R. Adamo, L. A. Herzenberg, L. A. Herzenberg and L. Steinman, *Proteomics*, 2007, **7**, 180-184.

26. Z. Pei, H. Yu, M. Theurer, A. Walden, P. Nilsson, M. Yan and O. Ramstrom, *Chembiochem*, 2007, **8**, 166-168.

27. The Consortium for Functional Glycomics (CFG), Available at http://www.functionalglycomics.org/fg/, Accessed 09/11/14.

28. CFG Mammalian Glycan Array Data, Available at http://www.functionalglycomics.org/static/consortium/resources/resourcecoreh8.shtml, Accessed 09/11/14.

29. A. B. Lowe, *Polym. Chem.*, 2014, **5**, 4820-4870.

30. B. T. Houseman and M. Mrksich, *Chem. Biol.*, 2002, **9**, 443-454.

31. Z. L. Zhi, N. Laurent, A. K. Powel, R. Karamanska, M. Fais, J. Voglmeir, A. Wright, J. M. Blackburn, P. R. Crocker, D. A. Russell, S. Flitsch, R. A. Field and J. E. Turnbull, *Chembiochem*, 2008, **9**, 1568-1575.

32. G. Nan, H. Yan, G. Yang, Q. Jian, C. Chen and Z. Li, *Curr. Pharm. Biotechnol.*, 2009, **10**, 138-146.

33. B. Donczo, J. Kerekgyarto, Z. Szurmai and A. Guttman, *Analyst*, 2014, **139**, 2650-2657.

34. J. Hirabayashi, M. Yamada, A. Kuno and H. Tateno, *Chem. Soc. Rev.*, 2013, **42**, 4443-4458.

35. M. Hermansson, *Colloids Surface B*, 1999, **14**, 105-119.

36. E. Ostuni, R. G. Chapman, R. E. Holmlin, S. Takayama and G. M. Whitesides, *Langmuir*, 2001, **17**, 5605-5620.

37. D. A. Dobrzanska, A. L. Cooper, C. G. Dowson, S. D. Evans, D. J. Fox, B. R. Johnson, C. I. Biggs, R. K. Randev, H. M. Stec, P. C. Taylor and A. Marsh, *Langmuir*, 2013, **29**, 2961-2970

38. K. Bebis, M. W. Jones, D. M. Haddleton and M. I. Gibson, *Polym. Chem.*, 2011, **2**, 975-982.

39. A. Hucknall, S. Rangarajan and A. Chilkoti, *Adv. Mater.*, 2009, **21**, 2441-2446.

40. J. Wang, M. I. Gibson, R. Barbey, S. J. Xiao and H. A. Klok, *Macromol. Rapid Commun.*, 2009, **30**, 845-850.

41. J. Nicolas, G. Mantovani and D. M. Haddleton, *Macromol. Rapid Commun.*, 2007, **28**, 1083-1111.

42. K. Matyjaszewski and J. Spanswick, *Mater. Today*, 2005, **8**, 26-33.

43. A. Goto and T. Fukuda, *Prog. Polym. Sci.*, 2004, **29**, 329-385.

44. C. J. Hawker, *J. Am. Chem. Soc.*, 1994, **116**, 11185-11186.

45. K. Matyjaszewski and J. Xia, *Chem. Rev.*, 2001, **101**, 2921-2990.

46. J. Chiefari, Y. K. Chong, F. Ercole, J. Krstina, J. Jeffery, T. P. T. Le, R. T. A. Mayadunne, G. F. Meijs, C. L. Moad, G. Moad, E. Rizzardo and S. H. Thang, *Macromolecules*, 1998, **31**, 5559-5562.

47. C. J. Hawker, A. W. Bosman and E. Harth, *Chem. Rev.*, 2001, **101**, 3661-3688.

48. J. Nicolas, Y. Guillaneuf, C. Lefay, D. Bertin, D. Gigmes and B. Charleux, *Prog. Polym. Sci.*, 2013, **38**, 63-235.

49. K. Matyjaszewski and N. V. Tsarevsky, *J. Am. Chem. Soc.*, 2014, **136**, 6513-6533.

50. H. Willcock and R. K. O'Reilly, *Polym. Chem.*, 2010, **1**, 149-157.

51. G. Moad, E. Rizzardo and S. H. Thang, *Aust. J. Chem.*, 2005, **58**, 379-410.

52. C. Boyer, M. H. Stenzel and T. P. Davis, *J. Polym. Sci., Part A: Polym. Chem.*, 2011, **49**, 551-595.

53. J. Skey and R. K. O'Reilly, *Chem. Commun.*, 2008, 4183-4185.

54. J. Hentschel, K. Bleek, O. Ernst, J. F. Lutz and H. G. Borner, *Macromolecules*, 2008, **41**, 1073-1075.

55. M. Bathfield, D. Daviot, F. D'Agosto, R. Spitz, C. Ladaviere, M. T. Charreyre and T. Delair, *Macromolecules*, 2008, **41**, 8346-8353.

56. M. Deletre and G. Levesque, *Macromolecules*, 1990, **23**, 4733-4741.

57. J. M. Spruell, B. A. Levy, A. Sutherland, W. R. Dichtel, J. Y. Cheng, J. F. Stoddart and A. Nelson, *J. Polym. Sci., Part A: Polym. Chem.*, 2009, **47**, 346-356.

58. C. W. Scales, A. J. Convertine and C. L. McCormick, *Biomacromolecules*, 2006, **7**, 1389-1392.

59. Z. Merican, T. L. Schiller, C. J. Hawker, P. M. Fredericks and I. Blakey, *Langmuir*, 2007, **23**, 10539-10545.

60. A. B. Lowe, B. S. Sumerlin, M. S. Donovan and C. L. McCormick, *J. Am. Chem. Soc.*, 2002, **124**, 11562-11563.

61. L. Nurmi, J. Lindqvist, R. Randev, J. Syrett and D. M. Haddleton, *Chem. Commun.*, 2009, 2727-2729.

62. M. A. Gauthier, M. I. Gibson and H. A. Klok, *Angew. Chem. Int. Ed.*, 2009, **48**, 48-58.

63. C. R. Becer, *Macromol. Rapid Commun.*, 2012, **33**, 742-752.

64. S.-J. Richards, M. W. Jones, M. Hunaban, D. M. Haddleton and M. I. Gibson, *Angew. Chem. Int. Ed.*, 2012, **51**, 7812-7816.

65. M. W. Jones, L. Otten, S. J. Richards, R. Lowery, D. J. Phillips, D. M. Haddleton and M. I. Gibson, *Chem. Sci.*, 2014, **5**, 1611-1616.

66. R. Tong, L. Tang, L. Ma, C. Tu, R. Baumgartner and J. Cheng, *Chem. Soc. Rev.*, 2014.

67. L. Zhai, *Chem. Soc. Rev.*, 2013, **42**, 7148-7160.

68. H. G. Schild, *Prog. Polym. Sci.*, 1992, **17**, 163-249.

69. E. Ruel-Gariépy and J.-C. Leroux, *Eur. J. Pharm. Biopharm.*, 2004, **58**, 409-426.

70. G. Vancoillie, D. Frank and R. Hoogenboom, *Prog. Polym. Sci.*, 2014, **39**, 1074-1095.

71. D. Roy, W. L. A. Brooks and B. S. Sumerlin, *Chem. Soc. Rev.*, 2013, **42**, 7214-7243.

72. D. Schmaljohann, *Adv. Drug Deliver. Rev.*, 2006, **58**, 1655-1670.

73. M. A. Ward and T. K. Georgiou, *Polymers*, 2011, **3**, 1215-1242.

74. C. de las Heras Alarcon, S. Pennadam and C. Alexander, *Chem. Soc. Rev.*, 2005, **34**, 276-285.

75. E. W. Edwards, M. Chanana, D. Wang and H. Möhwald, *Angew. Chem. Int. Ed.*, 2008, **47**, 320-323.

76. G. Chen and A. S. Hoffman, *Bioconj. Chem.*, 1993, **4**, 509-514.

77. C.-W. Chang, T. H. Nguyen and H. D. Maynard, *Macromol. Rapid Commun.*, 2010, **31**, 1691-1695.

78. H.-Y. Tsai, K. Vats, M. Z. Yates and D. S. W. Benoit, *Langmuir*, 2013, **29**, 12183-12193.

79. S. Dey, B. Kellam, M. R. Alexander, C. Alexander and F. R. A. J. Rose, *J. Mater. Chem.*, 2011, **21**, 6883-6890.

80. H. C. Kolb, M. G. Finn and K. B. Sharpless, *Angew. Chem. Int. Ed.*, 2001, **40**, 2004-2021.

81. W. H. Binder and R. Sachsenhofer, *Macromol. Rapid Commun.*, 2007, **28**, 15-54.

82. M. J. Kade, D. J. Burke and C. J. Hawker, *J. Polym. Sci., Part A: Polym. Chem.*, 2010, **48**, 743-750.

83. C. E. Hoyle, T. Y. Lee and T. Roper, *J. Polym. Sci., Part A: Polym. Chem.*, 2004, **42**, 5301-5338.

84. A. B. Lowe, *Polym. Chem.*, 2010, **1**, 17-36.

85. B. Yu, J. W. Chan, C. E. Hoyle and A. B. Lowe, *J. Polym. Sci., Part A: Polym. Chem.*, 2009, **47**, 3544-3557.

86. C. M. Dekeyser, C. C. Buron, K. Mc Evoy, C. C. Dupont-Gillain, J. Marchand-Brynaert, A. M. Jonas and P. G. Rouxhet, *J. Colloid Interface Sci.*, 2008, **324**, 118-126.

87. H. A. Biebuyck, C. D. Bian and G. M. Whitesides, *Langmuir*, 1994, **10**, 1825-1831.

88. S. P. Pujari, L. Scheres, A. T. M. Marcelis and H. Zuilhof, *Angew. Chem. Int. Ed.*, 2014, **53**, 6322-6356.

89. A. S. Duwez, P. Guillet, C. Colard, J. F. Gohy and C. A. Fustin, *Macromolecules*, 2006, **39**, 2729-2731.

90. P. VanDerVoort and E. F. Vansant, *J. Liq. Chromatogr. Relat. Technol.*, 1996, **19**, 2723-2752.

91. S. W. Lee and P. E. Laibinis, *Biomaterials*, 1998, **19**, 1669-1675.

92. M. E. McGovern, K. M. R. Kallury and M. Thompson, *Langmuir*, 1994, **10**, 3607-3614.

93. Y. H. Rogers, P. Jiang-Baucom, Z. J. Huang, V. Bogdanov, S. Anderson and M. T. Boyce-Jacino, *Anal. Biochem.*, 1999, **266**, 23-30.

94. J. J. Cras, C. A. Rowe-Taitt, D. A. Nivens and F. S. Ligler, *Biosens. Bioelectron.*, 1999, **14**, 683-688.

95. M. Baum and W. J. Brittain, *Macromolecules*, 2002, **35**, 610-615.

96. S. Tugulu, A. Arnold, I. Sielaff, K. Johnsson and H. A. Klok, *Biomacromolecules*, 2005, **6**, 1602-1607.

97. S. Edmondson, V. L. Osborne and W. T. S. Huck, *Chem. Soc. Rev.*, 2004, **33**, 14-22.

98. Z. G. Estephan, P. S. Schlenoff and J. B. Schlenoff, *Langmuir*, 2011, **27**, 6794-6800.

99. X. Ding, C. Yang, T. P. Lim, L. Y. Hsu, A. C. Engler, J. L. Hedrick and Y.-Y. Yang, *Biomaterials*, 2012, **33**, 6593-6603.

100. J. E. Raynor, T. A. Petrie, K. P. Fears, R. A. Latour, A. J. Garcia and D. M. Collard, *Biomacromolecules*, 2009, **10**, 748-755.

101. B. D. Ratner and S. J. Bryant, *Annu. Rev. Biomed. Eng.*, 2004, **6**, 41-75.

102. S. Tugulu and H. A. Klok, *Biomacromolecules*, 2008, **9**, 906-912.

103. X. W. Fan, L. J. Lin and P. B. Messersmith, *Biomacromolecules*, 2006, **7**, 2443-2448.

104. Q. Yu, P. Shivapooja, L. M. Johnson, G. Tizazu, G. J. Leggett and G. P. Lopez, *Nanoscale*, 2013, **5**, 3632-3637.

105. C. J. Weinman, J. A. Finlay, D. Park, M. Y. Paik, S. Krishnan, H. S. Sundaram, M. Dimitriou, K. E. Sohn, M. E. Callow, J. A. Callow, D. L. Handlin, C. L. Willis, E. J. Kramer and C. K. Ober, *Langmuir*, 2009, **25**, 12266-12274.

106. M. A. C. Stuart, W. T. S. Huck, J. Genzer, M. Mueller, C. Ober, M. Stamm, G. B. Sukhorukov, I. Szleifer, V. V. Tsukruk, M. Urban, F. Winnik, S. Zauscher, I. Luzinov and S. Minko, *Nat. Mater.*, 2010, **9**, 101-113.

107. M. E. Welch and C. K. Ober, *J. Polym. Sci., Part B: Polym. Phys.*, 2013, **51**, 1457-1472.

108. L. Moroni, M. K. Gunnewiek and E. M. Benetti, *Acta Biomater.*, 2014, **10**, 2367-2378.

109. S. Tugulu, P. Silacci, N. Stergiopulos and H.-A. Klok, *Biomaterials*, 2007, **28**, 2536-2546.

110. P. M. Mendes, *Chem. Soc. Rev.*, 2008, **37**, 2512-2529.

111. M. Lashkor, F. J. Rawson, A. Stepheson-Brown, J. A. Preece and P. M. Mendes, *Chem. Comm.*, 2014, **50**, 15589-15592.

112. A. D. Celiz, J. G. W. Smith, A. K. Patel, R. Langer, D. G. Anderson, D. A. Barrett, L. E. Young, M. C. Davies, C. Denning and M. R. Alexander, *Biomater. Sci.*, 2014, **2**, 1604-1611.

113. D. G. Anderson, S. Levenberg and R. Langer, *Nat. Biotechnol.*, 2004, **22**, 863-866.

114. Y. Mei, K. Saha, S. R. Bogatyrev, J. Yang, A. L. Hook, Z. I. Kalcioglu, S.-W. Cho, M. Mitalipova, N. Pyzocha, F. Rojas, K. J. Van Vliet, M. C. Davies, M. R. Alexander, R. Langer, R. Jaenisch and D. G. Anderson, *Nat. Mater.*, 2010, **9**, 768-778.

115. Kruss, *Drop Shape Analysis*, Availabe at http://www.kruss.de/products/contact-angle/dsa100/drop-shape-analyzer-dsa100/, Accessed 14/11/14.

116. D. Y. Kwok and A. W. Neumann, *Adv. Colloid Interface Sci.*, 1999, **81**, 167-249.

117. K. Grundke, T. Bogumil, T. Gietzelt, H. J. Jacobasch, D. Y. Kwok and A. W. Neumann, *Prog. Coll. Pol. Sci.*, 1996, **101**, 58-68.

118. H. Fujiwara, Spectroscopic Ellipsometry: Principles and Applications, John Wiley & Sons, New Jersey, 2007.

119. P. van der Heide, X-ray Photoelectron Spectroscopy: An introduction to Principles and Practices, John Wiley & Sons, New Jersey, 2012.

120. M. C. Dixon, *J. Biomol. Tech.*, 2008, **19**, 151-158.

121. C. I. Cheng, Y.-P. Chang and Y.-H. Chu, *Chem. Soc. Rev.*, 2012, **41**, 1947-1971.

122. B. D. Vogt, E. K. Lin, W. L. Wu and C. C. White, *J. Phys. Chem. B*, 2004, **108**, 12685-12690.

123. E. B. Zhulina, O. V. Borisov, V. A. Pryamitsyn and T. M. Birshtein, *Macromolecules*, 1991, **24**, 140-149.

124. G. M. Liu, H. Cheng, L. F. Yan and G. Z. Zhang, *J. Phys. Chem. B*, 2005, **109**, 22603-22607.

125. G. Zhang and C. Wu, *Macromol. Rapid Commun.*, 2009, **30**, 328-335.

126. G. Z. Zhang, *Macromolecules*, 2004, **37**, 6553-6557.

127. C. Wu and S. Q. Zhou, *Macromolecules*, 1995, **28**, 5388-5390.

128. G. Zhang and C. Wu, *Macromol. Rapid Comm.*, 2009, **30**, 328-335.

129. L. S. Penn, H. Huang, M. D. Sindkhedkar, S. E. Rankin, K. Chittenden, R. P. Quirk, R. T. Mathers and Y. Lee, *Macromolecules*, 2002, **35**, 7054-7066.

130. S. Slavin, A. H. Soeriyadi, L. Voorhaar, M. R. Whittaker, C. R. Becer, C. Boyer, T. P. Davis and D. M. Haddleton, *Soft Matter*, 2012, **8**, 118-128.

131. S. Slavin and D. M. Haddleton, *Soft Matter*, 2012, **8**, 10388-10393.

132. Y. Gou, S. Slavin, J. Geng, L. Voorhaar, D. M. Haddleton and C. R. Becer, *Acs Macro Lett.*, 2012, **1**, 180-183.

133. S. N. S. Alconcel, A. S. Baas and H. D. Maynard, *Polym. Chem.*, 2011, **2**, 1442-1448.

134. M. A. Cooperstein and H. E. Canavan, *Biointerphases*, 2013, **8,** 19-31.

135. J. F. Lutz and A. Hoth, *Macromolecules*, 2006, **39**, 893-896.

Chapter Two

2. Thiol–ene Immobilisation of Carbohydrates onto Glass and Silicon Surfaces

2.1. Chapter Summary

This chapter investigates techniques for the scalable and efficient immobilisation of carbohydrates onto glass and silicon substrates, as a stepping-stone towards the immobilisation of polymers onto these surfaces for the microarray applications. It was found that, although initially successful at changing the surface hydrophobicity, acryloyl chloride functionalisation is irreproducible and does not allow for detailed surface analysis. Silane functionalisation, however, has proved successful and reproducible and the acrylated silanes have been shown to give more even surface coatings. This work has developed new and versatile methodologies to functionalise both glass and silicon substrates with carbohydrates, using "click"-type reactions. The methodologies used within this work present an orthogonal handle, to enable the introduction of ligands of interest. The use of glass and silicon surfaces has allowed a variety of characterisation techniques (drop shape analysis, ellipsometry, X-ray photoelectron spectroscopy and fluorescent binding assays) to be used in order to show the successful functionalisation of the surfaces. Self-assembled monolayers on gold have been widely used for these microarray applications, to study the bimolecular interactions and create diagnostic devices, however gold is very expensive and analytical techniques are primarily limited to surface plasmon resonance. The use of glass slides for the same purpose provides a far more cost

effective solution and significantly increases the analytical options available. Aspects of this work have been published in Biomaterials Science.[1]

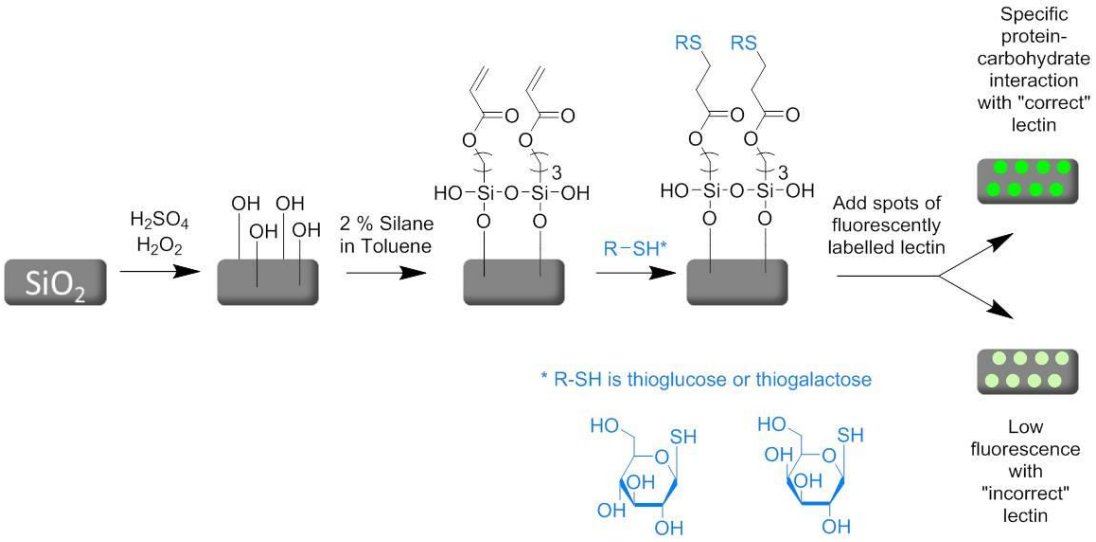

Figure 2.1: The ability to easily functionalise glass surfaces, rather than the more expensive and analytically challenging gold alternative, can provide a route towards improved microarray applications. The presence of the alkene end group in step three provides the orthogonal handle, to enable the introduction of ligands of interest, in this case thiolated sugars

2.2. Introduction

Due to a combination of the global decrease in the discovery of new antibiotics and the increase in antibiotic resistance,[2] the need for novel technologies to investigate bacterial infection and allow rapid diagnoses are more important than ever. Prior to the occurrence of infection, bacteria typically require adhesion onto the host cells, a process involving protein-carbohydrate interactions.[3] These adhesions can also be used to detect the bacteria and provide structural information on their adhesion proteins and carbohydrate specificities.[4] The presentation of carbohydrates in a microarray format, immobilised on a solid substrate, can provide an efficient way to probe the binding characteristics of the carbohydrates of interest. The microarray can be used to monitor multiple binding events between a variety of immobilised carbohydrates and their corresponding lectins. This is of particular

interest as the functions of carbohydrates within biological process have not yet been fully studied, despite the fact that more than 50% of proteins carry carbohydrate chains.[5] These protein-carbohydrate interactions are key to a large variety of cellular processes, including cellular recognition, adhesion and signalling.

Carbohydrate microarrays have been fabricated on a variety of solid supports, utilising a variety of immobilisation methods and surface analysis techniques, Figure 2.2. These immobilisation methods are broadly categorised into covalent and non-covalent and then further divided into site specific and site non-specific.[6] Options for the underlying substrate include gold, onto which self-assembled monolayers of alkenethiols have been reported, and glass, which is typically amino or epoxide functionalised.[7] Carbohydrate attachment techniques which are compatible with a variety of surfaces are highly desirable as they can allow more extensive characterisation techniques to be utilised and increase the applications for the resulting microarrays. We therefore rationalised that thiol-ene type chemistries would be the ideal method to install carbohydrates onto array-type surfaces, as thiolylated carbohydrates are readily accessible and orthogonal to most functional groups (amines, sulfates, phosphates, alcohols).The development of a facile synthetic route towards presenting carbohydrates on cheap and readily available glass surfaces is an attractive prospect for developing routes towards new diagnostic techniques and the investigation of carbohydrate binding and behaviour.

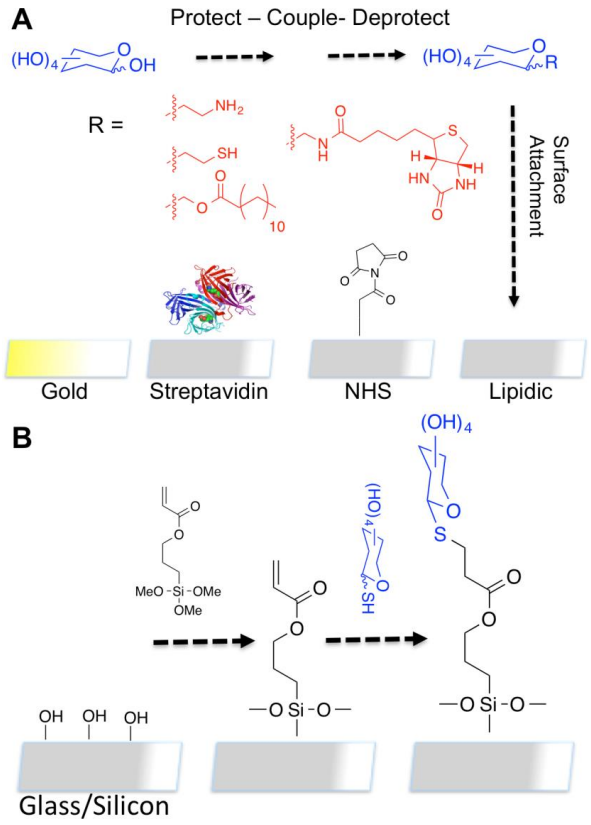

Figure 2.2: [A] Summary of some current technologies requiring specific surfaces and linkers: self-assembly of thiols onto gold, streptavidin coatings with biotinylated carbohydrates, *N*-Hydroxysuccinimide coatings and lipid coatimgs; [B] Proposed thiol-ene route using acrylate glass/silicon as template surface for forming covalently tethered monolayers

2.3. Results and Discussion

2.3.1. Glass and Silicon Surfaces

Glass slides are desirable and versatile surfaces for covalent carbohydrate immobilisation due to their availability, low cost and compatibility with most array scanners. However, these slides (in this work we have used microscope slides) and silicon wafers are not suitable for functionalisation in their natural state because they are not intrinsically reactive towards thiols, our desired bio-orthogonal group to introduce carbohydrates. In order to remove contaminants and create a hydroxyl-functionalised surface for further modification, the slides and wafers can be cleaned

with piranha solution, Figure 2.3. The procedure involves submersion of the slides in a chilled 3:1 H_2SO_4: H_2O_2 solution for 20 minutes, washing with Milli-Q water and drying under a stream of nitrogen.[8] Care was taken with the piranha solution due to its strongly oxidising and corrosive nature.

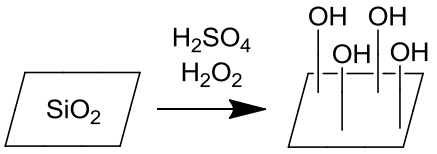

Figure 2.3: Cleaning of glass slides with piranha solution (3:1 H_2SO_4: H_2O_2)

2.3.2. Functionalisation with Acryloyl Chloride

Previously, acryloyl chloride has been shown to functionalise amine coated glass slides,[9] however, we desired a simpler approach, which did not rely on an amine coated glass starting substrate. Following cleaning, the slides were functionalised with neat acryloyl chloride (Figure 2.4) by submerging into the acryloyl chloride solution for three hours. It was found that washing with water or methanol was insufficient to remove the sticky residue. Sonication in chloroform, followed by rinsing with Milli-Q water and drying with a stream of nitrogen was found to be a successful washing technique, yielding apparently homogenous surfaces, as determined by drop shape analysis (DSA).

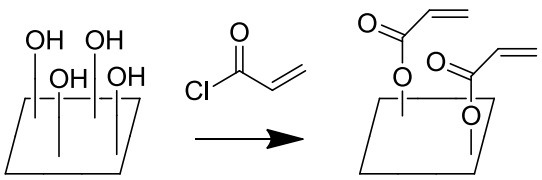

Figure 2.4: Functionalisation of cleaned glass surfaces with acryloyl chloride

Having functionalised the glass and silicon slides with acryloyl chloride, the surfaces could now be further modified using base catalysed thiol-ene "click" type reactions,[10] Figure 2.5, with the proposed mechanism shown in Figure 2.6. Initially two thiol-containing reagents (Table 2.1) were chosen in order to create a hydrophilic and hydrophobic surface, so that the functionalisation could be easily confirmed using DSA. The surfaces were submerged into neat solutions of the appropriate thiol and then washed with ethanol and Milli-Q water.

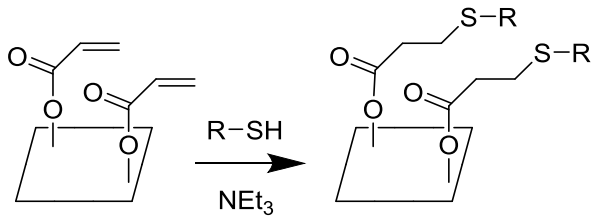

Figure 2.5: Thiol-ene functionalisation of the acrylated glass surfaces

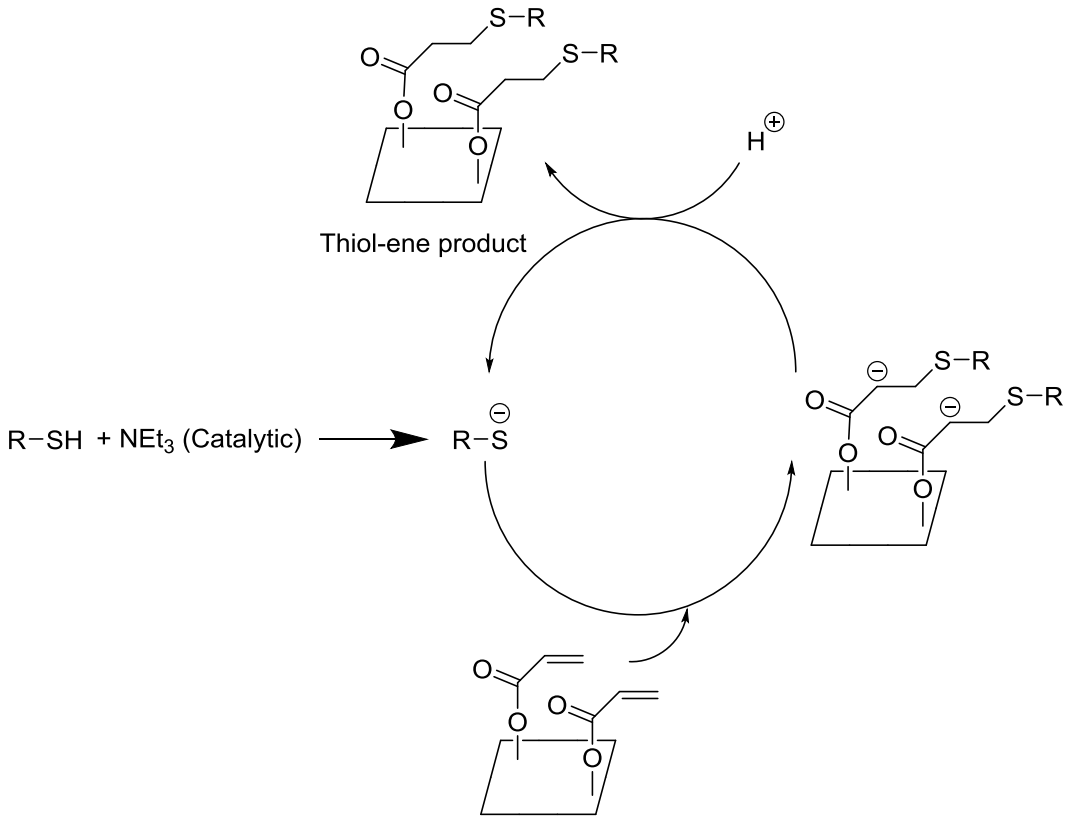

Figure 2.6: Proposed mechanism of base catalysed thiol-ene "click" reaction on the acrylate coated glass[11]

Table 2.1: Reagents for the functionalisation of the acrylate coated glass slides

Thioglycerol	Dodecanethiol
Relatively hydrophilic	Relatively hydrophobic
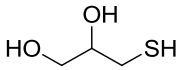	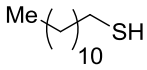

Contact angle measurements, taken using a drop shape analyser, can be used to observe the changes in the hydrophobicity of a surface as it is functionalised and therefore determine if the surface functionalisation has been successful. The changes in surface hydrophobicity for the three stages of surface functionalisation (cleaned glass to acryloyl chloride to thiol containing molecule of interest) are summarised in Figure 2.7. Cleaned glass exhibits a very low contact angle and acryloyl chloride surfaces coated with thioglycerol and dodecanethiol exhibit hydrophilic and hydrophobic characteristics respectively, as determined by contact angle measurements, as would be expected. Dodecanethiol and thioglycerol were also added to cleaned glass slides, without the acryloyl chloride functionalisation step, to see if significant functionalisation by non-specific adsorption was occurring. The results of this control experiment suggest that this is not the case. The contact angle increases for these two samples when compared to the cleaned glass, but the values are not similar to those observed for the acryloyl chloride *and* thiol functionalised samples and the values are within error of each other. It is likely that the increase in value is due to contamination of the chemically cleaned glass surfaces by submerging them in the thiol solutions and the subsequent washing procedure, along with small amounts of non-specific adsorption. This surface functionalisation process was then repeated using a silicon wafer as the substrate, with a summary of the results illustrated in Figure 2.8. The contact angles obtained for the thioglycerol

coating (39.0°) correspond well with literature data for the thiol-yne coupling of thioglycerol onto a silicon surface (38°).[12] Although initially promising, this functionalisation technique was poorly reproducible, particularly in the case of the silicon surfaces, and further surface analysis using infrared (IR) and X-ray photoelectron spectroscopy (XPS) proved unsuccessful.

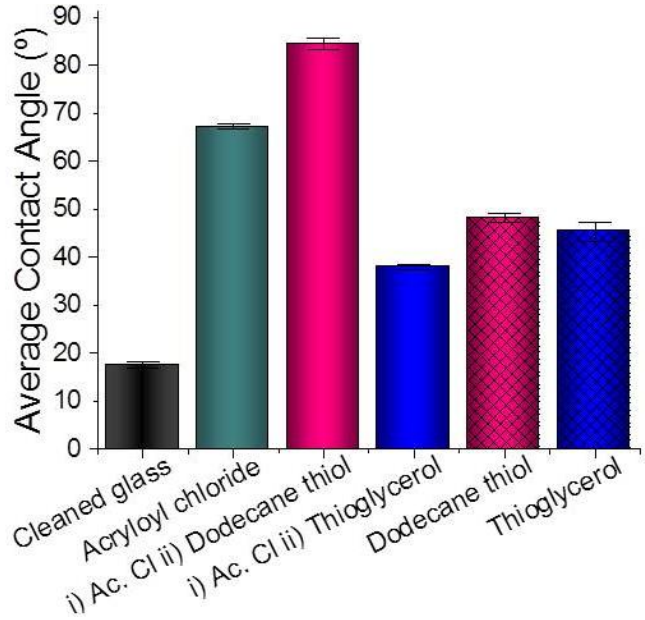

Figure 2.7: Water contact angle for the functionalised glass surfaces, shown with the standard deviation taken from a minimum of three independent measurements

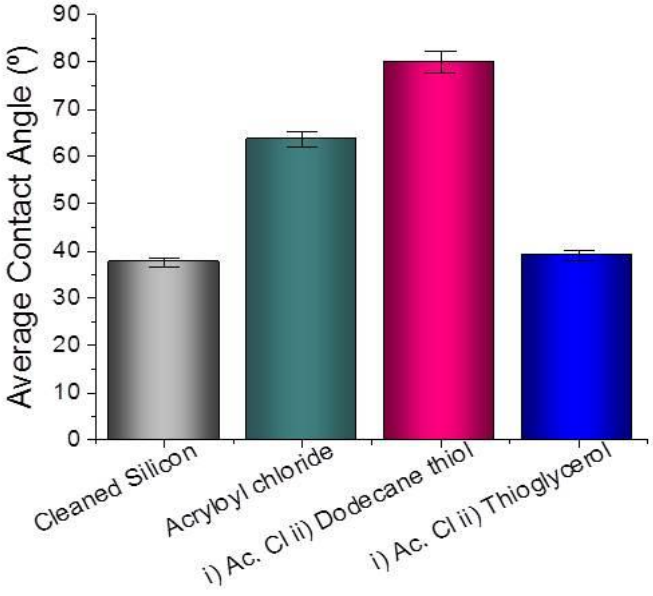

Figure 2.8: Water contact angle for the functionalised silicon surfaces, shown with the standard deviation taken from a minimum of three independent measurements

2.3.3. Functionalisation with Silanes

2.3.3.1. Solution Phase Silanisation

Due to the reproducibility problems that were encountered with the acryloyl chloride based coatings, an alternative functionalisation technique was sought. Silanisation was chosen, due to its proven success and prevalence in the literature.[13, 14] Additionally the desired linking functional group, the alkene, could still be accessible. The silanisation process involves covering a surface in a self-assembled layer of organo-functional alkoxysilane molecules. It is typically carried out on hydroxyl group containing surfaces such as cleaned glass and metal oxides and is therefore suited to the requirements of this work. The piranha cleaning method continued to be utilised and both glass and silicon surfaces could still be employed.

Many silanes are commercially available and examples that would allow further reaction with a thiol containing species was chosen; one acrylate functionalised and the other epoxy functionalised,[15] Table 2.2. The silanisation process, carried out by submerging the cleaned surfaces in a 2% silane solution in toluene, therefore generated a similar alkene-functionalised surface to that obtained using the acryolyl chloride method, Figure 2.9. It was found that the acrylated silane showed more even and reproducible surface modification and a better reactivity to the subsequent thiols and was therefore used for the remaining functionalisations. The optimum functionalisation time was found to be two hours, giving full modification without the sticky layer build-up. As with the acryloyl chloride functionalised surfaces dodecanethiol and thioglycerol were added to the surfaces in order to monitor the functionalisation by contact angle measurements. In addition to these two hydrophobic and hydrophilic control surfaces, thioglucose and thiogalactose were also added, as these surfaces are more relevant for the microarray

applications and can then be used for the later protein binding experiments in order to probe protein-carbohydrate binding events.

Table 2.2: Silanes chosen for surface modification

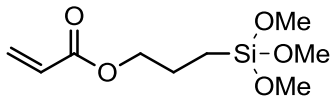	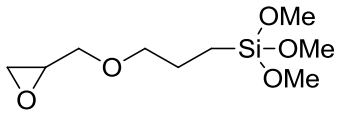
3-(trimethyoxysilyl)propyl acrylate	(3-glycidyloxypropyl)trimethoxysilane

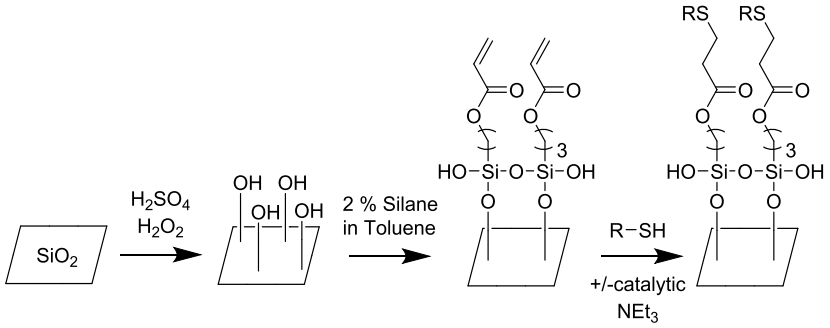

Figure 2.9: Surface functionalisation using silanes, shown using the 3-(trimethyoxysilyl)propyl acrylate as an example

The contact angles were recorded (Figure 2.10) and found to be reproducible, indicating that this is a suitable method. As expected, the thioglycerol modified surfaces are the most hydrophilic, with the dodecanethiol being hydrophobic. The contact angles correlate well with literature values. For example the cleaned glass (18°) is in agreement with stated values for chemically cleaned glass[16] and the silane coating (47°) is within the range of similarly hydrophilic systems studied by Dehaen *et al.*[17] The sugar (glucose and galactose) coated surfaces were found to have quite high contact angles, but this data was reproducible. This may indicate an incomplete coverage of monosaccharides onto the surfaces, which should not affect their application at this stage. No specific literature values could be found for comparison to the dodecane thiol and thioglycerol surfaces. However, contact angles of specific

surface functionalities are very susceptible to the linker molecule between the surface and the thiol-containing species. For example, values for the thiol-yne addition of thioglycerol onto silicon surfaces have been reported to vary between 38 degrees[12] and 58 degrees[18], depending on the method of linking the thioglycerol to the surface, making comparison between unlike systems unadvisable.

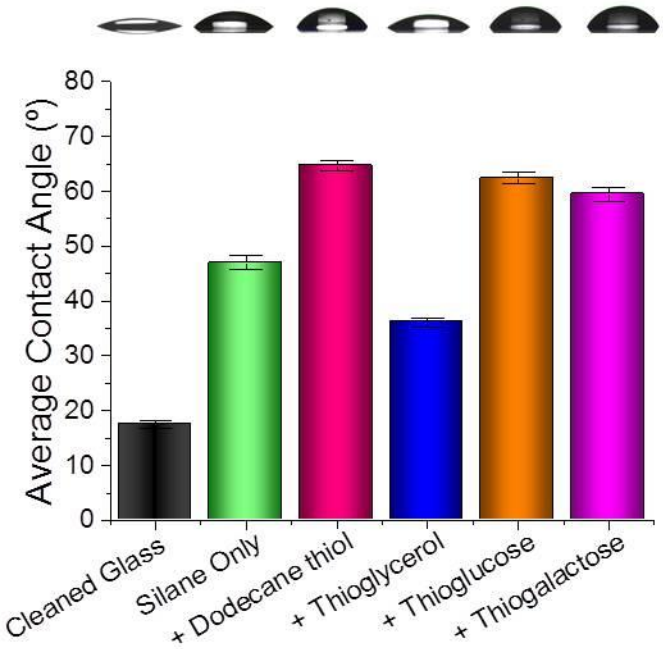

Figure 2.10: Water drop contact angles for the silane functionalised glass surfaces with the corresponding DSA images and the standard deviation taken from a minimum of three independent measurements. Each surface has undergone silane functionalisation and the "surface coating" refers to the layer which is bonded to the silane coated glass surface

The silane functionalisation process was also successfully carried out on the silicon wafer surfaces. The effect of adding ethanolamine to catalyse the addition of the thiol groups[14] onto the alkene support was also investigated, by adding the thiolated sugars to the surfaces in the absence of the amine as well as in its presence. The results, as illustrated in Figure 2.11 show the same trend as those for the glass surface (Figure 2.10) and indicate that the presence/absence of the amine has little effect on the resulting surface functionality. However, when obtaining the DSA data,

it was found that the baselines were calculated, by the software, much more easily for the samples which had been functionalised in the presence of amine, suggesting that it may increase the surface smoothness slightly.

The contact angles for the glass and silicon surfaces containing the same functionalilty are seen to be slightly different. For example, cleaned silicon produces contact angles of 27° whereas glass is much lower at (18°). When the silane layer is added the silicon surfaces exhibit angles of 75° whereas a much lower value of 48° is observed on glass. This is seen in previous literature and can be attributed to differences in surface energies and smoothness. For example, Wheeler *et al.* found that (3-glycidyloxypropyl)trimethoxysilane coatings on silicon produced angles of 44° compared to only 30° for the same system on a glass substrate.[15]

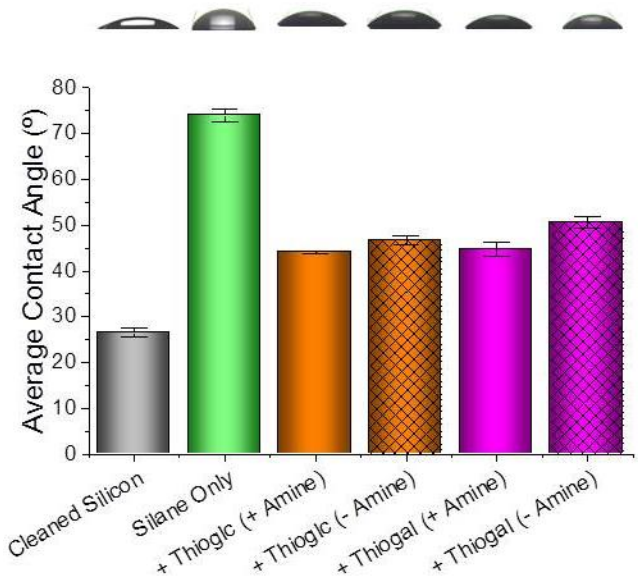

Figure 2.11: Water contact angle measurements for the silane functionalised silicon surfaces, shown with the standard deviation taken from a minimum of three independent measurements. Each surface has undergone silane functionalisation and the "surface coating" refers to the layer which is bonded to the silane coated silicon surface. Although the angles differ between this and the corresponding glass surface graph (Figure 2.10), due to different underlying surfaces and potential differences in the degree of coverage, the trends are the same for both

2.3.3.2. Optimising the Silanisation

Work towards optimising the silanisation process has found that sonication, for cleaning purposes, at any stage should be avoided as it can disrupt the silane crosslinking and result in detachment of the bound layer. Rinsing the silanised samples with toluene is sufficient to remove any unbound silane. The final washing step should always be carried out using water, regardless of the solvent used in the previous steps, in order to remove the water droplets from the surface and therefore prevent evaporation from the surfaces. No difference, as measured by ellipsometry and DSA, was observed in silane layer thickness if cured in the vacuum oven overnight prior to measuring. An indication of stability, measured by recording contact angle and ellipsometry measurements immediately after production of the sample and again at 1, 2 and 3 month time points, also produced no difference between the cured and uncured samples.

2.3.3.3. UV/Ozone Cleaning and Vapour Phase Silanisation

As an alternative to piranha solution cleaning, UV/Ozone cleaning can be used to remove organic contaminants from the surfaces and improve the surface wettability,[19] on both glass[20] and silicon surfaces.[21] The cleaning process introduces bound hydroxyl groups (and other reactive oxygen containing species) onto the surface, which are required for the further surface modification.[17] It was proposed that the acidic conditions used in piranha cleaning could result in protonated hydroxyl groups on the surface and this could be hindering the silane attachment, whereas UV/Ozone generates deprotonated hydroxyl groups, which may react better with the silanes (Figure 2.12). Additionally, this process can be carried out on polystyrene[22] or poly(ethylene terephthalate)[23] surfaces, without causing chemical degradation. This ability to apply the cleaning process to plastic surfaces opens up

new surface options, which would otherwise not have been possible as plastics are incompatible with the piranha cleaning.

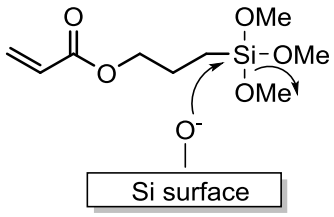

Figure 2.12: Deprotonated hydroxyl groups on the silicon surface may aid silane bonding

The use of UV/Ozone cleaning, in place of the piranha cleaning, had no effect on the resulting silanisation, when analysed by DSA and ellipsometry. Additionally, using the two methods in tandem (piranha clean then UV/Ozone clean) also produced no differences in surface thickness or uniformity. The data in Figure 2.13 shows the contact and resulting silane thickness (from ellipsometry, Section 2.3.4) for silicon surfaces that had been subjected to three different cleaning processes. The silicon wafers were cleaned with either piranha solution, five minutes UV/Ozone or 10 minutes UV/Ozone and then all placed into the same desiccator for silanisation. There are no significant differences between the three treatments and the error between the three repeats for each is very similar, indicating comparable uniformity, therefore it was concluded that the UV/Ozone procedure is not necessary. The UV/Ozone cleaning has the advantage of not requiring the very exothermic and corrosive piranha solution, but it does require the use of a UV/Ozone cleaner. Therefore, as the piranha cleaning proved sufficient and allowed the next functionalisation step to be carried out without moving the samples, this cleaning method has been used throughout the rest of this work.

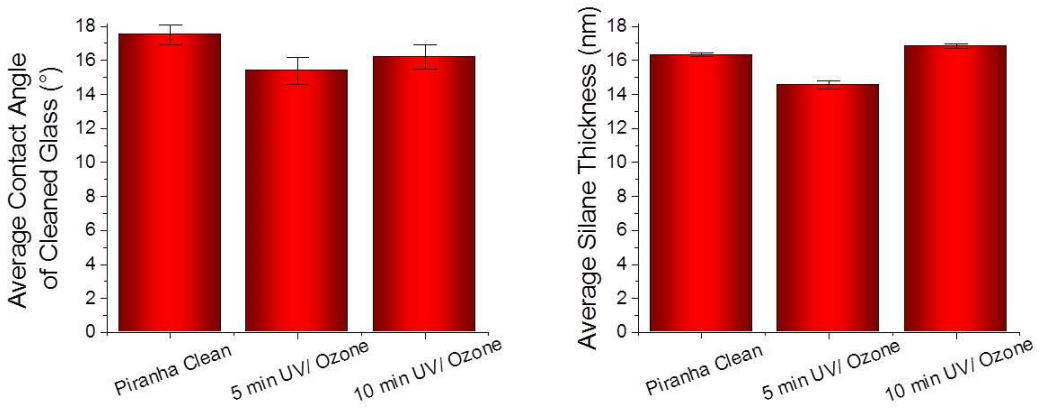

Figure 2.13: Contact angle data for cleaned glass and ellipsometry data for the resulting silane layer thickness for silicon surfaces, which had been subjected to different cleaning procedures. The error bars represent the standard deviation taken from a minimum of three independent measurements

Following this process the sample can be silanated using the solution phase method (Section 2.3.3.1.) or by vapour phase silanisation. The vapour phase process involves placing the cleaned sample into a desiccator with a few drops of the silane and leaving it at reduced pressure to allow the vaporised silane to bond to the surface. When initially trialled in the standard lab desiccator, it was found that the pressure could not be reduced and then subsequently held at this reduced pressure sufficiently. After 1 hour no silane layer was observed by ellipsometry (see Section 2.3.4), after two, three and 24 hours a silane build up was observed only around the perimeter of the wafers. The thickness of this layer ranged from 2.5 to 6.5 nm as determined by ellipsometry measurements. Due to the incompleteness of the silane coverage, this method was concluded to be inferior to the solution phase silanisation process, which was more suitable for our needs.

2.3.4. Surface Analysis by Ellipsometry

Ellipsometry has been used on the silicon surfaces to compliment the contact angle measurements and provide further confirmation of successful functionalisation. Angle of incidence variation, four-zone scans were used in order to obtain more data and allow more accurate calculations of the layer thicknesses. The values of psi and delta, which represent the raw measurement obtained from the change in polarization that occurs when the measurement beam interacts with a sample surface, were obtained. Using the WVase software,[24] it is possible to input these measured values (Ψ and Δ), alongside the wavelength of the incident light, into the software algorithms in order to produce a model that describes the interaction of light with the sample and therefore calculate the thickness, error and confidence interval for the layer in question.

The results can then be compared to the DSA data obtained for the glass and silicon surfaces. When calculating the thickness, firstly the silicon dioxide layer must be calculated from cleaned, unfunctionalised silicon wafer. The wafer can then be silanated and reanalysed in the same spot, giving the thickness of the silane layer, as the refractive indices of the oxide and silane layers are suitably different. Functionalised with the solution of interest, in this section that is the thiolated sugars, can then occur and a further ellipsometry measurement can be taken, again in the same spot. The thickness of the sugar layer can then be calculated by subtracting the previously obtained silane thickness from the value obtained for the whole organic layer.

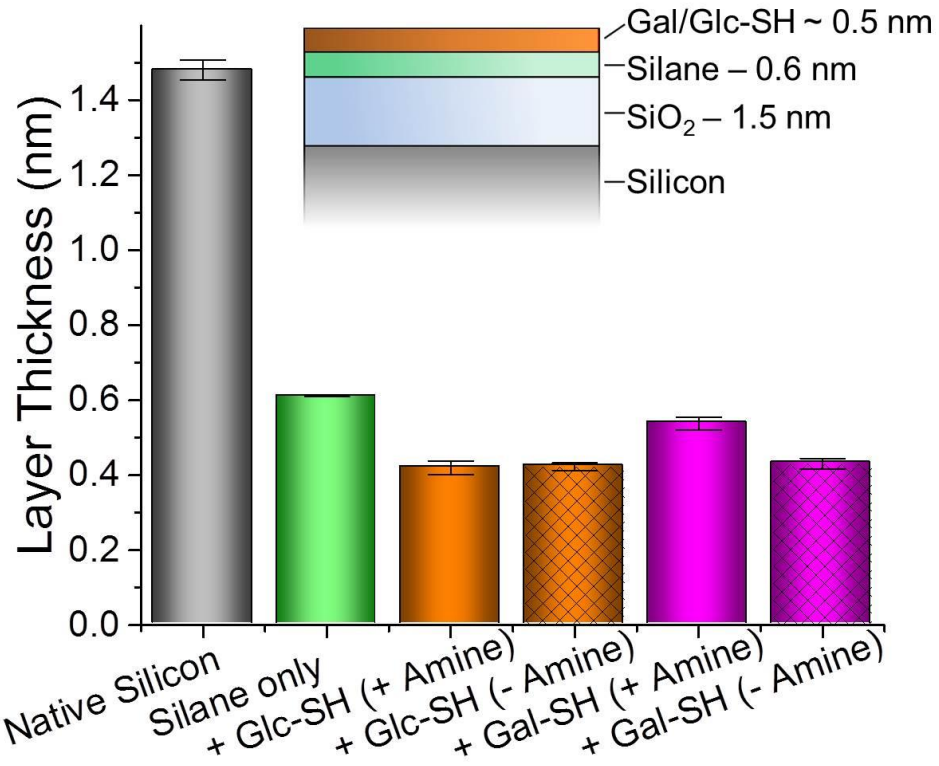

Figure 2.14: Ellipsometry data, giving the thickness of each layer for the silanated and then subsequently thio-sugar functionalised surfaces. The error bars represent the standard deviation taken from a minimum of three independent measurements

Ellipsometry data for vapour phase silanisation of the surfaces has already been depicted in Figure 2.13. For the vapour phase technique (Section 2.3.3.3.) the silane layer thickness, was around 15 nm. The ellipsometry data for the solution silanisation (Section 2.3.3.1.) is presented in Figure 2.14. It can be observed that the average oxide layer present on the cleaned silicon surface is 1.5 nm. The addition of the silane and the subsequent thiol-sugars in the presence and absence of amine show only small increases in thickness, this confirms that on the addition of sugars in proceeding in a thin layer, rather than as thick deposits caused by non-specific adhesion. No significant difference is observed between the samples thiolated in the presence of the amine compared to those in its absence, this corresponds to the findings from the DSA measurements in Section 2.3.3.1.

2.3.5. Surface Analysis by XPS

The surface analytical techniques employed thus far, DSA and ellipsometry, provide valuable data about the hydrophobicity/hydrophilicity of the surface and thickness of the organic layer; however they cannot give any detailed information about the functional groups present at the surface. For this reason XPS experiments were carried out to further confirm the surfaces had been successfully functionalised. The elemental analysis results are shown in Table 2.3. The values for the nitrogen content show a slight increase for the samples that had been functionalised in the presence of the amine, compared to those without any amine. However, the nitrogen percentages are still below the values calculated for the cleaned silicon sample, indicating that there is not a large build-up of bound ethanolamine in the surfaces. Additional XPS scans are available in Appendix One.

Table 2.3: XPS data showing the elemental analysis for silicon, silane, thioglucose and thiogalactose surfaces

Sample	C/ %	O /%	Si/ %	N/ %	Na/ %
Clean Silicon	12.7	27.4	59.3	0.7	0.0
Silane only	11.9	27.3	60.4	0.4	0.0
Thioglucose + amine	12.4	26.5	60.4	0.6	0.1
Thioglucose - amine	10.8	26.9	62.1	0.2	0.1
Thiogalactose + amine	14.8	26.7	57.7	0.7	0.1
Thiogalactose - amine	11.2	27.9	60.4	0.5	0.1

Key results to note from the XPS scans were the presence of peaks with binding energy corresponding to carbonyl groups present in the silanated surface, with an increase in the intensity of the CO peak and decrease in the carbonyl peak for the sugar coated surfaces, due to the silane groups now

being below the sugar and therefore less accessible. The data for the C-OH peak of the C 1s can be seen in Table 2.4. The peak is strong in the cleaned silicon, due to the hydroxyl functionalised surface; it is lower for the silane surface, as would be expected. The peak is then higher again for the carbohydrates due to the hydroxyl groups present on the glucose/galactose molecules. The presence of the amine is seen to increase the carbohydrate binding and galactose is consistently seen to bind more prolifically than glucose. These values are quoted as a percentage of the total elemental compositions, and thus it follows that in cleaned Si, although a value of 37.6% is obtained for the C 1s C-OH region, this is a much less significant value than for the functionalised surfaces, where the signals are more abundant.

Table 2.4: XPS Binding energies for the C-OH peak of the C 1s

Sample coating	**C 1s C-OH**	
Cleaned Si	287.19	37.6%
Silane only	287.09	22.0%
Glc-SH + amine	287.03	23.0%
Glc-SH - amine	286.83	22.2%
Gal-SH + amine	287.00	34.5%
Gal-SH - amine	287.07	24.1%

Figure 2.15 shows the carbon: silicon ratio upon addition of the thiols/amines. The clear increase in the relative carbon concentration following the addition of the glycosyl-thiols is indicative of successful thiol-ene coupling. Since the total layer thickness increases after coupling, as confirmed by ellipsometry, the limited penetration depth of XPS (typically 5-10 nm) results in less of the underlying

silicon being detected. For both Gal-SH and Glc-SH there was a significant increase in the carbon:silicon ratio upon addition of the amine catalyst. This is in contrast to the results of contact angle and ellipsometry that could not resolve these differences in grafting density. A representative C 1s region of the spectra for Gal-SH is shown in Figure 4B to demonstrate that the increased carbon signal is attributable to functionality consistent with a carbohydrate being present (e.g. C-C, C-O).[25] This analysis demonstrates the need for both molecular and surface property measurements for new array surfaces, otherwise the role of added amine would not have been elucidated from contact-angle/ellipsometry measurements alone.

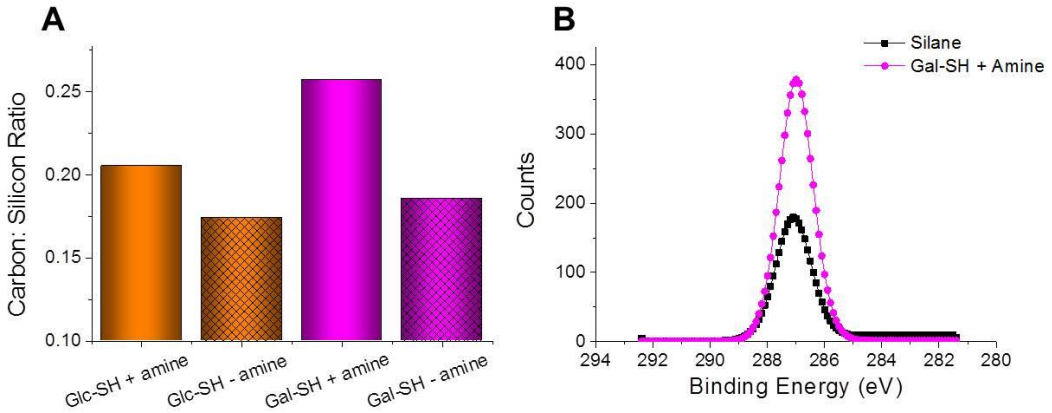

Figure 2.15: X-ray photoelectron spectroscopy analysis of carbohydrate functionalised surfaces; [A] Change in carbon:silicon ratio upon addition of different sugars; [B] Representative high-resolution XPS spectrum of C 1s region before and after addition of thiogalactose with amine catalyst

2.3.6. Lectin Binding Studies

In order for the surfaces to be utilised for microarray applications, they must be compatible with lectin binding interaction studies. A series of surfaces were prepared bearing either silane alone or Gal-SH/Glc-SH. Two fluorescently labelled lectins were chosen to investigate: Con A (exhibits some glucose binding specificity) and PNA (exhibits some galactose binding specificity). Initially the binding of PNA and Con A onto surfaces functionalised with glucose and galactose was investigated. It was found (Figure 2.16 and 2.17) that the PNA bound more strongly to the galactose surface and the Con A to the glucose surface, as indicated by the brighter fluorescent spot on the slide. This is to be expected due to the sugar binding specificities of the two lectins. As a control, both lectins were also added to just a silanated surface, with no carbohydrates present to interact with, and the binding for both lectins was observed to be very similar.

As mentioned in the introduction, carbohydrate-lectin interactions tend to be non-specific, and are better described as being preferential. Multivalent presentation has also been reported to affect specificity, which must be considered when applying arrays[26] along with considerations of the relative fluorescent labelling density of different proteins in comparative glycomics. Hence, there was still some binding of each lectin to their non-native carbohydrate target. Quantitative evaluation was obtained by analysing the images using Agilent Feature Extraction Software. The average fluorescent intensity was calculated for the sample area of interest (the lectin spot) by taking the average output value for the green channel for that set area. The background fluorescence (the average output value for the green channel for all of the areas of the sample without a lectin spot or pen mark) was calculated and manually subtracted from each value. The quantitative data is shown in Figure 2.16.

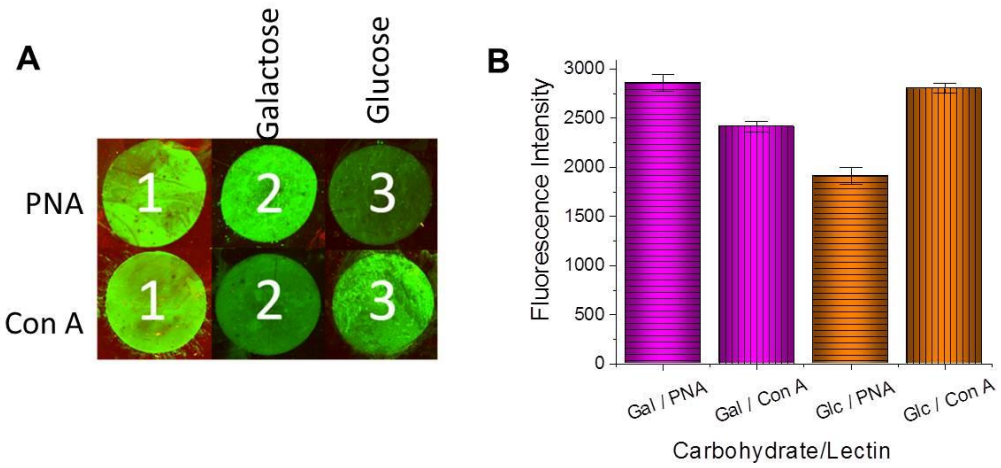

Figure 2.16: Lectin binding onto functionalised surfaces using 0.1 mg.mL^{-1} of FITC-lectin. [A] Collated array-scanner fluorescence micrographs (green/red channels); [B] Quantitative analysis of total green fluorescence (excitation 480 nm, emission 520 nm). (Error bars show standard deviation from minimum of 3 independent measurements)

A commonly employed array format is based on the SP8 linker ($(CH_2)_3NH_2$), which is used to immobilise amino sugars onto NHS-functional surfaces.[27] Figure 2.17 shows a comparison of our linkage method relative to SP8 linked carbohydrates, presenting a similar alkyl chain length (which is required to ensure the lectin can access the carbohydrate on the surface) and hence should enable comparisons to be made in the future between these surfaces, and those already used elsewhere.

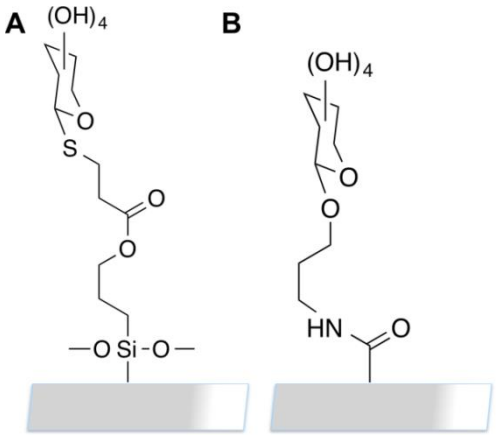

Figure 2.17: Comparison of [A] thiol-ene immobilisation verses [B] NHS/SP8 immobilisation.

2.3.7. Microtitre Plates

The microtitre plates, also referred to as microplates, used in this work are flat polystyrene plates containing 96 wells. Each well can be differently functionalised, incubated with a fluorescent-labelled protein, washed and then analysed in the microplate reader in order to detect the fluorescence intensity and therefore the extent of protein bound in each well. This provides a convenient way of obtaining large quantities of protein binding information quickly. Microplate studies form the basis of most high throughput screening platforms,[22] so the ability to use our methods on these platforms, along with the glass, silicon and gold surfaces, can allow any new technologies that we develop to have many more applications. As the plates are typically only subjected to aqueous solutions, suitable conditions for the acrylate functionalisation of the wells needed to be found. The reaction conditions were initially tested on standard uncoated plates, as these are much less expensive. Conditions and their outcomes are detailed in Table 2.5. It is important to note that the wells becoming inconsistently opaque will cause inconsistent fluorescent readings when used with the microplate reader and is therefore an unacceptable outcome. Also, it must be stressed that the solvent additions were carried out in very small volumes, with drop wise addition, in order to prevent excess exothermic reactions, particularly in the case of the acryloyl chloride: DMSO mixture. Increased proportions of DMSO in the acryloyl chloride: DMSO mixture were not investigated due to the potential for highly exothermic or explosive reactions.

Table 2.5: Microplate reagent compatibility testing reaction conditions and observations

Reaction Conditions	Observations and Results
Acryloyl chloride	Plate damaged in < 5 minutes
80:20 acryloyl chloride: DMSO	Plate damaged in < 10 minutes
Methacrylic anhydride	Plate turned opaque after 2 hours. Softened upon washing with water
Pyridine	No effect after 18 hours
75:25 methacrylic acid: pyridine	Plate turned opaque after 2 hours. Softened upon washing with water
75:25 methacrylic acid: pyridine. Isopropanol wash	Plate turned opaque after 2 hours. Softened upon washing with isopropanol
75:25 methacrylic acid: pyridine. Methanol wash	Plates incompatible with methanol
75:25 methacrylic acid: pyridine. Ethanol wash	Plates incompatible with ethanol

The acrylate functionalisation attempts were concluded to be unsuccessful, so a new method was trialled. It was proposed that as solid phase peptide synthesis is often carried out on polystyrene beads,[28] the techniques should be fully compatible with polystyrene plates. SPPS is typically carried out in DMF; however this is incompatible with the plates, so DMSO was trialled instead (again, this was carried out on the cheaper unfunctionalised plates, initially) and no compatibility issues were found with the reagents. The amine coated microplate could then be acrylated (Figure 2.18) ready for further modification with the thiols, to mimic the glass and silicon functionalisation.

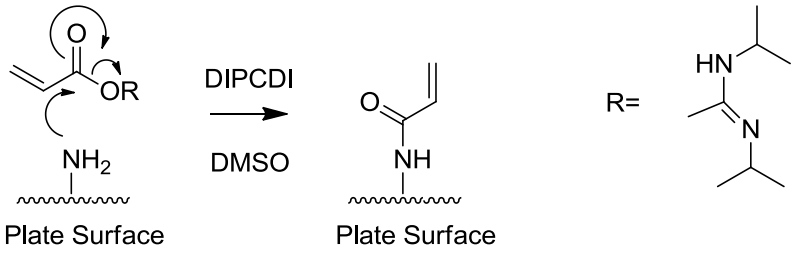

Figure 2.18: SPPS protocol to functionalise the amine-coated microplate surfaces

In order to test the surface functionalisation a variety of reagents were added to the wells of the amine coated plate, Table 2.6. TCEP was added to one of the thioglucose samples, as a phosphine catalyst, to see if it would improve the ability of the thiol to bond to the acrylic acid.[29] The third reagent for each well was fluorescently labelled Con A. This was added in equal quantities to each well, left in the dark for 30 minutes and then the excess lectin was removed by pipette. The plates were washed and allowed to dry, then tested in the microplate reader. The microplate reader records the fluorescence for each well in the plate and a higher reading indicates more fluorescent Con A remaining and therefore a greater extent of protein binding in that well.

Table 2.6: Functionalisation conditions for each of the amine coated microplates

First Reagent Added	Second Reagent Added	Third Reagent Added
Acrylic Acid	Thioglycerol (neat)	Fluorescent Con A (0.1 $mg.mL^{-1}$ in HEPES)
Acrylic Acid	Dodecanethiol (neat)	Fluorescent Con A (0.1 $mg.mL^{-1}$ in HEPES)
Acrylic Acid	Thioglucose (2 $mg.mL^{-1}$ in PBS)	Fluorescent Con A (0.1 $mg.mL^{-1}$ in HEPES)
Acrylic Acid	Thioglucose (2 $mg.mL^{-1}$ in PBS) + TCEP	Fluorescent Con A (0.1 $mg.mL^{-1}$ in HEPES)
Acrylic Acid	None	Fluorescent Con A (0.1 $mg.mL^{-1}$ in HEPES)

The results from the microplate reader are shown in Figure 2.19 and the plates were made in triplicate, with all of the repeat data shown. The values plotted are the average fluorescence reading for the 12 wells in that sample, with their corresponding standard deviation. As you can see the dodecanethiol results appear anomalous and unexpected. It was found that dodecanethiol caused discolouration of the plates and will therefore have disrupted the fluorescence measurement, so the data for these wells must be discounted. Within the remaining results, it is interesting to note that the presence of the amine with the thioglucose reduces the binding, but also increases the reproducibility. The Con A would be expected to bind to the thioglucose, as previously explained, however, without the presence of the TCEP the data is very unreproducible. The presence of the TCEP appears to help with the binding, which corresponds to the results found for adding amine to the thiolated sugars when reacting them with the functionalised glass and silicon surfaces. The thioglycerol surface results show fluorescence values that are much higher than expected, as thioglycerol is relatively hydrophilic it should have a relatively high

ability to resist non-specific protein adsorption.[30] Overall, the standard deviation between the wells within one sample and the discrepancies between the repeat data mean that this area of investigation was not pursued further.

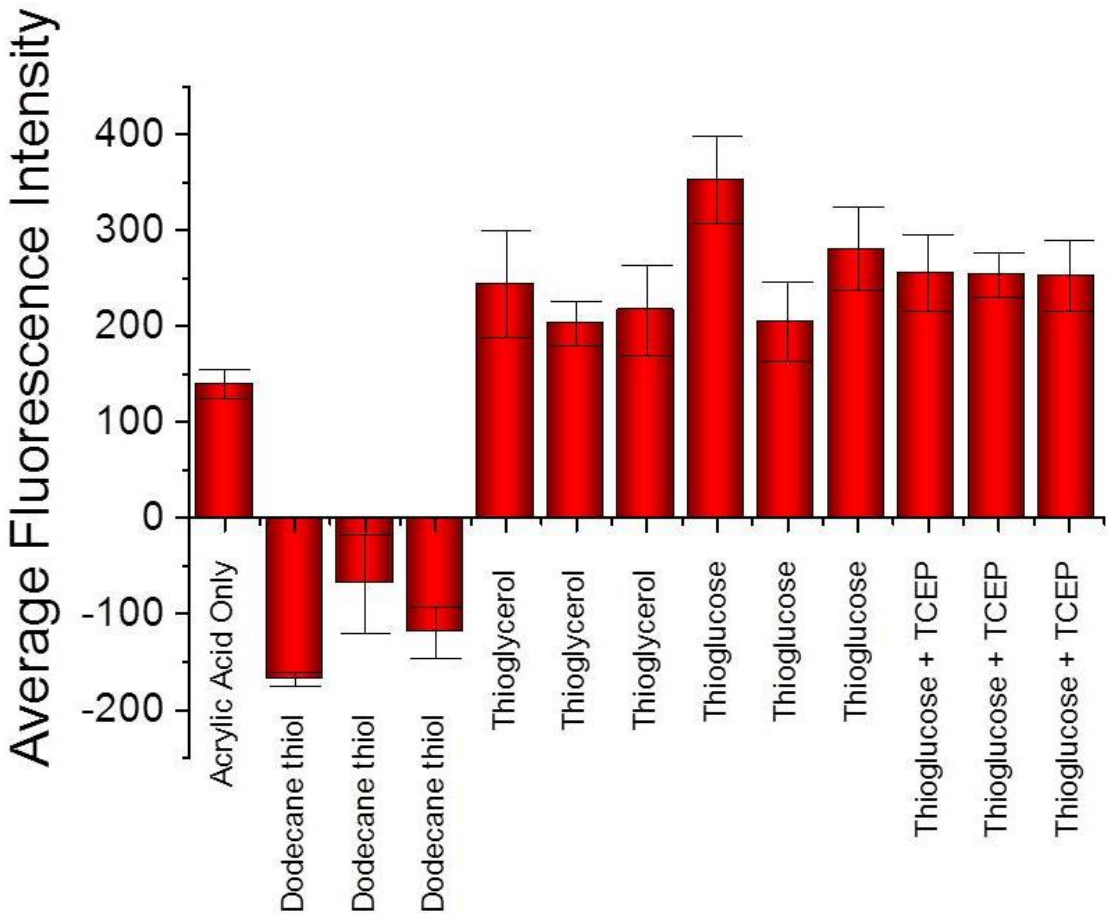

Figure 2.19: Microplate data for the acrylate functionalised microplate wells. Each well was functionalised with acrylic acid, then the coating stated in the graph, then fluorescent labelled Con A

2.4. Conclusions

This chapter has demonstrated how the feasibility and simplicity of thiol-gold self-assembled monolayers can be extended to cheaper and more readily available glass substrates, through the use of silane acrylate coatings. The addition of an acrylate-functional silane onto the glass or silicon surface provides an orthogonally reactive layer for the subsequent covalent immobilisation of thiolated carbohydrates. The characterisation, by DSA, ellipsometry, XPS and the fluorescence binding assay, demonstrated the successful modulation of surface properties. Importantly, the role of the amine catalyst was studied and shown to increase binding density, which was only revealed by elemental XPS analysis rather than surface properties only. Using fluorescence, the selectivity of the carbohydrates towards two model lectins was measured. This methodology's main strength lies in its simplicity and versatility, which can be extended to other biomolecules and surfaces.

2.5. Materials and Methods

2.5.1. General Experimental

All reagents and solvents were used as received from the supplier. Laboratory solvents were purchased from Fisher Scientific, 3-(trimethoxysilyl)propyl acrylate and (3-glycidyloxypropyl)trimethoxysilane from Sigma-Aldrich. Microscope slides were purchased from Fisher Scientific (ground edges,76 mm x 26 mm, 1.0 mm to 1.2 mm thick) and silicon wafers from IDB Technologies (kindly donated by the Macpherson Group (University of Warwick)) with a resistivity of 1-10 Ω. The flat bottomed 96-well polystyrene microtitre plates were purchased from Appleton Woods and the amine coated flat bottomed 96-well polystyrene microtitre plates were purchased from BD Biosciences.Phosphate-buffered saline (PBS) solution was prepared by dissolving a pre-formulated tablet (Sigma-Aldrich) in 200 mL Milli-Q. The resulting PBS solution has a composition of 0.01 M phosphate, 0.0027 M potassium chloride and 0.138 M sodium chloride, pH 7.4. 10 mmol HEPES buffer, containing 0.1 mmol $CaCl_2$, pH 6.5, was prepared in 250 mL Milli-Q. Ethanolamine was purchased from Sigma-Aldrich, thiosugars (1-thio-β-D-glucose sodium salt and 1-thio-β-D-galactose sodium salt) from Carbosynth and fluorescently labelled lectins (PNA, Con A) from Vector Labs (Fluorescein FLK-2100 labelled).

Any waste thiol solutions were treated with a sulfide oxidiser microemulsion solution (3% cyclohexane, 5% sodium dodecyl sulfate, 10% butan-1-ol and 82% water by weight) to kill the thiol smell. 1 ml of sulfide was dissolved in 15 ml of microemulsion and 5% aqueous sodium hypochlorite solution was then added in 2-fold excess. Thiol contaminated glassware was soaked in sulfide oxidiser microemulsion and aqueous sodium hypochlorite solution prior to washing.

2.5.2. General Surface Analysis

2.5.2.1. Contact Angle Measurements

The water contact angle measurements were conducted at room temperature using a Krüss drop shape analysis system DSA100 equipped with a movable sample table and microliter syringe. Milli-Q water was used as the wetting liquid and the drop size was set to 10 µL. Samples were placed onto the sample table, using tweezers, and aligned within the field of view of the camera. The microliter syringe was advanced until a drop of 10 µL was formed and suspended at the end of the syringe needle. The sample table was then elevated, until the sample touched the bottom of the drop, causing it to detach from the end of the needle and form on the surface. The sample table was the moved back to the original position and an image immediately recorded. The baseline and contact advancing angles were then computated from the image using the in-built software. This process was repeated five times for each sample and the reported values are the average taken from the repeat measurements.

2.5.2.2. Ellipsometry

Ellipsometry measurements were carried out on a Nanofilm auto-nulling imaging ellipsometer with a resolution of 0.001 deg (Delta and Psi) and a relative thickness error 0.001 nm. A 550 nm wavelength light source was used and all measurements were taken using an angle of incidence scan (four-zone) at 50, 60 and 70°. Analysis was carried out using WVase software.[24]

Firstly a cleaned silicon surface was tested. It was placed upon the sample table, under the alignment laser dot and automatically aligned to be level. Following the set up procedure (setting of Z-height to find the peak area of intensity, rotating

the polariser to find the brightest image and calibrating the focus based on a small contaminant, such as a speck of dust) the an angle of incidence scan was performed. The values of psi and delta for each angle were recorded and inputted into the WVase software. The thickness of the oxide layer present on the Silicon was calculated by adding a "SiO_2" layer (SiO_2 DATA, from Palik HOC Vol. 1, p. 759) into the model and fitting the data to the model, to obtain the thickness. The sample could then be silanated and the process repeated, this time modelling the layer using the "Cauchy" option from within the software. The "Cauchy" option was also used for any further layers added on top of the silane, the thickness of such layers was calculated by subtracting the value previously obtained for the silane away from the total "Cauchy" thickness. Three values for each sample were recorded and the values stated are the average of these repeats and the error bars represent the standard deviation within the measurements. Each value obtained from the software also has an experimental error associated with it and a mean-square error between fitted and measured delta and psi values.

2.5.2.3. X-ray Photoelectron Spectroscopy

The experiments were performed at the Science City Photoemission Facility, University of Warwick. The samples were mounted on to Omicron-style sample plates using electrically-conductive carbon tape and loaded in to the fast-entry chamber. Once the fast-entry chamber had been evacuated to an appropriate pressure, the samples were transferred in to the 12-stage carousel for storage at pressures of less than $1x10^{-10}$ mbar. XPS data were acquired in the main analysis chamber using an Omricron SPHERA analyser (Omicron Nanotechnology, UK). Core level XPS spectra were recorded using a pass energy of 10 eV (0.47 eV resolution), with the sample illuminated using an Omicron XM1000 Al K α x-ray

source (h\nu = 1486.6 eV). Analysis of the XPS data was carried out using the CasaXPS software, using mixed Gaussian-Lorentzian (Voigt) lineshapes. The transmission function of the analyser has been carefully determined using clean Au, Ag and Cu foils, whilst the work function of the analyser was determined using the Fermi edge of a polycrystalline Ag sample at regular intervals throughout the experiment, thereby allowing accurate composition and binding energy shifts to be determined. All binding energies have been referenced to the C 1s peak arising from adventitious carbon at 284.6 eV, a necessary correction due to the insulating nature of the oxide termination of the Si substrate.

2.5.2.4. Microarray Scanner

The fluorescence images were obtained using an Agilent G2565CA Scanner with a 2 μm resolution. Standard two colour scanning protocols were used with a SHG-YAG laser (532 nm) and a helium-neon laser (633 nm). The top left hand corner of each slide was marked with permanent pen, away from the lectin spots, and the slides were each placed into a sample holder. The samples were loaded and the standard two colour scan was run, producing the data as a Tagged Image File (Tif). The resulting image files were analysed using Agilent Feature Extraction Software. The average fluorescent intensity was calculated for the sample area of interest (the lectin spot) by taking the average output value for the green channel for that set area. The background fluorescence (the average output value for the green channel for all of the areas of the sample without a lectin spot or pen mark) was calculated and manually subtracted from each value.

2.5.3. Surface Modification

2.5.3.1. Piranha Cleaning

The solid surfaces used in this work (glass slides and silicon wafers) were cleaned using piranha solution [caution, exothermic, see notes below]. The surfaces were placed into a 3:1 (v/v) mixture of 98% sulfuric acid and 30% hydrogen peroxide (12 mL in total), on ice, for 20 minutes, then rinsed with Milli-Q water and dried in a gentle stream of dry nitrogen.

Safety Note: Piranha solution is strong oxidizing and is hazardous to prepare and use. It should be handled in small quantities, freshly prepared and never stored. The hydrogen peroxide solution should be slowly added to the acid and the reaction should be carried out on ice. After the cleaning procedure is complete, the piranha solution should be allowed to cool and then diluted slowly into one litre of deionised water, with 2-3 spoons of MnO_2. After 12 hours this solution can be neutralised with sodium bicarbonate and disposed of appropriately.

2.5.3.2.UV/Ozone Cleaning

The UV/Ozone cleaning process was carried out using a Novascan PSD-UVT, which contains a Hg lamp (185 nm and 254 nm, 20 mW cm^{-2}) as the UV source. The samples are placed in the sealed, air-filled chamber at a distance of 25 mm from the lamp. The 185 nm wavelength photons are absorbed by the atmospheric oxygen within the chamber, which forms O_3. The 254 nm wavelength photons are absorbed by the O_3 and by the hydrocarbons, which results in their decomposition. When the O_3 decomposes, atomic oxygen is formed and it is this very reactive species that is the main oxidising agent. The surfaces were treated for

either 5 or 10 minutes and then immediately removed and functionalised with the silane of interest.

2.5.3.3. Acryloyl Chloride Functionalisation

Immediately following the cleaning process, the samples were immersed into acryloyl chloride solution (12 mL, 3 hours, RT), then rinsed with chloroform (2 x 2 mL), sonicated in 10 mL of chloroform (5 min, RT), re-rinsed with chloroform (2 x 2 mL) and dried under a stream of nitrogen.

2.5.3.4. Thiol-ene "Click" Functinalisation of the Acrylate Surfaces

The acrylate functioalised samples were immersed into a neat solution of thiol (thioglycerol or dodecanethiol) containing catalytic ethanolamine (0.1 mL) for two hours. They were then washed with ethanol (5 x 2 mL) and water (5 x 2 mL), then blown under a stream of nitrogen until dry.

2.5.3.5. Solution Phase Silanisation

Immediately following the cleaning process, the samples were immersed into a (3-(trimethyoxysilyl)propyl acrylate or (3-glycidyloxypropyl)trimethoxysilane solution (each 5 mL, 2% v/v in toluene, 2 hours, RT), washed with toluene (5 x 2 mL), ethanol (5 x 2 mL) and water (5 x 2 mL), then blown under a stream of nitrogen until dry. This process applied to the glass slides and the silicon wafers.

2.5.3.6. Vapour Phase Silanisation

As with the solution phase silanisation, the samples from piranha or UV/Ozone cleaning were immediately silanated, in order to prevent any contamination to the cleaned surface. They were transferred to an empty, clean desiccator in which was placed a small watch glass containing 3 drops of the silane.

The desiccator was then put under vacuum, exposing the surfaces tothe vapour of 3-(trimethyoxysilyl)propyl acrylate at 5 mbar for 4 hours. The samples were then washed with ethanol (5 x 2 mL) and water (5 x 2 mL) and blown under a stream of nitrogen until dry.

2.5.3.7. Thiol-ene "Click" Functioalisation of Silane Coated Surfaces

Following silanisation, the samples were immersed into the chosen thiolated sugar solution (2 $mg.mL^{-1}$ in water) for 2 hours (RT) then washed with Milli-Q water (3 x 2 mL) and dried under a stream of nitrogen. For the samples that were functionalised in the presence of amine, ethanolamine (0.1 mL) was added into the thiolated sugar solution prior to addition of the sample.

2.5.4. Lectin Binding Studies

Samples were subjected to spots (2 µL) of each of the fluorescently labelled lectins (Con A (0.1 $mg.mL^{-1}$ in HEPES or PNA (0.1 $mg.mL^{-1}$ in PBS) for 30 minutes (RT, dark), the protein solutions were then removed by pipette and the surface was washed (5 mL appropriate buffer, 2 x 5 mL Milli-Q water) and dried under a stream of nitrogen. Samples were stored in the dark and in the fridge until tested on the fluorescence scanner. For the concentration dependant studies, a serial dilution of 0.1 $mg.mL^{-1}$ down to 6.025 $\mu g.mL^{-1}$ was used.

2.5.5. Microtitre Plate Functionalisation

2.5.5.1. Solvent Compatibility Testing

Prior to being able to use the microtitre plates for acrylate functionalisation, their solvent compatibility was investigated. 1 mL of each test solution was added to a different well of the polystyrene plate and the observations were recorded every 10 minutes for the first hour, then every 30 minutes for the following 4 hours, then

every hour for the next four hours. Wells showing no signs of damage after this nine hour test period were left for a further 18 hours. The plates were washed, as detailed above and allowed to dry. It must be stressed that the solvent additions were carried out drop wise addition, in order to prevent excess exothermic reactions, particularly in the case of the acryloyl chloride: DMSO mixture.

2.5.5.2. Acrylation of Amine Coated Plates

In a typical procedure acrylic Acid (0.09 mL) and N,N'-Diisopropylcarbodiimide (DIPCDI) (0.28 mL) were added into DMSO (4 mL) and left to activate for 10 minutes (RT). 25 µL of the activated acrylating solution was then added to each well in the amine coated microwell plate, except the bottom row, which was left empty as a control. The plates were left for 30 minutes (RT) then the excess solution was removed from each well by pipette, the plate washed with DMSO three times and allowed to dry. Each well of the plate was then functionalised with 25 µL of the correct thiol solution, as detailed in Table 2.7. The In each case an entire row (12 wells) was functionalised with each solution. After 2 hours the excess solution was removed, the plates washed with deionised Milli-Q three times and allowed to dry. Fluorescently labelled Con A (0.1 $mg.mL^{-1}$ in HEPES, 25 µL per well) was then added to each of the functionalised well, left for 30 minutes (RT, dark), washed three times with Milli-Q water and dried. The samples were then immediately tested in the microplate reader. The results show the average fluorescence from the 12 data points, with the background fluorescence from the blank wells subtracted, and the standard deviation between them.

Table 2.7: Functionalisation of the amine coated microplates

First Reagent Added	Second Reagent Added	Third Reagent Added
Acrylic Acid	Thioglycerol (neat)	Fluorescent Con A (0.1 $mg.mL^{-1}$ in HEPES)
Acrylic Acid	Dodecanethiol (neat)	Fluorescent Con A (0.1 $mg.mL^{-1}$ in HEPES)
Acrylic Acid	Thioglucose (2 $mg.mL^{-1}$ in PBS)	Fluorescent Con A (0.1 $mg.mL^{-1}$ in HEPES)
Acrylic Acid	Thioglucose (2 $mg.mL^{-1}$ in PBS) + TCEP	Fluorescent Con A (0.1 $mg.mL^{-1}$ in HEPES)
Acrylic Acid	None	Fluorescent Con A (0.1 $mg.mL^{-1}$ in HEPES)

2.5.5.3. Microplate Reader Measurements

Fluorescence measurements for the microplates were taken on a BioTek Synergy HT Microplate reader at excitation/emission wavelengths of 485/528 nm with a sensitivity of 75 nm and the readings were all taken at 20°C. The fluorescence measurements from the microplate reader were then converted into a numerical format by the Gen5 software. The background fluorescence (the average fluorescence reading from 12 completely unfunctionalised and empty wells) was recorded and subtracted from each of the data values.

2.6. References

1. C. I. Biggs, S. Edmondson and M. I. Gibson, *Biomater. Sci.*, 2015, **3**, 175-181.

2. H. C. Neu, *Science*, 1992, **257**, 1064-1073.

3. C. R. Bertozzi and L. L. Kiessling, *Science*, 2001, **291**, 2357-2364.

4. R. J. Pieters, *Med. Res. Rev.*, 2007, **27**, 796-816.

5. R. Apweiler, H. Hermjakob and N. Sharon, *BBA-Gen. Subjects*, 1999, **1473**, 4-8.

6. N. Laurent, J. Voglmeir and S. L. Flitsch, *Chem. Commun.*, 2008, 4400-4412.

7. G. Nan, H. Yan, G. Yang, Q. Jian, C. Chen and Z. Li, *Curr. Pharm. Biotechnol.*, 2009, **10**, 138-146.

8. N. Kim, C. T. Kim, Y. J. Cho and C. J. Kim, *Sens. Actuat. B-Chem.*, 2011, **160**, 563-570.

9. J. C. Tiller, C. J. Liao, K. Lewis and A. M. Klibanov, *Proc. Natl. Acad. Sci. U. S. A.*, 2001, **98**, 5981-5985.

10. C. E. Hoyle and C. N. Bowman, *Angew. Chem. Int. Ed.*, 2010, **49**, 1540-1573.

11. A. B. Lowe, *Polym. Chem.*, 2010, **1**, 17-36.

12. N. S. Bhairamadgi, S. Gangarapu, M. A. Caipa Campos, J. M. J. Paulusse, C. J. M. van Rijn and H. Zuilhof, *Langmuir*, 2013, **29**, 4535-4542.

13. S. P. Pujari, L. Scheres, A. T. M. Marcelis and H. Zuilhof, *Angew. Chem. Int. Ed.*, 2014, **53**, 6322-6356.

14. G. Z. Li, R. K. Randev, A. H. Soeriyadi, G. Rees, C. Boyer, Z. Tong, T. P. Davis, C. R. Becer and D. M. Haddleton, *Polym. Chem.*, 2010, **1**, 1196-1204.

15. Y. Nam, D. W. Branch and B. C. Wheeler, *Biosens. Bioelectron.*, 2006, **22**, 589-597.

16. J. J. Cras, C. A. Rowe-Taitt, D. A. Nivens and F. S. Ligler, *Biosens. Bioelectron.*, 1999, **14**, 683-688.

17. D. Janssen, R. De Palma, S. Verlaak, P. Heremans and W. Dehaen, *Thin Solid Films*, 2006, **515**, 1433-1438.

18. R. M. Hensarling, V. A. Doughty, J. W. Chan and D. L. Patton, *J. Am. Chem. Soc.*, 2009, **131**, 14673-14675.

19. S. K. So, W. K. Choi, C. H. Cheng, L. M. Leung and C. F. Kwong, *Appl. Phys. A: Mater. Sci. Process.*, 1999, **68**, 447-450.

20. J. R. Vig, *J. Vac. Sci. Technol., A*, 1985, **3**, 1027-1034.

21. S. Baunack and A. Zehe, *Phys. Status Solidi A*, 1989, **115**, 223-227.

22. R. J. Klein, D. A. Fischer and J. L. Lenhart, *Langmuir*, 2008, **24**, 8187-8197.

23. A. E. Ozcam, K. Efimenko, C. Jaye, R. J. Spontak, D. A. Fischer and J. Genzer, *J. Electron Spectrosc. Relat. Phenom.*, 2009, **172**, 95-103.

24. H. G. Tompkins and T. Tiwald, WVASE32 Software Training Manual for IR-VASE, 2009, Available at: https://wiki.kip.uni-heidelberg.de/KIPwiki/images/f/ff/IR-VASE_Training_Manual.pdf

25. NIST, X-ray Photoelectron Spectroscopy Database, Version 4.1, 2014, Available at: http://srdata.nist.gov/xps/

26. M. Mammen, S. K. Choi and G. M. Whitesides, *Angew. Chem. Int. Ed.*, 1998, **37**, 2755-2794.

27. O. C. Grant, H. M. K. Smith, D. Firsova, E. Fadda and R. J. Woods, *Glycobiology*, 2014, **24**, 17-25.

28. S. A. Sundberg, *Curr. Opin. Biotechnol.*, 2000, **11**, 47-53.

29. R. B. Merrifield, *Adv. Enzymol. Relat. Areas Mol. Biol.*, 1969, **32**, 221-296.

30. Y. Arima and H. Iwata, *Biomaterials*, 2007, **28**, 3074-3082.

Chapter Three

3. Surface Grafting RAFT Synthesised Polymers and a Comparison between pOEGMA and pNIPAM

3.1. Chapter Summary

The synthesis of poly(oligo(ethylene glycol)methyl ether methacrylate)s (pOEGMA)s and poly(*N*-isopropylacrylamide)s (pNIPAM)s, selected due to their desirable thermoresponsive behaviour, biocompatibility, and resistance to protein and cell adsorption, has been achieved through the reversible addition fragmentation transfer (RAFT) controlled radical polymerisation technique. RAFT polymerisation leads to functional groups at both ends of the polymer chain, allowing scope for further modifications. Of particular interest in our case is the thiocarbonylthio group present on the ω-end of the chain. The cleavage of this group to a thiol allows thiol-ene surface modifications and thiol-gold reactions.

Through the combination of these thiol-terminated polymers and the acrylate silane coating introduced in Chapter Two, thiol-ene "click" chemistry was employed in order to synthesise surface grafted polymer assemblies on both glass and silicon. The *grafting to* (attachment) technique, involving attaching pre-synthesised polymer chains onto a prepared substrate, was used as it is experimentally simpler then *grafting from* (growth) and allows full polymer characterisation to be undertaken prior to the grafting. Additionally, it

ensures that the polymers have identical properties, regardless of which substrate they are being added to and which experiment they are to be used in. The resulting polymer coatings have been characterised by drop shape analysis, ellipsometry and x-ray photoelectron spectroscopy. The presence of the thiol terminus also allows monolayer formation onto gold surfaces, which allowed the probing of the system using a Quartz Crystal Microbalance with Dissipation **(**QCM-D). This analytical tool was used to monitor the behaviour of polymers at the surfaces in real time and compare the efficiency of binding of the two different polymers, from which it was found that the pNIPAMs exhibit greater binding than the pOEGMAs. The thermoresponsive and non-fouling properties of the polymer coatings were also investigated and it was found that they can significantly reduce non-specific protein adsorption when compared to unfunctionalised glass substrates.

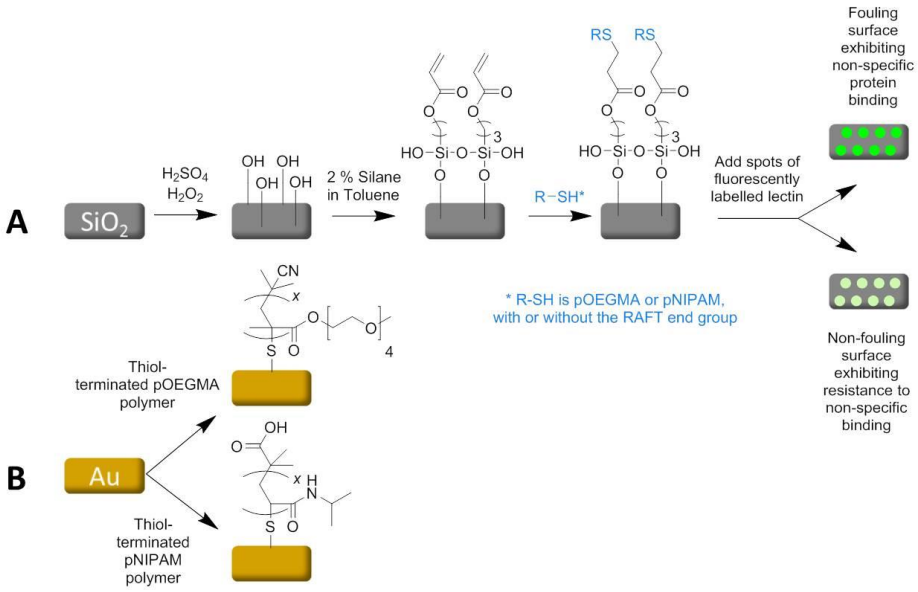

Figure 3.1: [A] Building on the silane acrylates detailed in Chapter Two, thermoresponsive pOEGMA and pNIPAM polymers were added onto both glass and silicon surfaces and their thermal switching behaviour and resistance to non-specific protein binding was studied. [B] The self-assembly of the same polymers onto gold surfaces was investigated as a comparison to the silane linked system and to obtain more details information regarding the polymer grafting

3.2. Introduction

The assembly of polymers onto solid supports has been widely researched, due in part to the large variety of their applications, including anti-corrosion, wetting, adhesion and lubrication. These polymer assemblies are defined as "polymer brushes" when the tethered polymer chains are attached to a substrate at one end and are grafted at a sufficiently high density, generally agreed to be when the distance between grafting sites is less than two radii of gyration of the polymer.[1] The properties of these brushes depends on a balance between the elastic free energy of the system and the chain-chain interactions. As the grafting density increases, the interaction between the chains is increased and they stretch away from the surface, forming the brush-like structure. A large number of polymers have been utilised for these surface grafting processes, often being selected due to their desirable solution properties. Polymers of oligo(ethylene glycol)methyl ether methacrylate (OEGMA) and *N*-isopropylacrylamide (NIPAM) have been of great interest to the polymer and materials science community due to their thermoresponsive behaviour,[2-5] biocompatibility[5, 6] and resistance to protein and cell adsorption.[7] This combination of properties and their ability to be synthesised using reversible addition fragmentation transfer (RAFT) polymerisation makes them highly desirable for thermoresponsive, biologically relevant, microarray applications.

The nature of the chain transfer agent used in RAFT polymerisation allows for control over the polymerisation reaction and leads to functional groups at both ends of the polymer chain, allowing scope for further modifications. Of particular interest is the thiocarbonylthio or dithioester

group present on the ω-end of the chain, which can be modified, or removed, post polymerisation.[8] The reduction of this group to a thiol allows an easy route towards thiol-ene Michael addition processes[9] and thiol-gold reactions.[10] These thiol-ene Michael-type additions can be used as an example of the *grafting to* polymer brush formation technique, involving attaching pre-synthesised polymer chains onto a prepared substrate,[11, 12] This method is experimentally simpler then *grafting from*, where polymers are grown *in situ* from a surface immobilised initiator.[13, 14] More importantly, it allows for full polymer characterisation to be undertaken prior to the grafting and ensures that the polymer samples have identical properties in each experiment, regardless of conditions or underlying substrate. Although the density of brushes formed using the *grafting to*[12] method can be limited, due to steric repulsion between the chains, previous work in the area has shown that covalently tethering of oligo(ethylene glycol) methacrylate (OEGMA) polymer chains can produce ultra-thin polymer brushes on a variety of solid supports, such as gold and glass.[15] The maximum thickness of polymer brushes grafted to surfaces is inherently limited, typically to 5-8 nm.[1] When long chain macromolecules are used it is very difficult for the solution-phase polymers to diffuse through the already bound chains and reach the grafting sites. In order to produce effective polymer brushes from the grafting to technique, the chains must therefore remain short and the resulting polymer coating therefore thin.[16] For this reason, short chain lengths of pOEGMA and pNIPAM have been utilised in this work.

The use of RAFT polymerisation to produce controlled surface grafted polymers has been extensively employed. In order to grow polymers from a

solid support, the RAFT agent is tethered to the surface by its R-group or Z-group, or alternatively the chains are grown from the surface immobilised initiator. Examples include the surface-initiated polymerisation of 6-azidohexyl methacrylate (AHMA) by the attachment of a dithiobenzoate RAFT agent onto silica nanoparticles (R-group tethering)[17] or the use of a silica supported RAFT agent to mediate the polymerisation of methyl acrylate, methyl methacrylate, butyl acrylate and styrene (Z-group tethering).[18] Interestingly, the Z-group tethering is often considered to be a *grafting to* approach, rather than *grafting from*, because the chain growth occurs away from the surface and the chains then react back onto the tethered RAFT agent.[19] More traditional *grafting to* approaches, where pre-synthesised polymer chains are attached onto functionalised solid supports, have also been reported and there are literature examples of the use of thiol-ene reactions for the functionalisation of silica nanoparticles with RAFT-synthesised polymers. In these cases the RAFT terminus of the polymer has been pre-reduced to a free thiol to allow the thiol-ene reaction to proceed. For example, the Narain Group has synthesised silica nanoparticles functionalised with surface vinyl groups and reacted them with thiol-terminated pNIPAM and poly(2-(diethylamino)ethyl methacrylate) (pDEAEMA), to produce temperature and pH responsive particles.[20] Silane coatings have also be used to introduce vinyl functionality for subsequent thiol addition; 3-(methacryloxy)propyl-trimethoxysilane has been used to coat silica nanoparticles and support the conjugation of thiol terminated poly(lauryl acrylate).[21]

The characterisation of surface grafted polymer brushes is typically achieved using a combination of techniques from: water contact angle

measurements, atomic force microscopy, ellipsometry, XPS and surface plasmon resonance. The presence of the thiol terminus on the reduced polymers also allows for layer formation onto gold surfaces, therefore opening up the possibilities to probe the system using a Quartz Crystal Microbalance with Dissipation **(**QCM-D) apparatus. This analytical tool can be used to monitor the behaviour of polymers at surfaces in real time and the kinetics of polymers grafting to surfaces.[22] For rigid, evenly distributed and sufficiently thin adsorbed layers, the Sauerbrey equation can be used as a good approximation for the mass adsorbed because Δf is proportional to Δm. This Sauerbrey mass takes into account the entire mass coupled to the sensor, including any water, other liquid or solvent molecules. The water (or other liquid) may couple *via* hydration, viscous drag or entrapment within cavities of the film and the bound layers should therefore be considered to be "hydrogel-like". This is in contrast to the frequently defined molar or dry mass, which excludes water and therefore the values should be quoted as "Sauerbrey mass" rather than simply "mass" in order to make this distinction clear.[23] The amount of liquid mass adsorbed within films obviously depends heavily on the properties of the film in question, however, estimations place the value for Sauerbrey mass to be between 1.5 and 4 times larger than the corresponding molar mass.[24] However, for comparative studies, such as in this work, the Sauerbrey mass provides a useful tool for assessing adsorption differences between the systems in question.

3.3. Results and Discussion

3.3.1. Polymerisations

3.3.1.1. Synthesis of poly(oligo(ethylene glycol)methyl ether methacrylate)s

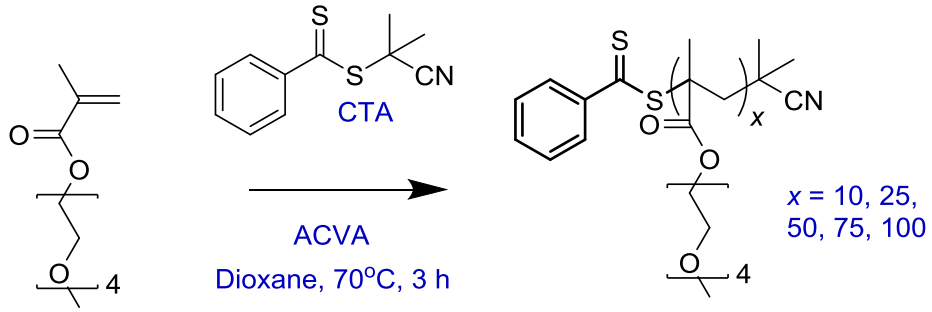

Figure 3.2: RAFT mediated polymerisation of OEGMA with CPBD as the RAFT agent

Four molecular weights of pOEGMA were synthesised from the RAFT polymerisation of PEG 300 OEGMA, Figure 3.2. 2-Cyano-2-propyl benzodithioate (CPBD) was chosen as the RAFT agent (CTA) due to its previous success in this synthesis[25] and ease of commercial availability and 4,4′-azobis(4-cyanovaleric acid) (ACVA) was added as a radical initiator. After 3 hours at 70°C the polymers were isolated by precipitation and the resulting waxy pink solids were characterised by nuclear magnetic resonance (NMR) spectroscopy, with an example assigned spectrum seen in Figure 3.3.

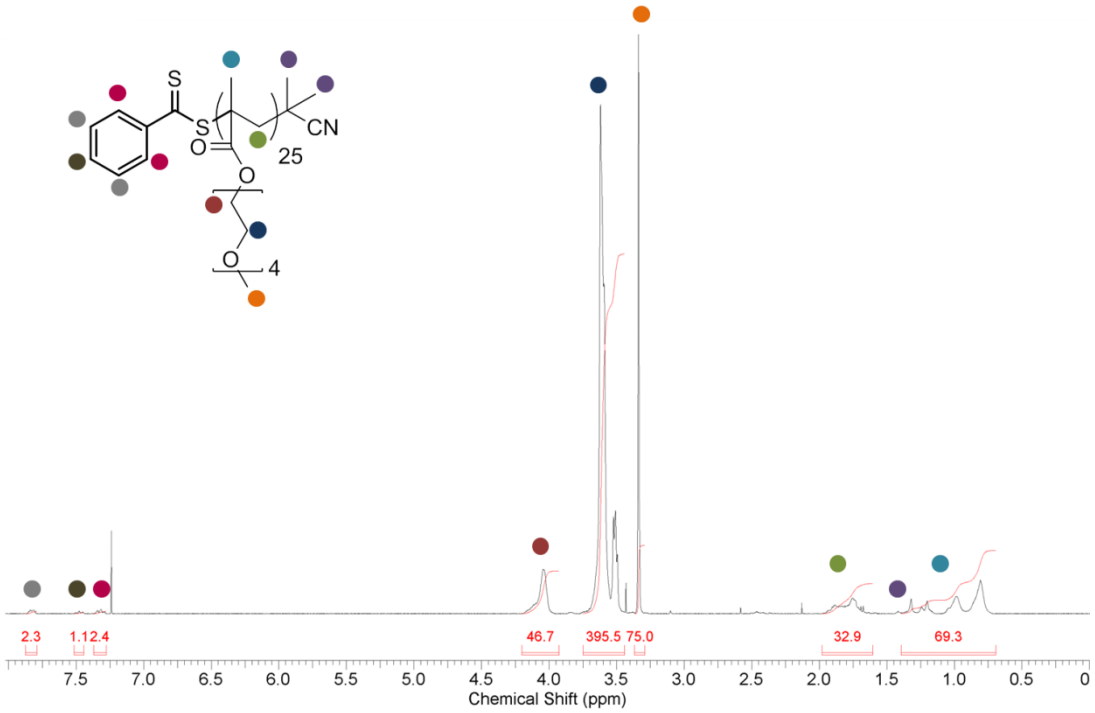

Figure 3.3: ^{1}H NMR spectroscopy characterisation poly(oligo(ethylene glycol)methyl ether methacrylate) in $CDCl_3$

The degree of polymerisation was calculated using ^{1}H NMR spectroscopy to determine the ratio of side chain methyl (δ 3.25-3.40) to aromatic end group protons (δ 7.20-7.95) and also by dimethylformamide (DMF) size-exclusion chromatography (SEC) against poly(methyl methacrylate) (pMMA) standards. The characterisation data is summarised in Table 3.1 and Figure 3.4, it is important to note that the SEC data is does not directly correlate with the theoretical molecular weights due to being compared to a pMMA standard, which has a different hydrodynamic volume. The obtained $DP_{(NMR)}$ agreed well with the SEC data for the shorter polymers, but for the longer chains, SEC gave an underestimate, which can be attributed to the bottle-brush structure of the polymer.

Table 3.1: Characterisation data for the pOEGMA polymers

[M]:[CTA][A]	$M_{n(NMR)}$[B]	DP (NMR)[B]	$M_{n\ (SEC)}$[C]	$M_{w\ (SEC)}$[C]	M_w/M_n (SEC)[C]
10:1	3300	11	3300	4300	1.32
25:1	5500	19	5000	6100	1.24
50:1	11000	39	7200	9200	1.28
100:1	28400	102	11000	14700	1.33

[A] Feed ratio of monomer to chain transfer agent; [B] Determined by ^{1}H NMR spectroscopy in $CDCl_3$; [C] Determined by SEC in dimethylformamide (DMF) using poly(methyl methacrylate) standards. M_w = weight average molecular weight, M_n = number average molecular weight

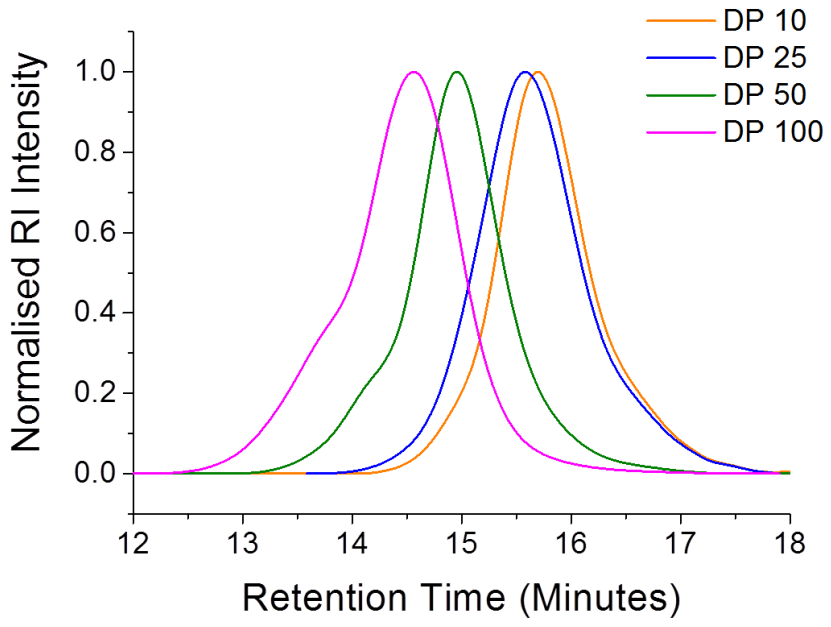

Figure 3.4: pOEGMA SEC data. Solvent = dimethylformamide (DMF)

The thermoresponsive behaviour of the polymers was confirmed by turbidimetric analysis, Figure 3.5. This technique involves measuring the loss of intensity of transmitted light in a sample, which is attributed to the scattering effect of particles suspended in it. For a thermoresponsive polymer, turbidimitry can be used to monitor the temperature at which the polymer transitions from soluble to

insoluble, known as the cloud point. The data shows both the normalised absorbance curves and the obtained cloud points (onset temperature and absorbance at 0.5 A.U.) and tells us that thermal transitions are occurring for each sample, with the temperature of the change depending on the molecular weight of the polymer, as would be expected.

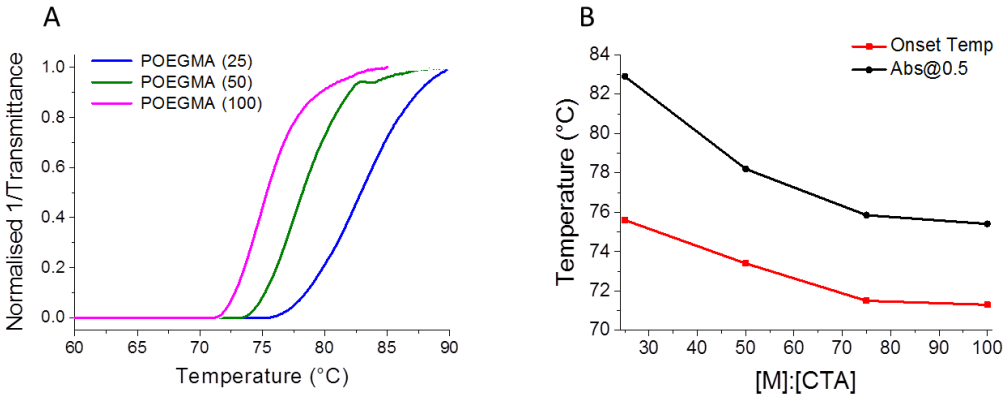

Figure 3.5: [A] Turbidimetric analysis of the pOEGMA samples and [B] Obtained cloud points according to onset temperature and normalised absorbance at 0.5. Polymer concentration = 1 mg.mL^{-1} in PBS

3.3.1.2. Synthesis of 2-(dodecylthiocarbonothioylthio)-2-methylpropanoic acid

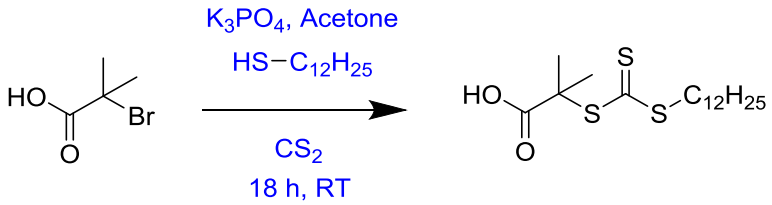

Figure 3.6: Synthesis of the 2-(dodecylthiocarbonothioylthio)-2-methylpropanoic acid RAFT agent

In order to obtain well defined pNIPAM, a dithiocarbonate RAFT agent was required. The 2-(dodecylthiocarbonothioylthio)-2-methylpropanoic acid RAFT agent (Figure 3.6), was synthesised from dodecanethiol, K_3PO_4, CS_2

and 2-bromo-2-methylpropionic acid using a standard procedure and characterised using ^{1}H NMR spectroscopy (Figure 3.7). The resulting yellow solid product was utilised as the RAFT agent for the polymerisation of NIPAM.

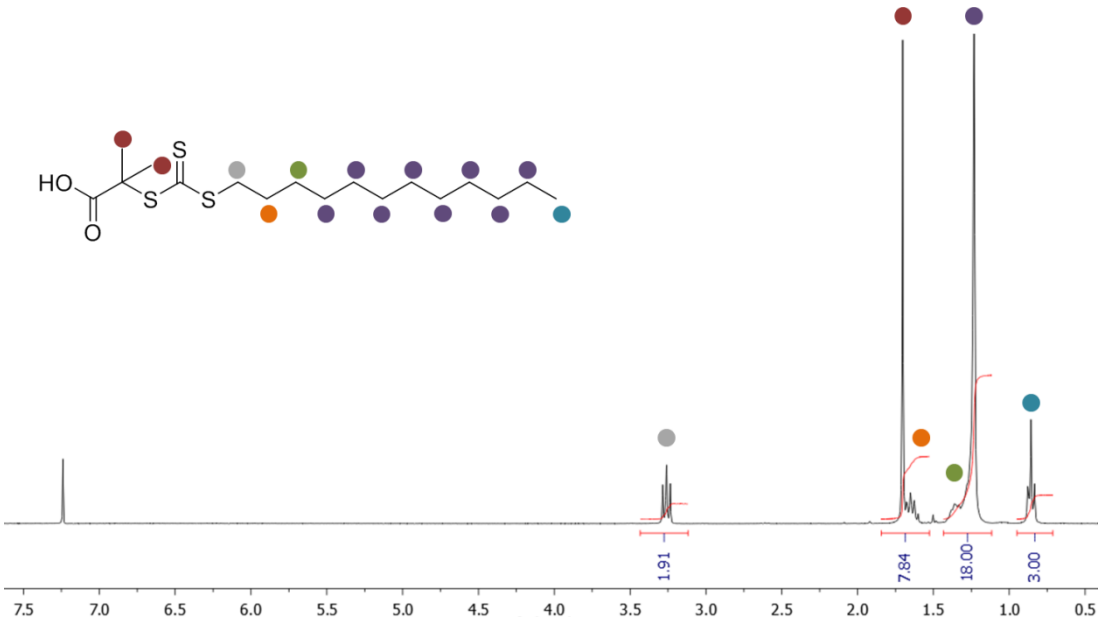

Figure 3.7: ^{1}H NMR spectroscopy characterisation of 2-(dodecylthiocarbonothioylthio)-2-methylpropanoic acid in $CDCl_3$

3.3.1.3. Synthesis of poly(*N*-isopropylacrylamide)s

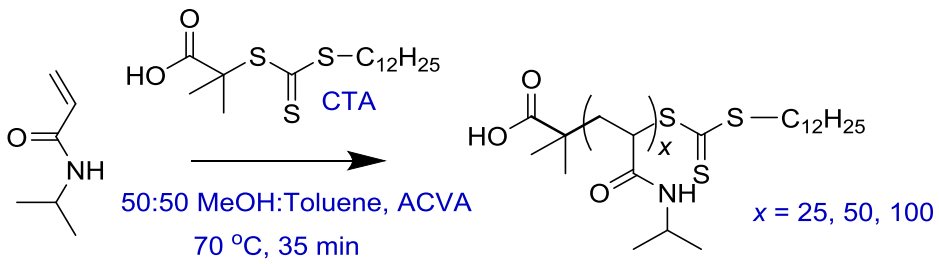

Figure 3.8: RAFT mediated polymerisation of NIPAM

Three molecular weights of pNIPAM were synthesised from the RAFT polymerisation of NIPAM (Figure 3.8), using 2-(dodecylthiocarbonothioylthio)-2-methylpropanoic acid as the RAFT agent. Following isolation, the resulting pale

yellow solid polymers were characterised by ^{1}H NMR spectroscopy, with an example assigned spectrum shown in Figure 3.9 and SEC, shown in Figure 3.10.

The degree of polymerisation was calculated using ^{1}H NMR spectroscopy, to determine the ratio of side chain methyl (δ 1.50- 1.85) to terminal CH_3 protons (δ 0.80- 0.90), and by DMF SEC. Conversion was calculated by ^{1}H NMR spectroscopy with reference to a mesitylene standard and each sample was found to have a conversion of 95%. The characterisation data is summarised in Table 3.2.

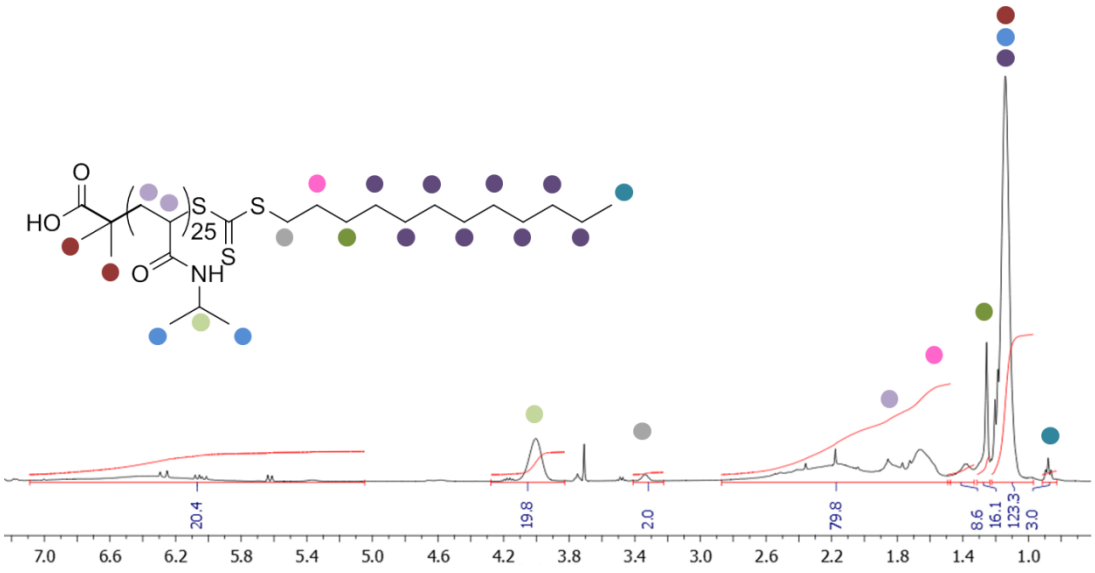

Figure 3.9: ^{1}H NMR spectroscopic characterisation of PNIPAM where *x* = 25 in $CDCl_3$

Table 3.2: Polymerisation characterisation data for the pNIPAM polymers

[M]:[CTA][A]	$M_{n(NMR)}$[B]	DP (NMR)[B]	$M_{n\ (SEC)}$[C]	$M_{w\ (SEC)}$[C]	M_w/M_n (SEC)[C]
25:1	2700	24	1200	1500	1.21
50:1	4200	37	5000	6200	1.23
100:1	5600	53	7000	8600	1.23

[A] Feed ratio of monomer to chain transfer agent; [B] Determined by ^{1}H NMR spectroscopy in $CDCl_3$; [C] Determined by SEC in dimethylformamide (DMF) using poly(methyl methacrylate) standards. M_w = weight average molecular weight, M_n = number average molecular weight

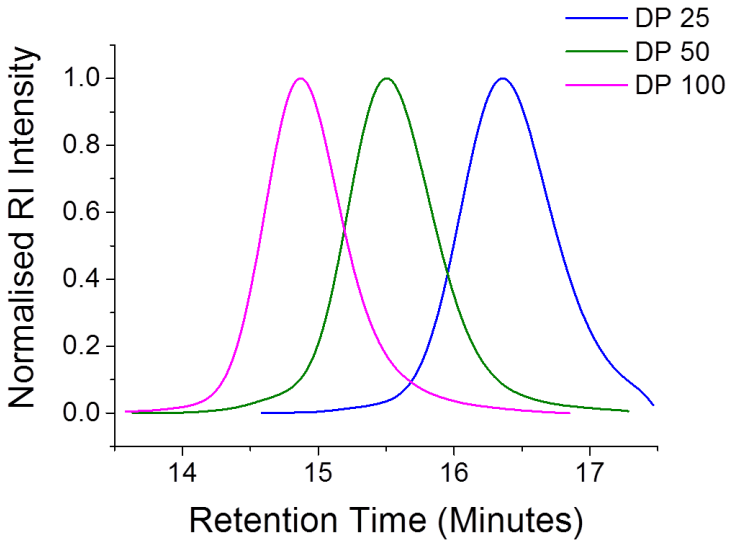

Figure 3.10: pNIPAM SEC data. Solvent = dimethylformamide (DMF)

As with the pOEGMA samples, the turbidimetric data, Table 3.3, confirms that the pNIPAM samples undergo a thermally induced collapse in solution. The temperature of this change is slightly higher than some of the literature values (typically around 32°C) due to carrying out the measurements in biologically relevant media (PBS buffer) rather than water and using a relatively dilute polymer solution, effects that are well known.[25] The carboxylic acid end group will also be unprotonated at pH 7.4, increasing water solubility and therefore increasing the cloud point.

Table 3.3: Turbidimetric data for pNIPAM polymers

[M]:[CTA][A]	Onset Temperature/°C[B]	Absorbance at 0.5/°C [C]
25:1	58.9	60.2
50:1	44.7	53.6
100:1	40.5	46.2

[A] Feed ratio of monomer to chain transfer agent; [B] Obtained cloud points according to onset temperature; [C] Normalised absorbance at 0.5 A.U. Data recorded at wavelength = 650 nm. Polymer concentration = 1 mg.mL^{-1} in PBS

3.3.2. Polymer Coatings on Silane Functionalised Surfaces

3.3.2.1. Formation of Polymer Coatings on Glass and Silicon

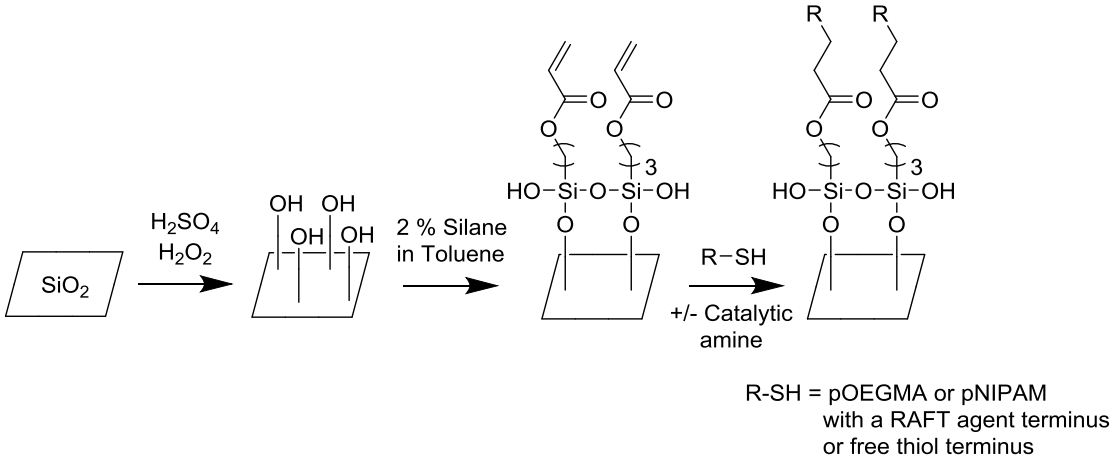

Figure 3.11: Schematic of the functionalisation of the glass or silicon surfaces with the silane acrylate and subsequently the polymers (pOEGMA and pNIPAM)

Polymer coated glass slides were fabricated using the silane acrylate coating introduced in Chapter Two, Figure 3.11. Briefly, glass slides were cleaned with piranha solution and then immersed into a (3-(trimethyoxysilyl)propyl acrylate (5 mL, 2% v/v in toluene) for two hours, then washed and dried under a stream of nitrogen. Following silanisation, the samples were submerged in solutions of the polymer, with or without the addition of ethanolamine, for a further two hours. This process was applied to the glass slides and the silicon wafers, the structure for the two different polymer coatings are shown in Figure 3.12.

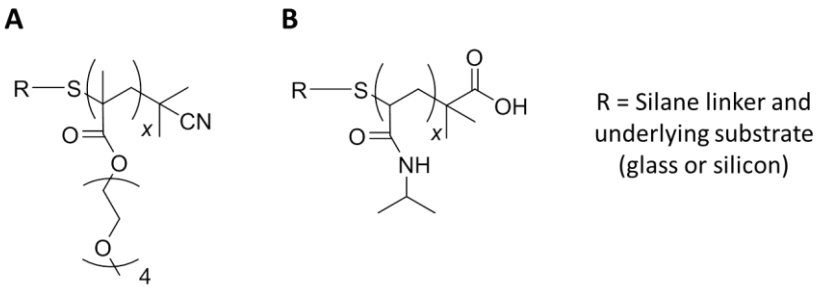

Figure 3.12: Coatings of [A] pOEGMA and [B] pNIPAM formed on the silane coated surfaces

3.3.3. Analysis of the Polymer Coated Surfaces

3.3.3.1. Drop Shape Analysis

Drop shape analysis remains a quick and cost effective way to confirm that the physical properties of a surface have been changed and can be easily applied to both glass and silicon substrates. By monitoring the contact angle changes we can begin to make conclusions about the functionalisation of the substrates. Figure 3.13 shows the static water contact angle measurements for glass and silicon surfaces with both pOEGMA and pNIPAM coatings. As was the case with the carbohydrate coatings, the effect of the amine in promoting the thiol-ene addition reaction cannot be seen by contact angle analysis alone. The data presented in Figure 3.13 contains the DSA data for both the surfaces functionalised in the presence of the amine and those functionalised without amine. The contact angles for the pOEGMA coatings on glass were 46.8° in the presence of amine and 45.2° in its absence. The standard deviation error between repeat experiments was found to be slightly smaller when amine is present (±2.0° compared to ±3.5°), suggesting potentially improved surface uniformity when the thiol-ene addition is promoted with ethanolamine. The trend remains the same with the pNIPAM coatings on glass; contact angles of 59.2±1.3° were obtained with amine and similar angles, but with slightly increased standard deviation values (58.0±1.9°) for samples without amine.

As would be expected, the chemically cleaned glass and silicon have the lowest contact angles (12.5 and 37.6° respectively), due to their hydroxyl functionality producing very hydrophilic surface properties. In common with the results in Chapter Two, the silane coatings on the glass and silicon exhibit different contact angles, potentially due to differences in efficiency of silane cross-linking or coverage of the silane layer. Consistently across the two substrates, the pOEGMA coatings exhibit lower contact angles than pNIPAM coatings, corresponding with the more hydrophilic nature of the pOEGMA structure.

The literature values for water contact angle on polymer brush coatings are very varied. For example the contact angles for pNIPAM brushes grown using surface-initiated ATRP have been reported at 65-67°[26] and 65.5±12.8° on gold surfaces[27] and in the region of 50–55° on silicon wafers,[28] but drop to 42° on pNIPAM gels,[29] all when measured below the LCST point of the polymer. For the pOEGMA brushes, the literature values are more consistent and correlate well with our data. Literature values for growing the brushes from silicon surfaces, by surface-initiated ATRP, range from 34-35° for a $OEGMA_{6.5}$ system[30] and 44±1.7° for a $OEGMA_9$ system.[31] The OEGMA used in our polymers is $OEGMA_4$, which is expected to be less hydrophilic and therefore produce larger water contact angles.

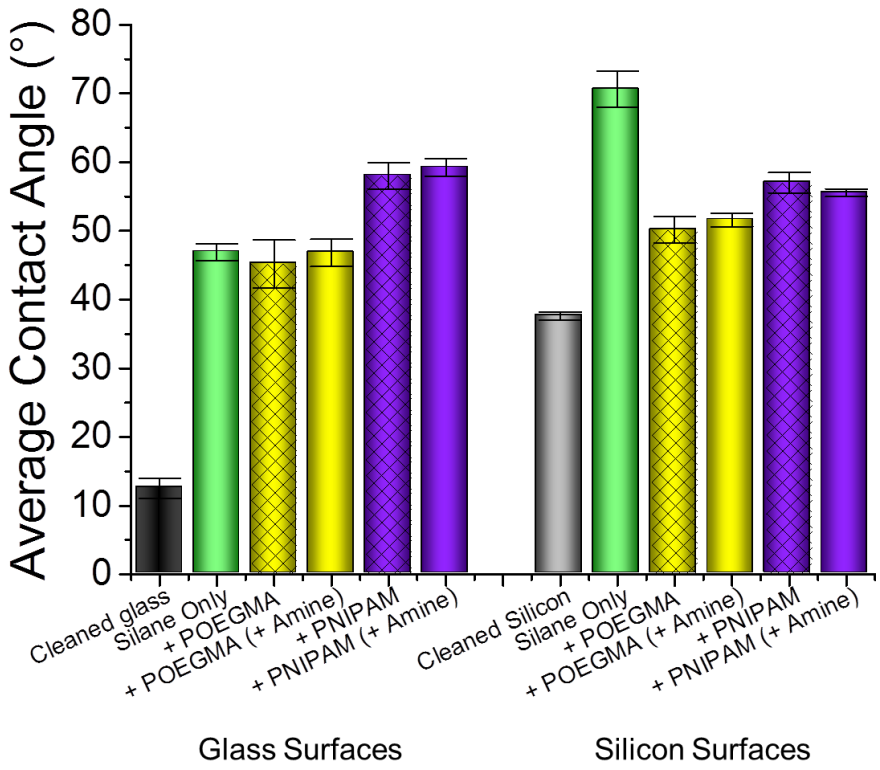

Figure 3.13: Static water drop contact angles for the silane functionalised glass and silicon surfaces, the error bars represent the standard deviation taken from a minimum of five independent measurements. Each surface has undergone silane functionalisation and then addition of either $pOEGMA_{25}$ or $pNIPAM_{25}$, with the inclusion or absence of catalytic amine in the polymer solution

3.3.3.2. Ellipsometry

To gain more surface structural information, the thickness of the polymer coatings on the silicon surfaces was investigated using ellipsometry. The experiments were performed using a two layer model. Initially the oxide layer thickness present on the cleaned surface (labelled as cleaned Si in Figure 3.14) was calculated using the "SiO_2" modelling option, as detailed in the experimental section, and then the subsequent organic layers were modelled using the "Cauchy" option. As shown in Figure 3.14, the polymer coatings were all in the region of 6 to 7 nm and the differences between the different polymer types and chain lengths are not significant. As would be expected, the

polymer layers are thicker than the silane coating and they are also thicker than the monosaccharide coatings seen in Chapter Two.

It is possible to estimate the expected layer thickness based upon the bond lengths present in the coatings. For example, in the silane coating, a 1.2 nm layer would be predicted, if the silanisation had formed a perfect monolayer. The layer thickness, as calculated by ellipsometry is thicker than this, indicating that the silane coverage is present as a multilayer. This is not detrimental to our application, providing that that silane coating remains relatively thin (< 5 nm) and the acrylate functionality is accessible for further surface modification and both of these requirements are fulfilled despite the multilayer silane coating. For the polymer coatings, we would expect 4.5 nm and 16.1 nm for the DP 25 and DP 100 coatings respectively, totalling 5.7 nm and 17.3 nm once the silane layer is taken into account. As can be seen in Figure 3.14, this corresponds well to the experimentally obtained thicknesses for the shorter (DP 25) polymers. For the longer polymers, the experimental thickness is much shorter than the predicted thickness, suggesting that the longer polymer chains are not fully stretched out away from the surface. This is to be expected for brushed obtained by “grafting-to”, where the density of the polymer chains is not high enough to force full chain extension, and does not detriment the intended applications for the coatings.

Previous work in this area has found that pNIPAM brushes grafted to silicon substrates form brushes with a dry thickness of 3 to 24 nm, depending on the molecular weight of the polymer, which is very comparable with our results.[32] These experiments were carried out on a different silicon oxide wafer source, with a much thicker native oxide layer. This should, however, not have

any effect on the surface functionalisation, as only the surface exposed hydroxyl groups are available to react with the silane. The underlying silicon and surface oxide groups, which are necessary for future functionalisation, will still be accessible.

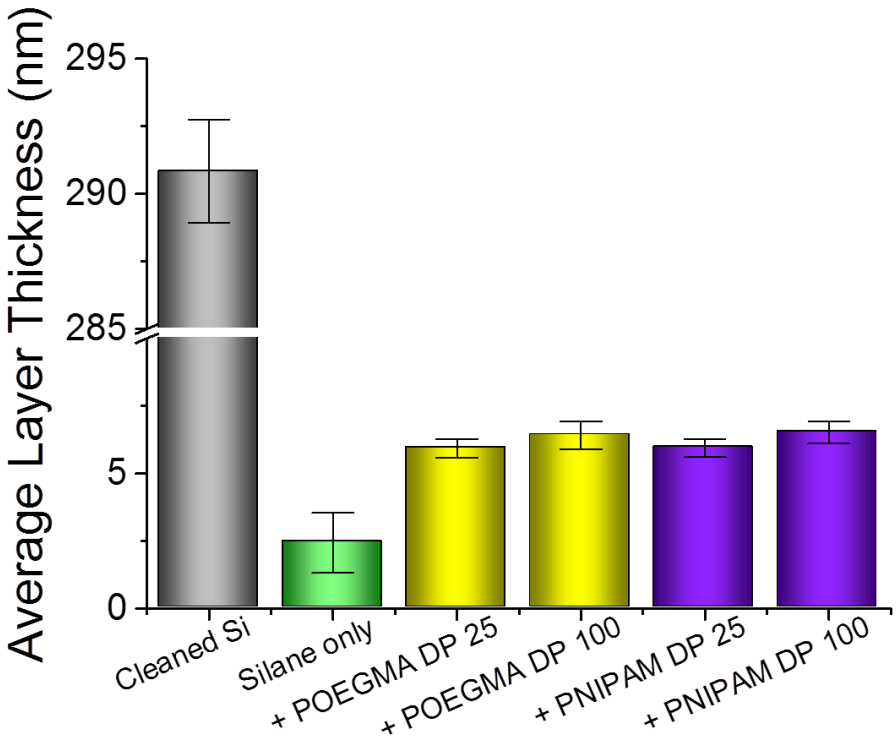

Figure 3.14: Ellipsometry data, giving the thickness of each layer for the silanated and then subsequently polymer functionalised silicon surfaces. The error bars represent the standard deviation taken from a minimum of three independent measurements

3.3.3.3. X-ray Photoelectron Spectroscopy (XPS)

To determine the chemical composition of the polymer functionalised surfaces, XPS was employed. Table 3.4 lists the samples prepared for XPS analysis. In addition to the silicon wafer, gold QCM-D sensors (used in Section 3.3.6) were also functionalised, in order to obtain a comparison between the thiol-gold self-assembly and the thiol-ene reaction occurring on the acrylated silicon. The gold surface preparation and functionalisation was

carried out by cleaning the surfaces with piranha solution and then placing into a polymer solution (2 $mg.mL^{-1}$) to allow self-assembly of the RAFT polymers onto the gold surface (this is further explained in Section 3.3.6.).

Table 3.4: Samples tested using XPS

Underlying Substrate	Silane Acrylate	Polymer
Silicon	No	
Silicon	Yes	
Silicon	Yes	pOEGMA DP 25
Silicon	Yes	pOEGMA DP 50
Silicon	Yes	pOEGMA DP 100
Silicon	Yes	pNIPAM DP 25
Silicon	Yes	pNIPAM DP 50
Silicon	Yes	pNIPAM DP 100
Gold	No	pNIPAM DP 25
Gold	No	pNIPAM DP 100

The Si 2p XPS spectra, Figure 3.15, shows the differences between the cleaned silicon surface and the silanated silicon surface. The spectrum for the cleaned silicon, Figure 3.15A, contains a lower energy peak (99.5 and 100.5 eV) corresponding to the electrons emitted from bulk silicon 2p orbitals and a higher energy peak corresponding to those from the native oxide layer present on the surface (103.4 and 104.0 eV). As is to be expected for silicon 2p data, each peak has a ratio 3:2. A larger component, corresponding to the 2p 3/2 spin state, is present at lower binding energy and a second component, corresponding to the 2p 1/2, is present at higher binding energy. By comparing

this spectrum to the peaks obtained for the silane coated silicon (Figure 3.15B), the successful addition of the silane coating is clear. In addition to the peaks for the bulk silicon and native oxide layer, a further pair of peaks (in a ratio of 3:2) is seen at higher binding energy. It is these peaks that correspond to the silane molecule. The ratio of native oxide to bulk silicon has increased for this sample due to the addition of the silane coating reducing the amount of underlying silicon available within the probing depth of the XPS beam.

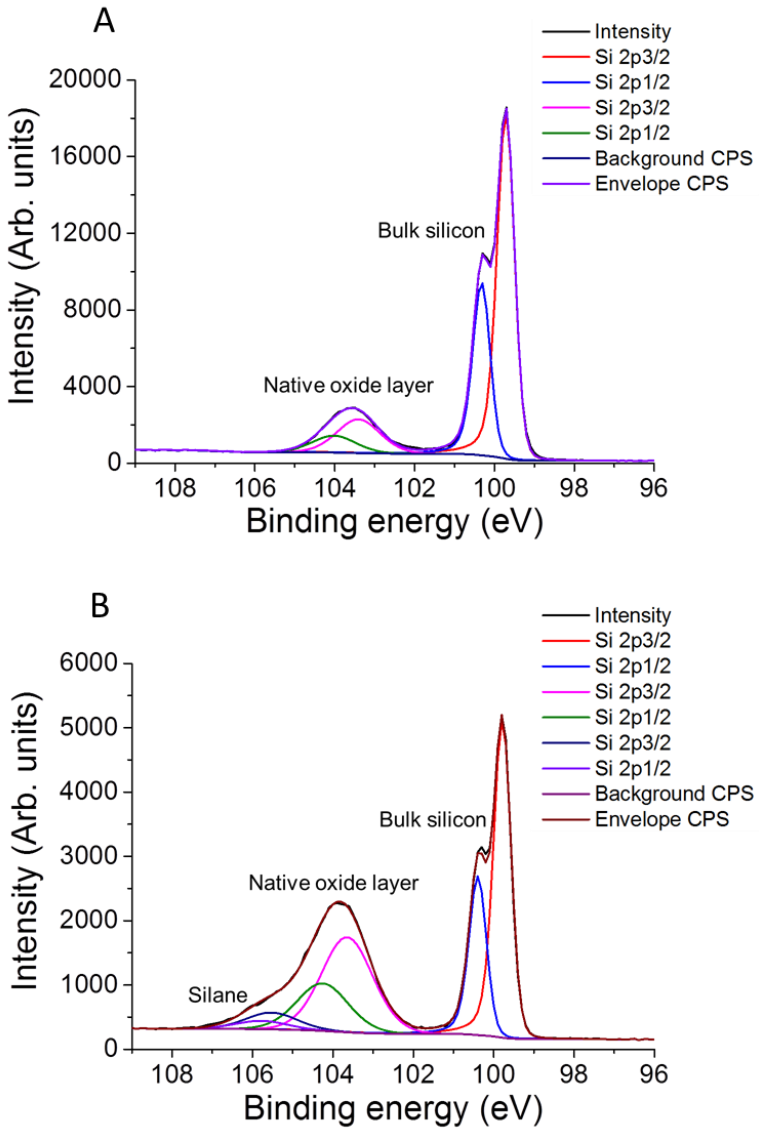

Figure 3.15:X-ray photoelectron spectroscopy data for the Si 2p peaks of both [A] cleaned silicon wafers and [B] silane coated silicon wafers

A typical spectrum for the XPS data of the C 1s peaks in pOEGMA is shown in Figure 3.16. This spectrum was taken from a pOEGMA DP 25 coating; however the data for each sample (DPs 25, 50 and 100) were all very similar. Four C 1s environments are visible, corresponding to the structure of the polymer. The most numerous carbon environment, corresponding to those carbon atoms present on the polymer backbone, indicated in red, results in the highest intensity peak. The intensity of the remaining peaks is also seen to appear in order of their prevalence within the structure. It is, however, inadvisable to compare the ratio of the peaks and attempt to correlate this data to the expected structure due to the incomplete coverage of the coatings. The Si 2p spectra for the pOEGMA coated samples still contains traces of bulk silicon, indicating small regions of incomplete polymer film formation. Additionally, there could be atmospheric contamination in the carbon 1s regions. The ratios between the peaks should therefore be used as a guide only.

The C 1s peaks have also been used to assign the components present in the pNIPAM coated surfaces, Figure 3.17. As with the pOEGMA coating, four components are seen and the intensity ratio of the peaks corresponds to the expected frequency of the environment within the molecule.

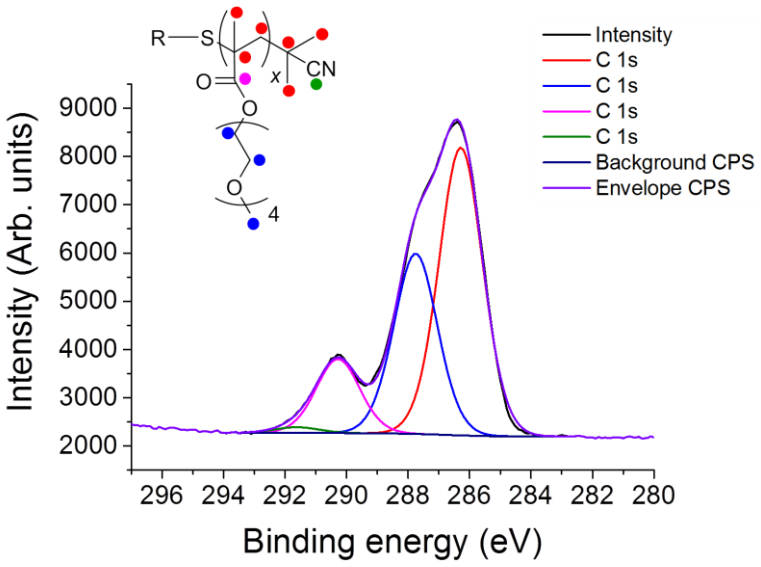

Figure 3.16: Representative high-resolution X-ray photoelectron spectroscopy spectrum of the C 1s for pOEGMA coated silicon. Data is shown for *x* = 25, but is representative for all pOEGMA polymers

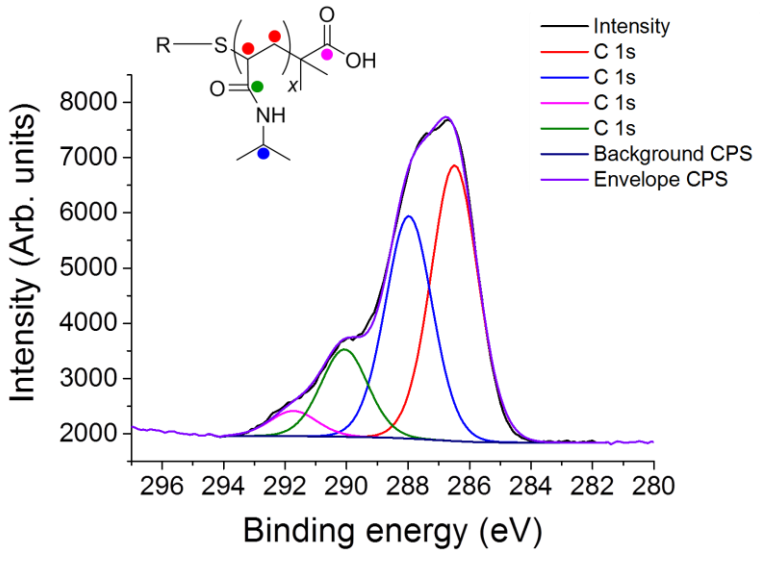

Figure 3.17: Representative high-resolution X-ray photoelectron spectroscopy spectrum of the C 1s for pNIPAM coated silicon. Data is shown for *x* = 25, but is representative for all pNIPAM polymers

In order to compare the surface coatings across the whole set of samples, the nitrogen composition as a percentage of the total surface elemental analysis (included in Table 3.5) can be analysed. The nitrogen signals indicate the presence of bound polymer because no nitrogen is present in the cleaned silicon or silane coated samples. The data shows that in general the pOEGMA coatings contain less nitrogen percentage than the pNIPAM coatings, whilst this likely indicates less effective binding, it should also be noted that nitrogen atoms are less prevalent in the pOEGMA (only the terminal CN) compared to the pNIPAM, which contains a nitrogen atom within the repeat unit. The differences in binding between these two polymer systems is explored in much more depth in Section 3.3.6. When comparing the addition of pNIPAM onto the silane coated silicon and onto cleaned gold, it is seen that more polymer is present on the gold surface. This is likely due to the incompleteness of the silane acrylate coating, however, the data pleasingly concludes that the polymer coatings are present on the silane acrylates. Due to the presence of background atmospheric contamination signals and incomplete polymer coverage, it would be inappropriate to calculate grafting density for any of the samples using this XPS data. For completeness, the total elemental analysis for all the surfaces is tabulated in Table 3.5 and additional spectra are presented in Appendix One. As would be expected, the relative percentage of carbon is greater on the functionalised surfaces than for the cleaned surface and the percentage of silicon signal detectable by the instrument is decreased once additional layers are added to the system. .

Table 3.5: X-ray photoelectron spectroscopy elemental surface analysis

Surface	Coating	C	O	Si	N	Au
Silicon	None	5.0%	36.4%	58.5%		
Silicon	Silane only	43.7%	40.0%	21.3%		
Silicon	POEGMA DP 25	43.6%	33.3%	21.9%	1.2%	
Silicon	POEGMA DP 50	45.4%	33.4%	19.8%	1.3%	
Silicon	POEGMA DP 100	41.3%	34.6%	22.4%	1.7%	
Silicon	PNIPAM DP 25	47.7%	31.2%	18.8%	2.3%	
Silicon	PNIPAM DP 50	48.0%	30.5%	18.7%	2.7%	
Silicon	PNIPAM DP 100	43.1%	32.1%	22.2%	2.6%	
Gold	PNIPAM DP 25	52.1%	7.9%		6.7%	33.3%
Gold	PNIPAM DP 100	59.9%	10.3%		8.8%	21.1%

3.3.4. Non-fouling Behaviour of Polymer Functionalised Surfaces

To test these coatings for compatibility with arraying applications and to assess the bio-inert nature of the surfaces, the surfaces were incubated with fluorescent-labelled lectin solutions. A fluorescent-labelled solution of Con A (a mannose/glucose binding lectin) in HEPES buffer was added to the pOEGMA, pNIPAM or silane-only coated glass slides. After 30 minutes, the surfaces were thoroughly and repeatedly washed with the same volume of Milli-Q water, to remove any unbound protein, and dried under a stream of nitrogen. The extent of protein binding was then visualised using a fluorescence scanner. A sample image for a pNIPAM coated slide, functionalised in the absence of the RAFT end group is shown in Figure 3.18, alongside an unfunctionalised glass surface and a silane coated slide.

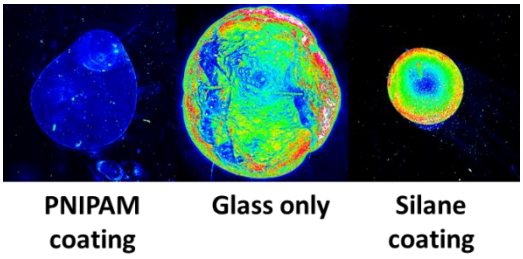

Figure 3.18: Fluorescence scanner images for the polymer coated ($pNIPAM_{100}$) glass slides after treating with a fluorescent-labelled Con A solution and washing off unbound lectin. A chemically cleaned glass slide and a silane coated glass surface, having been exposed to the same fluorescent-labelled lectin, are shown for comparison. Box size for each sample is 10 mm

The images show that the polymer coating is successfully reducing the non-specific binding of the lectin onto the surface. In the glass only sample, the fluorescence is clearly brighter. The spot size is much larger due to the hydrophilic nature of the chemically cleaned glass substrate, lectin spot volumes were constant throughout the experiments but spot diameters were unavoidably varied, due to the differences in underlying surface hydrophilicity. The silane coated surface is also exhibiting significant non-specific binding, confirming that the polymer functionality is responsible for exhibiting the non-fouling behaviour.

We hypothesised that when the polymer solutions were added in the presence of catalytic amine, to promote the thiol-ene addition, the resulting polymer coatings would be more complete and uniform than for the corresponding amine-free polymer solutions. This proved to be the case; when experiments were carried out on surfaces functionalised with polymer solutions in absence of amine (and therefore presence of their RAFT terminus), brighter fluorescence images were obtained. These trends, obtained for both the pOEGMA and pNIPAM systems, Figure 3.19, suggest that these polymers do not bind as well to the silane based acrylate surface and therefore exhibit less resistence to the protein binding. These images were also observed to have less homogenous fluorescence values across the surface, indicating a

potentially less uniform surface coating. POEGMA and pNIPAM *with* a free thiol terminus, having been deprotonated with amine, exhibit minimal protein binding, in agreement with previous literature about the protein-resistant nature of these surfaces.[25, 33, 34] These results confirm that the addition of the amine into the polymer solution is beneficial for the efficient conjugation of the polymers to the silane acrylate. The amine will be having a two-fold effect; firstly by removal of the RAFT end group[8] the free thiol terminus is better able to access the alkene end group of the silane acrylate and secondly it can catalyse the thiol-ene addition,[9, 35] as was also deduced in Chapter Two with the addition of the thiolated monosaccharaides. It also suggests that covalent polymer attachment is occurring, rather than the far less desirable non-specific adsorption.

As a positive control, a set of silane coated glass slides were functionalised with thioglucose and also tested for Con A binding, alongside the polymer coated samples. As would be expected, the Con A bound strongly to the glucose functionalised surface and a high level of fluorescence remained after washing. For each sample the average fluorescence intensity over the whole lectin spot area was calculated, as this should be proportional to the amount of adsorbed protein, with the data for both polymer coatings and the thioglucose, glass and silane controls depicted in Figure 3.19.

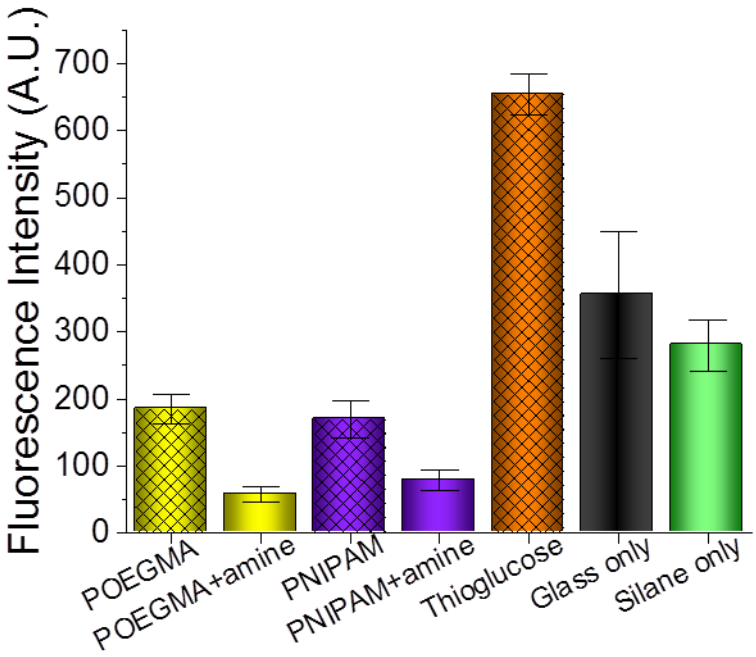

Figure 3.19: Numerical data taken from the fluorescence scanner images for the polymer coated glass slides, after treating with a fluorescent-labelled Con A solution and washing off unbound lectin. The surface has been functionalised with DP 100 pOEGMA and pNIPAM either with or without the addition of amine (to cleave the RAFT end group and catalyse the thiol-ene) or thioglucose with amine. The final two samples are chemically cleaned glass and silane coated glass. Error bars represent the standard deviation from a minimum of three independent measurements

Along with confirming that for both polymer systems, the addition of the amine is beneficial in producing low-fouling coatings, the results also show that even when the polymers were added in the absence of the amine, they also exhibit an increased resistance to the lectin than the glass or silane only samples. This suggests that although the binding is much improved with the addition of the amine, some polymer is still present without it, which is in agreement with our DSA and ellipsometry data. Interestingly, the error bars for the polymer + amine samples are smaller than for the corresponding amine free samples, indicating a more uniform polymer layer coverage when the catalyst is present. The data in Figure 3.19 is shown for the longer chain polymers (DP 100), the results for the shorter (DP 25) still exhibited low fouling, as indicated by low fluorescence values, but the fouling-

reduction was less dramatic than for the longer polymers. The results overall show that our polymer functionalised glass surfaces can produce effective fouling-resistant coatings, as indicated by the minimal fluorescence visible on the surface and that the effect is far more pronounced when the polymers had been added in the presence of catalytic amine.

3.3.5. Thermoresponsive Behaviour of Polymer Functionalised Surfaces

The thermoresponsive behaviour of both pOEGMA and pNIPAM in solution was investigated by UV-Vis spectroscopy, to monitor the temperature at which the polymer transitions through the LCST and becomes insoluble, Section 3.3.1. It is known that surface bound polymer brushes also exhibit this behaviour,[27, 28, 32] however the restriction imposed by the surface tether can alter the properties of the transition. The presence of the surface limits the available configurational space and increases the repulsions between chains, especially within dense polymer brushes. In order to investigate the thermoresponsive behaviour of our polymer coated surfaces, initially a system was devised in which the glass slides were heated, using a heat gun and then quickly transferred to the drop shape analyser in order to assess how the contact angles differed on the heated surfaces compared to those at room temperature. Unfortunately, this proved experimentally unviable as the heat losses from the glass slides during the transfer, and especially when placed onto the cool stage of the DSA, were such that it had returned to room temperature prior to dosing of a water droplet. Instead, it was decided to record the hydrophilic to hydrophobic switching through monitoring of the droplet size, rather than the contact angle, and therefore remove the need for the lengthy process of aligning the sample with the DSA, which was allowing for extensive heat loss.

Water droplets, of a known volume, were administered onto the glass surface, which had been placed over a template. Due to the transparent nature of the glass surfaces, the template was visible through the sample and the drop could be aligned to match up with the template circles, see Figure 3.20. The droplets could then be photographed using a camera phone and the drop sizes, relative to the template, calculated through image analysis using ImageJ, which is freely available from http://imagej.nih.gov/ij/.

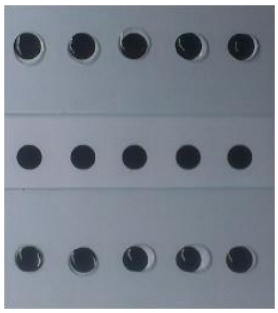

Figure 3.20: Water droplets administered onto the glass surfaces, which have been placed over a template image. The size of the droplets relative to the template can then be calculated and a comparison between droplet size on heated, cooled and room temperature surfaces obtained

Two methods of heating were trialled; firstly the samples were heated directly on a hot plate, set to 80°C for five minutes. Secondly, the samples were placed into a beaker of water at 80°C for five minutes, followed by very quickly drying them with nitrogen. Similarly, the cooling was carried out by placing the samples into the fridge simply in a dry petri-dish or within a petri-dish of water. It was proposed that heating or cooling in the presence of water would facilitate the collapse or expansion of polymer chains and hence their switch from hydrophilic to hydrophobic, or *vice versa*. However, the drying step that was necessary following heating in hot water immediately reduced the temperature, preventing reliable data from being obtained. The dry heating method was therefore adopted instead. This was compared to the combined

data for the wet and dry cooling, for which there were no significant differences. The results in Figure 3.21 show the size of the water droplets on each sample, relative to the size of the template. Both pOEGMA and pNIPAM coatings were tested and DP 25 and 100 polymers were used, to see if the switching behaviour is effected by degree of polymerisation and each surface was tested at three different temperatures: room temperature (24°C), hot (80°C) and cold (5°C).

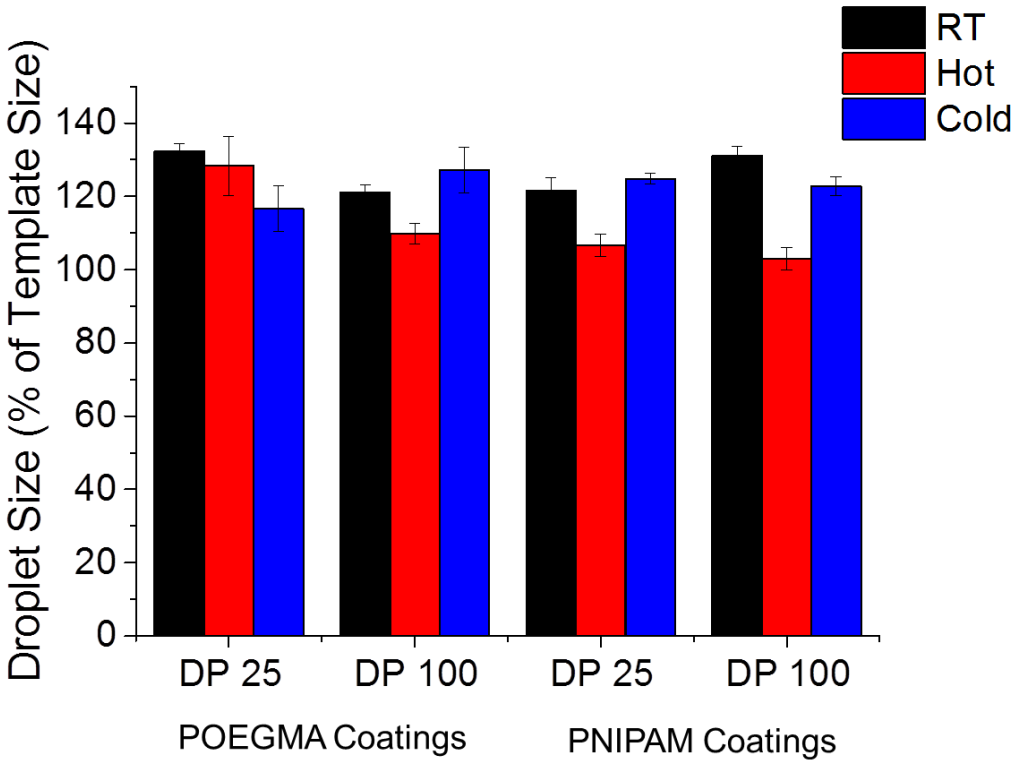

Figure 3.21: Numerical data obtained for water droplets administered onto the glass surfaces, which have been placed over a template image. The size of the droplets relative to the template has been calculated for each polymer at two different molecular weights and at three temperatures. Error bars represent the standard deviation from a minimum of three independent measurements

Overall, the general trends in droplet diameter are as we would expect. When the surfaces are heated the polymers should pass through their LCST and collapse, to form a more hydrophobic surface. The water droplets on a more hydrophobic surface will exhibit less spreading and wetting and therefore the diameter will be smaller. The opposite is true for the cold surfaces, where the more hydrophilic surfaces

should promote spreading and wetting and result in larger droplets. The pNIPAM surfaces appear to undergo a greater switch then the pOEGMA surfaces, potentially due to the more accessible LCST point of pNIPAM (32°C), whereas the LCST for POEGMA is far higher (around 64°C for $pOEGMA_{300}$ polymers)[36] and the samples, although initially heated to 80°C will be cooler than this by the time the measurement has been made. This data shows the proof of concept that the polymer coated surfaces exhibit thermal switching, but in order to probe the transition in more detail a new method was needed.

A temperature controlled stage fitted with a microscope was used to observe the growth and shrinkage of water droplets on functionalised glass surfaces. The slides were placed onto the temperature controlled stage platform to equilibrate for 10 minutes, 2.5 µL water droplets were deposited onto glass slides, the lid was added to retain humidity and the microscope positioned above the sample. The temperature of the stage could then be set at a constant level or programmed to change at a given rate. Initially the functionalised slides were simply held at either 0 or 25°C for 10 minutes on the temperature controlled stage, to see if each surface is affected equally by evaporation. A photograph of the droplet on the surface was taken at the start of the experiment and a further photograph was taken after 10 minutes, the diameter of the final drop could them be recorded relative to the original diameter. This experiment was also attempted at 50°C, however at this elevated temperature evaporation begins to occur at four minutes and the resulting condensation on stage window prevented visualisation of the drops and therefore the measurement. The data for silane and pNIPAM functionalised surfaces, Figure 3.22, shows that the droplet stability is very similar for each type of surface and that over 10 minutes the

droplet shrinkage at steady temperature is minimal, suggesting that a 10 minute time scale is appropriate for monitoring the droplet size changes.

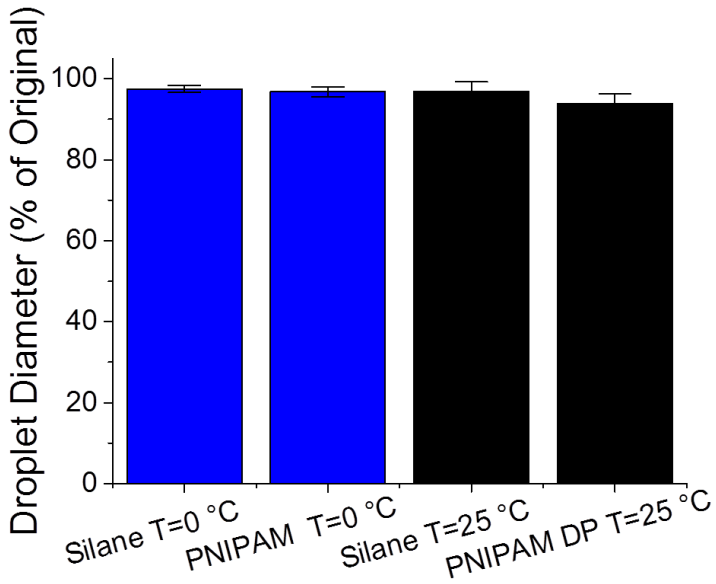

Figure 3.22: Droplet diameter as a percentage of the original droplet diameter, after being held for ten minutes at either 0 or 25°C. Data shown for both silane and pNIPAM functionalised glass slides. Error bars represent the standard deviation from five independent measurements

Having ascertained that the droplets experienced minimal shrinkage at constant temperature over a 10 minutes time scale, the water droplets were then monitored as the temperature was changed. The initial temperature was set to 50°C and end temperature set to 0°C with cooling rate of set at 5°C.min^{-1}. Again 2.5 µL droplets were dosed onto the glass slide and photographs of the drops taken at the beginning and end of the experiment, so the final diameter can be calculated relative to the original. The results, Figure 3.23 show that when the temperature is varied, the behaviour of the droplets is different for the different functionalised surfaces. The shrinkage of the droplets in the polymer coated surfaces is retarded compared to the glass and silane controls and the effect is more pronounced on with the longer chain pNIPAM.

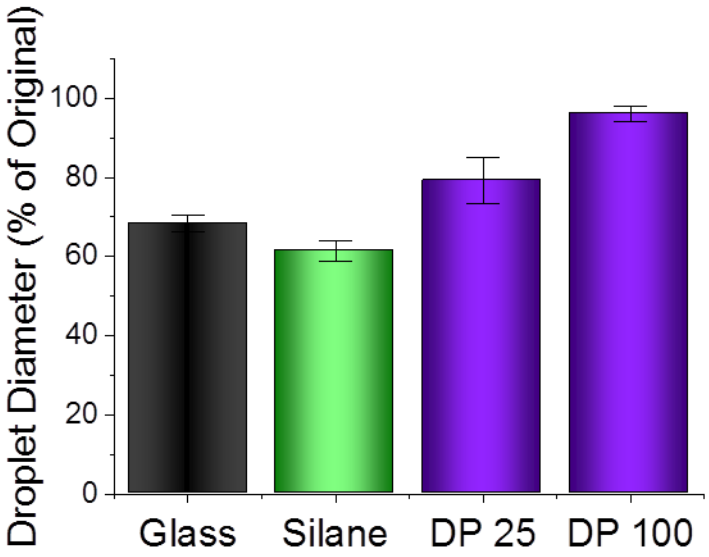

Figure 3.23: Droplet diameter as a percentage of the original droplet diameter, after 10 minutes with a starting temperature of 50°C and a cooling rate of 5 °C.min^{-1}. Data shown for chemically cleaned glass, silane and pNIPAM (DP 25 and 100) functionalised glass slides. Error bars represent the standard deviation from five independent measurements

This behaviour is very interesting, but does not give an indication of whether the droplet size changes are occurring at a steady rate throughout the temperature change. The experiments were therefore repeated under the same conditions, but with a photograph of the drop recorded every 5°C. The images in Figure 3.24 show the droplets on a silane and pNIPAM DP 25 coated surface. Although images are taken every 1 minute, only every other image has been shown for clarity. It is clear to see that the droplet on the silane surface has experienced significant shrinkage, whereas the drop on the polymer functionalised surface retains much of its original size by the end of the experiment.

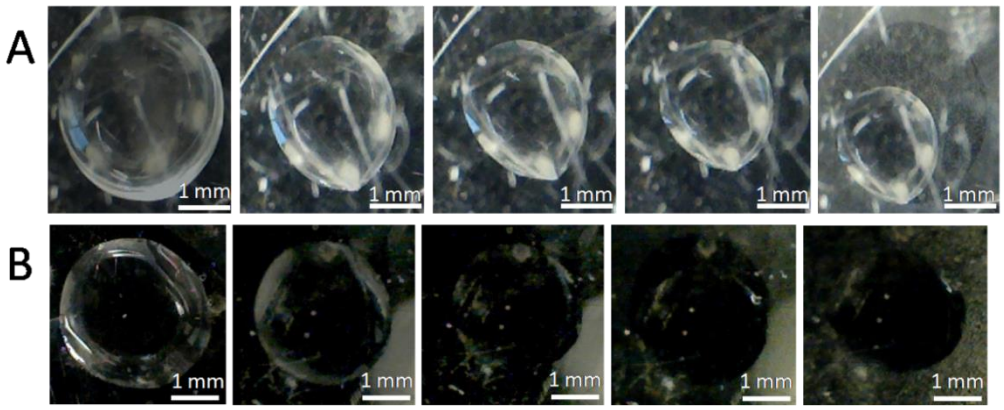

Figure 3.24: Photographs of the water droplets on [A] silane coated glass and [B] pNIPAM DP 25 coated glass, photographs have been taken every 2 minutes, with the first image at a temperature of 50°C and the final image at 0°C and a cooling rate of 5°C.min^{-1}

Plotting the diameter of the droplet at each temperature point throughout the experiment provides a clearer a picture of how the size changes as a function of temperature and time. Figure 3.25 displays this data as both droplet diameter in millimetres (A) and as a percentage of the original droplet size (B). In Figure 3.25A it is clear that the droplet shrinkage, as a function of temperature and time, differs with the differently functionalised underlying substrates. Minimal/no diameter reduction is occurring on the pNIPAM coatings, compared to steep size-reduction gradients for just glass and silane coated glass. It also shows the large variation in starting droplet diameter for the different surfaces, as would be expected due to the different surface hydrophobicity. For this reason, the size data has also been presented as a function of the original droplet size in Figure 3.25B. With the data normalised, the trends are clearer to see and data sets fall into two distinct regions; the shallow and flat gradient of the droplets on the pNIPAM coated surfaces and the steep gradients for the control surfaces (uncoated glass and silane coated glass). If the surfaces were exhibiting thermoresponsive behaviour, they would be expected to switch from hydrophilic to hydrophobic when the temperature moves through the LCST point, and therefore they should exhibit spreading. In the case of the longer

chain pNIPAM coating, this switch appears to be happening just after 20°C, shown by the increase in droplet size at that point. It is difficult to say if that temperature of the actual polymer film is experiencing a temperature corresponding exactly to the temperature of the stage because there may be a slight thermal lag as the cooling temperature permeates through the glass slide and into the polymer film layer. It is therefore possible that this switch is occurring at a slightly higher temperature, closer to the LCST of free pNIPAM chains in solution. In the case of the shorter DP 25 pNIPAM, coating this upward size trend is not seen, however, if you were to subtract the baseline from the control surfaces (either silane or just glass), then the net effect would be droplet growth. It can therefore be concluded that the thermoresponsive behaviour of both pNIPAM coatings is being seen, however the majority of the droplet growth is being overshadowed by the baseline shrinkage of the droplets, which always occurs over the timescale of the experiment. Overall, the thermoresponsive behaviour of the polymer coated surfaces differs from the control surfaces and the longer pNIPAM coatings exhibit greater thermoresponsive behaviour in all of our experiments. The changes also appear to be occurring in an easily accessible temperature region, which is very promising for the glycoarray applications.

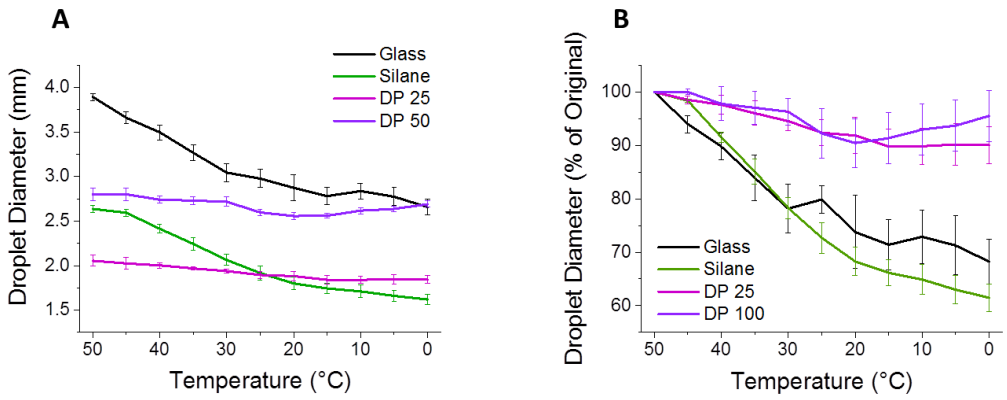

Figure 3.25: Size of water droplets on glass, silane coated glass and pNIPAM DP 25 and DP 100 coated glass, as [A] droplet diameter in mm and [B] droplet diameter relative to the starting diameter, with temperature (also correlating to time, 5°C = 1 min) along the *x*-axis. Measurements were taken every 2 minutes, with the first at a temperature of 50°C (time = 0 min) and the final image at 0°C (time = 10 minutes) and a cooling rate of 5°C.min^{-1}

3.3.6. QCM-D Studies into Gold-Polymer Binding

3.3.6.1. POEGMA Binding with and without the RAFT End Group

Self-assembly of thiol-containing species onto gold substrates is a commonly used technique, producing covalently bound monolayers, referred to as self-assembled monolayers (SAMs) and there are examples of RAFT polymer immobilisation onto gold.[37] However, these gold based systems are unsuitable for microarray applications because the gold surfaces are incompatible with the fluorescence scanners. Additionally, gold surfaces are costly and therefore less applicable to real-world diagnostic and sensor applications than the low cost and readily available glass slides. There is, however, great benefit in carrying out control experiments on gold surfaces in order to compare the assembly of thiolated polymer species onto gold surfaces with their thiol-ene grafting onto acrylated silicon.

One method for doing this is through the use of Quartz Crystal Microbalance with Dissipation (QCM-D), which allows us to monitor the addition of thiol containing species (in our case RAFT-synthesised pOEGMA and pNIPAM) to the gold surface in real time. The QCM-D monitors the change in frequency (*f*) of the

underlying quartz crystal, with an increase in surface mass represented by a decrease in resonant frequency.[38] At the same time, the dissipation (*D*) of the system is also recorded, providing information on the rigidity of the films or brushes which are being formed. An absorbed layer with a high Δ*D* is said to be soft, whereas a low Δ*D* indicated rigidity.[23]

Initially, we wanted to investigate the how the presence of the RAFT end group, as opposed to the free thiol terminus, affects the ability of the polymers to assemble and bind onto the gold surface, Figure 3.26. It has been known for many years that dithioesters and trithocarbonates can be used as anchoring points for grafting onto gold,[37] however, we were interested to see how this would work with the pOEGMA polymers and how the rate of binding and subsequent total mass of polymer bound would differ for the two different approaches.

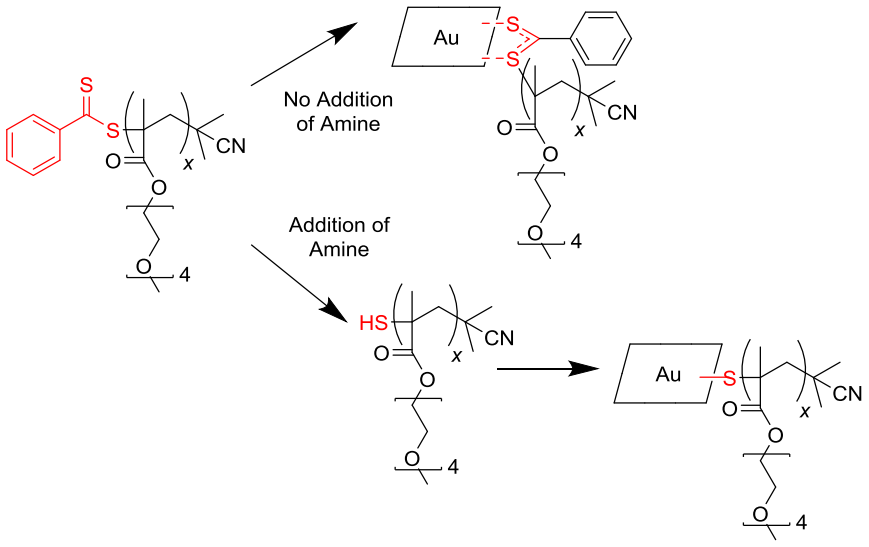

Figure 3.26: Self-assembly of pOEGMA polymers onto a gold surface *via* the dithioester RAFT end group (top) or free thiol end group (bottom)

We initially began with the addition of low molecular weight pOEGMA, which had not been exposed to any amine and therefore, as confirmed by ^{1}H NMR, still retained RAFT end groups. An annotated plot obtained for the DP 25 pOEGMA polymer is seen in Figure 3.27. Immediately prior to each experiment the gold QCM sensors were cleaned using the piranha cleaning procedure detailed in Chapter Two. Once in the machine the surfaces were exposed to Milli-Q water at a flow rate of 200 $\mu L.min^{-1}$ until the sensors' resonant frequencies equilibrated for at least 30 minutes. The measurement was then restarted, in order to prevent a large initial baseline from being displayed and solution changed to the polymer in question (2 $mg.mL^{-1}$ in water) and this was flowed over until a new equilibrium was reached. Then the flowing solution was changed back to water, in order to remove any unbound polymer which was just sat on the surface or entangled within the bound chains. A concentration of 2 $mg.mL^{-1}$ was chosen as this was seen to be significantly concentrated enough to result in adsorption. The experiments were carried out at 30°C. This temperature was chosen because it lies below the critical point for pOEGMA and pNIPAM and will therefore maximise adsorption, without causing phase separation and ensures that the changes in frequency are due to conjugation rather than non-specific deposition of chains onto the surface. Additionally, the temperature of the room frequently surpassed 30°C and it is experimentally beneficial to keep the measurement chamber and solution liquid at approximately the same temperature (±2°C). It is also important not to set the measurement chamber temperature higher than the sample liquid temperature or bubbles may form in the inlet tubing and/or chamber.

The data in Figure 3.27 shows that as the polymer binds to the surface the frequency begins to decrease, which is to be expected because there is increased mass present on the surface. It is, however, important to also take into account the frequency change upon switching back to a water flowing solution. This increase in frequency shows that a significant proportion of the original frequency change can be attributed to unbound polymer chains, which are then washed away from the surface. Failure to collect data for the removal of unbound polymer can lead to incorrectly high mass calculations. The data is displayed showing the 7^{th}, 9^{th} and 11^{th} frequency harmonics, with their corresponding dissipation harmonics. The QCM software presents the data showing all harmonics between 1 and 13 (odd numbers only), however for clarity only three are displayed in this report. The fundamental (first) harmonic is typically disregarded due to a poorer signal: noise ratio and the seventh overtone is often chosen because it avoids the adverse effects due to energy trapping found in the lower harmonics and the interference of anharmonic sidebands found in the high harmonics.[39] For this work harmonics 7, 9 and 11 were chosen as a good representative sample. Presenting the data with more than one overtone displayed is highly beneficial as the spreading of the harmonics provides information regarding the rigidity of the films and the validity of the modelling systems. When the harmonics remain closely packed, as is the case in our system, a rigid film is present and the Sauerbrey equation may be used to obtain mass values from the frequency shifts. The low dissipation change also suggests that the polymers are producing a rigid film which fully couples to the sensor.[38]

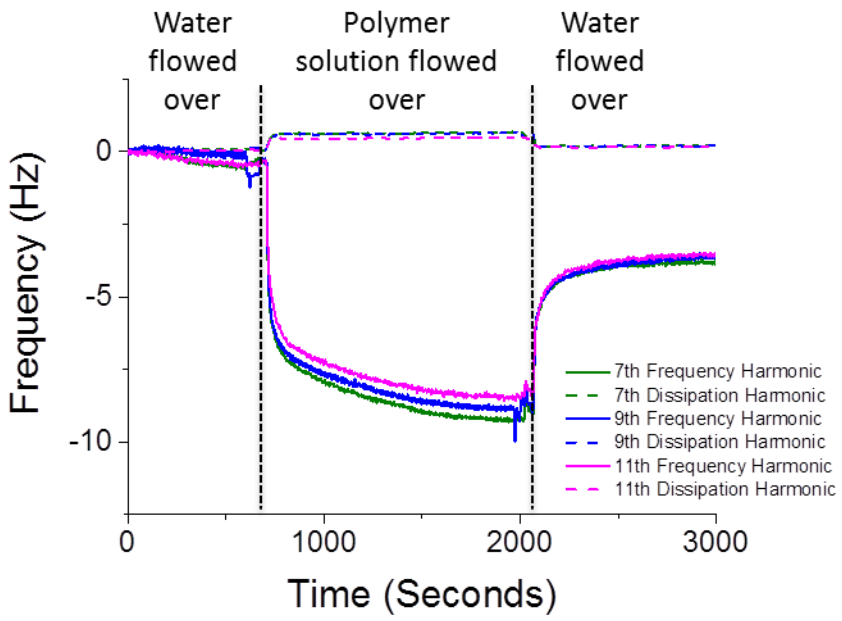

Figure 3.27: QCM trace for the grafting of DP 25 pOEGMA, without cleavage of the RAFT end group, to the gold surface of the QCM chip. The frequency and dissipation changes associated with the polymer binding and removal of unbound polymer are shown

It was proposed that the larger polymers would induce a large change in the frequency, due to the increased mass of their individual chains. Therefore the DP 50 and 100 pOEGMA polymers were tested using the same conditions. The results, shown in Figure 3.28, disprove this hypothesis. Although the binding of the DP 50 polymer produces a slightly larger frequency shift, the data for the largest (DP 100) sample exhibits no greater mass change than for the smallest. Combined with the increase in the mass of each individual chain, this shows that fewer chains of the larger polymers are binding that for the smaller polymers. Overall, the frequency changes for each sample and therefore the mass bound to the surface is seen to be very low.

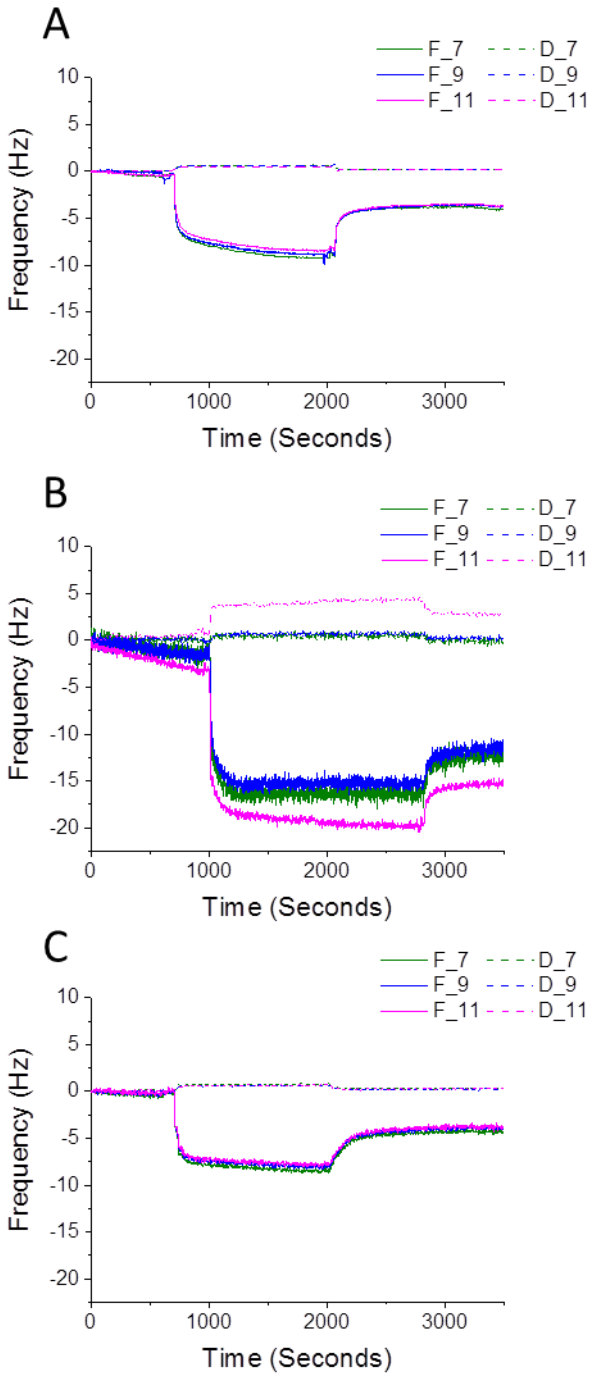

Figure 3.28: Typical QCM-D traces for the addition of pOEGMA polymers to the cleaned gold surface, without the removal of the RAFT end group. [A] pOEGMA DP 25, [B] pOEGMA DP 50, [C] pOEGMA DP 10

For adsorbed films with only small ΔD values the adsorbed mass is proportional to the change in frequency and the Sauerbrey equation, shown below, may be applied. This relationship states that the frequency shift of a quartz crystal resonator is directly proportional to the added mass. Δf_n is the

change in frequency associated with overtone n, C is the mass sensitivity constant (C = 17.7 ng.cm^{-2}.Hz^{-1} at 5 MHz) and *n* is the overtone number (i.e. 1,3,5,7 etc.). Using this formula it is possible to calculate the adsorbed mass value for different overtones in the same experiment and also compare the adsorbed mass for different experiments. The result of converting frequency change into Sauerbrey mass for the binding of the DP 25 pOEGMA is seen in Figure 3.29. As the time increases the mass bound to the surface increases, and then reduces again when the unbound chains are washed away.

$$\Delta m = \frac{-\,\mathrm{C}\,\Delta f_n}{n}$$

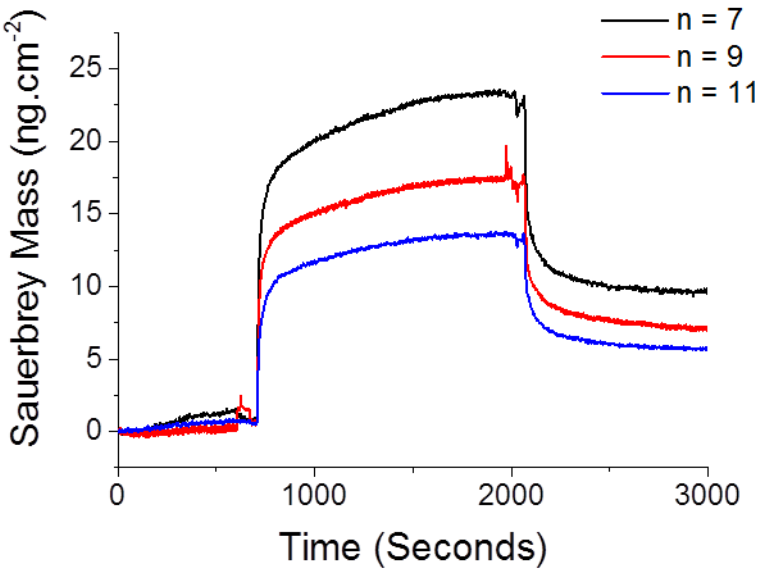

Figure 3.29: Sauerbrey mass corresponding to the frequency changes shown in Figure 3.27 for the binding of pOEGMA DP 25 onto gold with respect to time. Each line represents a different overtone (7, 9 11)

To see if the cleavage of the RAFT end group to a free thiol can increase the polymer binding, the experiments were repeated but with the addition of 1 drop of ethanolamine into the polymer solution 30 minutes prior

to the experiment, to cleave the RAFT end group. As can be seen in Figure 3.30, this was not the case. Rather than increasing the binding, the addition of the amine resulted in no overall mass binding at all. Again, the importance of continuing the experiments to include a washing step is seen, if the experiment had been stopped after the second baseline was observed than a misleading mass change would be concluded. It is proposed that the amine may be binding to the gold preferentially over the polymers; however this overall mass may not be observed as it is below the detection limits and therefore the overall frequency change is displayed as being zero. The initial decrease in frequency when changing from water to the polymer and amine solution most likely due to the change in solution properties, we observe similar changes whenever the solvent is changed (water to buffer for example) despite no mass binding occurring.

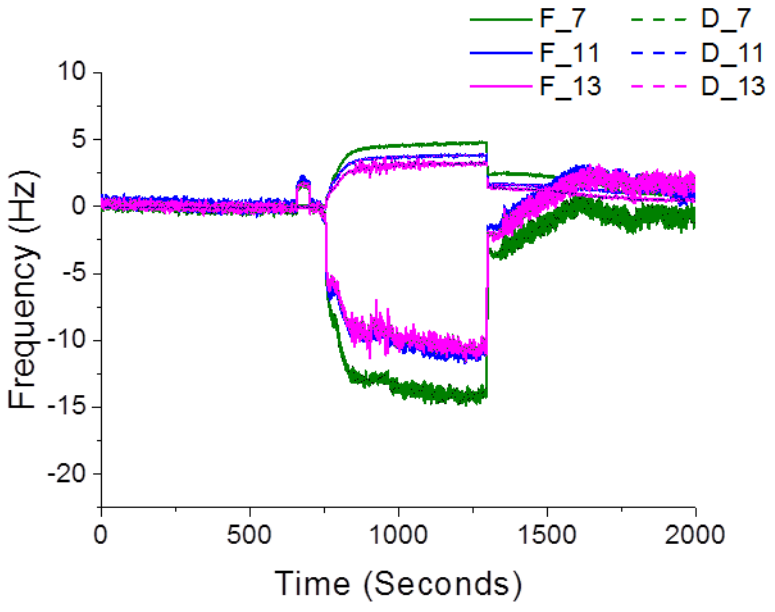

Figure 3.30: Typical QCM trace for the addition of free-thiol terminated pOEGMA polymers onto the cleaned gold surfaces. This data is for the DP 50 system, however similar data was observed for all polymer samples

There are literature reports of the restructuring of grafted polymer chains when observed by QCM. These reports state that as the density of chains increases the transition from the "pancake" to "brush" chain conformations can be observed. Previous work has demonstrated that, due to the balance between segment-segment repulsion and the elasticity of the chains, a conformational change occurs after around 10 minutes of polymer flow.[40] To investigate if this change was occurring within our system, long timescale experiments were run, a typical plot of which is shown in Figure 3.31. The results demonstrated that no significant re-ordering is occurring in our systems, the initial frequency decrease occurs swiftly, as expected, and then the frequency remains relatively stable for the remainder for the 62.5 hour experiment. The small deviations are most likely due to temperature changes that occur overnight and the standard Hertz shift expected from longer measurements. The polymers used in this work are much shorter than those that have been seen to exhibit re-arrangement; it is likely that the shortness of the chains reduces the segment-segment repulsion and steric crowding effects to an extent where brush-like structures form very quickly, without transitioning through the pancake-like state. We therefore do not need to consider the problem of conformational changes occurring in our system.

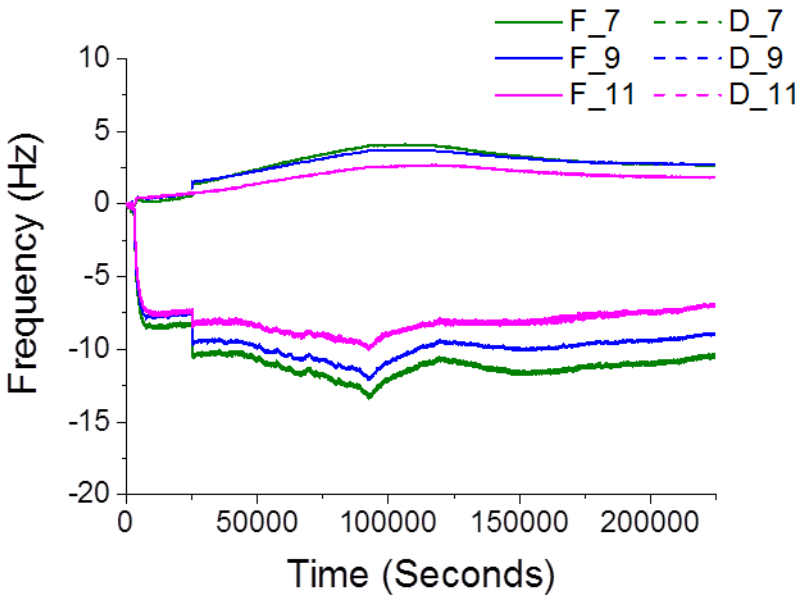

Figure 3.31: Extended (62.5 h) pOEGMA DP 25 binding experiment. Polymer solution is continually flowed over, washing step not shown

3.3.6.2. PNIPAM Binding

A critical comparison between the binding of the pOEGMA polymers and the PNIPAM polymers was required and therefore the QCM-D binding experiments were repeated using solutions of pNIPAM. Pleasingly, these pNIPAM polymers showed much larger frequency shifts when added onto the same gold surfaces under the same experimental conditions. The QCM-D trace for pNIPAM DP 25 is shown in Figure 3.32. As with the pOEGMA results, this trace displays low dissipation shifts and closely packed harmonics, indicating rigid films that are well coupled to the sensor.

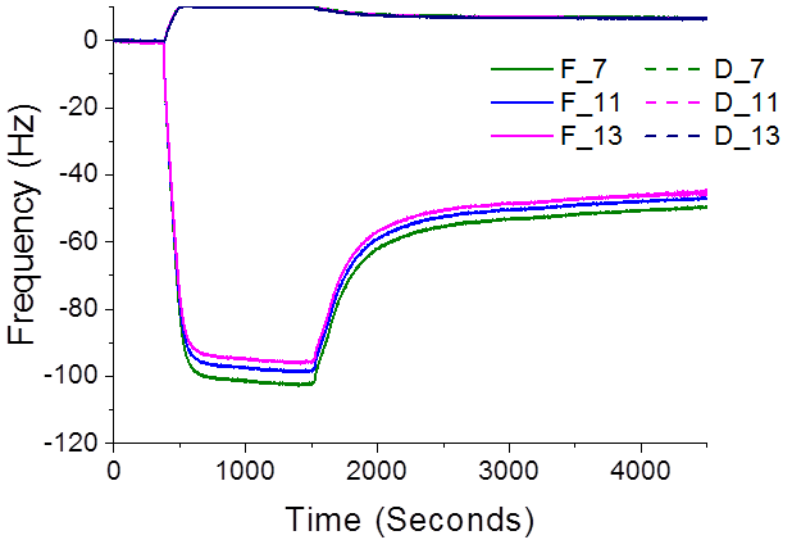

Figure 3.32: QCM trace for the grafting of DP 25 pNIPAM, without addition of amine to cleave of the RAFT end group, to the gold surface of the QCM chip, showing the frequency and dissipation change associated with the binding

In Figure 3.33 typical QCM-D traces obtained from the addition of three different molecular weights of pNIPAM are shown. As with the pOEGMA experiments it was predicted that the frequency shifts would be greater for the larger polymers, however, this was not observed. Interestingly, as the length of polymer chain increased, the frequency shift decreased. The longer polymer chains are more hindered and the ratio of conjugation sites (terminal thiol or terminal RAFT group) to polymer backbone decreases as the chain length increases. The frequency shifts are therefore a balance between the increasing mass of the polymer chains competing with the increasing hindrance towards successful conjugation to the surface and the effects of steric crowding.

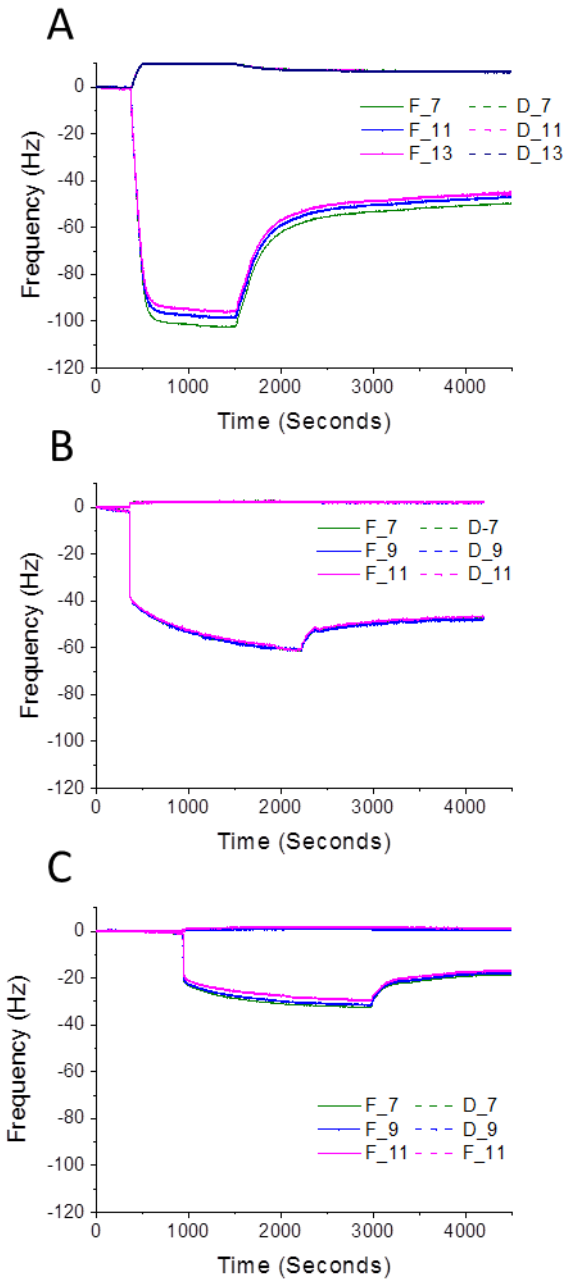

Figure 3.33: Typical QCM-D traces for the addition of pNIPAM polymers to the cleaned gold surface, without addition of amine to facilitate the removal of the RAFT end group. [A] pNIPAM DP 25, [B] pNIPAM DP 50, [C] pNIPAM DP 100

When amine was added into the polymer solution prior to the QCM-D measurement, in order to cleave the RAFT end group and allow surface conjugation via the free thiol-terminus, no net binding of the polymers was observed by QCM-D. The traces typically stabilised, after washing, at a frequency above the original

baseline. Additionally, the traces were seen to be much noisier than for the corresponding amine free samples, Figure 3.34. This data is in agreement with the results obtained for the pOEGMA system.

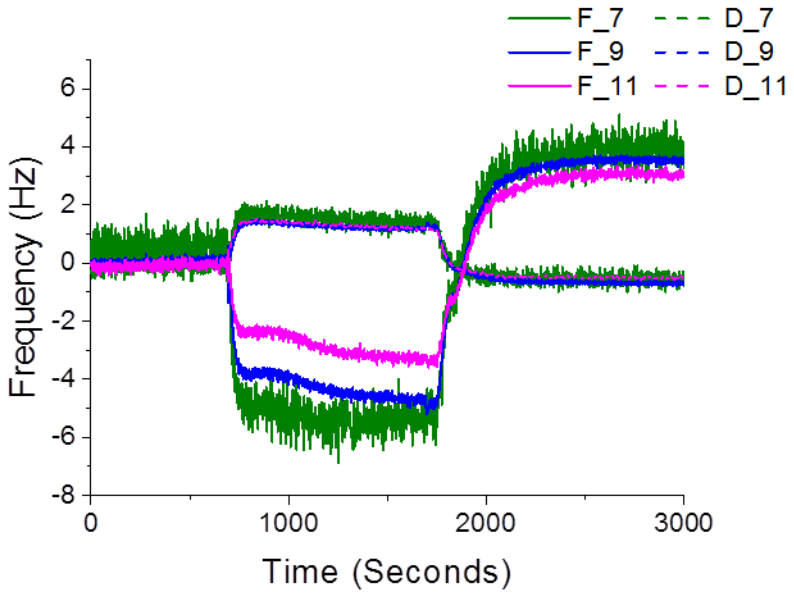

Figure 3.34: Typical QCM trace for the addition of free-thiol terminated pNIPAM polymers onto the cleaned gold surfaces. This data is for the DP 50 system, however similar data was observed for all polymer samples

3.3.6.3. Comparison of the Binding of pNIPAM and pOEGMA

When comparing the binding of pOEGMA and pNIPAM to gold surfaces, as monitored by QCM-D, larger frequency shifts and therefore larger mass changes are observed for the pNIPAM polymers. Figure 3.35A shows binding data for the two different polymers, plotted on the same axis for ease of comparison and Figure 3.35B presents this data when converted to Sauerbrey mass. A summary for each different molecular weight of each polymer, also showing the errors encountered in repeat measurements, is depicted in Figure 3.36. Removing time as an axis and plotting frequency versus dissipation directly (D-*f* plots) can provide information regarding the properties of the polymer films. It allows one to examine the dissipation change per unit adsorbed onto the surface and identify if or when

conformational changes are occurring. If there is a constant linear relationship between ΔD and Δ*f* then the adsorbed polymer is not changing conformation, whereas non-linear trends or sudden points of deviation indicate such changes are occurring.[41] Figure 3.37 depicts this data for all three molecular weights of both pNIPAM and pOEGMA, on the same scale. For the pNIPAM polymers, in each case the addition process is occurring without conformational change and the dissipation changes for the pOEGMA system are too small to suggest any structural changes occurring. The only changes in trend lines are occurring at the point when the rinsing step was commenced and the dissipation and frequency changes are therefore reversed, as is to be expected.

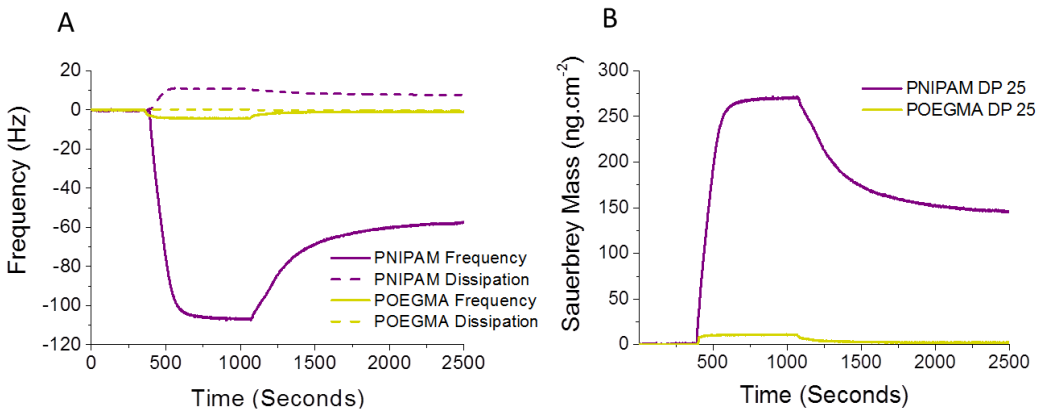

Figure 3.35: [A] QCM-D traces showing the frequency and dissipation changes upon binding of pOEGMA and pNIPAM polymers to the gold surfaces, both for the DP 25 polymers. [B] Sauerbrey mass changes upon binding of pOEGMA and pNIPAM polymers to the gold surfaces, both for the DP 25 polymers

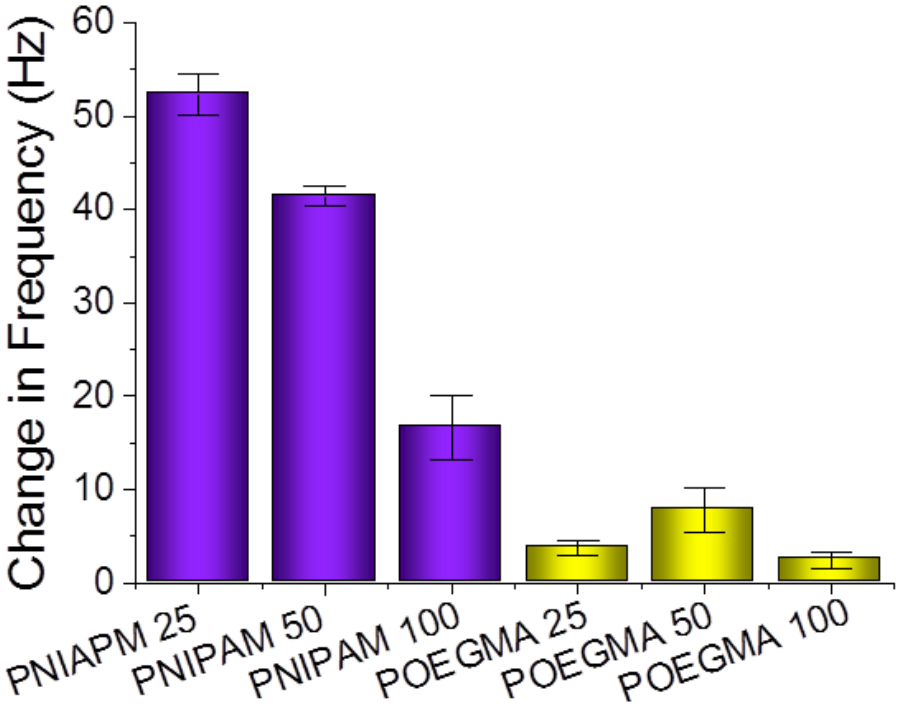

Figure 3.36: Average change in frequency value attributed to the binding of three molecular weights each of pNIPAM and pOEGMA. Data taken from at least three independent repeats for each sample

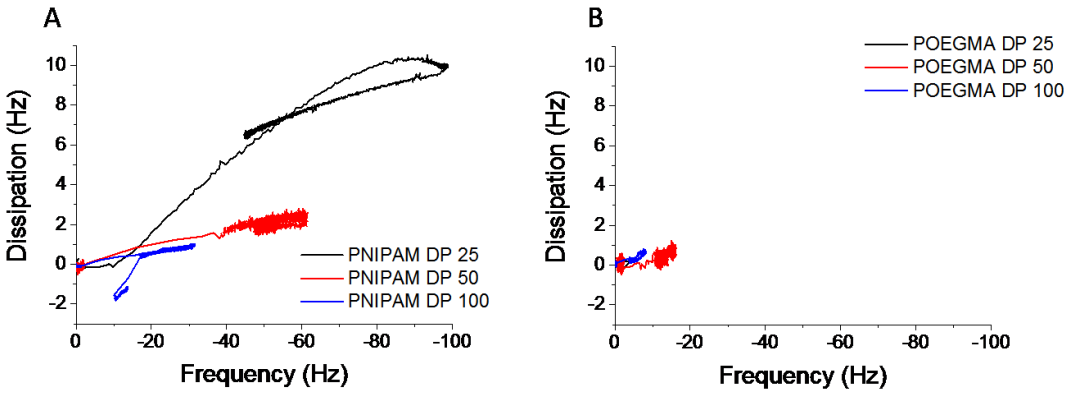

Figure 3.37: Frequency vs dissipation plots for the adsorption of [A] pNIPAM DP 25, 50, 100 and [B] pOEGMA DP 25, 50, 100 onto gold QCM sensors

It is proposed that the differences in binding for the two polymers may be due primarily to steric factors, when you compare the brush structures formed from each polymer, as shown in Figure 3.38, the huge steric bulk of the comb-like pOEGMA is clear and it is reasonable to assume that it will be a hindrance to the grafting of neighbouring polymer chains.

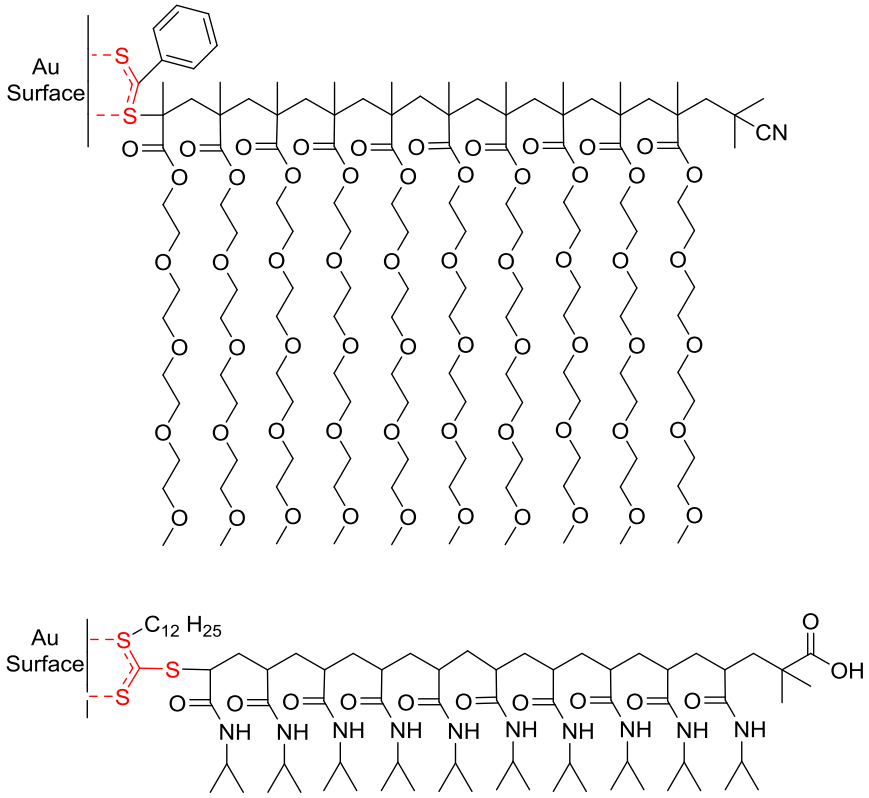

Figure 3.38: Representations of the brushes formed from the addition of pOEGMA (top) and pNIPAM (bottom) polymers onto the gold QCM-D sensors. Only ten repeat units are shown for clarity, but even at these short chain lengths it is clear that the comb-like structure of the pOEGMA will be far more sterically hindering towards the grafting of neighbouring polymer chains

In order to check that the differences in binding were not due to the differences in RAFT end group structure, the addition of just the RAFT agents to the cleaned gold was tested. Typical plots are seen in Figure 3.39. Despite the initial drop in frequency, indicating potential binding, after washing the harmonics returned to a frequency level very close to the baseline and the results for the two different

RAFT agents were seen to be very similar. The DMP RAFT agent does appear to bind slightly better, although the frequency changes were very low and the mass of RAFT agent that bound is at the detection limits for the system. As no significant differences were observed, it can be concluded that the different polymer chain are producing the differences in frequency change, rather than the different RAFT agents.

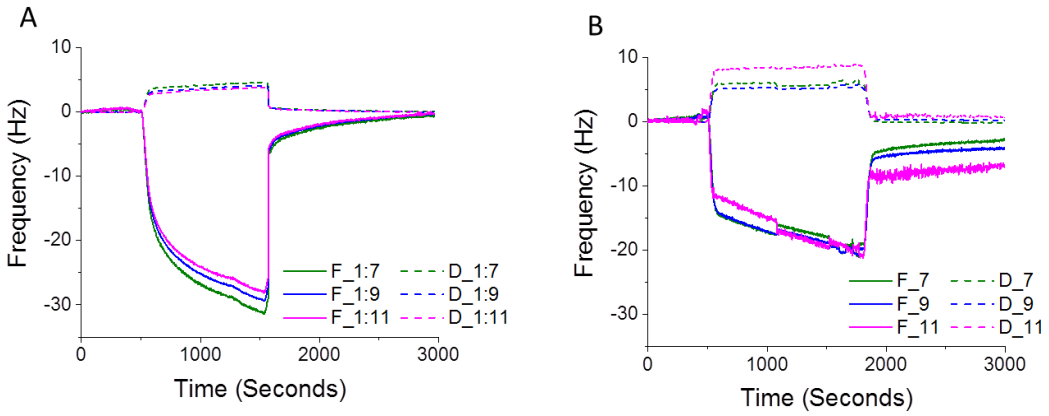

Figure 3.39: Typical QCM-D traces for the addition RAFT agents to the cleaned gold surface [A] CPDB RAFT agent (used to polymerise pOEGMA), [B] DMP RAFT agent (used to polymerise pNIPAM)

3.3.6.4. QCM-D to Demonstrate Thermo-responsive Behaviour

The QCM-D instrument has a temperature change function; therefore the effect of temperature upon the properties of bound polymers could be investigated.[42, 43] The polymer brushes should exhibit the same thermal switching behaviour when surface bound as they have been seen to do in solution (Section 3.3.1.), i.e. below their LCST they should be hydrophilic and fully solvated, then above the LCST they should collapse and release bound water. This should be observed by an increased in frequency, corresponding to a reduction in the mass of the brush layer (grafted polymer and associated bound water molecules).These experiments were carried out with pNIPAM polymer due to previous experiments showing that pNIPAM binds much more effectively to the surface than pOEGMA.

The gold chips were functionalised with the pNIPAM in the QCM-D, any unbound polymer was washed off and the measurement restarted without pausing the flow. This results in the stable baseline, corresponding to the polymer brushes in the water flow, being reset to $f = 0$. The results in Figure 3.40 show the typical frequency changes following on from this measurement reset. As the temperature is reduced the frequency decreases, indicating increased mass, which could be deduced as being due to water binding. The opposite then occurs when the temperature is raised. Whilst this initially appears to be showing the thermoresponsive behaviour of the polymer brushes, when control experiments were carried out on unfunctionalised gold sensors, Figure 3.41, it is seen that these frequency changes occur even when a polymer brush system is not present. These changes are because quartz crystals are affected by variations in temperature and these inherent crystal effects must be discounted prior to investigating the polymer switching behaviour.[39] However, the crystal effects are seen to be affecting Δf to a greater extent that for the polymer brushes. These experiments may suggest that the grafting density of the polymers is too low for LCST behaviour to be observed on these surfaces or that the associated frequency changes are too small to be observed.

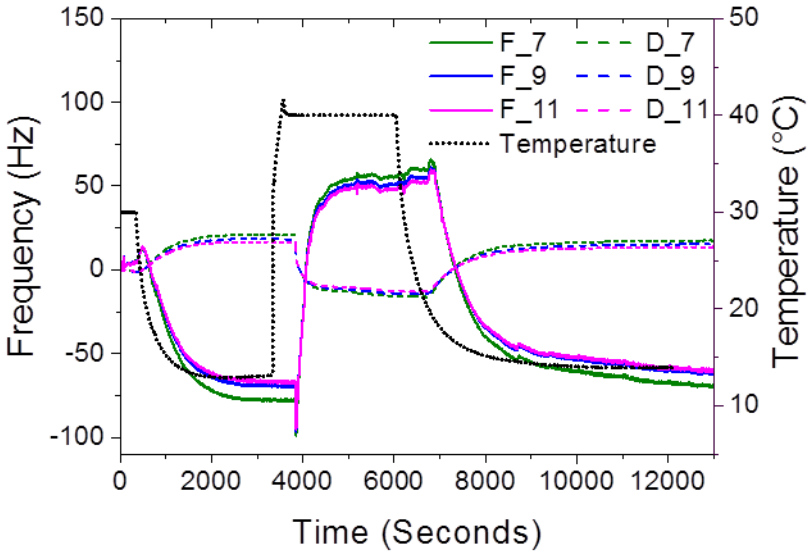

Figure 3.40: Frequency and dissipation shifts for pNIPAM DP 50 adsorbed onto the QCM sensor, with respect to varying temperature. The small drop in *f* seen at approximately 3900 s was caused by a knock to the system

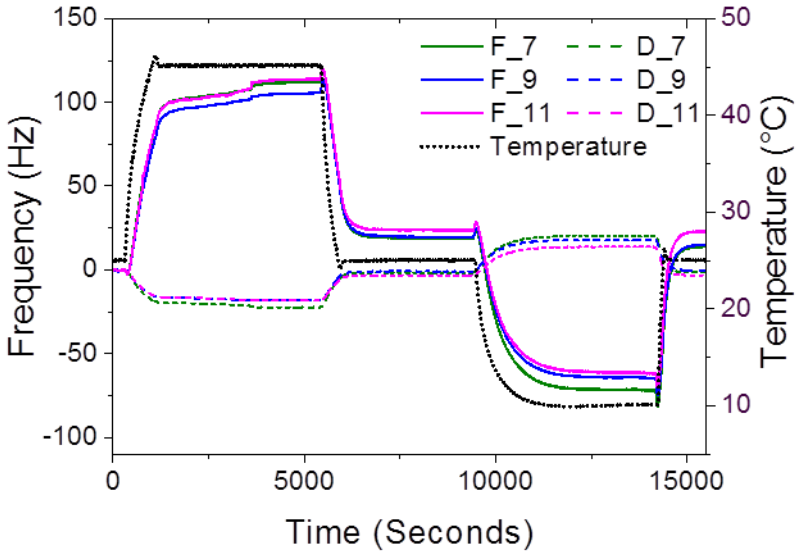

Figure 3.41: Frequency and dissipation shifts for a clean, unfunctionalised gold sensor in the presence of flowing Milli-Q water, with respect to varying temperature

3.3.7. QCM-D Studies into Silicon-Polymer Binding

3.3.7.1. Polymer Binding with and without the Silane Acrylate

Having concluded that the adsorption of pNIPAM onto gold resulted in much greater Δf values than for pOEGMA and that the smaller chain lengths of polymer resulted in greater Δf values than for their longer chain counterparts, it was decided to see if these finding were consistent with our SiO_2 surfaces and silane acrylate coatings. Silicon coated QCM sensors were purchased in order to more directly compare the gold QCM-D work to the previous surface analysis obtained on the silicon wafers. Firstly, a control experiment was carried out. Polymer solutions were flowed over the cleaned silicon sensors, in the same manner that the polymer solutions were added to the cleaned gold sensors. The data for the addition of pNIPAM DP 25 and 50 is seen in Figure 3.42. Although an initial sharp Δf is observed in both cases when the polymer is flowed over, when the solution is reverted to water this change is reversed and the frequency shifts back to the original baseline at 0 Hz. This confirms that no polymer is adsorbing onto the SiO_2, providing a negative control.

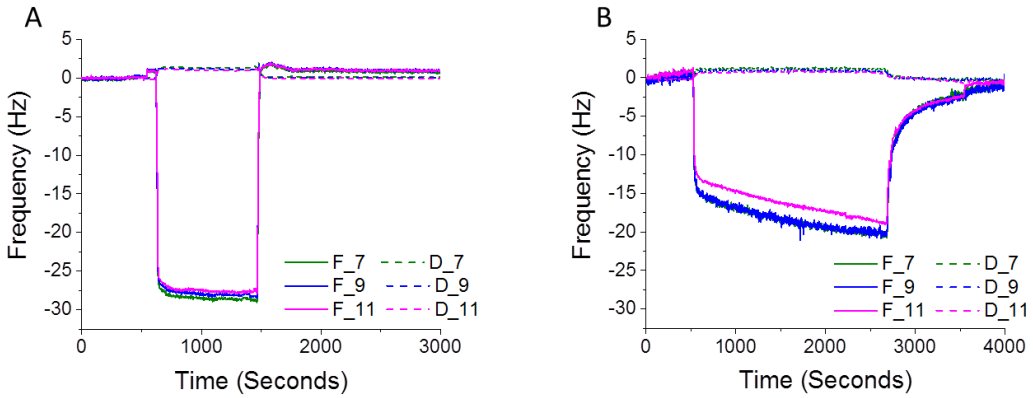

Figure 3.42: Flowing over [A] pNIPAM DP 25 and [B] pNIPAM DP 100 onto cleaned silicon QCM wafers, without silane acrylate coatings

Having confirmed that the native SiO_2 is not receptive to pNIPAM adsorption, the silane acrylate system was investigated. The silicon sensors were silanated outside of the QCM-D apparatus, following the procedure described in Section 2.6.5. and then subjected to the same polymer flowing conditions as used for the gold sensors. As can be seen in Figure 3.43, the initial Δf upon flowing of the polymer solution is comparable to the results for the unsilanated sensors (Figure 3.43). However, this is where the similarities end, after the washing step has been completed, the frequency stabilises at approximately 15 Hz, compared to 0 Hz for the native silicon surfaces. Therefore, we can conclude that polymer mass has added onto the silane surface and that it remains bound during the washing step. A D-f plot for the adsorption of pNIPAM onto the silane coated silicon is shown in Figure 3.44. The change in the gradient of the plot for the longer chain (DP 100) pNIPAM suggests that there is some small surface conformational rearrangement occurring at the higher grafting density, this could however be attributed to changes in polymer hydration. For the shorter chains, the linear relationship suggests that no rearrangement is occurring during the addition.

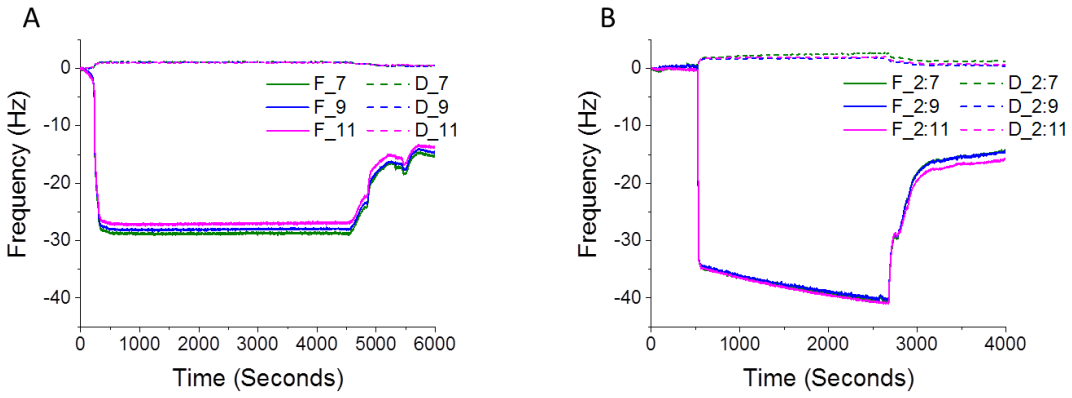

Figure 3.43: Frequency shifts obtained from the adsorption of [A] pNIPAM DP 25 and [B] pNIPAM DP 100 onto silanated silicon QCM wafers

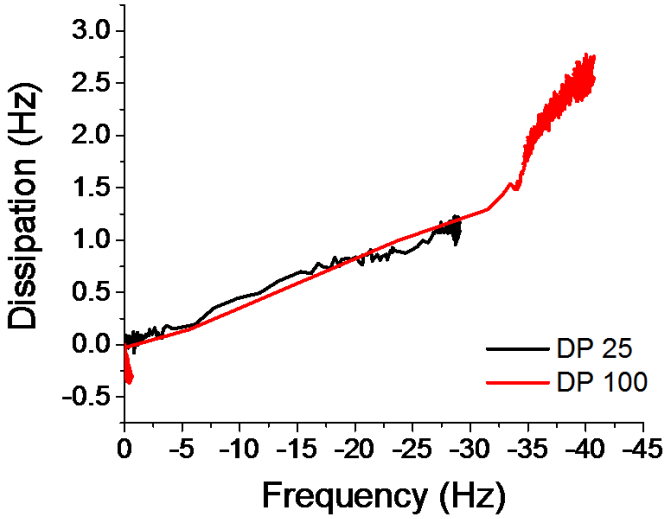

Figure 3.44: Frequency *vs* dissipation plots for the adsorption of pNIPAM DP 25 and pNIPAM DP 100 onto acrylate silane coated QCM wafers

A summary of the differences in addition of the polymers with and without the silane acrylate, with respect to Sauerbrey mass, is shown in Figure 3.45. The Sauerbrey mass with respect to time for the binding of pNIPAM onto the silane coated silicon is shown in red and the addition without the silane is shown in blue. The data concludes that the net mass bound in the absence of the silane acrylate is negligible and that mass addition does occur when the silane acrylate is in place.

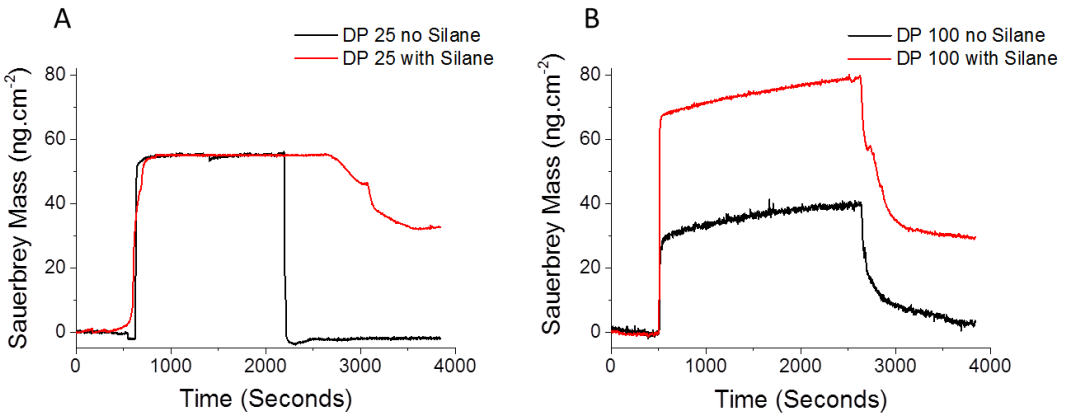

Figure 3.45: Sauerbrey mass values obtained from the adsorption of [A] pNIPAM DP 25 and [B] pNIPAM DP 100 onto both silanated and native (not silanated) silicon QCM wafers

The graph in Figure 3.46 summarises the data for the four different systems (DP 25 and 100 pNIPAM onto native and silanated silicon). When comparing this data to the frequency changes for the assembly of the polymers directly onto the gold QCM sensors (Figure 3.36), the frequency shifts are smaller for these silicon wafers, but the differences in binding between the different chain lengths are no longer seen. This suggests that the silane acrylate may be acting to circumvent some of the steric crowding issues that occurred with the direct assembly onto gold. This is advantageous as the longer chain polymers exhibit greater non-fouling and thermoresponsive behaviour (Section 3.3.4.) and it is therefore very pleasing to see that these more desirable longer chains bind equally efficiently to our silane coated silicon.

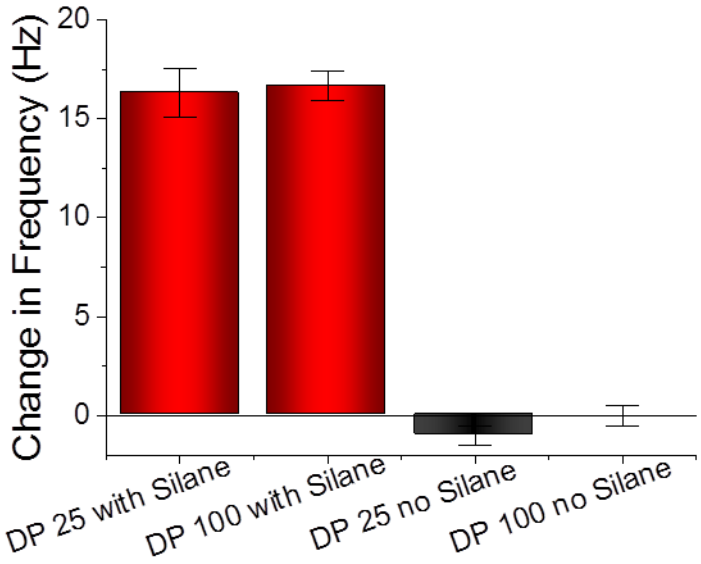

Figure 3.46: Average change in frequency attributed to the binding of two molecular weights of pNIPAM onto native SiO_2 and silane coated SiO_2. Data taken from at least two independent repeats for each sample

3.3.7.2. Static Silicon QCM-D measurements

The QCM-D apparatus can be used to obtain static data, in addition to using the pumped flow function. In this case, samples are placed into the chamber and the frequency shift for each sample, at each overtone is recorded. The samples are then functionalised outside the chamber, before being retested. The graph in Figure 3.36A shows this data plotted for a chemically cleaned and silanated sensor, from which the change in frequency value is untraceable. However, when the *x*-axis is expanded (Figure 3.47B) it can be seen that a frequency shift of around 600 Hz has occurred. The data in Figure 3.48 shows the frequency shifts resulting from the silanation of three separate sensors, with the 7^{th}, 9^{th} and 11^{th} resonance (overtone) included. As is to be expected, the frequency change increases with increasing overtone number, which is why the Sauerbrey equation includes the overtone number, n, as a denominator. When the equation is applied, the Sauerbrey mass for each sensor (Figure 3.48B) is much more similar. The values, however, are very large and would correspond to a mass of approximately 0.65 ng.sensor^{-1} and therefore a silane thickness of approximately 800 nm. These values are much larger than we found by both ellipsometry and XPS and when compared to the thin film colour chart in Figure 3.49, seem to be an unrealistic answer. Our sensors (when the thin oxide layer substrates are used) still appear grey-brown after functionalisation, corresponding to thicknesses of $\leq$ 8 nm, whereas 800 nm films would appear magenta. These static measurements therefore have value in confirming the functionalisation of the surfaces, by exhibiting mass addition, however extensive extraction of data from the frequency shifts

should be avoided due to the number of approximations required in each step reducing the validity of the conclusions.

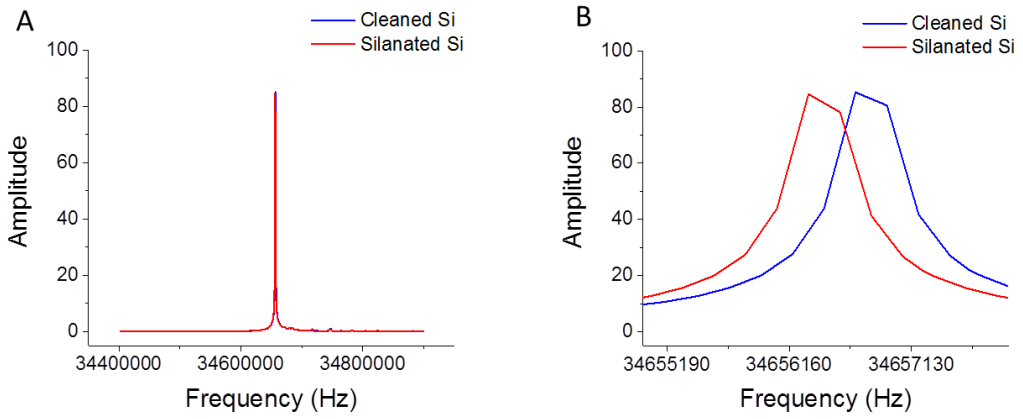

Figure 3.47: Static frequency *vs* amplitude plots for silicon QCM sensors, [A] shows the sweep obtained from Q-Soft package, with the peak frequency obtained for the cleaned silicon sensor and silane coated silicon sensor appearing to overlay, whereas [B] shows that the difference in peak frequency is visible when viewed on a small section of the *x*-axis

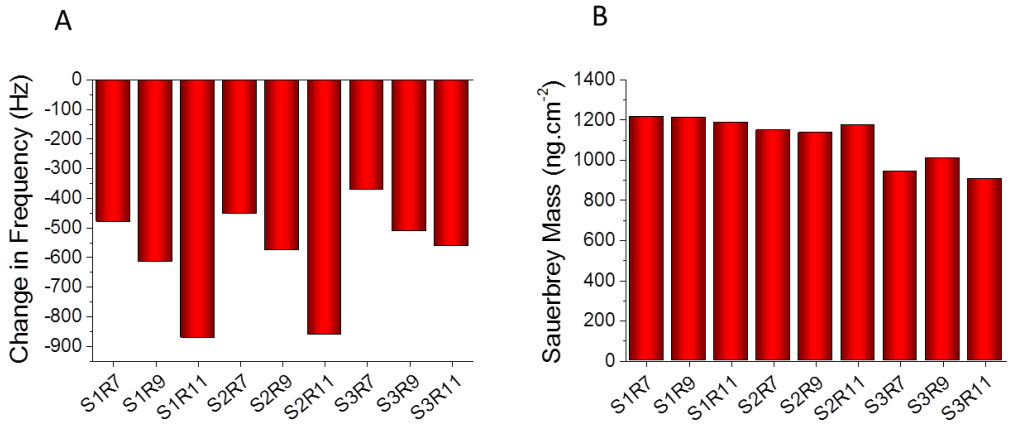

Figure 3.48: [A] Frequency change upon addition of the silane coating to the cleaned silicon sensor, data is shown for overtones 7 to 11 for three different sensors. [B] Sauerbrey masses calculated from the change in frequency for each sensor at overtones 7, 9 and 11

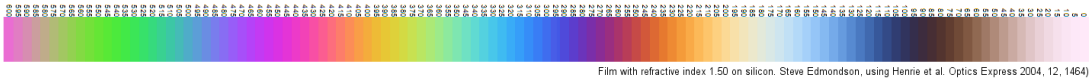

Figure 3.49: Thin film colours on silicon wafers (for a refractive index of 1.50), image designed by Dr. Steve Edmondson, based on the work of Henrie[44]

3.4. Conclusions

Polymers of poly(oligo(ethylene glycol) methyl ether methacrylate) (pOEGMA) and poly(*N*-isopropylacrylamide) (pNIPAM), were successfully synthesised using the RAFT controlled radical polymerisation technique. These polymers were then grafted to glass, silicon and gold substrates, to form brush-like coatings. The use of an alkene terminated silane coating allowed the successful chemisorption of the polymers onto the glass and silicon and the inherent reactivity of thiol groups with gold facilitated the gold surface functionalisation.

Analysis of the surfaces using DSA, ellipsometry, XPS and QCM-D confirmed that successful surface functionalisation had occurred. In addition to probing the nature of the surface coatings it was also found that the pNIPAMs exhibit significantly greater binding to both glass/silicon than the corresponding pOEGMAs. Investigations into the non-fouling and thermoresponsive behaviour indicated that the longer chain pNIPAMs exhibit both of these desirable properties more significantly than the shorter pNIPAMs, both of which are exhibiting these characteristics more than the pOEGMAs. Although the QCM-D experiments suggested that the shorter chain pNIPAMs bound more effectively to the gold surfaces, when the silicon surfaces were probed, this difference was not seen. Equally, it was not seen by XPS.

We can therefore conclude that a surface (glass/silicon) functionalised with the silane acrylate and then with the longer chain pNIPAMs will be very appropriate for the smart microarray applications we will explore in Chapter

Four. These coatings have been seen to exhibit effective polymer binding, good fouling-resistance and potential thermal switching behaviour, within an experimentally obtainable temperature range.

3.5. Materials and Methods

3.5.1. General Experimental

All reagents and solvents were used as received from the supplier. Laboratory solvents were purchased from Fisher Scientific and 3-(trimethoxysilyl)propyl acrylate from Sigma-Aldrich. Microscope slides were purchased from Fisher Scientific (ground edges, 76 mm x 26 mm, 1.0 mm to 1.2 mm thick) and silicon wafers from IDB Technologies (kindly donated by the Macpherson Group (University of Warwick)) with a resistivity of 1-10 Ω. QCM-D sensors were purchased from Q-Sense.

Phosphate-buffered saline (PBS) solution was prepared by dissolving a pre-formulated tablet (Sigma-Aldrich) in 200 mL ultra-high quality water. The resulting PBS solution has a composition of 0.01 M phosphate, 0.0027 M potassium chloride and 0.138 M sodium chloride, pH 7.4. 10 mmol HEPES buffer, containing 0.1 mmol $CaCl_2$, pH 6.5, was prepared in 250 mL ultra-high quality water. Fluorescently labelled lectins (PNA, Con A) from Vector Labs (Fluorescein FLK-2100 labelled) Mesitylene (analytical standard) PEG 300 oligo(ethylene glycol) methyl ether methacrylate (95.0%), and *N*,*N*-dimethylacrylamide (99.0%) were purchased from Sigma-Aldrich.

Any waste thiol solutions were treated with sulfide oxidiser microemulsion solution (3% cyclohexane, 5% sodium dodecyl sulfate, 10% butan-1-ol and 82% water by weight) to kill the thiol smell. 1 ml of sulfide was dissolved in 15 ml of

microemulsion and 5% aqueous sodium hypochlorite solution was then added in 2-fold excess. Thiol contaminated glassware was soaked in sulfide oxidiser microemulsion and 5% aqueous sodium hypochlorite solution prior to washing.

3.5.1.1. Nuclear Magnetic Resonance Spectroscopy

All NMR spectra were obtained using a Bruker DPX-300 (300 MHz) or DPX-400 (400 MHz) spectrometer. The deuterated solvents were used as supplied by Aldrich. Chemical shifts were recorded as δ values in parts per million (ppm) and referenced to the solvent used.

3.5.1.2. Size Exclusion Chromatography

SEC analysis was performed on a Varian 390-LC MDS at 30°C. The system is equipped with a PL-AS RT/MT autosampler, a PL-gel 3 μm (50 × 7.5 mm) guard column and two PL-gel 5 μm (300 × 7.5 mm) mixed-D columns. Detection is achieved using a differential refractive index and a Shimadzu SPD-M20A diode array detector. The eluent was a solution of dimethylformamide (DMF) with 1 $mg.mL^{-1}$ lithium bromide and the flow rate was set to 1.0 $mL.min^{-1}$. Data analysis was carried out on Cirrus 3.2 SEC software. The molecular weight calculations were carried out against narrow molecular weight PMMA standards (200 - 1.0×10^6 $g.mol^{-1}$).

3.5.1.3. Cloud Point Measurements (Turbidimetric Analysis)

The thermal transitions were measured using an Agilent Technologies Cary60 UV/Vis spectrometer equipped with a Quantum Northwest TC1 temperature controller. Samples were heated for 10°C to 90°C at $2°C.min^{-1}$. The polymers are fully solubilised at the starting temperature, resulting in near perfect optical transmittance at 650 nm. Upon approaching the LCST, the

polymer solutions turn opaque and the cloud point is measured as the temperature at which 50% of the original transmittance is lost.

3.5.1.4. Infrared Spectroscopy

IR spectra were collected on a Bruker Alpha Platinum-ATR spectrometer. A total of 64 scans were taken for each sample and all samples were presented in a dry state.

3.5.1.5. Mass Spectrometry

Mass spectra were recorded on a Bruker Esquire2000 TOF machine in positive mode, with ethanol as the sample solvent.

3.5.1.6. Surface Cleaning Procedure

The surfaces used in this work (glass, silicon and gold) were cleaned using piranha solution. The surfaces were placed into a 3:1 (v/v) mixture of 98% sulfuric acid and 30% hydrogen peroxide, on ice, for 10 minutes, then rinsed with deionized water, then ethanol and then further Milli-Q water and blown dry in a gentle stream of dry nitrogen.

Safety Note: Piranha solution is strong oxidizing and is hazardous to prepare and use. It should be handled in small quantities, freshly prepared and never stored. The hydrogen peroxide solution should be slowly added to the acid and the reaction should be carried out on ice. After completion of the piranha cleaning process, the piranha solution should be allowed to cool and then diluted slowly into one litre of deionised water, with 2-3 spoons of MnO_2. After 12 hours this solution can be neutralised with sodium bicarbonate and disposed of appropriately.

3.5.2. General Surface Analysis

3.5.2.1. Contact Angle Measurements

The water contact angle measurements were conducted at room temperature using a Krüss drop shape analysis system DSA100 equipped with a movable sample table and microliter syringe. Deionized water was used as the wetting liquid and the drop size was set to 10 µL. Samples were placed onto the sample table, using tweezers, and aligned within the field of view of the camera. The microliter syringe was advanced until a drop of 10 µL was formed and suspended at the end of the syringe needle. The sample table was then elevated, until the sample touched the bottom of the drop, causing it to detach from the end of the needle and form on the surface. The sample table was the moved back to the original position and an image immediately recorded. The baseline and contact advancing angles were then computated from the image. This process was repeated five times for each sample and the reported values are the average taken from the repeat measurements.

3.5.2.2. Ellipsometry

Ellipsometry measurements were carried out on a Nanofilm auto-nulling imaging ellipsometer with a resolution of 0.001 deg (Delta and Psi) and a relative thickness error 0.001 nm. A 550 nm wavelength light source was used and all measurements were taken using an angle of incidence scan (four-zone) at 50, 60 and 70°.

Firstly a cleaned silicon surface was tested. It was placed upon the sample table, under the alignment laser dot and automatically aligned to be level. Following the set up procedure (setting of Z-height to find the peak area of intensity, rotating the polariser to find the brightest image and calibrating the focus based on a small

contaminant, such as a speck of dust) the an angle of incidence scan was performed. The values of psi and delta for each angle were recorded and inputted into the WVase software. The thickness of the oxide layer present on the Silicon was calculated by adding a "SiO_2" layer (SiO_2 DATA, from Palik HOC Vol. 1, p. 759) into the model and fitting the data to the model, to obtain the thickness. The sample could then be silanated and the process repeated, this time modelling the layer using the "Cauchy" option from within the software. The "Cauchy" option was also used for any further layers added on top of the silane, the thickness of such layers was calculated by subtracting the value previously obtained for the silane away from the total "Cauchy" thickness. Three values for each sample were recorded and the values stated are the average of these repeats and the error bars represent the standard deviation within the measurements. Each value obtained from the software also has an experimental error associated with it and a mean-square error between fitted and measured delta and psi values.

3.5.2.3. X-ray Photoelectron Spectroscopy

The experiments were performed at the Science City Photoemission Facility, University of Warwick, by Dr. Marc Walker. The samples were mounted on to Omicron-style sample plates using electrically-conductive carbon tape and loaded in to the fast-entry chamber. Once the fast-entry chamber had been evacuated to an appropriate pressure, the samples were transferred in to the 12-stage carousel for storage at pressures of less than $1x10^{-10}$ mbar. XPS data were acquired in the main analysis chamber using an Omricron SPHERA analyser (Omicron Nanotechnology, UK). Core level XPS spectra were recorded using a pass energy of 10 eV (0.47 eV resolution), with the sample illuminated using an Omicron XM1000 Al K α x-ray source (h\nu = 1486.6 eV). Analysis of the XPS data was carried out using the

CasaXPS software, using mixed Gaussian-Lorentzian (Voigt) lineshapes and references to the NIST database.[45] The transmission function of the analyser has been carefully determined using clean Au, Ag and Cu foils, whilst the work function of the analyser was determined using the Fermi edge of a polycrystalline Ag sample at regular intervals throughout the experiment, thereby allowing accurate composition and binding energy shifts to be determined. All binding energies have been referenced to the C 1s peak arising from adventitious carbon at 284.6 eV, a necessary correction due to the insulating nature of the oxide termination of the Si substrate.

3.5.2.4. Microarray Scanner

The fluorescence images were obtained using an Agilent G2565CA Scanner capable of one- and two-colour scanning and compatible with glass slide arrays. The scanner is fitted with a 48-slide carousel autoloader and can scan up to 2 μm resolution. Standard two colour scanning protocols were used with a SHG-YAG laser (532 nm) and a helium-neon laser (633 nm). The data was exported as a Tagged Image File (Tif) file and numerical data was then obtained using Agilent Feature Extraction Software. The average fluorescence intensity was taken across the whole sample or whole sample area of interest and the background fluorescence subtracted.

3.5.2.5. Quartz Crystal Microbalance with Dissipation

Gold and silicon dioxide QCM sensors were purchased from Q-Sense. The sensors have a resonant frequency of 4.95 MHz ±50 kHz with a diameter of 14 mm and a surface roughness of $\leq$ 3 nm. The experiments were carried out using a Q-Sense E4 QCM-D instrument with the temperature set to 30°C throughout the experiments using the in-built temperature controller. The surfaces were cleaned

with piranha solution (Section 2.6.1.) prior to use. Should a sensor have been stored between cleaning and testing, it was rinsed (ethanol 2 x 5 mL and water 2 x 5 mL) and dried with nitrogen, immediately prior to usage. Solutions of pOEGMA and pNIPAM (2 $mg.mL^{-1}$in water with and without amine) were prepared and sonicated and thermally equilibrated for 20 minutes prior to the experiment, in order to remove any air from the solutions. The sensors were placed in the chambers and sonicated Milli-Q water was pumped at a rate of 200 $\mu L.min^{-1}$ until the sensors' resonant frequencies equilibrated. The bathing solution was then changed to 2 $mg.mL^{-1}$ of the relevant polymer and allowed to equilibrate, whereupon the solution was changed back to water to remove any polymer simply resting on the surface and the flow was continued until a stable baseline was achieved. At each solution change the pump was stopped and restarted to avoid any air intake to the system. Following the experiment, the system was cleaned (sodium dodecyl sulfate, 2 $mg.mL^{-1}$, followed by water, both pumped over at maximum speed for 10 minutes each) in order to remove any remaining traces of unbound polymer. The sensors were washed with water and dried with nitrogen, then stored in their original boxes until they were cleaned for use in a further experiment.

The thermoresponsive measurements were carried out in the same way, however rather than keeping the temperature 30°C throughout the experiment; it was varied using the in-built temperature control software.

The silicon sensors were placed into the QCM-D machine either in their native state (chemically cleaned silicon dioxide surface) or having been previously functionalised with silane (Section 3.5.4.). The experiments were then carried out as for the gold sensors.

The static measurement were obtained by placing the cleaned sensors into the measurement chambers, without turning on the pump or adding any flow solution, and then performing a frequency sweep. The resulting frequency values were then plotted against their amplitude in order to deduce the maximum frequency obtained for each overtone. The process was then repeated with functionalised sensors and the differences in frequency value for each overtone compared.

3.5.3. Polymerisations

3.5.3.1. Synthesis Poly(oligo(ethylene glycol) methyl ether methacrylate)s

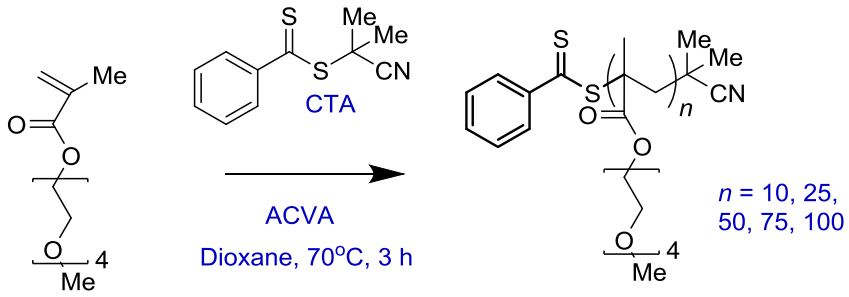

To a solution of PEG 300 oligo(ethylene glycol) methyl ether methacrylate OEGMA (1.29 mL, 4.5 mmol) and CPBD (100 mg, 0.45 mmol) in dioxane (7 mL) was added ACVA (25.2 mg, 0.09 mmol). Further polymerisation solutions were prepared, as detailed in Table 3.6. The solutions were degassed with nitrogen, immersed into an oil bath (70°C) for three hours then opened and cooled on ice. Each solution was concentrated, precipitated into petroleum ether (35 mL) and re-precipitated from THF into ether twice. The resulting pink waxy polymers were dried overnight in a vacuum oven.

Table 3.6: Polymerisation reagent compositions for the synthesis of pOEGMAs

Theoretical Degree of Polymerisation [M]:[CTA]		Initiator (ACVA)	RAFT Agent (CPBD)	Monomer (OEGMA 300)
10:1	Ratio	0.2	1	10
	Moles/ mmol	0.09	0.45	4.5
	Mass/ mg	25.2	100	1.35×10^3
25:1	Ratio	0.2	1	25
	Moles/ mmol	0.036	0.18	4.5
	Mass/ mg	10.09	39.78	1.35×10^3
50:1	Ratio	0.2	1	50
	Moles/ mmol	0.018	0.09	4.5
	Mass/ mg	5.045	19.89	1.35×10^3
100:1	Ratio	0.2	1	100
	Moles/ mmol	0.009	0.045	4.5
	Mass/ mg	2.52	9.95	1.35×10^3

The polymers were characterised by ^{1}H NMR spectroscopy. The degree of polymerisation was also determined by ^{1}H NMR spectroscopy by calculating the ratio of side chain methyl (δ_{ppm} 3.25-3.40) to aromatic protons (δ_{ppm} 7.20- 7.95). Analysis was also carried out by DMF SEC against PMMA standard. The characterisation data is summarised in Table 3.1.

3.5.3.2. Synthesis of 2-(dodecylthiocarbonothioylthio)-2-methylpropanoic acid

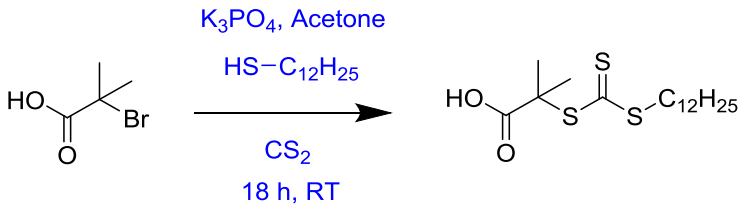

The method previously published by the Gibson group was followed.[46] To a stirred suspension of K_3PO_4 (4.20g, 19.76 mmol) in acetone (60 mL) was added dodecanethiol (4.00 g, 19.76 mmol) dropwise over 25 minutes. CS_2 (4.10 g, 53.85 mmol) was added and stirred for 10 minutes; the solution turned bright yellow. 2-bromo-2-methylpropionic acid (3.00 g, 17.96 mmol) was added; a precipitation of KBr was noted. The reaction was stirred for 18 hours and then the solvent was removed under reduced pressure and the residue was extracted into CH_2Cl_2 (2 x 200 mL) from 1M HCl (200 mL). The organic layer was washed with water (200 mL) and brine (200 mL) then dried over $MgSO_4$. The solvent was removed under reduced pressure to yield the crude product. Purification was carried out by column chromatography on silica (eluting with 75:24:1 40 – 60°C petroleum ether: diethyl ether: acetic acid) to yield a bright yellow solid (4.20 g, 64%).

^{1}H NMR (300 MHz, $CDCl_3$) δ_{ppm}: 3.20 (2H, t, S-C**H**$_2$-$(CH_2)_{10}$- CH_3); 1.66 (6H, s, C-(CH_3)$_2$); 1.60 (2H, p, S-CH_2-C**H**$_2$-$(CH_2)_9$-CH_3); 1.31 (2H, m, S-CH_2-CH_2-C**H**$_2$-$(CH_2)_8$-CH_3); 1.25-1.15 (16H, m, S-CH_2-CH_2-CH_2-$(CH_2)_8$-CH_3); 0.82 (3H, t S-CH_2-$(CH_2)_{10}$- C**H**$_3$).

^{13}C NMR (125 MHz, $CDCl_3$) δ_{ppm}: 220.90 (S-(**C**=S)-S), 177.15 (HO-(**C**=O)-C), 55.45 (O=C-(**C**-$(CH_3)_2$-S), 37.10 (S-**C**H_2-CH_2), 31.94, 29.71, 29.64, 29.58, 29.46, 29.30, 29.11, 22.70 (S-CH_2-CH_2-CH_2-(**C**H_2)$_8$-CH_3), 28.97 (S-CH_2-CH_2-

CH_2-($CH_{2)8}$-CH_3), 27.81 (S-CH_2-**C**H_2-CH_2-), 25.26 (C-(C**H**$_3)_2$), 14.15 (S-($CH_{2)11}$-**C**H_3).

IR cm^{-1}: 2955 (alkyl-H stretch); 1712 (C=O stretch), 1069 (S-(C=S)-S) stretch).

MS (ESI +) m/z: 387.1 $[M+Na]^+$; expected 387.1

3.5.3.3. Synthesis of poly(*N*-isopropylacrylamide)s

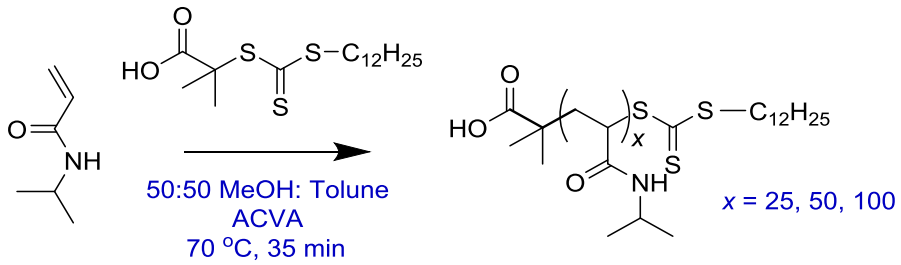

In a typical procedure *N*-isopropylacrylamide (1.00 g, 8.837 mmol), 2-(dodecylthiocarbonothioylthio)-2-methylpropanoic acid (128.9 mg, 0.353 mmol), 4,4'-azobis(4-cyanovaleric acid) (19.7 mg, 70.6 µmol) were added to a vial fitted with stir bar and rubber septum and dissolved in methanol:toluene (50:50) (4 mL). Mesitylene (200 µL) was added as internal reference and the mixture was then stirred (5 min). Further polymerisation solutions were prepared, as detailed in Table 3.7. The solutions were degassed with nitrogen (30 min), immersed into an oil bath (70°C, 35 min) then opened and cooled on ice. Each solution was concentrated, precipitated into petroleum ether (35 mL) and re-precipitated from acetone into diethyl ether three times. The resulting solid was isolated by centrifugation and dried to yield a pale yellow solid product.

Table 3.7: Polymerisation reagent compositions for the synthesis of pNIPAMs

Theoretical Degree of Polymerisation [M]:[CTA]		**Initiator (ACVA)**	**RAFT Agent (CPBD)**	**Monomer (OEGMA 300)**
25:1	Ratio	0.2	1.0	25.0
	Moles/ mmol	0.070	0.353	8.837
	Mass/ mg	19.7	128.9	1.0×10^3
50:1	Ratio	0.2	1.0	50.0
	Moles/ mmol	0.00353	0.1767	8.837
	Mass/ mg	9.91	64.44	1.0×10^3
100:1	Ratio	0.2	1.0	50.0
	Moles/ mmol	0.00018	0.0883	8.837
	Mass/ mg	4.9	32.2	1.0×10^3

The polymers were characterised by ^{1}H NMR spectroscopy. The degree of polymerisation was calculated using ^{1}H NMR spectroscopy to determine the ratio of side chain methyl (δ 1.50- 1.85) to terminal CH_3 protons (δ 0.80- 0.90), and by DMF SEC. Overall monomer conversion was calculated by ^{1}H NMR spectroscopy by measuring the decrease in intensity of the vinyl peaks associated with the monomer relative to mesitylene. The characterisation data is summarised in Table 3.2.

3.5.4. Polymer Coatings on Silane Functionalised Surface

3.5.4.1. Glass and Silicon Surface Functionalisation

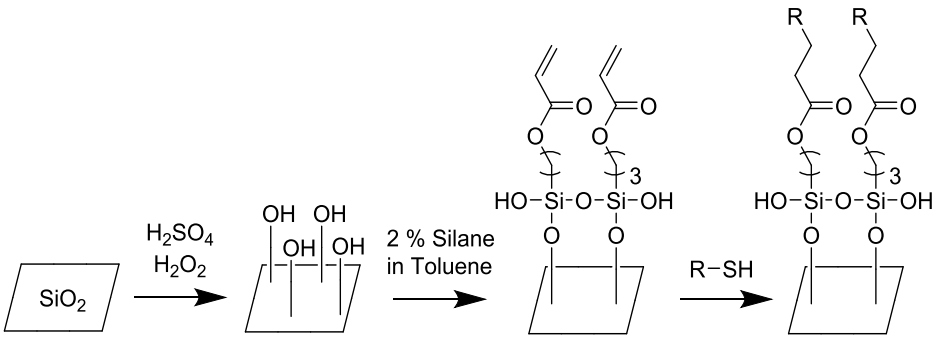

Immediately following the cleaning process (Section 2.6.1.), the samples were immersed into a (3-(trimethyoxysilyl) propyl acrylate (5 mL, 2% v/v in toluene, 2 hours, RT), washed with toluene (5 x 2 mL), ethanol (5 x 2 mL) and water (5 x 2 mL), then blown under a stream of nitrogen until dry. This process applied to the glass slides and the silicon wafers.

Following silanisation a solution of the selected polymer (pOEGMA or pNIPAM) was prepared (2 $mg.mL^{-1}$ in water) and ethanolamine (0.1 mL) was added if required. The samples were immersed into the polymer solution for 2 hours (RT) then washed with Milli-Q water (3 x 2 mL) and dried under a stream of nitrogen.

3.5.4.2. Non-fouling Behaviour of Polymer Functionalised Surfaces

Samples were either totally immersed into solutions of fluorescently labelled lectin (Con A (0.1 $mg.mL^{-1}$ in HEPES) for 30 minutes (RT, dark) or the same procedure was followed but spots (5 µL) of lectin were administered onto the surface. The samples were then removed from the solution, excess lectin solution

was pipetted from the surface and the sample was washed (2 x 5 mL HEPES buffer, 5 x 5 mL Milli-Q water) and dried under a stream of nitrogen. Samples were stored in the dark and in the fridge until tested on the fluorescence scanner.

3.5.4.3. Thermoresponsive Behaviour of Polymer Functionalised Surfaces

3.5.4.3.1. Direct Heating of Glass slides

Glass slides were held with plastic tweezers at one end and heated with a hot air gun for 2 minutes on each side. The air flow was continually moved to ensure even heating. The slides were immediately transferred to the measurement stage of the drop shape analyser.

3.5.4.3.2. Hot Plate Heating of Glass Slides

A hot plate was covered in a protective layer of clean aluminium foil and set to heat to 80°C. Upon reaching the set temperature, the samples were added onto the foil and heated for 5 minutes. They were then carefully removed and tested immediately. For the hydrated samples, they were placed into a beaker of Milli-Q water at 80°C for five minutes. The cold samples were placed into either an empty petri-dish or a dish containing Milli-Q water, they were then refrigerated (5°C) for 15 minutes.

Testing was carried out by placing the sample over the size template and administering water droplets (5 µL) onto the surface from an autopipette. The pipette was depressed until a droplet was formed at the end of the tip, but without falling. The tip was then brought into contact with the surface, allowing the water drop to transfer. The drops were added over the template circles and immediately photographed using a camera phone. The drop sizes, relative to the template, were then calculated through image analysis using ImageJ.

3.5.4.3.3. Temperature Controlled Stage Facilitated Heating and Cooling of Glass Slides

The sample was placed onto a pre-temperature set temperature controlled stage (Linkam BCS196 cryostage (Linkam Scientific Instruments Ltd, Guildford, Surrey, UK)) and allowed to anneal at the pre-set temperature for 10 minutes. Droplets of Milli-Q water (2.5 µL) were administered onto the surface from an autopipette. The pipette was depressed until a droplet was formed at the end of the tip, but without falling, the tip was then brought into contact with the surface, allowing the water drop to transfer. The lid of the temperature controlled stage was then fitted and the timer started. The programmed cooling process was then begun, if required. Photographs were taken using a Veho 40-400x USB microscope, images taken using Veho MicroCapture Version 1.3 and the images analysed using ImageJ. The diameter of each droplet was calculated by comparison to the size of the central hole in the stage (1 mm).

3.6. References

1. W. J. Brittain and S. Minko, *J. Polym. Sci. A Polym. Chem.*, 2007, **45**, 3505-3512.

2. J. F. Lutz and A. Hoth, *Macromolecules*, 2006, **39**, 893-896.

3. C. de las Heras Alarcon, S. Pennadam and C. Alexander, *Chem. Soc. Rev.*, 2005, **34**, 276-285.

4. Z. Li, Y.-H. Kim, H. S. Min, C.-K. Han and K. M. Huh, *Macromol. Res.*, 2010, **18**, 618-621.

5. Z. Li, Y.-H. Kim, H. S. Min, C.-K. Han and K. M. Huh, *Macromol. Res.*, 2010, **18**, 618-621.

6. S. N. S. Alconcel, A. S. Baas and H. D. Maynard, *Polym. Chem.*, 2011, **2**, 1442-1448.

7. X. W. Fan, L. J. Lin and P. B. Messersmith, *Biomacromolecules*, 2006, **7**, 2443-2448.

8. H. Willcock and R. K. O'Reilly, *Polym. Chem.*, 2010, **1**, 149-157.

9. A. B. Lowe, *Polym. Chem.*, 2010, **1**, 17-36.

10. Z. L. Zhi, N. Laurent, A. K. Powel, R. Karamanska, M. Fais, J. Voglmeir, A. Wright, J. M. Blackburn, P. R. Crocker, D. A. Russell, S. Flitsch, R. A. Field and J. E. Turnbull, *Chembiochem*, 2008, **9**, 1568-1575.

11. M. Baum and W. J. Brittain, *Macromolecules*, 2002, **35**, 610-615.

12. S. Tugulu, A. Arnold, I. Sielaff, K. Johnsson and H. A. Klok, *Biomacromolecules*, 2005, **6**, 1602-1607.

13. R. Barbey, L. Lavanant, D. Paripovic, N. Schuewer, C. Sugnaux, S. Tugulu and H.-A. Klok, *Chem. Rev.*, 2009, **109**, 5437-5527.

14. S. Edmondson, V. L. Osborne and W. T. S. Huck, *Chem. Soc. Rev.*, 2004, **33**, 14-22.

15. J. Wang, M. I. Gibson, R. Barbey, S. J. Xiao and H. A. Klok, *Macromol. Rapid Commun.*, 2009, **30**, 845-850.

16. A. D. Price and D. L. Huber, *Polym. Chem.*, 2013, **4**, 1565-1574.

17. Y. Li and B. C. Benicewicz, *Macromolecules*, 2008, **41**, 7986-7992.

18. Y. L. Zhao and S. Perrier, *Macromolecules*, 2006, **39**, 8603-8608.

19. Y. Zhao and S. Perrier, *Reversible Addition-Fragmentation Chain Transfer Polymerization from Surfaces*, Springer International Publishing, 2016.

20. Y. Kotsuchibashi, M. Ebara, T. Aoyagi and R. Narain, *Polym. Chem.*, 2012, **3**, 2545-2550.

21. K. Chen, Y. Zhao and X. Yuan, *Chem. Res. Chinese U.*, 2014, **30**, 339-342.

22. E. B. Zhulina, O. V. Borisov, V. A. Pryamitsyn and T. M. Birshtein, *Macromolecules*, 1991, **24**, 140-149.

23. F. Hook, B. Kasemo, T. Nylander, C. Fant, K. Sott and H. Elwing, *Anal. Chem.*, 2001, **73**, 5796-5804.

24. N. C. Fawcett, R. D. Craven, P. Zhang and J. A. Evans, *Anal. Chem.*, 1998, **70**, 2876-2880.

25. K. Bebis, M. W. Jones, D. M. Haddleton and M. I. Gibson, *Polym. Chem.*, 2011, **2**, 975-982.

26. S. Balamurugan, S. Mendez, S. S. Balamurugan, M. J. O'Brien and G. P. Lopez, *Langmuir*, 2003, **19**, 2545-2549.

27. C. D. H. Alarcon, T. Farhan, V. L. Osborne, W. T. S. Huck and C. Alexander, *J. Mater. Chem.*, 2005, **15**, 2089-2094.

28. C. Xue, N. Yonet-Tanyeri, N. Brouette, M. Sferrazza, P. V. Braun and D. E. Leckband, *Langmuir*, 2011, **27**, 8810-8818.

29. J. Jhang, R. Pelton and Y. L. Deng, *Langmuir*, 1995, **11**, 2301-2302.

30. F. J. Xu, L. Y. Liu, W. T. Yang, E. T. Kang and K. G. Neoh, *Biomacromolecules*, 2009, **10**, 1665-1674.

31. M. Kobayashi, Y. Terayama, H. Yamaguchi, M. Terada, D. Murakami, K. Ishihara and A. Takahara, *Langmuir*, 2012, **28**, 7212-7222.

32. E. Bittrich, S. Burkert, M. Mueller, K.-J. Eichhorn, M. Stamm and P. Uhlmann, *Langmuir*, 2012, **28**, 3439-3448.

33. A. Hucknall, S. Rangarajan and A. Chilkoti, *Adv. Mater.*, 2009, **21**, 2441-2446.

34. E. Ostuni, R. G. Chapman, R. E. Holmlin, S. Takayama and G. M. Whitesides, *Langmuir*, 2001, **17**, 5605-5620.

35. B. Yu, J. W. Chan, C. E. Hoyle and A. B. Lowe, *J. Polym. Sci., Part A: Polym. Chem.*, 2009, **47**, 3544-3557.

36. J.-F. Lutz, *J. Polym. Sci., Part A: Polym. Chem.*, 2008, **46**, 3459-3470.

37. A. S. Duwez, P. Guillet, C. Colard, J. F. Gohy and C. A. Fustin, *Macromolecules*, 2006, **39**, 2729-2731.

38. M. C. Dixon, *J. Biomol. Tech.*, 2008, **19**, 151-158.

39. M. A. Plunkett, Z. H. Wang, M. W. Rutland and D. Johannsmann, *Langmuir*, 2003, **19**, 6837-6844.

40. G. Zhang and C. Wu, *Macromol. Rapid Commun.*, 2009, **30**, 328-335.

41. I. G. Sedeva, R. Fetzer, D. Fornasiero, J. Ralston and D. A. Beattie, *J. Colloid Interface Sci.*, 2010, **345**, 417-426.

42. M. Annaka, C. Yahiro, K. Nagase, A. Kikuchi and T. Okano, *Polymer*, 2007, **48**, 5713-5720.

43. A. Dirani, X. Laloyaux, A. E. Fernandes, B. Mathy, O. Schicke, O. Riant, B. Nysten and A. M. Jonas, *Macromolecules*, 2012, **45**, 9400-9408.

44. J. Henrie, S. Kellis, S. M. Schultz and A. Hawkins, *Opt. Express*, 2004, **12**, 1464-1469.

45. NIST, X-ray Photoelectron Spectroscopy Database, Version 4.1, 2014, Available at: http://srdata.nist.gov/xps/

46. D. J. Phillips and M. I. Gibson, *Biomacromolecules*, 2012, **13**, 3200-3208.

Chapter Four

4. Contact Printing of Glycosylated Polymers

4.1. Chapter Summary

Having successfully functionalised surfaces with both carbohydrates (Chapter Two) and polymers (Chapter Three) this chapter explored combining these and functionalising surfaces with carbohydrate terminated poly(*N*-isopropylacrylamide) (pNIPAM) in order to generate arrays. The polymers were synthesised by the reversible addition fragmentation transfer (RAFT) controlled radical polymerisation technique, to generate well defined polymers. Polymers were synthesised using a pentafluorophenyl (PFP) RAFT agent, resulting in PFP terminated pNIPAMs, which were subsequently glycosylated with 2-deoxy-2-aminomannose ($ManNH_2$), 2-deoxy-2-aminoglucose ($GlcNH_2$) and 2-deoxy-2-aminogalactose ($GalNH_2$). By virtue of RAFT synthesised polymers as linkers, surface grafting through the thiol-containing RAFT terminus and glycan conjugation at the other end is possible.

Orthogonal functionalisation of both acrylate silane and epoxide coated glass microscope slides with these glycosylated polymers successfully produced surface grafted glycans which could be interrogated with model lectins, as monitored by scanning fluorescence spectroscopy. It was found that the longer chain glycosylated polymers ($pNIPAM_{100}$) exhibited better discrimination with regard to lectin binding specificities than the shorter

($pNIPAM_{25}$) polymers and when the entire slide was coated, both surface coatings (silane acrylate and epoxide) behaved comparably.

The work was then concluded with the direct-microcontact printing of the small library of glycosylated polymers onto both acrylate silane and epoxide slides in order to produce high density glycopolymer arrays, with 400 polymer spots present on one microscope slide. These arrays were then tested for their interaction with a soybean agglutinin (SBA) and wheat germ agglutinin (WGA). It was found that the lectins bound to the glycan according to their expected binding profiles and that the epoxide surfaces were superior for these printing applications. Again, the longer chain polymers produced better discrimination between carbohydrate-lectin binding events. The use of these glycan arrays to probe the binding patterns of model lectins shows the potential of this system as a biologically-relevant screening tool.

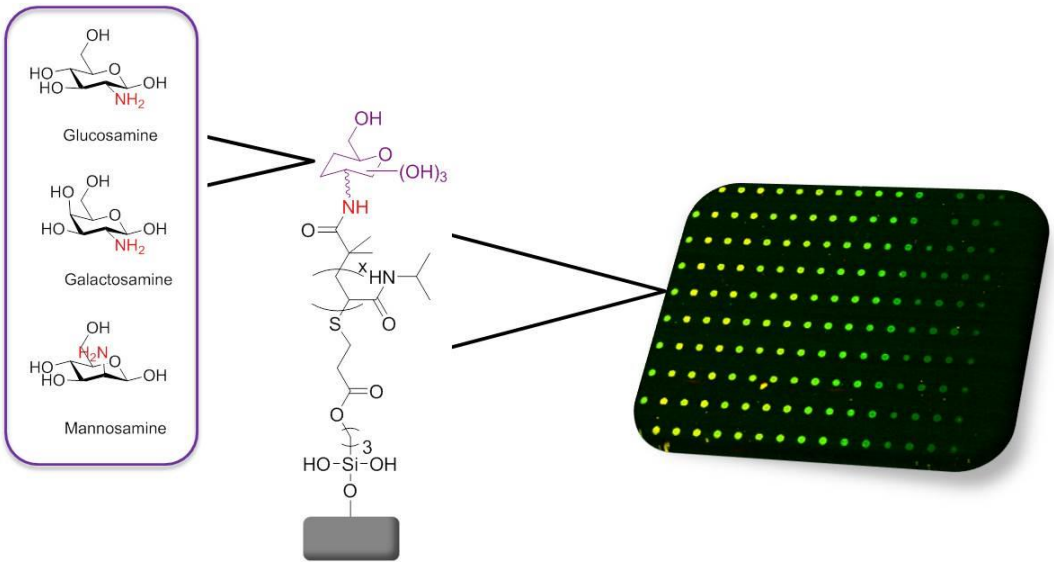

Figure 4.1: Building on the silane acrylate coatings detailed in Chapter Two and grafting of pNIPAM polymers to glass in Chapter Three, the printing of mannose, glucose and galactose terminated pNIPAM glycosylated polymers was studied. Acrylate silane coated slides were compared to the commercially available epoxide coatings and the interactions of the printed polymers with fluorescently labelled lectins was investigated

4.2. Introduction

Post-polymerisation modification allows access to functional polymers that may otherwise be difficult to access and also has the significant advantage of knowing that the properties of the polymer scaffold are consistent across a library of materials. Direct polymerisation of a number of differently functionalised monomers would be unlikely to produce polymers with identical degrees of polymerisation and dispersity values, a problem that can be circumvented by the use of the post-polymerisation technique. This method involves preparing a single batch of the precursor polymer scaffold and then subsequently functionalising this polymer chain. The use of activated ester-type monomers has been well investigated due to their ease of accessibility and ready availability of the amine functional moieties to be attached. The addition of both amines and alcohols onto polymers containing activated esters of pentafluorophenol (PFP), *N*-hydroxysuccinimide and 4-nitrophenol has been described. Typically amines are preferred due to their greater nucleophilicity compared to alcohols.[1]

The use of PFP functionality for post-polymerisation modification was introduced by the Théato group[2] and has been applied to the process of RAFT polymerisation by the Gibson group. In that work poly(pentafluorophenyl methacrylate) (pPFPMA) was synthesised as a reactive scaffold for the synthesis of glycosylated polymers, amongst other functionalities.[3] Recent work from the Gibson group has expanded these concepts and developed a tandem post-polymerisation strategy for the synthesis of glycopolymer libraries through side chain modification, Figure 4.2. This method had the key advantage of producing glycosylated polymers with precisely controlled chain

length, carbohydrate density and defined backbone-carbohydrate liner lengths, whilst also avoiding the problems associated with radical polymerisation of alkyne or alkene monomers.[4]

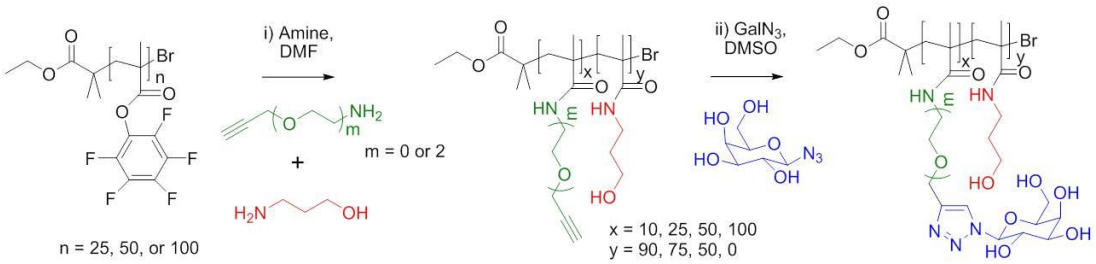

Figure 4.2: Synthesis of pendant functionalised glycopolymer libraries using tandem post-polymerisation modification, adapted from the work of S-J. Richards[4]

The same synthetic concepts have also been applied to terminal functionalised glycosylated polymers. RAFT polymerisation was utilised to generate poly(*N*-hydroxyethyl acrylamide) (pHEA) polymers with a PFP group at one terminus and a masked thiol at the other. The carbohydrates were then introduced by reacting the PFP-polymers with 2-deoxy-2-aminomannose ($ManNH_2$) and 2-deoxy-2-aminogalactose ($GalNH_2$).[5] In this work, the free thiol terminus of the polymers was reacted with the surface of gold nanoparticles. However, this thiol functionality will also allow for conjugation to an acrylate or epoxide coated surface,[6, 7] as we have demonstrated in Chapter Three.

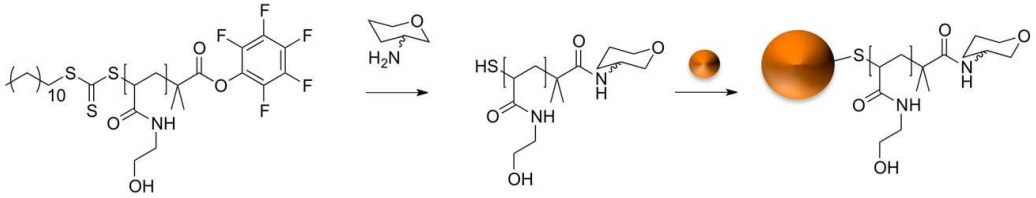

Figure 4.3: Synthesis of glycopolymer functionalised gold nanoparticles, via a post-polymerisation route. Taken from the work of S-J. Richards[5]

In contrast to the previous work which has involved immobilising these glycosylated polymers onto gold nanoparticles,[4] immobilisation onto glass slides utilising direct-microcontact printing in order to generate high density arrays is desirable for high-throughput and low volume applications. Microcontact printing (μCP) is a form of soft lithography that was originally developed by the Whitesides group at Harvard University. The technique involved the use of master polydimethysiloxane (PDMS) soft polymer stamps that were used to transfer patterns of a solution onto the surface of a substrate, an evolution of the ancient art of stamp printing being combined with lithography and using alkanethiols as the "ink".[8] The potential of these microscale self-assembled monolayers to be used as biosensors or for biologically relevant applications was quickly established and surfaces were developed to resist or promote the adsorption of proteins and cells.[9]

More recent work has developed these early principles into sophisticated high-throughput screening devices, which have applications in the fields of biomaterials discovery and sensor development. These high-throughput methodologies involve the deposition of probe molecules onto a surface and then using the resulting microarrays to screen large libraries of materials of molecules for biological responses. These microarray surfaces, with their large number of immobilised probes, allow large numbers of experiments to be performed in parallel, on the same surface, where they are subjected to identical reagents and conditions. Work on DNA microarrays, which are significantly more advanced than the carbohydrate microarray field, has developed techniques by which thousands of unique nucleotide sequences are presented on a surface and screened for their hybridisation with the target

DNA strands. The positive pairings are then visualised using a fluorescence scanner. There are many challenges associated with these readouts, primarily that the fluorescence must be discrete, the background must be dark and the immobilised probe molecules must survive any washing steps that are deemed essential to the investigation.[10]

The techniques for the immobilisation of the probes onto the array surfaces must be chosen such that there are minimal defects within the printed materials, there is good adhesion of the printed material and the non-specific adsorption of unwanted material is minimised during the bioassay. In addition to the soft lithography based μCP techniques already discussed,[9] direct contact printing has also been developed as a viable alternative. In this process a pin filled with the printing solution is brought into direct or close-to contact with the substrate, allowing solution transfer. Through the use of a robotic arm, the location of "ink" spots can be precisely controlled and very high density arrays can be produced. This method is adaptable to a large variety of solutions, but does suffer from the challenges of surface damage if the printing pin is used on a soft gel coated substrate.[10] A further option is ink-jet printing, a non-contact technique which avoids the problems arising from contact printing causing damage to the substrate but instead suffers from susceptibility to nozzle blocking and a more problematic cleaning procedure.[11] The two processes are summarised in Figure 4.4. For use on glass substrates, where surface damage is not a concern, direct contact printing offers an experimentally more accessible route towards array fabrication.

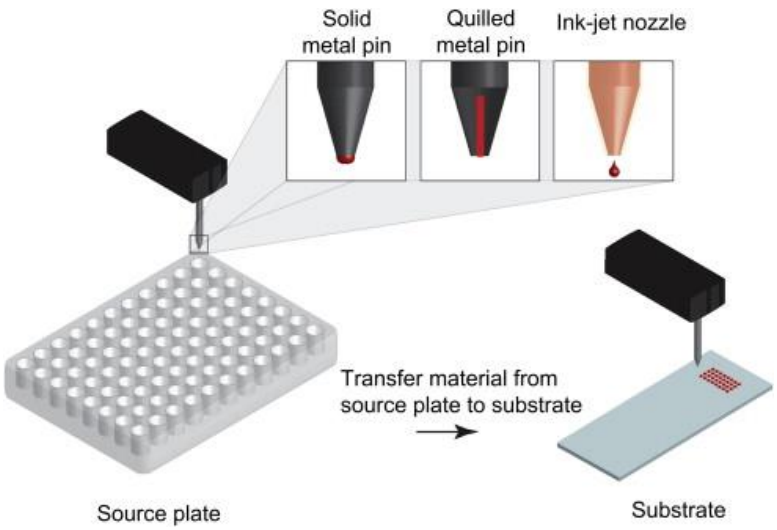

Figure 4.4: The use of robotically controlled direct-contact or ink-jet printing to produce high density and highly ordered arrays of materials on a solid substrate. The two options for direct-contact printing (solid metal pins and quilled pins) are shown alongside the in-jet nozzle option. Taken from the work of A.L. Hook *et al.* [11]

The first use of direct contact printing for the production of polymer microarrays to be used for screening cell responses was reported in 2004. These array systems were used to study the growth of human embryonic stem cells and demonstrated on-chip polymerisations and the use of polyhydroxyethylmethacrylate (pHEMA) slide coatings. The pHEMA serves to resist cell attachment as well as providing a matrix into which printed material can penetrate and physically entangle, thus improving the stability of the spotted polymers.[12] One year later, new arrays were produced from the immobilisation of pre-synthesised polymers and their interactions with the stem cells were studied.[13] Within the field of glycan printing, commercially available amino-reactive (*N*-hydroxysuccinimide) glass slides have been used as the substrate for the printing of synthetic and natural amine functionalised glycan sequences. These printed arrays build upon the methods for carbohydrate binding discussed in Chapter Two, but with the advantage of much higher density systems, made possible through robotically-controlled

printing techniques. The application of the already well developed scanning and image processing techniques utilised by the DNA microarray community,[14] has significantly aided progress in this area.[15] Combining the polymer printing technologies previously mentioned with the desire to have printed glycans, has led to the development of a printed glycopolymer functionalised surfaces. For example, mucin-like synthetic glycopolymers, with the ability to control the polymer linker length and glycan density, have been shown to create more physiologically authentic platforms for probing glycan-binding events, summarised in Figure 4.5.[16] These is still a need, however, for facile glycopolymer immobilisation techniques which are compatible with glass substrates and can be used to probe glycan interactions.

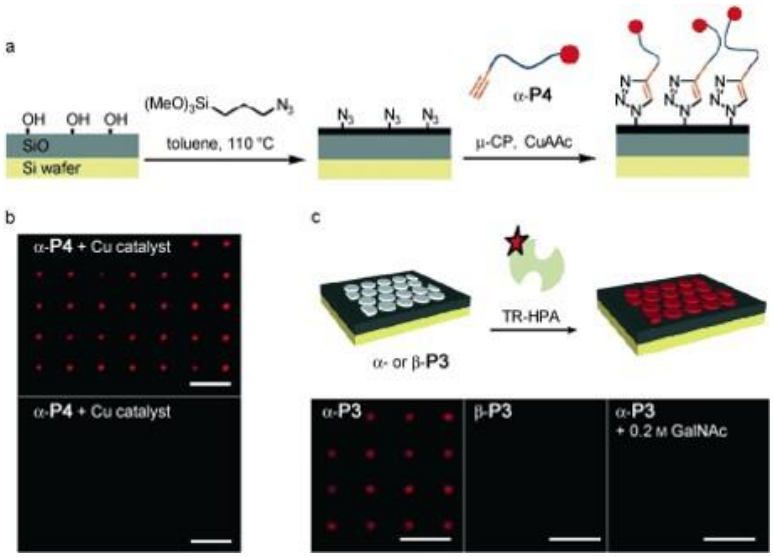

Figure 4.5: Glycopolymer microarrays printed onto silicon wafer substrates adapted from the work of K. Godula *et al.*[16] Printing is achieved through the use of a PDMS stamp with 2 μm features for transfer of the glycopolymer "ink". [A] The arrays are generated through preparing azide coatings on the silicon oxide wafers and covalent microcontact printing of alkyne terminated. [B] Fluorescence micrograph showing the success of the alkyne-azide reaction. [C] Binding of HPA lectin to glycopolymer surfaces

4.3. Results and Discussion

4.3.1. Comparison of Silane Coating and Commercially Available Epoxide Coatings

The direct-microcontact printing, which is crucial to the progression of this work into a high-throughput system, requires microscope slides of maximum size 75 mm x 25 mm, which is smaller than the dimensions of the slides used in previous work. New slides were therefore sourced from Corning Scientific. As a comparison to our silane coating, commercially available epoxide coated glass slides were also purchased. These epoxide coatings have traditionally been used for the immobilisation of glycans for microarray applications, either via the secondary amine group of reductively aminated glycans[17] or via hydrazide-conjugated carbohydrates.[18] However, epoxides react very quickly with thiols, a process which is sometimes called "thiol-epoxy click" and is orthogonal, allowing hydroxyl groups to be present. In order to compare the two substrates, both acrylate coated and epoxide coated glass slides were functionalised with two thiols; dodecanethiol (chosen as a hydrophobic control) and thioglycerol (chosen as a hydrophilic control). The functionalisation process was conducted in the same reaction vessel for each type of surface (i.e. the epoxide and silane coated slides were both placed into the same dish of thiol) in order to minimise experimental variation and better directly compare the two processes (Figure 4.6). Catalytic ethanolamine was added, as this had been shown to improve surface functionalisation (Chapters Two and Three).

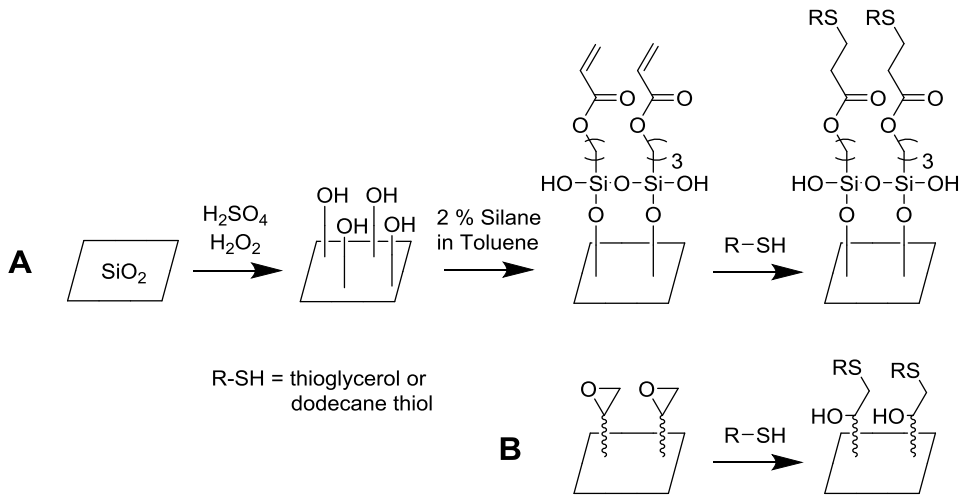

Figure 4.6: Schematic of the functionalisation of [A] the native glass slides with the silane acrylate coating and subsequently the model thiol solutions and [B] the commercially available epoxide coated glass slides with the model thiol solutions

The surfaces were then compared visually and characterised through drop shape analysis. The contact angle measurements for the new smaller plain glass slides and commercially available epoxide coated glass slides are shown in Figure 4.7. The trends for both surfaces are reassuringly the same and the contact angles for each pair of thiol-functionalised coatings are very similar, despite the differences in hydrophobicity of the underlying coating. This data provides satisfactory evidence for using the two systems (acrylate silane coating and commercial epoxide coating) in parallel for the remaining investigations. However, from an economic viewpoint, it is far more preferable to use the plain glass slides and coat them with the acrylate silane. The cost savings involved in coating silane acrylates onto the glass are very significant (£0.19/slide for the plain glass compared to £13.20/slide for the epoxide coated slides).

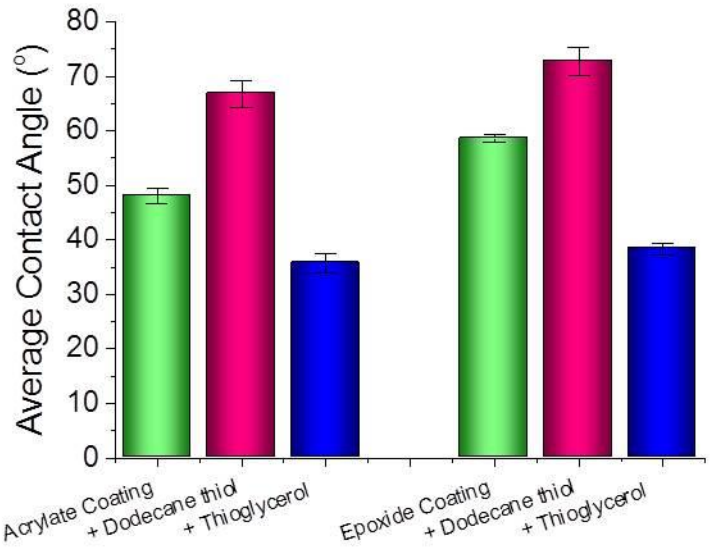

Figure 4.7: Water drop contact angle measurements for the acrylate (left) and epoxide (right) with two different thiols. Error bars show the standard deviation taken from a minimum of five independent measurements.

4.3.2. Synthesis of Glycosylated Polymers

Encouraged by the results above, end-glycosylated polymers were synthesised for immobilisation onto the glass surfaces. In order to produce well defined polymers with the appropriate α and ω end functionality, a pentafluorophenyl containing RAFT agent was required.

4.3.2.1. Synthesis of PFP RAFT Agent

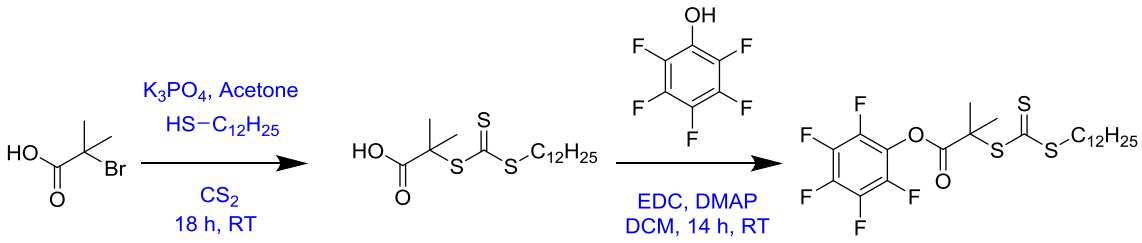

Figure 4.8: Synthesis of the pentafluorophenyl 2-(dodecylthiocarbonothioylthio)-2-methylpropionic acid RAFT

The 2-(dodecylthiocarbonothioylthio)-2-methylpropanoic acid RAFT agent (Figure 4.8), was synthesised from dodecanethiol, K_3PO_4, CS_2 and 2-bromo-2-methylpropionic acid, as described in Chapter Three. The resulting yellow solid product was then further reacted with Pentafluorophenol to yield the pentafluorophenyl 2-(dodecylthiocarbonothioylthio)-2-methylpropionic acid (PFP-DMP) to be utilised as the RAFT agent for the polymerisation of NIPAM. A pentafluorophenyl (PFP) trithiocarbonate RAFT agent was chosen in order to enable further modification with amino-glycosides, for production of the glycosylated polymers, and also for the presence of the masked-thiol end group to allow coupling with the alkene or epoxide functionalised surfaces. An assigned ^{1}H NMR spectrum for the PFP-DMP RAFT agent is shown in Figure 4.9.

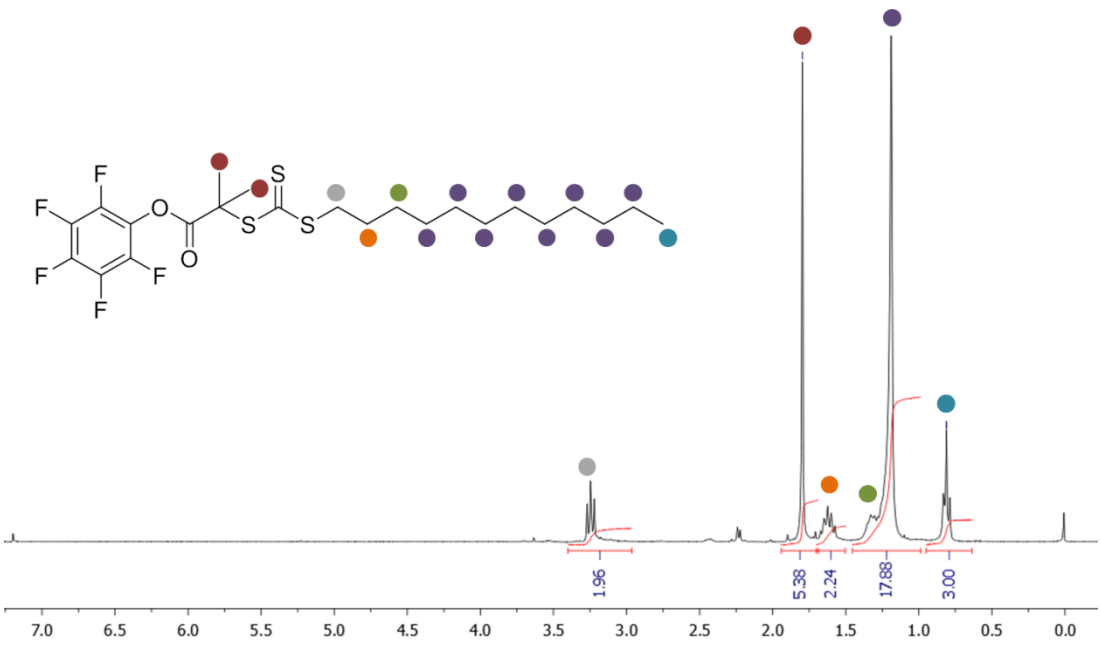

Figure 4.9: ^{1}H NMR spectrum of pentafluorophenyl 2-(dodecylthiocarbonothioylthio)-2-methylpropanoic acid in $CDCl_3$

4.3.2.2. Synthesis of Pentafluorophenyl Terminated pNIPAM Polymers

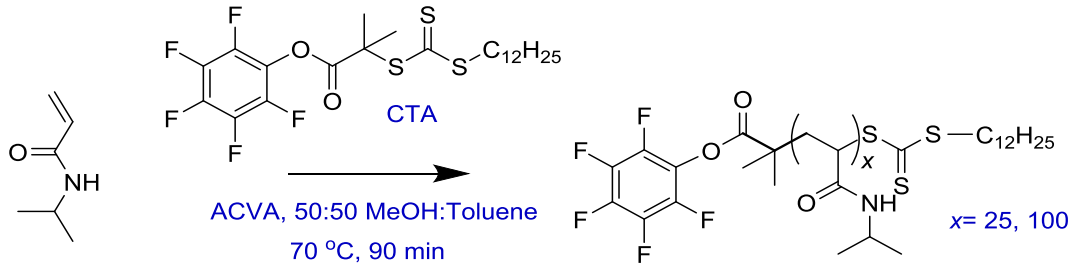

Figure 4.10: RAFT mediated polymerisation of NIPAM using the PFP RAFT agent

Using the pentafluorophenyl 2-(dodecylthiocarbonothioylthio)-2-methylpropionic acid RAFT agent and 4,4′-azobis(4-cyanovaleric acid) (ACVA) as a radical initiator, two molecular weights of PFP-terminated pNIPAM were synthesised (targeted degree of polymerisation 25 and 100), Figure 4.10. Following a 90 minute polymerisation time and isolation of the polymers through precipitation, the resulting pale yellow solids were characterised by NMR spectroscopy and the molecular weight distribution was determined by size exclusion chromatography, indicating low dispersities (Table 4.1 and Figure 4.11). The M_n values obtained from SEC were in reasonable agreement with those predicted from [M]:[CTA] and conversion obtained from NMR. The NMR spectrum was indistinct from the spectrum for pNIPAM polymerised with the DMP RAFT agent without the PFP group present; the assigned spectrum for this can be seen in Figure 3.9.

Table 4.1: Characterisation data for the PFP-pNIPAM polymers

[M]:[CTA][A]	Conv. (NMR)[B]	DP_{Theo} (NMR)[B]	M_n (NMR)[B]	$M_{n(SEC)}$[C]	$M_{w(SEC)}$[C]	M_w/M_n[C]
25:1	88%	22	2480	3980	4450	1.12
100:1	92%	92	10410	9200	9890	1.08

[A] Feed ratio of monomer to chain transfer agent; [B] Determined by ^{1}H NMR spectroscopy in $CDCl_3$; [C] Determined by SEC in dimethylformamide (DMF) using poly(methyl methacrylate) standards. M_w = weight average molecular weight, M_n = number average molecular weight

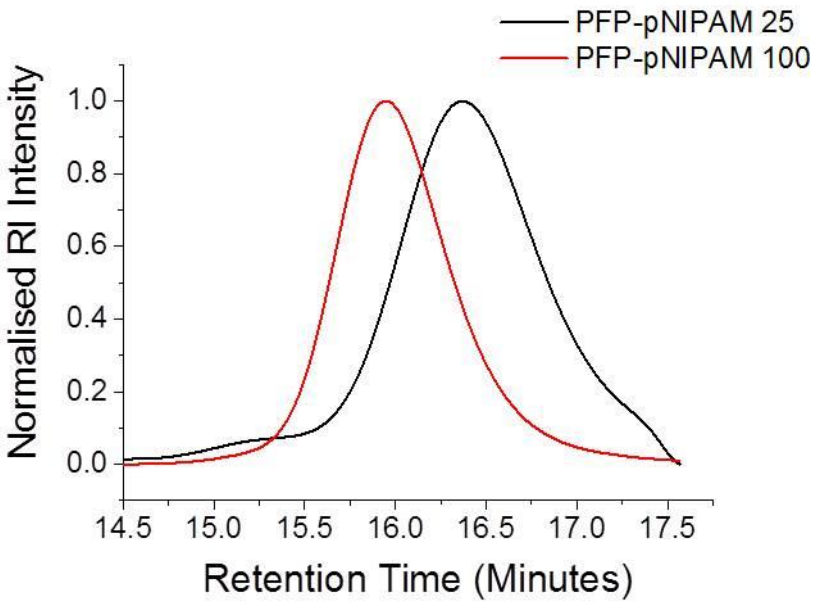

Figure 4.11: PFP-pNIPAM SEC traces, run in DMF

As a further confirmation of the successful polymerisation and to check if the polymer chains retained both the PFP unit and the thiol-containing RAFT end group, MALDI-ToF was employed. The data, Figure 4.12, shows a distribution of mass peaks, as is expected, and the difference between each peak is 113 Daltons, corresponding to the mass of one NIPAM repeat unit. The peak assignments, detailed in Table 4.2, confirm that the polymer chains retain both end groups because each peak correspond to *x* NIPAM repeat units plus the mass of both parts of the RAFT agent and one sodium ion. This shows the efficacy of the RAFT process and

that the polymers are suitable to use for the immobilisation process. An ESI mass spectrum is presented in Appendix One.

Table 4.2 : MALDI-ToF peak assignment for PFP-pNIPAM$_{25}$

Entry	m/z	NIPAM Repeat Units	Ion
1	1232.01	6	Na^+
2	1347.15	7	Na^+
3	1461.99	8	Na^+
4	1576.57	9	Na^+
5	1691.91	10	Na^+
6	1806.02	11	Na^+
7	1919.94	12	Na^+
8	2032.70	13	Na^+
9	2147.31	14	Na^+
10	2260.79	15	Na^+
11	2374.18	16	Na^+
12	2487.47	17	Na^+
13	2600.70	18	Na^+
14	2713.88	19	Na^+
15	2826.01	20	Na^+
16	2939.14	21	Na^+

Mass corresponds to end groups present on both ends of the polymer, plus the number of NIPAM repeat units and ion indicated

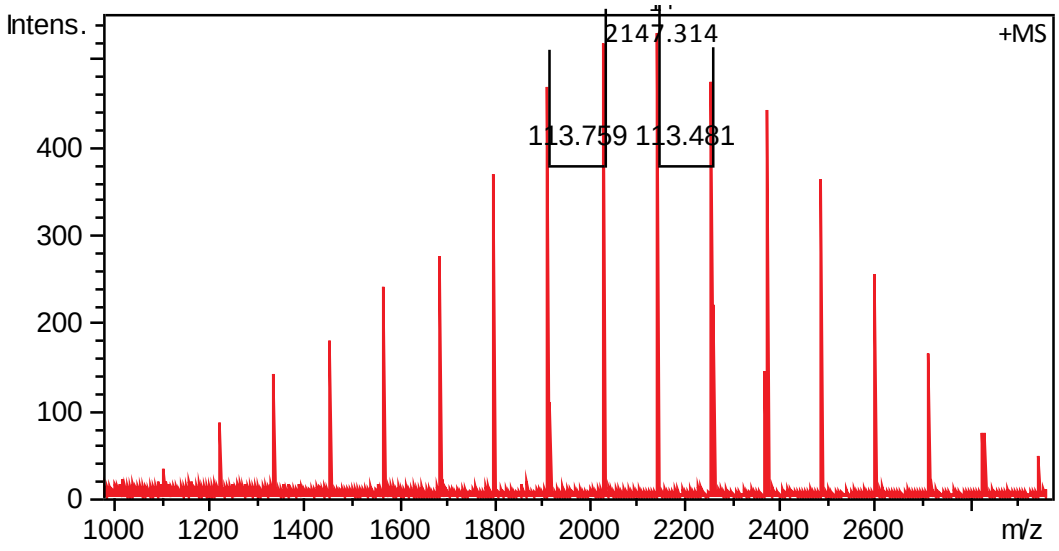

Figure 4.12: MALDI-Tof spectrum for PFP-PNIPAM$_{25}$

4.3.2.3. Glycosylation of PFP-pNIPAM polymers

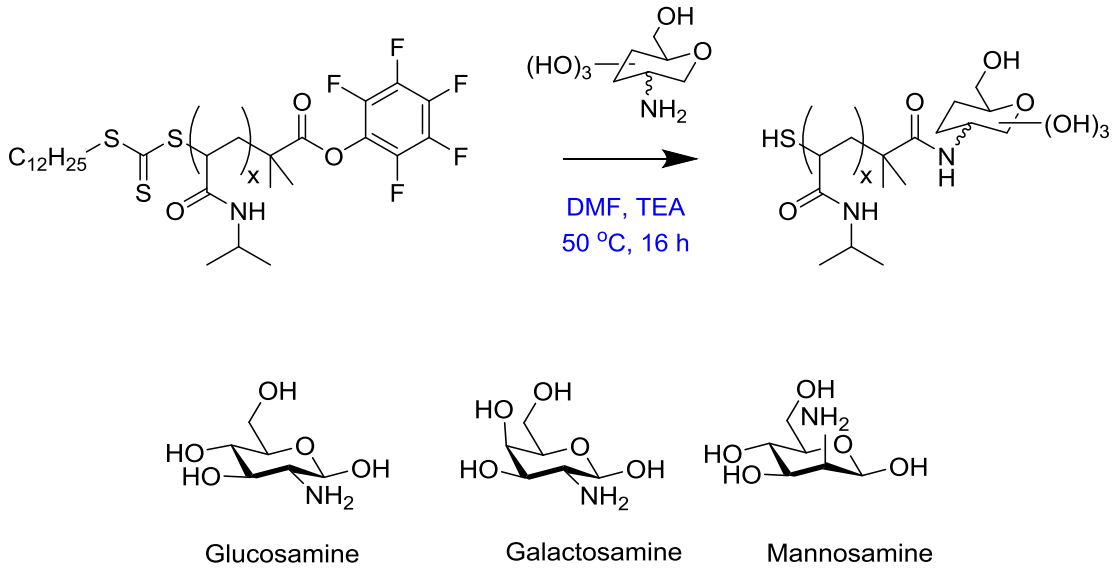

Figure 4.13: Reaction of the PFP terminated pNIPAMs with amino-monosaccharaides

Carbohydrate moieties were introduced onto the polymer chains via the reaction of the PFP end group with amino sugars (2-deoxy-2-aminomannose ($ManNH_2$), 2-deoxy-2-aminoglucose ($GlcNH_2$) and 2-deoxy-2-aminogalactose ($GalNH_2$), see Figure 4.13. This glycosylation step also serves to cleave the trithiocarbonate end group from the ω-end of the polymer, yielding the terminal thiol group, which we can later use for surface conjugation. The small library of monosaccharide terminated pNIPAM molecules that were synthesised is detailed in Table 4.3.

Table 4.3: Monosaccharide terminated polymers synthesised

Sample code	pNIPAM chain length	Terminal Sugar
A	100	Glc
B	100	Gal
C	100	Man
D	100	-
E	25	Glc
F	25	Gal
G	25	Man
H	25	-

Successful conversion of the PFP group into the monosaccharide of interest was confirmed by the use of infrared spectroscopy. In Figure 4.14 the disappearance of the C=O stretch, corresponding to the carbonyl group present in the PFP terminus (small peak observed at 1770 cm^{-1}, due to the C=O group being part of an activated ester)[4] is observed in the glycosylated polymer sample. As pNIPAM should be thermoresponsive, it is possible to check for successful end group modification by turbidimetric analysis. It has been established that for short, <10,000 $g.mol^{-1}$ pNIPAM, changing the end group has a profound effect on LCST/cloud point.[19] Comparing the pre-glycosylated PFP-pNIPAM polymers to their glycosylated counterparts, the turbidimetery data exhibits a dramatic shift in both onset temperature (from 16 to 35°C) and the temperature at which $absorbance_{650nm}$ = 0.5 (from 19 to 35°C). This is consistent with an increase in hydrophilicity. Sample data for the comparison of PFP-$pNIPAM_{25}$ to Glc-$pNIPAM_{25}$ is shown in Figure 4.15. The retention of thermoresponsive behaviour of the short pNIPAM chains, despite the presence of the monosaccharide end group is pleasing and could prove beneficial

to any future work investigating the use of these coatings for thermoresponsive behaviour.

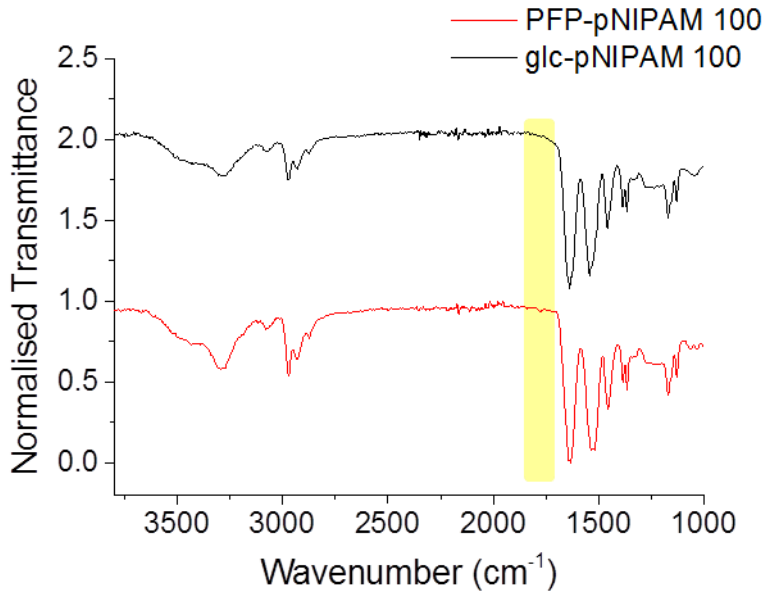

Figure 4.14: IR spectra show the removal of the PFP ester. Region of interest is highlighted

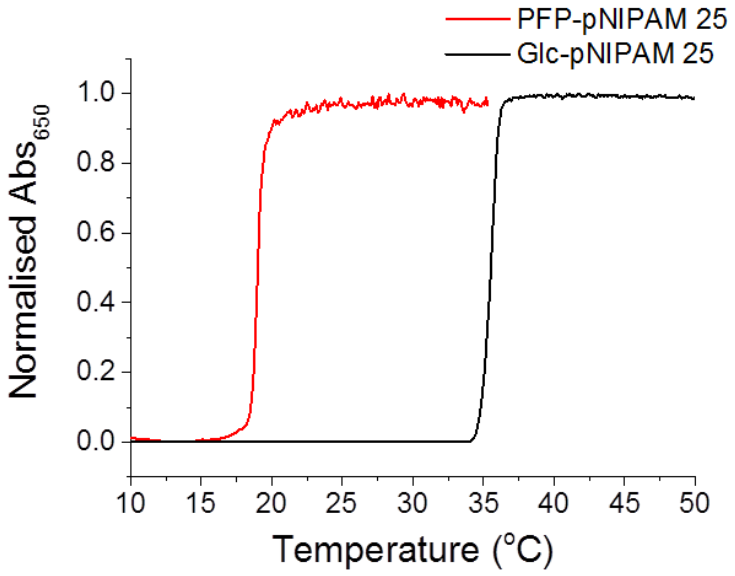

Figure 4.15: Turbidimetric analysis of the PFP-pNIPAM$_{25}$ and Glc-pNIPAM$_{25}$. Polymer concentration = 1 mg.mL^{-1} in water

Size exclusion chromatography data comparing one pair of glycosylated polymers (Glc-pNIPAM$_{100}$ and Glc-pNIPAM$_{25}$), depicted in Figure 4.16, confirms that the differences in polymer chain length characterised in Table 4.1 remain in the glycosylated species and that the end group modification does not affect the polymer M_w, nor dispersity.

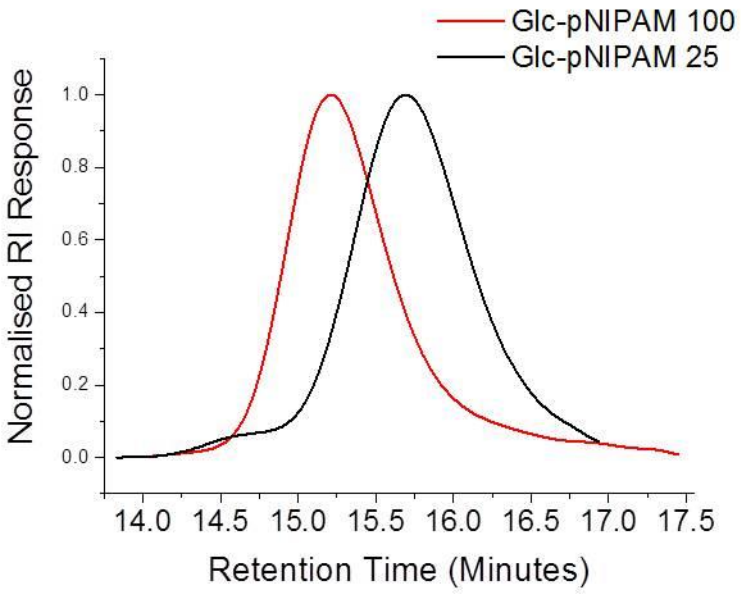

Figure 4.16: SEC traces for Glc-pNIPAM$_{25}$ and Glc-pNIPAM$_{100}$, run in DMF

Table 4.4: SEC Characterisation data for the glycosylated-pNIPAM polymers

[M]:[CTA]	Terminal Sugar	$M_{n(SEC)}^{[C]}$	$M_{w(SEC)}^{[C]}$	$M_w/M_n^{[C]}$
25:1	Glc	4200	4700	1.10
25:1	Gal	3600	4400	1.25
25:1	Man	3100	4200	1.34
100:1	Glc	8100	9900	1.13
100:1	Gal	8300	9300	1.11
100:1	Man	8600	9400	1.09

SEC experiments run in DMF using poly(methyl methacrylate) standards. M_w = weight average molecular weight, M_n = number average molecular weight

MALDI-ToF analysis was attempted in order to characterise the glycosylated polymers, however side-reactions with the matrix components were observed. The peak separation of 113 was still clearly seen though, confirming the presence of the NIPAM monomers. High-resolution electrospray ionisation MS was therefore employed instead. The spectrum depicted in Figure 4.17, shows the peaks resulting from the analysis of Glc-PNIPAM$_{25.}$ Since the glycosylation reaction was carried out in TEA, it is highly probable that the thiol end group (trithiocarbonate) of the polymer was replaced with the TEA salt. In the MS process, using positive mode, this can be subsequently converted to the sodium salt. The peaks in this spectrum are doubly charged species, indicated by the peak splitting difference being half that of a NIPAM monomer, and therefore the 1587.07 peak can be attributed to [Glc-pNIPAM$_{25}$-SNa+2Na]$^{2+}$.

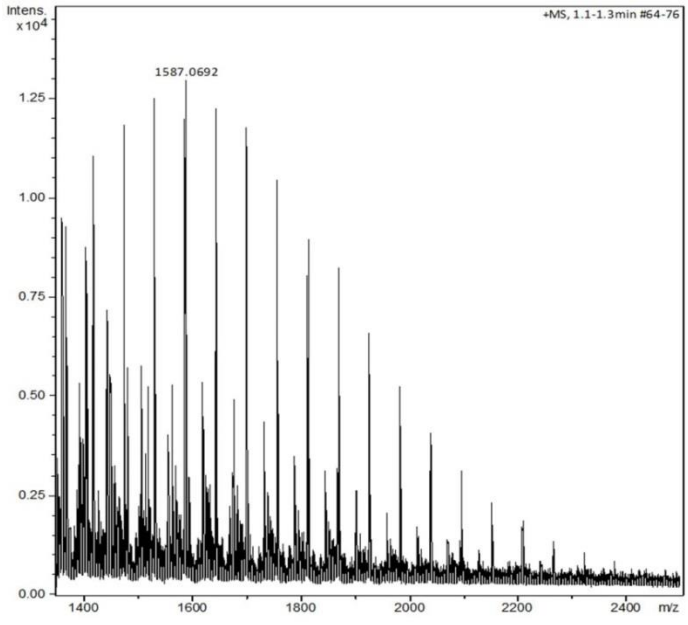

Figure 4.17: High resolution ESI-ToF MS spectrum for Glc-PNIPAM$_{25}$

Taken together, these data confirm installation of the sugar and generation of the thiol end group.

4.3.3. Immobilisation of Glycosylated Polymers onto Glass Substrates

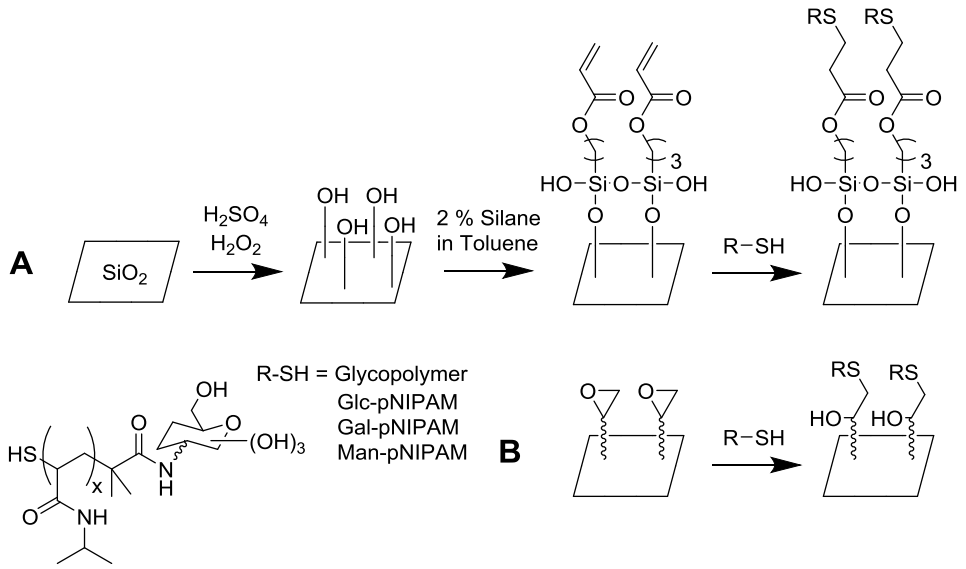

Figure 4.18: Schematic for polymer immobilisation onto [A] acrylate silane and [B] epoxide coated glass

Figure 4.18 shows the synthetic scheme to immobilise polymers onto acrylate or epoxide surfaces. The glycosylated pNIPAMs were added using the same protocols used for the pNIPAM and pOEGMA polymers in Chapter Three. Briefly, the glycopolymer solutions were prepared at 2 $mg.mL^{-1}$ in water and incubated at room temperature for 2 hours before washing.

4.3.3.1. Drop Shape Analysis of the Glycopolymer Functionalised Glass

Water contact angle measurements were taken in order to confirm immobilisation. The glass slides were functionalised with each of the six glycopolymers detailed in Table 4.3, in triplicate. The results in Figure 4.19 show that although the acrylate and epoxide coated glass initially have different contact angles (48.0° and 58.6° respectively), once functionalised with the polymers, in both cases the contact angles exhibit a shift, indicating successful surface modification. In the case of the silane acrylate, the

modification from surface acrylate to glycosylated polymer can be seen in the change in contact angle from 48.0° to an average value of 58.9° and on the epoxide coating a change from 58.6° to 48.5° is observed. Interestingly, the values for the glycosylated-pNIPAM on the silane acrylate are very similar to those obtained for the thioglucose and thiogalactose functionalised surfaces prepared in Chapter Two (62.4° and 59.5° respectively) and also the pNIPAM functionalised glass discussed in Chapter Three (58.0°), whereas those on the epoxide coating are lower. This suggests that the epoxy surface may be better able to structure the sugars on the surface than the acrylated silane surface. Detailed characterisation of pNIPAM polymer functionalised surfaces was carried out in Chapter Three, so no further characterisation was undertaken.

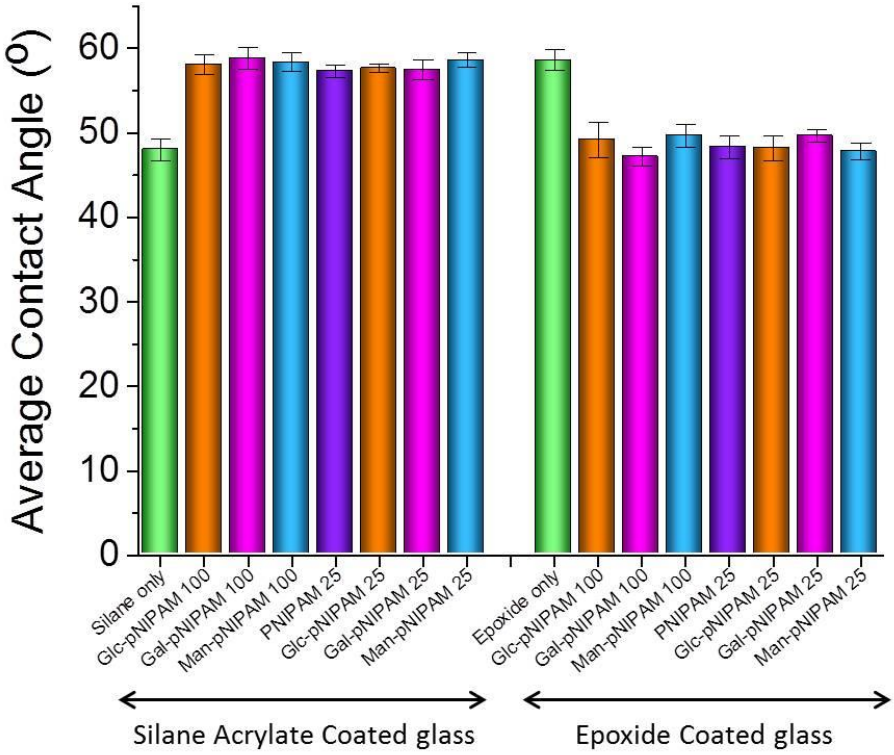

Figure 4.19: Water drop contact angles for the acrylate (left) and epoxide (right) functionalised glass with and without the subsequent glycosylated-pNIPAM functionalisation. Error bars show the standard deviation taken from a minimum of five independent measurements

4.3.4. Interaction of Surface Bound Glycopolymers with Lectins

With the successfully preparation of surface bound glycosylated polymers, lectin binding could be studied. Glass slides were fully submerged in solutions of each of the 8 polymers from Table 4.3 to generate polymer coatings, which were then washed and dried. Spots of fluorescent labelled Con A were then administered onto the surfaces. These lectin spots were allowed to incubate with the glycopolymers for 30 minutes, in the dark, the excess lectin was then removed and the slides were washed, dried and scanned in the microarray scanner. This process was carried out on both acrylate and epoxide coated glass slides.

The results, shown in Figure 4.20, show that the binding specificity trends are much more pronounced for the longer chain polymers ($pNIPAM_{100}$) than the shorter polymer ($pNIPAM_{25}$) on both the acrylate and epoxide substrates. When looking at the data for the $pNIPAM_{100}$ polymers, on both types of surface, the Con A is exhibiting more binding (indicated by higher fluorescence values) to the glucose and mannose functionalised polymers than the galactose functionalised polymers. These results are in correspondence with the expected binding profiles of Con A, which is known to show preferential binding for α-D-mannosyl and α-D-glucosyl groups.[20] For the shorter glycopolymers, the trends are less distinct, although there is still a slight preferential binding for glucose and mannose over galactose. From the QCM-D experiments in Chapter Three, we concluded that the grafting density of the $pNIPAM_{25}$ polymers was higher than the longer $pNIPAM_{100}$ chains. Assuming that this is still the case for the glycopolymers, it is reasonable to conclude that the reduced number of bound polymer chains and therefore

reduced number of terminal glycans for the $pNIPAM_{100}$ will affect the binding process. When the number of surface bond polymers is greater there are therefore more glycans present and they are more tightly packed, as is the case for the shorter $pNIPAM_{25}$ polymers. The increased sugar concentration will increase the affinity of all sugars to the point where it is saturated and hence less discrimination can be observed. At lower grafting densities, the multivalency is lower and hence the Con A binding will be stronger to Man/Glc than Gal. The numerical fluorescence values are lower for the epoxide coating because the more hydrophilic surface present on these samples, compared to the silane acrylate coating, resulted in more spreading of the lectin spots and therefore less concentrated FITC signals.

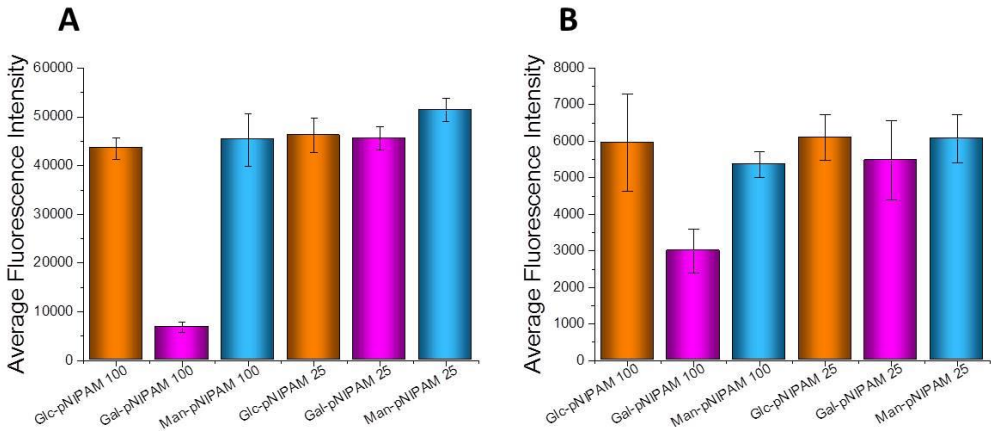

Figure 4.20: Lectin binding onto glycopolymer functionalised surfaces [FITC-Con A] =0.025 mg.mL^{-1} [A] Acrylate and [B] Epoxide coated glass. Fluorescence values correspond to quantitative analysis of average green fluoresce (excitation 480 nm, emission 520 nm) over the sample area. Error bars represent the standard deviation between 3 independent measurements

Whilst the functionalisation of whole glass slides with a glycopolymer is of interest and subsequent addition of lectin spots allows for the protein-carbohydrate binding specificities to be observed, it does not permit high-throughput data collection because each sample can only be used to monitor

the interaction of one surface bound polymer with a limited set of test lectin spots and furthermore droplet spreading can reduce the resolution. It would be far more preferable to functionalise the surface with many different test polymers, for which the number of different glycopolymer species are limited only by the time required to synthesise large libraries of compounds, and then incubate these multi-functionalised surfaces with one test lectin per slide. This is particularly important because of the limited number of commercially available fluorescently labelled test lectins. In this way, far greater numbers of interactions can be probed on one sample, reducing preparation and scanning time and costs.

The presentation of large numbers of glycopolymer species on a glass slide is best achieved through the use of printing methods, such as direct contact printing or inkjet printing. Direct microcontact printing was chosen for this work, due to this system not suffering from the frequent blocking problems often associated with the inkjet printers. Prior to employing the direct microcontact printer, however, control experiments involving manually printing the glycopolymers onto the silane coated glass slides were performed. This allowed for the development of an incubating, blocking and washing protocol and these experiments gave us the opportunity to optimise the process without the challenges of obtaining access to a microcontact printer.

Firstly, the slides were functionalised with three different glycopolymers (pNIPAM$_{100}$ with terminal glucose, galactose or mannose) so that the lectin could be administered in spots, to prevent the challenges of non-specific background protein binding. Glass slides were cleaned and functionalised with the silane solution, as previously described in Chapters

Two and Three, then 100 µL spots of the 10 mg.mL^{-1} glycopolymer solutions, in water, were added and allowed to react whilst contained within a sealed, humidified, Petri dish, in order to minimise evaporation. The spot size was chosen to be large enough to allow a large area for administering the lectin onto, but without allowing the solutions to spread into each other. After washing and drying, spots of Con A FITC (0.025 mg.mL^{-1}) were added, allowed to react, washed and then dried. The resulting data, Figure 4.21, showed that the Con A was exhibiting preferential binding to the glucose and mannose functionalised regions, shown by increased fluorescence values. These results are in good correspondence with the values obtained when functionalising whole glass slides (see Figure 4.20) and confirms the potential of the system.

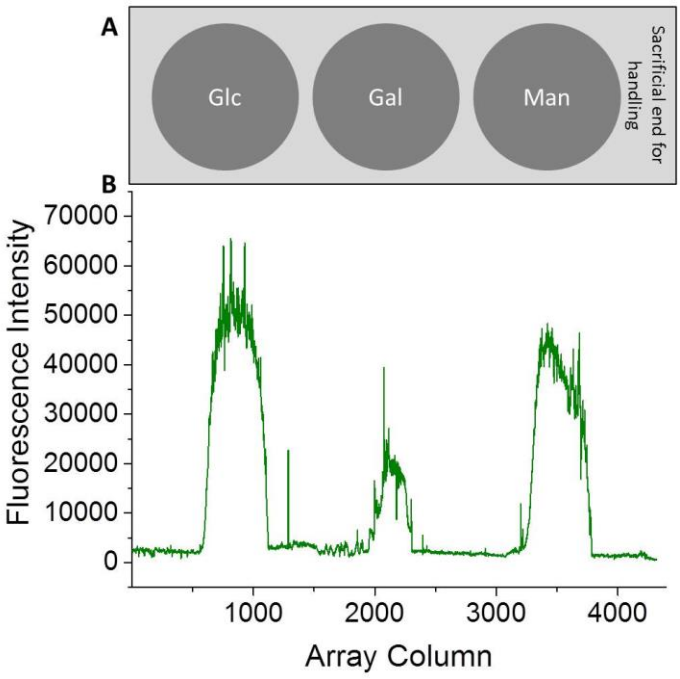

Figure 4.21: Microarray scanner fluorescence intensity trace for functionalised slides. [A] Schematic of surface coating. [B] Fluorescence intensity after Con A incubation

After achieving successful binding onto glycopolymer functionalised surfaces, the next step was to add an increased number of glycopolymer spots onto the surface and then incubate by submerging the whole sample in a lectin solution. Each of the glycopolymers from Table 4.3 was added onto an acrylate functionalised glass slide in the form of 5 µL spots, as shown in Figure 4.22. As can be seen, the polymer spots themselves exhibit some inherent low level fluorescence, which is advantageous in terms of confirming surface modification and identifying the precise location of the spots. The "coffee-ring" shape of the spots, where the edges exhibit greater fluorescence than the centre, is a well-known defect occurring when a droplet containing solute dries onto a surface.[10] This heterogeneity can be prevented by using smaller droplets, which will be the case when the direct-microcontact printer in employed for droplet delivery (see later). The 5 µL spots achieved through manual pipetting are typically 5.0 mm in diameter, whereas the 2.4 nL droplets obtained through the direct microcontact printing are only 0.2 mm in diameter.

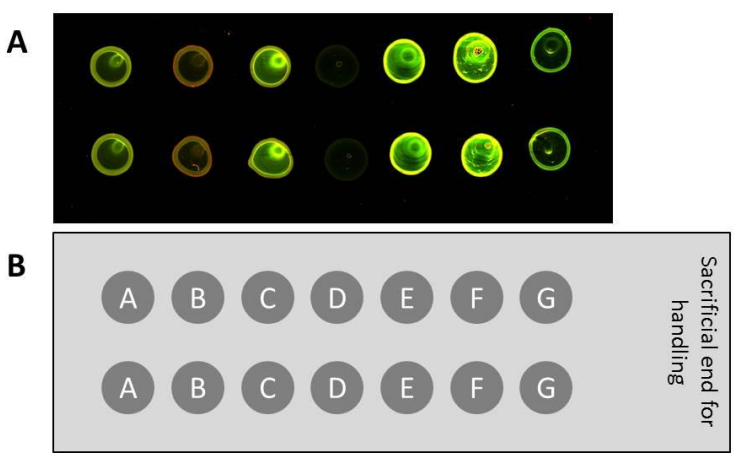

Sample code	pNIPAM chain length	Terminal Sugar
A	100	Glc
B	100	Gal
C	100	Man
D	100	-
E	25	Glc
F	25	Gal
G	25	Man

Figure 4.22: [A] Microarray scanner image of the glycopolymers solutions (see table for solution details) spotted onto a silane coated glass slide and [B] pictorial representation of the functionalised slides, showing the location of the sacrificial end, which is left unfunctionalised in order to facilitate handing

The slides were incubated with a test lectin (soy bean agglutinin (SBA) 0.2 $mg.mL^{-1}$ in HEPES buffer) for 30 minutes in the dark, to allow for interaction between the protein and the surface bound carbohydrates. The data in Figure 4.23 shows the problems obtained when the surfaces are incubated with the lectin, in the absence of a blocking procedure. Although the polymer coatings have been designed to resist non-specific interactions, the areas surrounds the polymer spots consist of silane functionality and large amounts of non-specific lectin binding can be seen in these regions. The image in Figure 4.23A shows the un-manipulated data from the scanner and the very high fluorescence values across the sample make any trends very difficult to observe. In part [B] the intensity of the colour has been reduced by 25% and it can now been observed that the fluorescence is brightest and most uniform in the galactose functionalised region, which corresponds to the known binding specificity for SBA (preferential binding to *N*-acetylgalactosamine). However, there is still significant binding to both glucose and mannose and the background regions. Pleasingly, the un-glycosylated pNIPAM appears to be resisting the non-specific adsorption to a greater extent than some of the background regions. In the intensity graph, the values are all up near to the maximum, which is undesirable. However, only the region corresponding to the galactose functionalisation reaches the maximum value and is cut off, suggesting that this area has the largest amount of FITC-SBA.

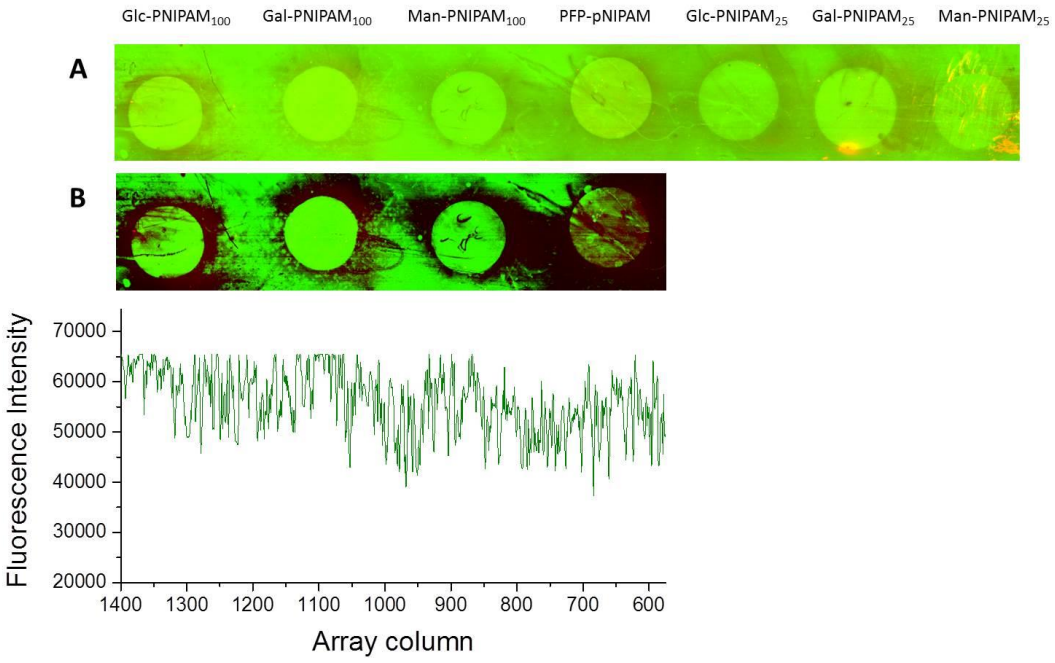

Figure 4.23: Typical microarray scanner images of glycosylated polymer arrays [A] Is the unprocessed image and [B] has the colour intensity reduced by 25%. The intensity graph is the fluorescence intensity taken from the green channel for the row corresponding to the mid-point through the polymer spotted regions

From this data it became very clear that a blocking procedure was required, prior to the lectin incubation step, in order to minimise non-specific interactions between the lectins and the surface. Firstly, a blocking procedure involving a 30 minute soak in a 2 $mg.mL^{-1}$ solution of bovine serum albumin (BSA), followed by washing to remove unbound material, was employed. Unfortunately, the BSA proved to bind indiscriminately across the whole sample, rather than just to the areas around the polymer spots. This problem remained when lower concentrations of BSA were trialled. At high BSA concentrations (2 $mg.mL^{-1}$), intrinsic fluorescence from the protein was observed across the whole sample, prior to addition of the FITC-lectin, and at low concentrations (0.02 $mg.mL^{-1}$) low levels of green fluorescence were detected across the whole sample, even after addition of the FITC-lectin.

Following the procedure used by the CFG on their streptavidin-biotin arrays,[21] a tween (polyethylene glycol sorbitan monolaurate, a non-ionic detergent) blocking procedure was trialled. This proved far more successful, the tween did not add significant amounts of background fluorescence onto the sample and nor did it appear to coat the entire slide, including the polymer spots. Other literature techniques recommend including tween in the lectin solution, but we found the results comparable to just using HEPES buffer. [22] Therefore, we progressed to using a tween blocking procedure for the microarray printing process.

4.3.5. Direct-Microcontact Printing of Glycopolymers onto Glass

To increase the density of information present on each slide and reduce droplet-to-droplet variance, a direct-microcontact printer was employed to generate nanospots of the polymer solutions on the surface. Samples of polymer solutions were prepared, see Table 4.3 for details of the polymers, at 10 $mg.mL^{-1}$ in Milli-Q water and then diluted to produce concentrations of 5, 2.5, 1.25 and 0.6125 $mg.mL^{-1}$. The solutions were then printed onto both acrylate and epoxide coated glass microscope slides to produce high density arrays of polymer. The chamber of the printer was set to 25°C and 45% humidity in order to prevent rapid evaporation of the polymer spot solution and therefore facilitate the reaction between the thio-terminus of the pNIPAM chain and the acrylate or epoxide group present on the surface. The resulting arrays contain eight polymer solutions, each in five concentrations, with ten repeats of each sample. In total this results in the ability to probe 40 different lectin-glycopolymer binding events, each repeated ten times, on one glass slide, Figure 4.24.

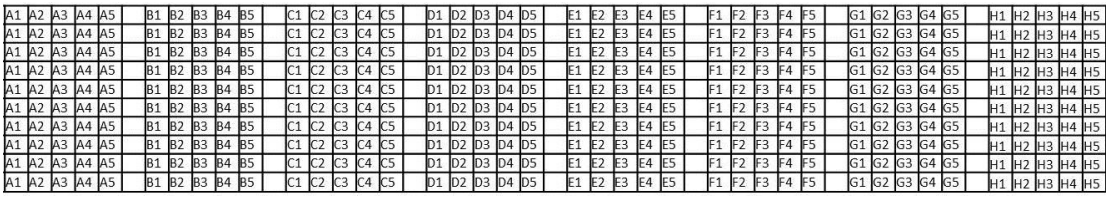

Figure 4.24: Diagrammatic representation of the presentation of polymer solution spots on the glass slide. A1 represents sample A at concentration 1 (10 mg.mL^{-1}) with A2 representing this polymer at half the concentration of A1 etc. Each sample solution is spotted 10 times (from the top to the bottom of the slide) and the eight different polymers are spotted working across the slide from left to right

As with the manually spotted glycopolymers, an inherent fluorescence was observed for the printed polymer solutions, as seen in Figure 4.25, confirming that the spots had correctly printed and that the concentrations were decreasing as would be expected. The data in Figure 4.25 shows a section of the slide with five decreasing concentrations of the Man-pNIPAM$_{25}$ and then five decreasing concentrations of the PFP-pNIPAM$_{25}$. The fluorescence intensity, both of the spots and the corresponding graph, decreases with decreasing concentration, as would be expected. Also, the glycosylated polymers appear to have bound more successfully with the surface than the PFP-terminated pNIPAMs, which is to be expected considering that only the glycosylated polymers have a free thiol terminus. As we have described in Chapter Three, the free thiol allows for better thiol-ene surface conjugation that the corresponding RAFT end group.

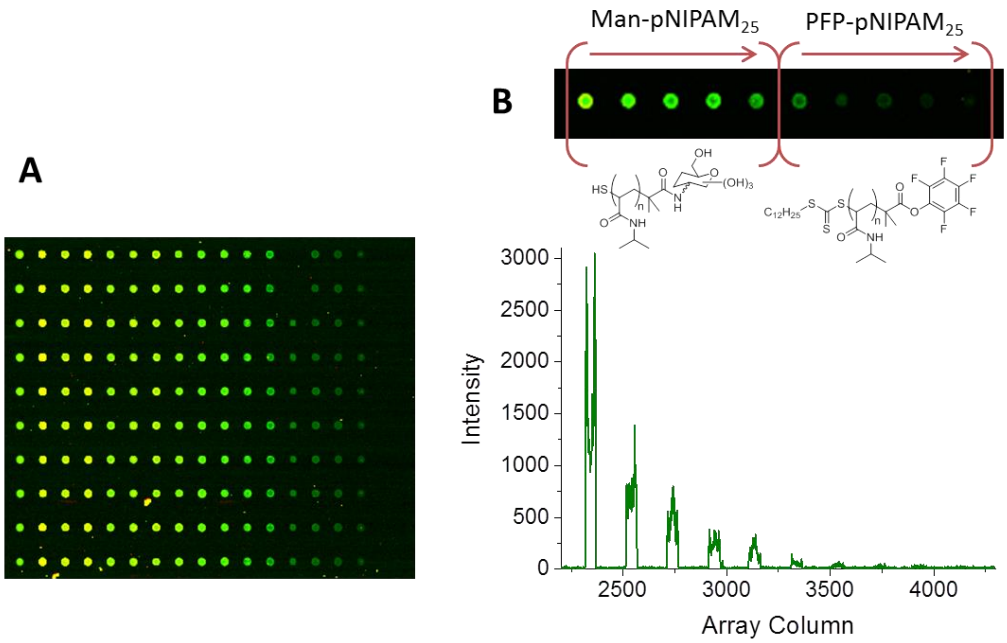

Figure 4.25: [A] Microarray scanner image for the printed polymers. [B] Microarray scanner image and corresponding fluorescence intensity trace for a section of the glycopolymer spots printed onto the glass slide with five decreasing concentrations of Man-pNIPAM$_{25}$ and five decreasing concentrations of PFP-pNIPAM$_{25}$, on the epoxide coated glass

4.3.6. Interaction of Printed Glycopolymers with Lectins

Having confirmed that the polymers were successfully printed onto the surfaces, the arrays could be used to probe glycopolymer-lectin interactions. The tween blocking procedure was utilised and the surfaces were then submerged in a solution of SBA and allowed to incubate for 30 minutes. Following washing , the surfaces were scanned and the fluorescence intensity was plotted for the array rows containing the printed spots. The data in Figure 4.26 shows a section of the slide containing the Gal-pNIPAM$_{100}$, Man-pNIPAM$_{100}$ and PFP-pNIPAM$_{100}$ polymers, each in five decreasing concentrations, after interaction with SBA. Firstly, the glycopolymer-lectin interactions appear to be concentration dependent; the highest binding is observed for the highest concentration of glycopolymer. Also, the SBA appears to be binding preferentially to the Gal-PNIPAM$_{100}$, which is in correspondence with the expected binding profiles. The SBA is also binding to the

Man-pNIPAM$_{100}$, due to the binding specificities of the lectins being preferential rather than totally specific, which is to be expected. The SBA is not exhibiting any significant binding to the regions coated with un-glycosylated polymers. The fluorescence values for these regions do not exhibit the characteristic peaks and the fluorescent spots are not observed in the array image.

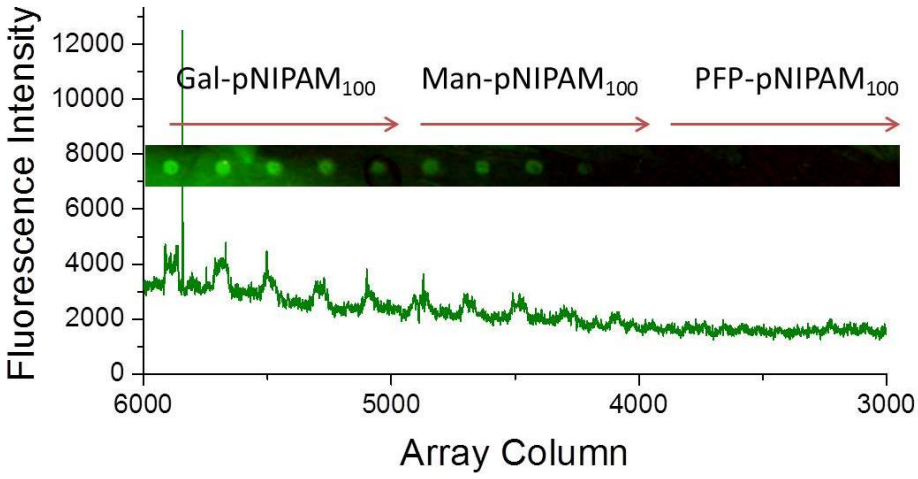

Figure 4.26: Microarray scanner image and corresponding fluorescence intensity trace for a Gal-, Man- and PFP- glycopolymer spots printed onto the epoxide coated glass slide after incubation with SBA

This process was then repeated using WGA as the lectin. The data in Figure 4.27 shows the binding of the WGA to the Glc- pNIPAM$_{100,}$ Gal-pNIPAM$_{100}$, Man-pNIPAM$_{100}$ and PFP-pNIPAM$_{100}$ functionalised regions of the epoxide coated slide. The WGA appears to be binding preferentially to the galactose functionalised region, but also binding to glucose and mannose to a lesser extent. If the baseline values are taken into account, then the glucose binding is higher than those observed for the mannose. This agrees well with previous research in the group.[23] Again, there is no specific binding occurring in the un-glycosylated polymer functionalised region.

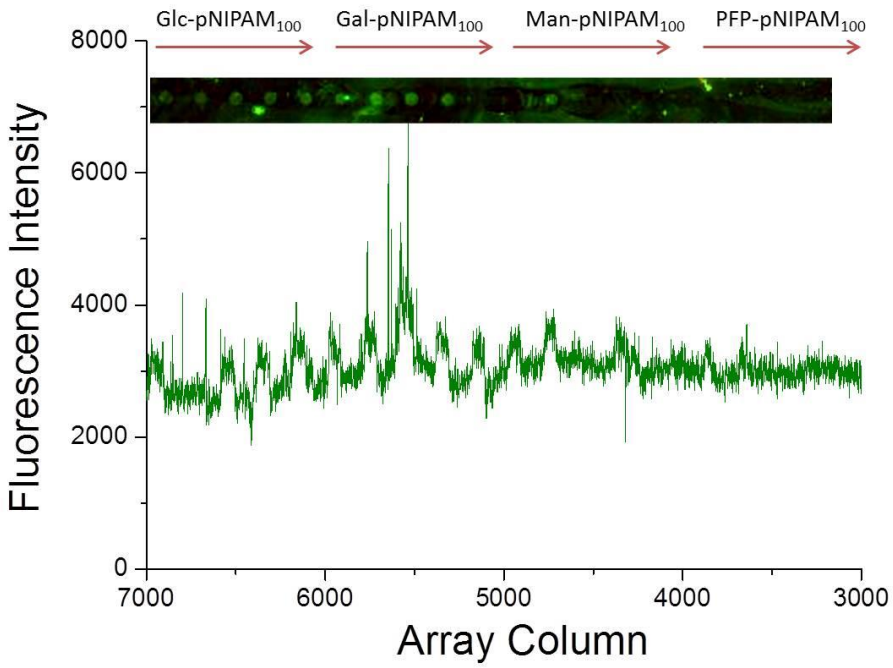

Figure 4.27: Microarray scanner image and corresponding fluorescence intensity trace for a Glc-, Gal-, Man- and PFP- glycopolymer spots printed onto the epoxide coated glass slide after incubation with WGA

It should be noted that there is still heterogeneity across the slides and ideally more optimisation is required to probe the biological binding effects, but in principle we have demonstrated that all the synthetic steps were successful. Future work will focus on applying this to probe medically relevant lectin interactions and optimising the washing steps to ensure maximum resolution.

4.4. Conclusions

Pentafluorophenyl-terminated poly(*N*-isopropylacrylamide)s (PFP-pNIPAM), were successfully synthesised using the RAFT controlled radical polymerisation technique. These polymers were glycosylated in a post-polymerisation modification step involving the reaction of the terminal PFP group with 2-deoxy-2-aminomannose ($ManNH_2$), 2-deoxy-2-aminoglucose ($GlcNH_2$) and 2-deoxy-2-aminogalactose ($GalNH_2$) to produce a small library of glycan-terminated polymers. These polymers were successfully immobilised onto the acrylate silane coated glass slides utilised throughout Chapters Two and Three and also onto commercially available epoxide coated glass slides. The resulting surface grafted glycans were then probed for their suitability as glycoarrays through their interactions with model lectin systems, which was found to be successful and greater differences in carbohydrate-lectin binding specificity were achieved through the use of the longer chain ($pNIPAM_{100}$) glycopolymers.

In order to increase the information density and reduce the problems that arise due to large polymer spots (namely uneven fluorescence distributions within the test areas) the glycopolymers were printed onto glass slides using a BioDot direct contact printer. This allowed the generation of glass slides with 400 2.4 nL polymer spots present on the surface. These surfaces were then used to investigate the carbohydrate-lectin binding specificity using SBA (preferential binding to galactose residues) and WGA (preferential binding to glucose and galactose residues), demonstrating the proof concept that these arrays have potential to be used as biological screening tools.

4.5. Materials and Methods

4.5.1. General Experimental

All reagents and solvents were used as received from the supplier. Laboratory solvents were purchased from Fisher Scientific and 3-(trimethoxysilyl)propyl acrylate from Sigma-Aldrich. Plain Microscope slides were purchased from Corning Scientific (plain, soda-lime glass, ground edges, 75 mm x 25 mm, 0.9 mm to 1.1 mm thick). Epoxide coated microscope slides were purchased from VWR and supplied by Corning Scientific (25.3 mm x 75.5 mm x 1.1 mm).

10 mmol HEPES buffer, containing 0.1 mmol $CaCl_2$, pH 6.5, was prepared in 250 mL Milli-Q water. Tris-HCl buffer was prepared at 20 mM, pH 7.4. Fluorescently labelled lectins (Con A, SBA) from Vector Labs (Fluorescein FLK-2100 labelled). All other reagents were purchased from Sigma-Aldrich.

Any waste thiol solutions were treated with sulfide oxidiser microemulsion solution (3% cyclohexane, 5% sodium dodecyl sulfate, 10% butan-1-ol and 82% water by weight) to kill the thiol smell. 1 ml of sulfide was dissolved in 15 ml of microemulsion and 5% aqueous sodium hypochlorite solution was then added in 2-fold excess. Thiol contaminated glassware was soaked in sulfide oxidiser microemulsion with 5% sodium dodecyl sulfate prior to washing.

4.5.1.1. Nuclear Magnetic Resonance Spectroscopy

All NMR spectra were obtained using a Bruker DPX-300 (300 MHz) or DPX-400 (400 MHz) spectrometer. The deuterated solvents were used as supplied by Aldrich. Chemical shifts were recorded as δ values in parts per million (ppm) and referenced to the solvent used.

4.5.1.2. Size Exclusion Chromatography

SEC analysis was performed on a Varian 390-LC MDS at 30°C. The system is equipped with a PL-AS RT/MT autosampler, a PL-gel 3 μm (50 × 7.5 mm) guard column and two PL-gel 5 μm (300 × 7.5 mm) mixed-D columns. Detection is achieved using a differential refractive index and a Shimadzu SPD-M20A diode array detector. The eluent was a solution of dimethylformamide (DMF) with 1 $mg.mL^{-1}$ lithium bromide and the flow rate was set to 1.0 $mL.min^{-1}$. Data analysis was carried out on Cirrus 3.2 SEC software. The molecular weight calculations were carried out against narrow molecular weight PMMA standards (200 - 1.0×10^6 $g.mol^{-1}$).

4.5.1.3. Cloud Point Measurements (Turbidimetric Analysis)

The thermal transitions were measured using an Agilent Technologies Cary60 UV/Vis spectrometer equipped with a Quantum Northwest TC1 temperature controller. Samples were heated for 10°C to 90°C at $2°C.min^{-1}$. The polymers are fully solubilised at the starting temperature, resulting in near perfect optical transmittance at 650 nm. Upon approaching the LCST, the polymer solutions turn opaque and the cloud point is measured as the temperature at which 50% of the original transmittance is lost.

4.5.1.4. Infrared Spectroscopy

IR spectra were collected on a Bruker Alpha Platinum-ATR spectrometer. A total of 64 scans were taken for each sample and all samples were presented in a dry state.

4.5.1.5. Mass Spectrometry

Mass spectra were recorded on a Bruker Esquire2000 TOF machine in positive mode, with ethanol as the sample solvent. High resolution mass spectra were recorded on a Bruker Electrospray Ultra-High Resolution tandem TOF mass spectrometer using electrospray ionisation in positive mode on samples prepared in water-THF, then diluted with 80% methanol. MALDI-ToF (matrix-assisted laser desorption ionisation time-of-flight mass spectrometry) data was obtained using a Bruker Daltonics Ultraflex Extreme MALDI-ToF mass spectrometer, equipped with a SmartBeam 2 laser. Detection (positive ion) was performed using a voltage of 25 kV. Polymer samples were dissolved in water, then diluted with 80% methanol and prepared on a DHB:CHCA 50:50. The data was calibrated using PEG standards.

4.5.1.6. Surface Cleaning Procedure

The plain microscope slides used in this work were chemically cleaned according to the method described in Chapters Two and Three using piranha solution. The commercially coated epoxide slides were rinsed with Milli-Q water and blown dry in a gentle stream of dry nitrogen before use.

Safety Note: Piranha solution is strong oxidizing and is hazardous to prepare and use. It should be handled in small quantities, freshly prepared and never stored. The hydrogen peroxide solution should be slowly added to the acid and the reaction should be carried out on ice. After completion of the cleaning process, the piranha solution should be allowed to cool and then diluted slowly into one litre of deionised water, with 2-3 spoons of MnO_2. After 12 hours this solution can be neutralised with sodium bicarbonate and disposed of appropriately.

4.5.2 General Surface Analysis

4.5.2.1. Contact Angle Measurements

The water contact angle measurements were conducted at room temperature using a Krüss drop shape analysis system following the same experimental procedure detailed in Chapter Three.

4.5.2.2. Microarray Scanner

The fluorescence images were obtained using an Agilent G2565CA Scanner capable of one- and two-colour scanning and compatible with glass slide arrays. The scanner is fitted with a 48-slide carousel autoloader and can scan up to 2 μm resolution. Standard two colour scanning protocols were used with a SHG-YAG laser (532 nm) and a helium-neon laser (633 nm). The data was exported as a Tagged Image File (Tif) file and numerical data was then obtained using Agilent Feature Extraction Software. The background intensity was taken as the average fluorescence intensity across the whole sample where no specific interactions were being observed (i.e. the area away from the lectin or glycopolymer spotted solutions) and was subtracted from the fluorescence intensity for the area of interest. The intensity values quoted are for the green channel.

4.5.3. Synthetic Procedures

4.5.3.1. Synthesis of Pentafluorophenyl 2-(dodecylthiocarbonothioylthio)-2 methylpropanoic acid (PFP-DMP)

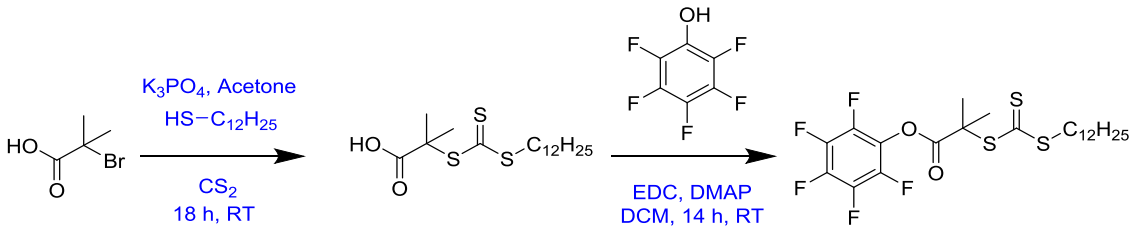

2-(dodecylthiocarbonothioylthio)-2-methylpropanoic acid (DMP) was synthesised and characterised as per the method previously described in Chapter Three. To the DMP (0.50 g, 1.37 mmol) was added *N*-(3-Dimethylaminopropyl)-*N'*-ethylcarbodiimide hydrochloride (EDC) (0.39 g, 2.05 mmol), and 4-(dimethylamino)pyridine (DMAP) (0.25 g, 2.05 mmol) in 40 mL DCM and the solution was stirred for 20 minutes under N_2. Pentafluorophenol (0.78 g, 4.24 mmol) in 5 mL DCM was then added and the reaction was stirred overnight at room temperature. The reaction was washed successively with 3 M HCl, 1 M $NaHCO_3$ and 0.5 M NaCl, dried over $MgSO_4$, filtered and concentrated *in vacuuo* to yield a yellow oil (0.51 g, 70.0 %).

^{1}H NMR (300 MHz, $CDCl_3$) δppm: 3.29 (2H, t, J = 7.3 Hz, $SC\mathbf{H}_2$); 1.86 (6H, s, $C_9C\mathbf{H}_3)_2$); 1.67 (2H, q, J = 7 Hz, $SCH_2C\mathbf{H}_2$); 1.37 (2H, m, $C\mathbf{H}_2CH_3$); 1.23 (16H, br. s, $SCH_2CH_2(C\mathbf{H}_2)_8$); 0.86 (3H, t, J = 6.5 Hz, $CH_2C\mathbf{H}_3$).

^{13}C NMR (500 MHz, $CDCl_3$) δppm: 220.20 (**C**=S), 169.28 (**C**=O), 54.91(**C**$(CH_3)_2$), 36.46 (S**C**H_2), 31.41, 29.02, 28.95, 28.84, 28.74, 28.60, 28.36, 28.08, 27.19 (**S**$(CH_2)_9$), 22.60 (**C**H_2CH_3), 13.52 ($S(CH_2)_{11}$**C**H_3).

IR ν/cm^{-1}: 2960 (alkyl-H stretch); 1779 (C_6F_5C=O stretch); 1070 (S-(C=S)-S stretch).

MS (ESI +) m/z: 553.2 $[M+Na]^+$; expected 553.1

4.5.3.2. Synthesis of PFP-pNIPAM polymers

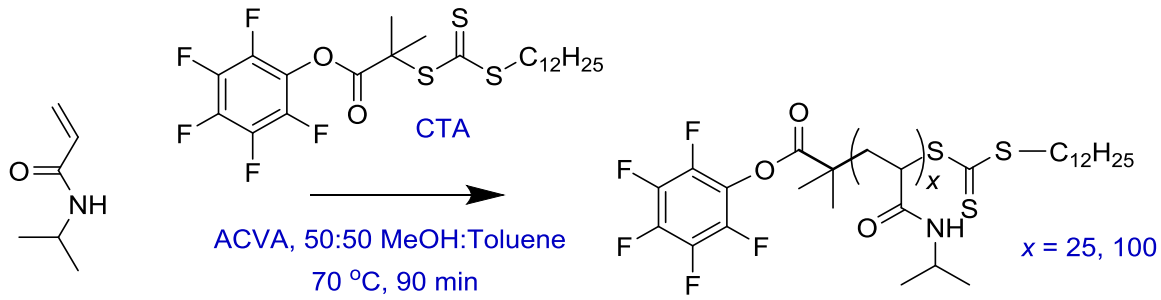

In a typical procedure, *N*-isopropylacrylamide (1.00 g, 8.837 mmol), pentafluorophenyl 2-(dodecylthiocarbonothioylthio)-2-methylpropanoic acid (188.0 mg, 0.35 mmol), 4,4'-azobis(4-cyanovaleric acid) (19.7 mg, 70.6 µmol) were added to a vial fitted with stir bar and rubber septum and dissolved in methanol:toluene (50:50) (4 mL). Mesitylene (200 µL) was added as internal reference and the mixture was then stirred (5 min). Further polymerisation solutions were prepared, as detailed in Table 4.5. The solutions were degassed with nitrogen (30 min), immersed into an oil bath (70°C, 90 min) then opened and cooled on ice. Each solution was concentrated, dissolved in the minimum of THF, precipitated into hexane (35 mL) and re-precipitated from THF into hexane a further three times. The resulting solid was isolated by centrifugation and dried to yield a pale yellow solid product.

Table 4.5: Polymerisation reagent compositions for the synthesis of PFP-pNIPAMs

Theoretical Degree of Polymerisation [M]:[CTA]		Initiator (ACVA)	RAFT Agent (PFP-DMP)	Monomer (NIPAM)
25:1	Ratio	0.2	1	25
	Moles/ mmol	0.070	0.35	8.84
	Mass/ mg	19.7	188.0	1.0×10^3
100:1	Ratio	0.2	1	100
	Moles/ mmol	0.03	0.14	8.84
	Mass/ mg	7.8	75.0	1.0×10^3

The polymers were characterised by ^{1}H NMR spectroscopy. The degree of polymerisation was also estimated from the conversion (from ^{1}H NMR spectroscopy). Analysis was also carried out by DMF SEC against PMMA standard. The characterisation data is summarised in Table 4.6.

Table 4.6: Characterisation data for the PFP-pNIPAM polymers

[M]:[CTA][A]	Conver. (NMR)[B]	DP_{Theo} (NMR)[B]	Mn (NMR)[B]	M_n (SEC)[C]	M_w (SEC)[C]	M_w/M_n[C]
25:1	88%	22	2480	3980	4450	1.12
100:1	92%	92	10410	9200	9890	1.08

[A] Feed ratio of monomer to initiator; [B] Determined by ^{1}H NMR spectroscopy in $CDCl_3$; [C] Determined by SEC in dimethylformamide (DMF) using poly(methyl methacrylate) standards. M_w = weight average molecular weight, M_n = number average molecular weight

4.5.3.3. Glycosylation of PFP-pNIPAMs

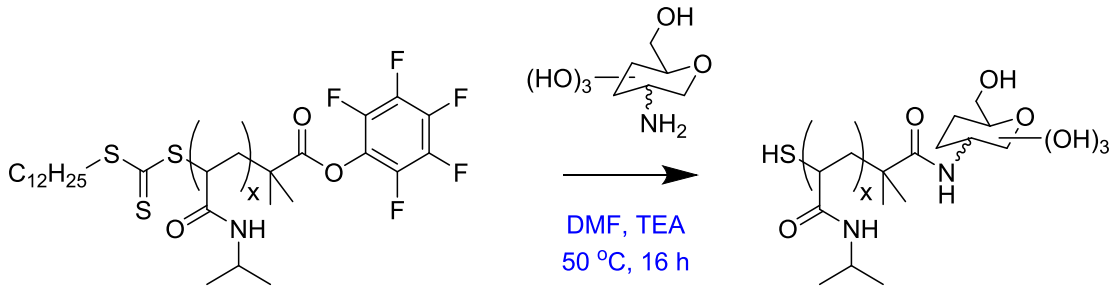

In a typical procedure, PFP-pNIPAM$_{25}$ (100.0 mg, 0.03 mmol) and mannosamine (25.0 mg, 0.13 mmol) were dissolved in DMF (2 mL) with TEA (5 µL) and the reaction stirred for 16 hours at 50°C. The reaction mixture was concentrated and resolubilised in THF. The polymer was then isolated by precipitation into hexane and re-precipitated from THF into hexane a further three times. The pale cream solid was then dried.

4.5.4. Glycopolymer Coatings on Glass Substrates

4.5.4.1. Functionalisation of Plain Microscope Slides

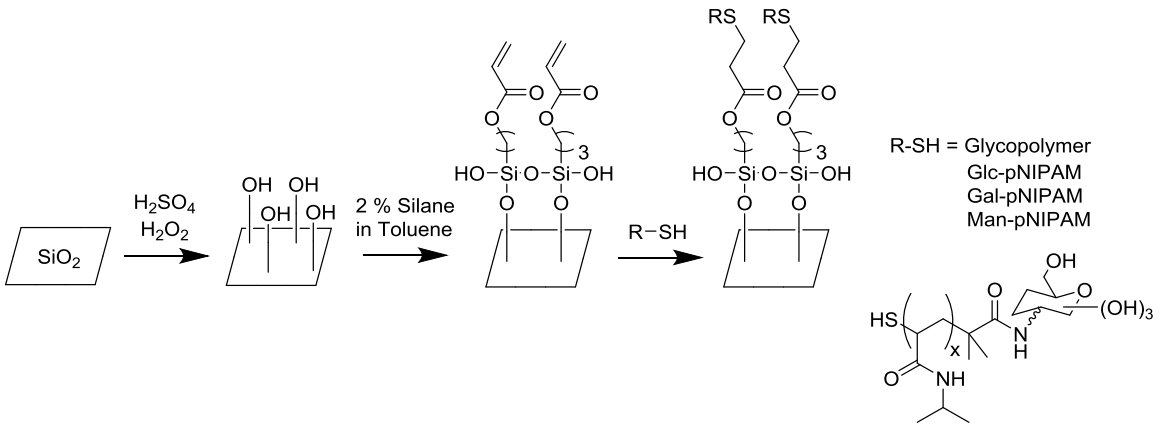

Immediately following the cleaning process (Section 2.6.1.), the samples were immersed into a (3-(trimethyoxysilyl)propyl acrylate (5 mL, 2% v/v in toluene, 2 hours, RT), washed with toluene (5 x 2 mL), ethanol (5 x 2 mL) and water (5 x 2 mL), then blown under a stream of nitrogen until dry.

Following silanisation, a solution of the selected glycopolymer (Glc-pNIPAM, Gal-pNIPAM or Man-pNIPAM) was prepared (2 mg.mL^{-1} in water with 1 µL of ethanolamine added) and the samples were immersed into the polymer solution for 2 hours (RT) then washed with Milli-Q water (3 x 2 mL) and dried under a stream of nitrogen.

When glycopolymer spots were required (as opposed to entre surface functionalisation), the process remained the same, except that 2 µL droplets of the glycopolymer solution were dosed onto the silane functionalised surface in place of complete submersion of the slides into the glycopolymer solution. Reaction conditions and washing processes remained as above.

4.5.4.2. Functionalisation of Epoxide Coated Glass

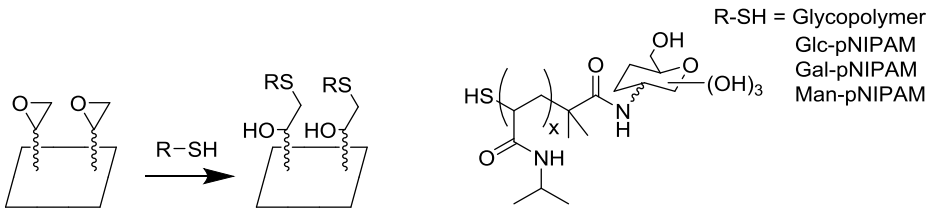

The epoxide coated glass slides were washed with Milli-Q water and dried under a stream of nitrogen prior to use. They were then submerged into a solution of the selected glycopolymer (Glc-pNIPAM, Gal-pNIPAM or Man-pNIPAM) (2 mg.mL-1 in water 1 µL of ethanolamine added) for 2 hours (RT) then washed with Milli-Q water (3 x 2 mL) and dried under a stream of nitrogen. When glycopolymer spots were required (as opposed to entre surface functionalisation), the process remained the same, except that 2 µL droplets of the glycopolymer solution were dosed onto the epoxide functionalised surface in place of complete submersion of the slides into the glycopolymer solution.

4.5.5. Direct Micro-Contact Printing of Polymers onto Glass

Polymer solutions prepared (10 $mg.mL^{-1}$) in Milli-Q water and sonicated for 20 minutes to facilitate solubilisation. The solutions were then diluted in a 384 well plate to produce concentrations of 5, 2.5, 1.25 and 0.6125 $mg.mL^{-1}$.

Printing was then carried out using a XYZ3200 dispensing workstation (Biodot). Approximately 2.4 nL of solution was printed onto a slide (10 replicate spots per slide) using 946PM6B pins (ArrayIt) at 25ºC, 45% humidity. Between samples slides were washed with ultra-pure water (18.2 MΩs) and dried under vacuum. The first 5 mm of the slide on all edges was left unprinted to allow for handling.

4.5.6. Lectin-Glycopolymer Interactions

Contact printed or manually spotted samples were removed from the refrigerator and left at room temperature for 30 minutes prior to use. The slides were then either subjected to a blocking procedure (BSA in concentrations ranging 2% to 0.02% in HEPES or water, Tween 20 in concentrations ranging from 2% to 0.02% in water or Tris-HCl, Tween 20 at 0.05% with 1% BSA in Tris-HCl) for 1 hour at room temperature, or not blocked. The most successfully blocking procedure was found to be Tris-HCl with 0.05% Tween 20. The slides were then dip washed in HEPES, rinsed with Milli-Q water and dried under a stream on nitrogen. They were then submerged in the lectin of interest (Con A, SBA or WGA at 0.01 $mg.mL^{-1}$ in HEPES) for 30 minutes in the dark at room temperature. The dip washing, rinsing and drying process was repeated and the samples were immediately scanned.

4.6. References

1. M. A. Gauthier, M. I. Gibson and H. A. Klok, *Angew. Chem. Int. Ed.*, 2009, **48**, 48-58.

2. M. Eberhardt, R. Mruk, R. Zentel and P. Theato, *Eur. Polym. J.*, 2005, **41**, 1569-1575.

3. M. I. Gibson, E. Froehlich and H.-A. Klok, *J. Polym. Sci. A Polym. Chem.*, 2009, **47**, 4332-4345.

4. S.-J. Richards, M. W. Jones, M. Hunaban, D. M. Haddleton and M. I. Gibson, *Angew. Chem. Int. Ed.*, 2012, **51**, 7812-7816.

5. S.-J. Richards and M. I. Gibson, *Acs Macro Lett.*, 2014, **3**, 1004-1008.

6. A. B. Lowe, *Polym. Chem.*, 2010, **1**, 17-36.

7. C. E. Hoyle, A. B. Lowe and C. N. Bowman, *Chem. Soc. Rev.*, 2010, **39**, 1355-1387.

8. J. L. Wilbur, A. Kumar, E. Kim and G. M. Whitesides, *Adv. Mater.*, 1994, **6**, 600-604.

9. M. Mrksich and G. M. Whitesides, *Trends Biotechnol.*, 1995, **13**, 228-235.

10. M. S. Algahtani, D. J. Scurr, A. L. Hook, D. G. Anderson, R. S. Langer, J. C. Burley, M. R. Alexander and M. C. Davies, *J. Controlled Release*, 2014, **190**, 115-126.

11. A. L. Hook, D. G. Anderson, R. Langer, P. Williams, M. C. Davies and M. R. Alexander, *Biomaterials*, 2010, **31**, 187-198.

12. D. G. Anderson, S. Levenberg and R. Langer, *Nat. Biotechnol.*, 2004, **22**, 863-866.

13. D. G. Anderson, D. Putnam, E. B. Lavik, T. A. Mahmood and R. Langer, *Biomaterials*, 2005, **26**, 4892-4897.

14. P. O. Brown and D. Botstein, *Nat. Genet.*, 1999, **21**, 33-37.

15. O. Blixt, S. Head, T. Mondala, C. Scanlan, M. E. Huflejt, R. Alvarez, M. C. Bryan, F. Fazio, D. Calarese, J. Stevens, N. Razi, D. J. Stevens, J. J. Skehel, I. van Die, D. R. Burton, I. A. Wilson, R. Cummings, N. Bovin, C. H. Wong and J. C. Paulson, *P. Natl. Acad. Sci. USA*, 2004, **101**, 17033-17038.

16. K. Godula, D. Rabuka, K. T. Nam and C. R. Bertozzi, *Angew. Chem. Int. Edit.*, 2009, **48**, 4973-4976.

17. A. R. de Boer, C. H. Hokke, A. M. Deelder and M. Wuhrer, *Anal. Chem.*, 2007, **79**, 8107-8113.

18. S. Park, M. R. Lee and I. Shin, *Nat. Protoc.*, 2007, **2**, 2747-2758.

19. M. J. Summers, D. J. Phillips and M. I. Gibson, *Chem. Commun.*, 2013, **49**, 4223-4225.

20. Y. Gou, J. Geng, S.-J. Richards, J. Burns, C. R. Becer and D. M. Haddleton, *J. Polym. Sci. A Polym. Chem.*, 2013, **51**, 2588-2597.

21. Functional Glycomics Gateway, Protocol : cfgPTC_242 (Biotinylated Samples), 2009.

22. K. Godula and C. R. Bertozzi, *J. Am. Chem. Soc.*, 2010, **132**, 9963-9965.

23. S.-J. Richards, PhD Thesis, The University of Warwick, 2015.

Chapter Five

5. Conclusions

Carbohydrate arrays are a key tool within glycobiology and hold the potential to further our knowledge in field of protein-carbohydrate interactions and their role in pathogenicity. Low cost, high resolution and highly reproducible glycoarrays have the potential to revolutionise modern healthcare, from point-of-care diagnostics to elucidating new drug targets. However, the immobilisation of carbohydrates onto surfaces remains challenging, both synthetically and analytically.

In this work we have developed an acrylate silane coating, which has demonstrated how the feasibility and simplicity of thiol-gold self-assembled monolayers can be extended to cheaper and more readily available glass substrates. The silane acrylate serves as an orthogonally reactive layer for the subsequent covalent immobilisation of thiolated species, in our case carbohydrates or RAFT synthesised polymers. The resulting immobilised monosaccharides or polymers have been thoroughly characterised (using drop shape analysis, ellipsometry, XPS, QCM-D and fluorescence binding assays) and the successful modulation of surface properties has been demonstrated. A comparison between the conjugation of two different RAFT synthesised polymer species concluded that poly(*N*-isopropylacrylamide) (pNIPAM) polymers grafted in a higher density than poly(oligo(ethylene glycol) methyl ether methacrylate) (pOEGMA) onto both glass/silicon and gold surfaces. It was also found that the pNIPAM polymer coatings were exhibiting desirable

non-fouling properties and that the longer chain ($pNIPAM_{100}$) polymers were more non-fouling than their shorter counterparts ($pNIPAM_{25}$). Neither was seen to exhibit extensive thermoresponsive switching behaviour within an experimentally accessible temperature range. The synthesis of glycosylated pNIPAM polymers allowed the presentation of polymer linked glycans onto the glass surfaces and these surface grafted glycosylated polymers were studied for their compatibility with current array scanning protocols. The successful direct microcontact printing of the glycans onto silane and epoxide coated glass was achieved. The resulting high density arrays were used to investigate the carbohydrate-lectin binding specificity using a variety of model lectins.

In conclusion, the main strength of the acrylate silane coating lies in its simplicity and versatility. It can be applied to both glass and silicon surfaces and allows the thiol-ene immobilisation of thiolated molecules of interest, as we have demonstrated with the successful conjugation of monosaccharides, polymers and glycan terminated polymers. These polymer tethers enhance the surface functionality relative to traditional arrays. The use of direct microcontact printing facilitated the generation of high density arrays of surface immobilised glycosylated polymers and we have demonstrated their potential for investigating protein-carbohydrate interactions. There is great scope to further optimise these binding experiments, surface graft other glycopolymer species and incubate with a wide variety of lectins or even whole bacteria. These systems could then be used to generate a global library of specific binding interactions, which have the potential to transform personal diagnostic healthcare.

Appendix One

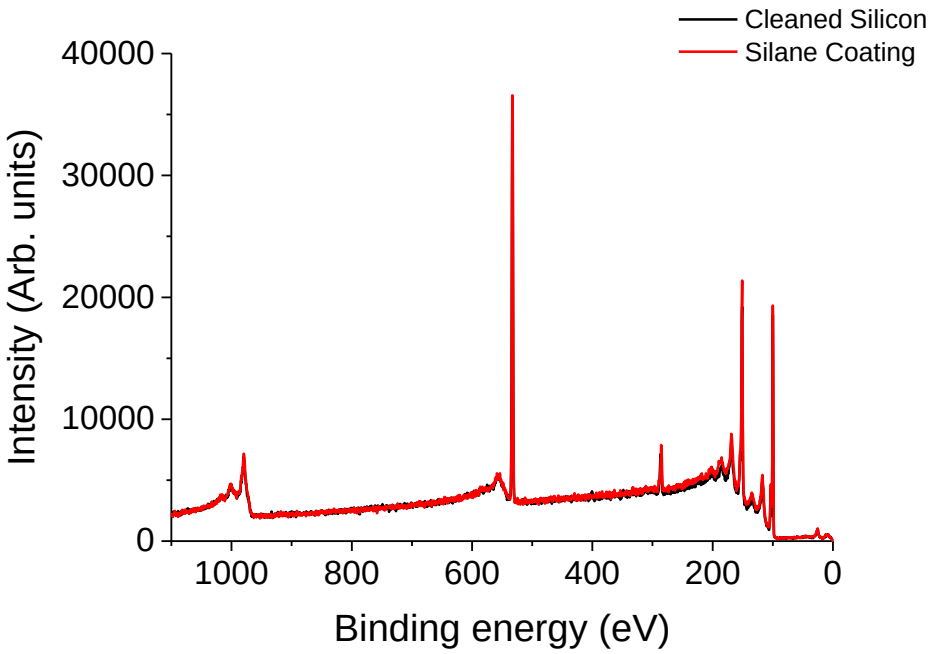

Figure 1: X-ray photoelectron spectroscopy survey scans for the cleaned silicon oxide and silane coated surfaces described in Chapter Two

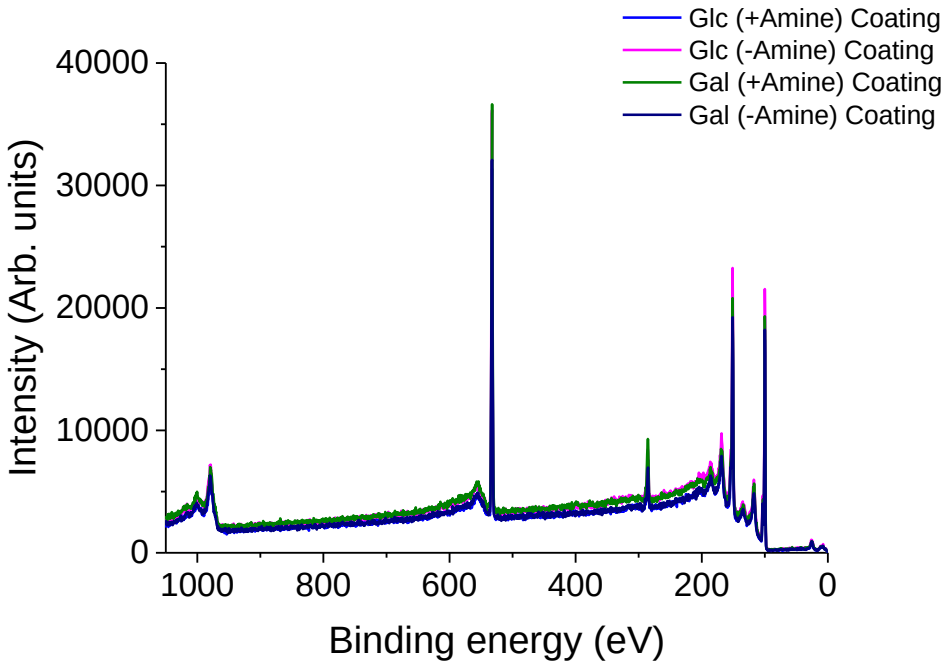

Figure 2: X-ray photoelectron spectroscopy survey scans for the thiolated monosaccharide coated silicon surfaces described in Chapter Two

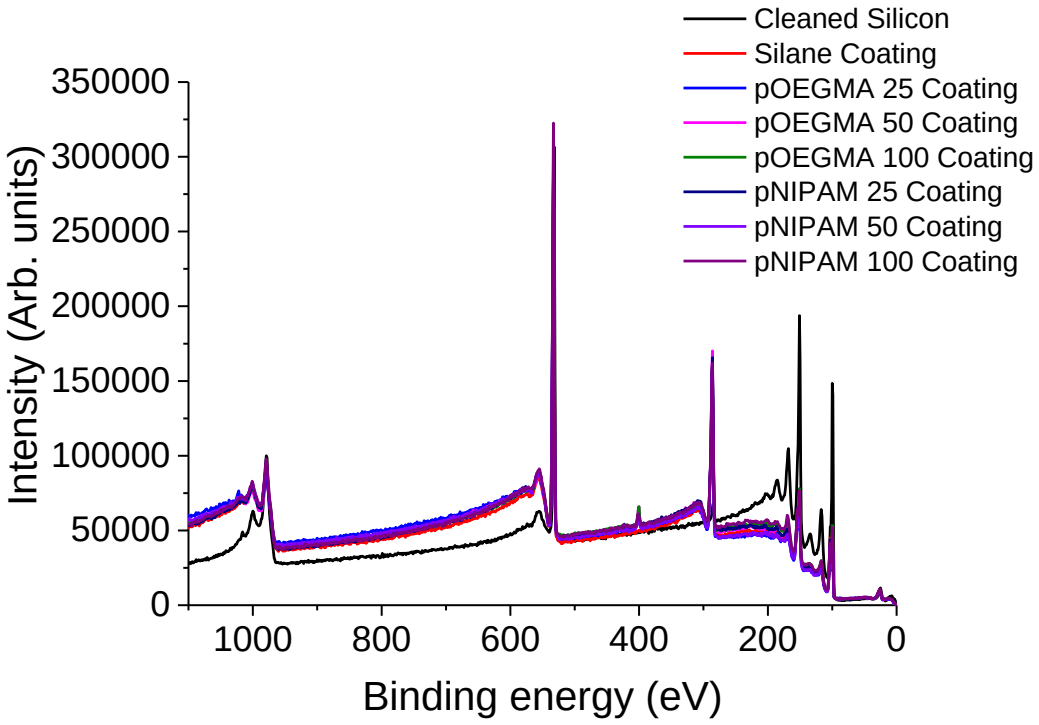

Figure 3: X-ray photoelectron spectroscopy survey scans for the pOEGMA and pNIPAM coated silicon surfaces described in Chapter Three

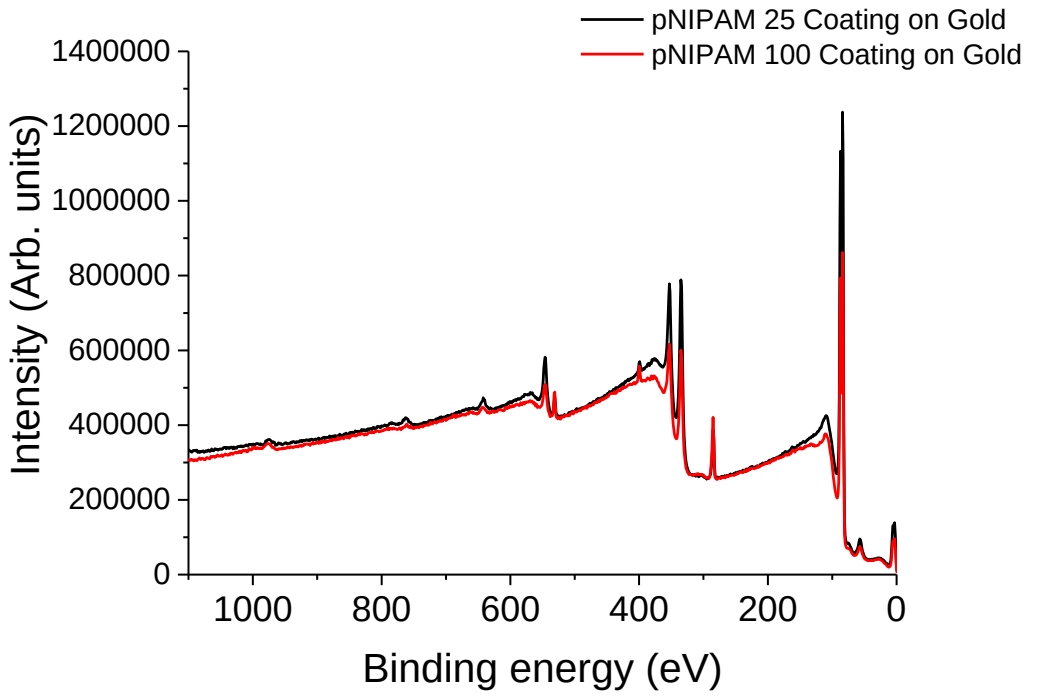

Figure 4: X-ray photoelectron spectroscopy survey scans for the pNIPAM coated gold surfaces described in Chapter Three

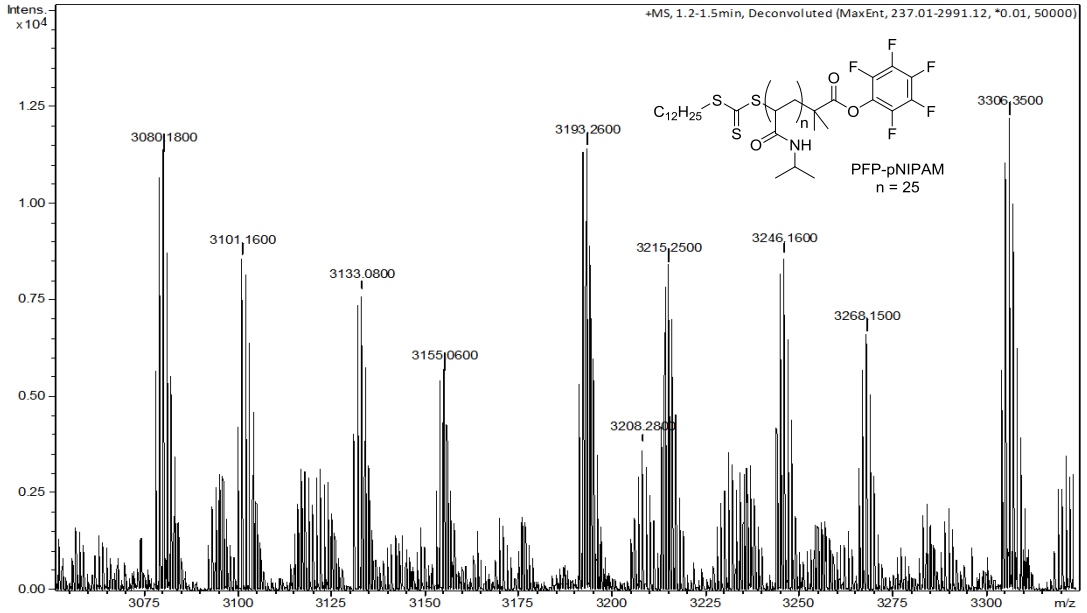

Figure 5: High resolution ESI-ToF MS spectrum for PFP-pNIPAM$_{25}$ described in Chapter Four

Appendix Two

This appendix contains collaborative works that I have been involved in during my PhD, but that are not directly related to the content of this thesis. Firstly is a recent publication in the field of ice nucleation and secondly is an invited book chapter, which is due for publication in November 2015.

Article

pubs.acs.org/Biomac

Probing the Biomimetic Ice Nucleation Inhibition Activity of Poly(vinyl alcohol) and Comparison to Synthetic and Biological Polymers

Thomas Congdon, Bethany T. Dean, James Kasperczak-Wright, Caroline I. Biggs, Rebecca Notman, and Matthew I. Gibson*

Department of Chemistry, University of Warwick, Coventry, CV4 7AL, United Kingdom

Supporting Information

ABSTRACT: Nature has evolved many elegant solutions to enable life to flourish at low temperatures by either allowing (tolerance) or preventing (avoidance) ice formation. These processes are typically controlled by ice nucleating proteins or antifreeze proteins, which act to either promote nucleation, prevent nucleation or inhibit ice growth depending on the specific need, respectively. These proteins can be expensive and their mechanisms of action are not understood, limiting their translation, especially into biomedical cryopreservation applications. Here well-defined poly(vinyl alcohol), synthesized by RAFT/MADIX polymerization, is investigated for its ice nucleation inhibition (INI) activity, in contrast to its established ice growth inhibitory properties and compared to other synthetic polymers. It is shown that ice nucleation inhibition activity of PVA has a strong molecular weight dependence; polymers with a degree of polymerization below 200 being an effective inhibitor at just 1 mg.mL^{-1}. Other synthetic and natural polymers, both with and without hydroxyl-functional side chains, showed negligible activity, highlighting the unique ice/water interacting properties of PVA. These findings both aid our understanding of ice nucleation but demonstrate the potential of engineering synthetic polymers as new biomimetics to control ice formation/growth processes

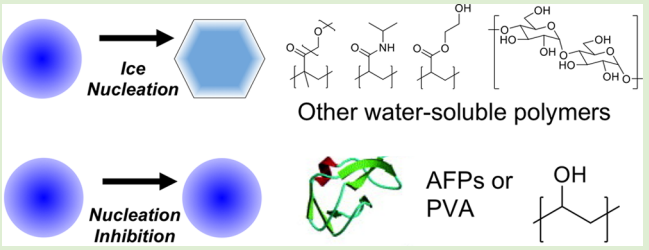

INTRODUCTION

Ice formation via heterogeneous nucleation is crucial in the context of atmospheric science,[1] cryopreservation,[2] cryomedicine,[3] cryosurgery,[4] and also food science.[5] The challenges in understanding, and in particular, predicting homogeneous and heterogeneous nucleation temperatures cannot be understated. For example, in the vitreous cryopreservation of cells and tissue for transplantation medicine, ice nucleation must be suppressed until the glass transition temperature is reached to ensure a glassy, rather than ice-rich phase.[6] In frozen foods, ice nucleation at relatively high temperatures generates larger ice particles than at lower temperatures. A difference in ice grain size, from 15 to 20 to 40 μm, will cause an unpalatable difference in the quality and taste of ice cream.[7]

While ice formation in water (freezing) is thermodynamically favorable at temperatures below 0 °C, there is a large kinetic barrier, resulting in the homogeneous (for ultrapure water) nucleation/freezing temperature being ∼−38 °C; the temperature when pure water spontaneously turns to ice at ambient pressure. In practice, the presence of impurities in water (dust, salts, bacteria, etc.) provide nucleation sites enabling nucleation to occur typically in the range of 0 to −20 °C in bulk samples. This complex phase behavior has proven to be challenging to understand, in part due to nucleation being a rare event, meaning computational modeling of the process is very challenging. The ability to predictably control ice nucleation temperature, however, would be technologically significant in applications ranging from the seeding of rain clouds to controlling ice build-up on wind turbines. Several inorganic minerals, such as kaolinite[8] and feldspar, have been shown to be very potent ice nucleators and may play a role in rain cloud formation via Saharan dust clouds.[9,10]

A large range of ice nucleating proteins exist, both in anthropods[11] and on the surface of bacteria.[12] The plant pathogen *Pseudomonas syringae* is capable of inducing ice nucleation on the leaves of plants, promoting frost formation and releasing nutrients for the bacteria.[13] Antifreeze proteins, which are highly effective at inhibiting ice growth, display some weak nucleation inhibition,[14] believed to arise due to the interactions with ice nucleating proteins. Extracellular proteins known as ice nucleating proteins have found commercial use in snow making.[15] In contrast to the above, many extremophile organisms have evolved antifreeze (glyco)proteins (AF(G)Ps) to protect themselves from cold damage (in some cases in response to ice nucleating bacteria). While the primary roles of AF(G)Ps are to depress the equilibrium freezing point and inhibit ice recrystallization (growth/ripening), they also show complex behavior in ice nucleation, both promoting[16] and

Received: June 10, 2015
Revised: August 8, 2015

DOI: 10.1021/acs.biomac.5b00774
Biomacromolecules XXXX, XXX, XXX−XXX

inhibiting[17] dependent on the conditions.[18] Extremophiles will often exploit a range of these methods in parallel in order to survive.[19,20]

The major challenge with the study of AF(G)Ps and ice nucleating proteins is that they are synthetically challenging to access. Ben et al. have developed small molecule mimics of AF(G)Ps,[21,22] and Gibson et al. have shown that synthetic polymers can reproduce the ice recrystallization inhibition properties of AF(G)Ps, and applied this to nonvitreous cryopreservation, but far fewer examples exist of polymers with ice nucleation properties. Poly(vinyl alcohol) (PVA) is established as a highly potent inhibitor of ice growth in frozen and vitrified media,[23,24] and in particular lower molecular weight fractions display anomalously strong ice growth inhibition.[25] Polyglycerol has been reported to bind to and inhibit the ice nucleation activity of some proteins, and the combination of polyglycerol with poly(vinyl alcohol) was shown to be particularly effective for reducing ice formation in vitrified solutions.[26] The ice nucleation inhibition behavior of poly(vinylpyrrolidone) (PVP) and AF(G)P mixtures has been studied by Franks et al.,[27] but there remains a huge gap in the understanding of the design rules for the synthesis of ice nucleation inhibitors. PVA in combination with antifreeze proteins have been used to control ice crystal growth in ice slurries.[28] Lu et al. conducted detailed experiments into the inhibition of nucleation and growth of ice by PVA in vitrified solutions.[29] Nucleation inhibition activity using droplet freezing has been interrogated using a range of methods, including microfluidics,[30] suspension in oil,[31] or using electrodynamic balances.[32,33] Murray et al. have measured homogeneous and heterogeneous freezing of water using a hydrophobic substrate and an optical microscope,[34] and this method has also been used to examine the effect of surface topography on droplet nucleation.[35] Using a multipoint freezing assay, highly disperse, partly acetylated PVA has been shown to display ice nucleation inhibition activity.[16] Conversely, studies using commercial PVA (with no additional purification) at relatively high concentrations result in nucleation promotion rather than inhibition, showing the complexity of this process.[36,37]

While the above examples indicate that synthetic polymers could be useful tools to modulate and understand ice nucleation phenomena, all previous studies have been undertaken using either poorly defined PVA materials with high dispersities and unknown degrees of acetylation or using limited analytical methods that do not take into account the stochastic nature of ice nucleation (i.e., single measurements are not sufficient). In this work we employ RAFT/MADIX polymerization methodology to access a library of well-defined polymers to investigate how their structural features (molecular weight, side chains) influence nucleation as a first step to understanding and predicting new synthetic materials capable of reproducing extremophile function.

EXPERIMENTAL SECTION

Materials. Hydrophobic slides made of glass with a PTFE coating were purchased from Thermo Scientific, stored at 80 °C, and allowed to cool to ambient temperature prior to use. 4,4′-Azobis(4-cyanovaleric acid) (98%), dextran (9−10 kDa, 98%), hydrazine hydrate (80%) solution, *N*-hydroxyethyl acrylamide (97%), *N*-isopropylacrylamide (98%), poly(ethylene glycol) (M_n = 300), methyl ether methacrylate (99%), poly(vinyl alcohol) (75−100 kg mol^{-1}, 98%), poly(vinyl alcohol) (85−124 kg mol^{-1}, 98%), and vinyl acetate (99%) were purchased from Sigma-Aldrich. Hexane, methanol, and tetrahydrofuran were purchased from Fluka. *O*-Ethyl-*S*-1-phenyl carbonodithioate, 2-(pyridyldisulfanyl) ethyl 2-(dodecylthiocarbonothioylthio)-2-methylpropanoic acid, and poly(hydroxy ethyl acrylate) were synthesized using previously reported methods.[38,39]

Analytical and Physical Methods. ^{1}H and ^{13}C NMR spectra were recorded on Bruker DPX-300 and DPX-400 spectrometers using deuterated solvents purchased from Sigma-Aldrich. Chemical shifts are reported relative to residual nondeuterated solvent. Size exclusion chromatography (SEC) was used to examine and differentiate between the molecular weights and the dispersities of the synthesized polymers. The SEC analysis was performed on a Varian 390-LC MDS system equipped with a PL-AS RT/MT autosampler, a PL-gel 3 μm (50 × 7.5 mm) guard column, and two PL-gel 5 μm (300 × 7.5 mm) mixed-D columns held at 30 °C, and the instrument was equipped with a differential refractive index and a Shimadzu SPD-M20A diode array detector. Dimethylformamide (including 5 mM ammonium tetrafluoroborate) was used as the eluent at a flow rate of 1 mL min^{-1}. The THF SEC system comprised of a Varian 390-LC-Multi detector suite fitted with differential refractive index (DRI), light scattering (LS), and ultraviolet (UV) detectors equipped with a guard column (Varian Polymer Laboratories PLGel 5 μm, 50 × 7.5 mm) and two mixed D columns of the same type. The mobile phase was THF with 5% triethylamine (TEA) eluent at a flow of 1.0 mL/min, and samples were calibrated against Varian Polymer Laboratories EasiVials linear poly(styrene) and poly(methyl methacrylate) standards (162−2.4 × 10^5 g/mol) using Cirrus v3.3. The temperature of the ice and water droplets was controlled on a Linkam Biological Cryostage BCS196 with T95-Linkpad system controller equipped with a LNP95-liquid nitrogen cooling pump, using liquid nitrogen as the coolant (Linkam Scientific Instruments UK, Surrey, U.K.). Image and droplet monitoring was conducted using a Veho Discovery VMS-004 Deluxe USB microscope and Veho Microcapture software V 1.3.

Ice Nucleation Assay. This example is for a single polymer, but the same method was employed for each sample. PVA was dissolved in Milli-Q water over 24 h to give the desired concentration for the assay and to ensure complete solvation of the polymer. A total of 10 droplets (0.5 μL) were pipetted onto each slide, and the slide was placed inside a Linkham Scientific cryostage. The cryostage was rapidly cooled to 5 °C at a rate of 50 °C/min and then held at this temperature for 3 min to allow the temperature of the glass slide and droplets to equilibrate. The samples were then cooled from 5 °C to −40 °C at a rate of 2 °C/min. Ice nucleation was observed using a Veho Discovery VMS-004 Deluxe USB microscope and Veho Microcapture software V 1.3. The experiment was repeated with fresh droplets from the same stock solution until at least 20 droplet freezing temperatures were recorded.

Polymerization of Vinyl Acetate Using *O*-Ethyl-*S*-1-phenyl Carbonodithioate. As a representative example, *O*-ethyl-*S*-1-phenyl carbonodithioate (0.069 g, 0.35 mmol), vinyl acetate (4.67 g, 2.64 mmol), and ACVA (4,4′-azobis(4-cyanovaleric acid)) (0.005 g, 0.029 mmol) were added to a stoppered vial. The solution was thoroughly degassed under a flow of N_2 for 20 min, and the reaction mixture was then allowed to polymerize at 68 °C for typically 15 h. For short chain oligomers of PVAc, under these conditions, conversion proceeds at approximately 1% per minute, so for $PVAc_{13}$, the reaction was quenched using liquid nitrogen and exposing the vial to air after 10 min heating at 68 °C. The yellow solutions were then cooled to room temperature. Poly(vinyl acetate) was then recovered as a yellow sticky solid after precipitation into hexane. The hexane was decanted and the poly(vinyl acetate) was redissolved in THF, which was then concentrated in vacuo and thoroughly dried under vacuum at 40 °C for 24 h, forming an off-white solid. Representative characterization data for $PVAc_{183}$: ^{1}H NMR (400 MHz, $CDCl_3$): δ 4.61 (1H, br, C*H*O−CH_2), 1.74 (3H, br, CO−CH_3), 1.53 (2H, br, CH_2); M_n^{SEC}(THF) = 15800 Da, M_w/M_n = 1.16.

Hydrolysis of Poly(vinyl acetate) to Poly(vinyl alcohol). As a representative example, poly(vinyl acetate) (0.3 g, M_n 15800 g·mol^{-1}, $Đ$ = 1.16) was dissolved in a methanol (4 mL) in a round-bottom flask. Hydrazine hydrate solution (6 mL, 80% in water) was added, and the reaction mixture was stirred at 40 °C for 1 h until the solution became clear. The reaction mixture was then dialyzed using distilled water and poly(vinyl alcohol) was recovered as a spongy white solid by

DOI: 10.1021/acs.biomac.5b00774
Biomacromolecules XXXX, XXX, XXX−XXX

Scheme 1. RAFT/MADIX Polymerization of Vinyl Acetate and Subsequent Hydrolysis to PVA Using Hydrazine Hydrate Solution

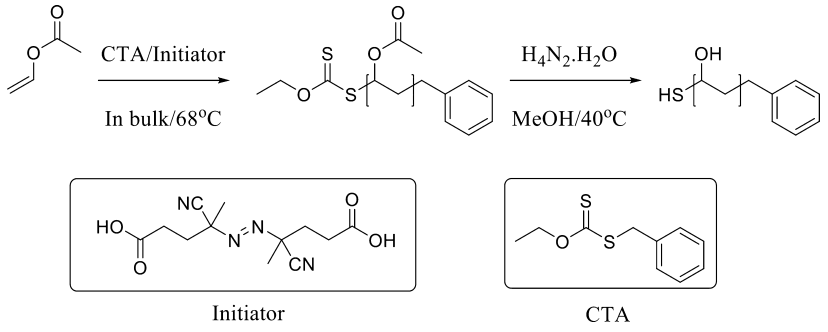

Table 1. PVA and PVA·PVAc Used in This Study

entry	[M]/[CTA]	M_n(Theo)[a] [g mol^{-1}]	M_n(SEC)[b] [g mol^{-1}]	$Đ$[b]	DP$_n$[c]	PVA[d]
PVAc$_{13}$	110	9500	1300	1.33	13	PVA$_{13}$
PVAc$_{73}$	70	6000	6300	1.11	73	PVA$_{73}$
PVAc$_{126}$	120	10300	10900	1.31	126	PVA$_{126}$
PVAc$_{183}$	155	13300	15800	1.16	183	PVA$_{183}$
PVAc$_{322}$	168	14500	27800	1.40	322	PVA$_{322}$
PVAc$_{366}$	395	34000	31500	1.48	366	PVA$_{366}$

[a]Theoretical number-average degree of polymerization, assuming 100% conversion. [b]Determined by SEC in THF using PMMA polymer standards. [c]Number-average degree of polymerization, determined from conversion of monomer to polymer by ^{1}H NMR. [d]Corresponding PVA prepared by complete hydrolysis of PVAc, determined by ^{1}H NMR.

freeze-drying the dialysis solution. For short chain PVA$_{10}$, the solution was diluted with water and washed with toluene (4 × 60 mL) to remove the organic solvents. The solution was then freeze-dried, and poly(vinyl alcohol) was recovered as a spongy white solid by freeze-drying the dialysis solution. Complete hydrolysis was confirmed by ^{1}H NMR. Representative characterization data for PVA$_{183}$: ^{1}H NMR (400 MHz, D_2O): δ 4.00 (1H, br, C*H*OH), 1.68−1.60 (2H, br, CH_2).

Polymerization of *N*-Isopropylacrylamide. Prepared according to a method adapted from literature.[40] *N*-isopropylacrylamide (1.00 g, 8.84 mmol), 2-(pyridyldisulfanyl) ethyl 2-(dodecylthiocarbonothioylthio)-2-methylpropanoic acid (43.0 mg, 0.118 mmol), and 4,4′-azobis(4-cyanovaleric acid) (6.60 mg, 23.6 μmol) were dissolved in methanol/toluene (1:1; 4 mL) in a glass vial containing a stir bar. The vial was degassed under a flow of nitrogen for 10 min and then heated at 70 °C for 1 h, after which the reaction mixture was opened to air and quenched in liquid nitrogen. The product was precipitated into cold diethyl ether and dried under vacuum to give a yellow solid. ^{1}H NMR (400 MHz, $CDCl_3$): δ 3.85−4.10 (1H, br, C*H*), 1.95−2.30 (2H, br, CH_2), 1.55−1.70 (1H, m, NC*H*), 1.0−1.20 (6H, d, CH_3). M_n^{SEC}(THF) = 9280 Da; M_w/M_n = 1.05.

Polymerization of Oligo(ethylene glycol) Methyl Ether Methacrylate. Poly(ethylene glycol) (M_n = 300) methyl ether methacrylate (2.00 g, 6.67 mmol), 2-(dodecylthiocarbonothioylthio)-2-methylpropanoic acid (3.74 mg, 10.3 μmol), and 4,4′-azobis(4-cyanovaleric acid). The vial was degassed under a flow of nitrogen for 10 min and then heated at 70 °C for 4 h. The reaction mixture was opened to air and quenched in liquid nitrogen. The product was precipitated into diethyl ether, isolated by centrifugation, and dried under vacuum overnight to give a waxy, yellow solid. Representative characterization data for p(OEGMA)$_{224}$. ^{1}H NMR (400 MHz, $CDCl_3$) δ 3.50−4.15 (16H, br d, PEG), 2.00 (3H, s, OCH_3), 1.55−1.90 (2H, m, CH_2), 0.75−1.75 (3H, m, CH_3). M_n^{SEC}(THF) = 175750 Da; M_w/M_n = 1.92.

General Procedure for Polymerization of *N*-Hydroxyethyl Acrylamide. 4,4-Azobis(4-cyanovaleric acid) (5 mg, 0.018 mmol), 2-(dodecylthiocarbonothioylthio)-2-methylpropanoic acid (32 mg, 0.088 mmol), and *N*-hydroxyethyl acrylamide (1 g, 8.8 mmol) were dissolved in 1:1 methanol/toluene (4 mL) in a glass vial containing a stir bar. The reaction mixture was degassed under a flow of nitrogen for 10 min, sealed then heated at 70 °C for 30 min. The reaction mixture was opened to air and quenched in liquid nitrogen. The polymer was precipitated into diethyl ether to give a light yellow solid. ^{1}H NMR (400 MHz, D-MeOH): δ 4.79−4.94 (br s, CONH-CH_2-CH_2-OH), 3.58−3.80 (br s, CONH-CH_2-CH$_2$-OH), 3.07−3.23 (br s, CONH-CH_2-CH$_2$-OH), 1.36−2.32 (br, polymer backbone). M_n^{SEC}(THF) = 4900 g·mol^{-1}; M_w/M_n (SEC) = 1.12.

RESULTS AND DISCUSSION

Previous reports on the role of PVA on ice nucleation have been in vitrified solutions (i.e., containing >20% of an organic cosolvent) and using poorly defined materials with broad molecular weight distributions and variable degrees of acetate hydrolysis (as is found in most commercial samples). Our previous work on the impact of synthetic polymers on ice crystal growth (again, not to be confused with nucleation) has shown that both molecular weight and degree of hydrolysis are crucial parameters in their activity.[25] Therefore, a RAFT/MADIX methodology was employed in order to access well-defined polymers such that the effect of polymer chain size could be reliably interrogated. Using a xanthate chain transfer agent (Scheme 1), the molecular weight of the polymer can be tuned by controlling the monomer to initiator ratio. Following polymerization and isolation, the polymers were characterized by ^{1}H NMR and SEC, the results are shown in Table 1, and example SEC traces are shown in Figure 1. All the reactions were conducted in bulk, which has been shown to be an efficient method to polymerize vinyl acetate in a controlled fashion when the ratio of monomer to chain transfer agent is around 100−200. Short chain oligomers of PVAc were prepared by quenching the reaction at low conversion. Using this strategy, well-defined polymers were obtained with dispersity values ($Đ$ = M_w/M_n) below 1.5 (which is expected for deactivated monomers such as VAc, especially at higher [M]/[CTA] ratios) and molecular weights close to that predicted by the feed ratio. The obtained PVAc polymers were hydrolyzed using hydrazine hydrate solution, which gives

DOI: 10.1021/acs.biomac.5b00774
Biomacromolecules XXXX, XXX, XXX−XXX

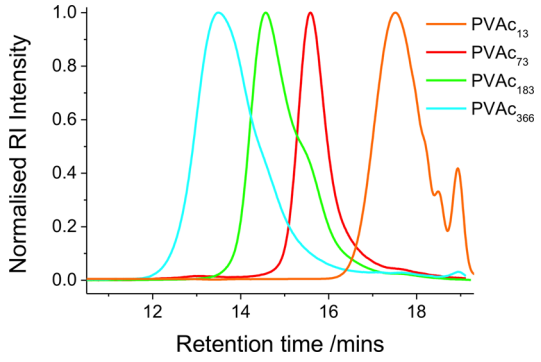

Figure 1. Size exclusion chromatography (SEC) traces of polymers. The low molecular weight shoulder seen in $PVAc_{183}$ can be attributed to termination via chain transfer.

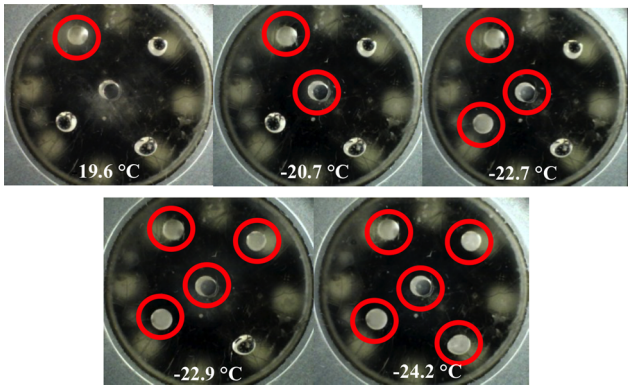

Figure 2. Pictures of the multipoint freezing assay. Nucleating droplets are circled in red, the concentric ring is the reflection of the microscope LEDs.

quantitative deprotection, unlike saponification with KOH or NaOH, as we have previously reported.[41]

A key aim of this study is to study the underlying structural features of synthetic polymers, which enable ice nucleation inhibition. Therefore, a panel of other water-soluble, synthetic polymers, poly(hydroxyethyl acrylamide) (pHEA), poly(*N*-isopropylacrylamide) (pNIPAM), and poly((oligo ethylene glyco)methacrylate (pOEGMA), were prepared by RAFT/MADIX polymerization. (Table 2). In all cases well-defined polymers were obtained, except for pOEGMA, which gave a larger than expected dispersity which was thought to be due to column-interactions in the SEC analysis. This dispersity, in this case, does not affect the later discussion (see below).

Ice nucleation is a stochastic process; essentially this means that, in sufficiently small samples (to reduce the number of unwanted nucleators), the temperature of freezing will always vary and therefore single-point measurements do not give reliable nor useful data, such as that from bulk DSC (differential scanning calorimetry) freezing measurements.[42] To reduce these effects, a droplet freezing assay, was employed.[9] Briefly, very small volume (0.5 μL) droplets of ultrapure (Milli-Q) water were added to a hydrophobic glass slide. Small droplets reduce the probability of competing nucleators being present and enable a true "average" nucleation temperature to be determined. These droplets were cooled on a cryostage, under an atmosphere of dry nitrogen, and the freezing point of each droplet recorded by visual observation using a microscope. An example is shown in Figure 2. Differential ice nucleation plots can then be obtained by recording the percentage of droplets frozen versus freezing temperature.

Using the multipoint freezing assay, concentrated (10 mg·mL^{-1}) PVA solutions were prepared and evaluated. Differential ice nucleation plots are shown in Figure 3A, and the temperature at which 50% of all the droplets were frozen for each sample are displayed in Figure 3B to facilitate comparison.

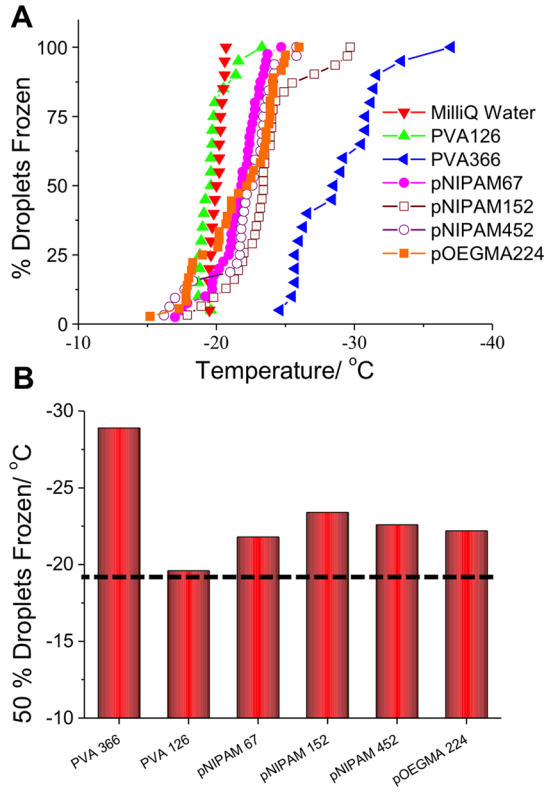

Figure 3. Ice nucleation measurements activity of polymers at 10 mg·mL^{-1} of polymer in solution. (A) Differential ice nucleation plots; (B) Temperature at which 50% of the droplets were frozen, for each polymer sample (no error bars shown to prevent confusion between error and the stochastic processes). Dotted line is to guide the eye toward nucleation temperature of Milli-Q water.

Table 2. Polymers Prepared for Use in This Study

entry	[M]/[CTA]	conv.[a]	M_n(NMR)[a] [g mol^{-1}]	M_n(SEC)[b] [g mol^{-1}]	$Đ$[b]	DP_n[a]
$p(NIPAM)_{67}$	75	88.8	7500	9280	1.05	67
$p(NIPAM)_{152}$	600	25.3	17000	15500	1.27	152
$p(NIPAM)_{452}$	600	75.4	51000	55900	1.12	452
$p(OEGMA)_{224}$	650	34.4	67100	175749	1.92	224
$pHEA_{83}$	100	83.0	9900	10000[c]	1.17	83

[a]Determined from conversion of monomer to polymer by ^{1}H NMR. [b]Determined by SEC in THF using PMMA polymer standards. [c]Determined by SEC in DMF (inc. 5 mM NH_3BF_4) relative to PMMA standards.

DOI: 10.1021/acs.biomac.5b00774
Biomacromolecules XXXX, XXX, XXX−XXX

The other polymers in Table 2 were also tested using this methodology.

In line with previous reports using highly disperse PVA, some inhibition was observed relative to that of the water sample alone (−19 °C, see Figure 4). A very short PVA

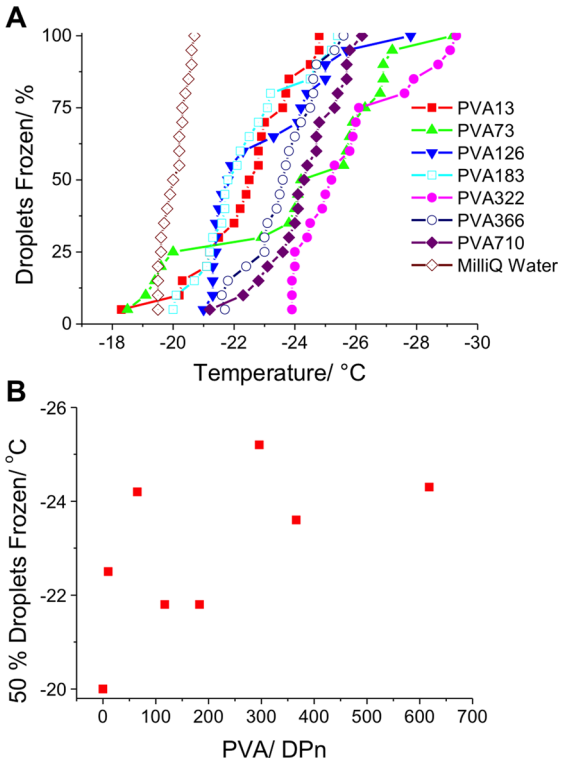

Figure 4. Ice nucleation inhibition activity of RAFT/MADIX synthesized PVA. All assays were run using a concentration of 1 mg·mL^{-1} of polymer in solution. (A) Differential ice nucleation plots; (B) Temperature at which 50% of the droplets were frozen for each PVA sample (no error bars shown to prevent confusion between error and the stochastic process). DP = number-average degree of polymerization.

(PVA13) was tested but gave inconsistent results at these concentrations; purification of short polymers by dialysis is not possible, which may explain this observation. Also, at equal mass concentration, the molar concentration of the short polymer is significantly larger, which we cannot rule out playing a role. Lower concentration data is included later in this paper. The longest chain tested (DP = 366) depressed the temperature to −29 °C. This is a remarkable shift in nucleation and considering the total mass of polymer (and, hence, [OH]) was constant (compared to shorted polymers), this suggests a complex mechanism of interaction to promote this inhibition. We have previously observed similar trends in the ice-growth inhibition activity of PVA, but we believe these are mechanistically unrelated.[25,43] To rule out viscosity as the reason for this behavior, the pNIPAM and pOEGMA polymers (with high molecular weights) were also tested. These all displayed similar freezing point depression irrespective of molecular weight or functionality. In fact, both these polymers gave droplet freezing points of around −23 °C, which is lower than Milli-Q water, which displays a nucleation temperature in the range of −19 °C.[44] Clearly, the activity of PVA is rather unique, even though some activity was observed here with the other polymers. These results mirror observations in ice recrystallization inhibition assays, where the activity of PVA has been shown to be strongly weight (M_n) dependent. To investigate this further, a larger number of PVAs were tested, but with a lowering of the concentration to 1 mg·mL^{-1} to enable any concentration-dependent effects to be separated but also to ensure it is predictive of any applications (i.e., biomedical) where lower concentrations are desirable, Figure 4.

Figure 4 shows that even at 1 mg·mL^{-1} concentration the longer PVAs still had significant ice nucleation inhibition activity. The trend was not linear, potentially as a result of the inherent dispersity of the polymers and the stochastic nature of the assays employed here. Nonetheless this observation confirms that macromolecular engineering of PVA enables the magnitude of the inhibition activity to be controlled, and presents a new tool toward predictable and controllable nucleation.

The results shown above confirm that molecular weight and the structure of PVA relative to other synthetic polymers both contribute to its activity. However, the control polymers used above (pNIPAM and pOEGMA) do not contain hydroxyl groups in their side chain. A simplistic consideration of the possible mechanisms of nucleation inhibition could involve hydrogen bond formation between ice nuclei and the polymers, meaning that other poly(hydroxylated) macromolecules should also be tested. Therefore, $pHEA_{83}$ and also the polysaccharide dextran (9−10 kDa) were tested at 10 mg·mL^{-1} (to ensure effects are pronounced) and the results are shown in Figure 5.

Figure 5 shows that high molecular weight PVA is more effective at depressing the freezing point of water compared to other poly ols at a similar concentration. PVA_{126} (M_n = 5550 g·

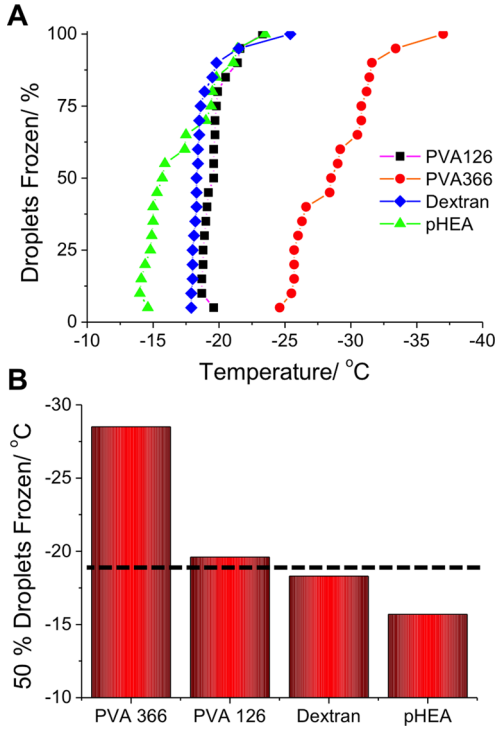

Figure 5. Ice nucleation inhibition activity of PVA, pHEA, and dextran. All assays were run using a concentration of 10 mg·mL^{-1} of polymer in solution. (A) Differential ice nucleation plots; (B) Temperature at which 50% of droplets were frozen for each sample (no error bars shown to prevent confusion between error and stochastic processes).

DOI: 10.1021/acs.biomac.5b00774
Biomacromolecules XXXX, XXX, XXX−XXX

mol^{-1}) shows no activity, similar to Dextran (MW = 9000−10000) and pHEA (M_n = 9900), despite its comparatively low molecular weight, suggesting that this behavior in part arises from a property intrinsic to PVA. Although the pHEA samples do slightly lower the nucleation temperature, we are not willing to claim it is strongly promoting this, but may warrant further study. Classical nucleation theory suggests that nucleation probability decreases with solution viscosity, which can explain molecular weight trends, but not the underlying activity seen here. The reasons for the inhibition properties of these polymers remains unclear; the polymers may be directly interacting with the small ice nuclei that form, inhibiting them, or by blocking the activity of other ice nucleators in solution. There is precedent both of these phenomena. For example, PVP and poly(caprolactam)s are capable of inhibiting the formation of methane hydrate crystals[45] in gas pipelines by directly interacting with and disrupting the formation when the crystals have just nucleated and begun to crystallize.[46,47]

However, considering the body of evidence showing how polymers and proteins nullify ice nucleators, this may be the more likely of the two mechanisms. Wowk and Fahy observed polymers interacting with nucleating agents; polyglycerol was found to bind and inhibit the ice nucleation activity of some proteins, and the combination of polyglycerol with poly(vinyl alcohol) was shown to be particularly effective for reducing ice formation in vitrified solutions.[26] Inada et al. have demonstrated that PVA is very effective at blocking silver iodide induced ice nucleation, which is hypothesized to be due to it binding to the surface of the AgI nucleators.[48,49] PVA has also been shown to deactivate the nucleating ability of the ice nucleating proteins from *Pseudomonas syringae*.[16] In contrast to these reports, our assay made every attempt to exclude nucleators, but from the freezing point of around −20 °C observed for Milli-Q, here it appears that heterogeneous nucleation still dominates, even with the high purity water. The fact that PVA solutions display a depressed ice nucleation temperature, taken with the above reports, lead us to believe that PVA is interacting with whatever nucleators exist in Milli-Q water, but we cannot rule out direct interaction with the ice nuclei.

For in vivo application, the polymer must either be degradable (which PVA is not in the human body) or sufficiently small that it can be excreted by glomerular filtration, while maintaining activity. It is interesting to observe here that longer polymers are also more active at inhibition, although a mechanism is not yet presented. Conversely, we have previously shown that PVA with just a DP of 20 is required for significant ice recrystallization (growth) inhibition, implying that these related, but separate, processes may have different structural requirements. The results shown here suggest that, in addition to the chemical composition, the macromolecular architecture of polymers can hugely influence ice nucleation properties and offers a synthetically accessible tool for probing this most fundamental, but misunderstood (often conflated with freezing point depression or ice growth), process. Identifying the molecular weight of the polymers that are most efficient is also crucial in the development of these for biomedical applications. Future work will focus not only on understanding the INI activity of these and other synthetic polymers, but their ability to influence the heterogeneous as well as homogeneous nucleation and how this links with their other known "antifreeze" properties of thermal hysteresis (freezing point depression) and ice recrystallization inhibition.

CONCLUSIONS

Here, the ice nucleation inhibition activity of poly(vinyl alcohol) has been studied in detail. RAFT/MADIX polymerization was employed to access polymers with predictable molecular weights and low dispersity (M_w/M_n) values. Using differential ice nucleation analysis, the heterogeneous nucleation temperature of the "pure" water used here was determined to be −19 °C. The well-defined polymers revealed a significant molecular weight dependent ice nucleation inhibition effect, with the shortest polymers decreasing nucleation by only 2 °C, but the longest by almost 10 °C. These preliminary findings show that, in addition to affecting ice crystal growth, PVA also has the unique effect of inhibiting ice nucleation, which may provide insight into this complex process, controlled by seemingly simple polymers. Furthermore, this work shows that polymer architecture may also be used as a tool to modulate ice nucleation activity. These polymers will enable us to study the unique ice nucleation process in detail, and the results help to design new macromolecular tools for extreme-cold environments.

ASSOCIATED CONTENT

Supporting Information

Details on the synthesis of both RAFT agents and the conversion of PVAc to PVA. The Supporting Information is available free of charge on the ACS Publications website at DOI: 10.1021/acs.biomac.5b00774.

(PDF)

AUTHOR INFORMATION

Corresponding Author

*Fax: +44 247 652 4112. E-mail: m.i.gibson@warwick.ac.uk.

Notes

The authors declare no competing financial interest.

ACKNOWLEDGMENTS

The Leverhulme Trust are thanked for funding for a studentship to T.C. via the Research Grant RPG-144. The University of Warwick is thanked for providing undergraduate bursaries (URSS and via the Materials Global Research Priority) for B.D. The cryostage used here was purchased with support from a research grant from the Royal Society, U.K. Equipment used was supported by the Innovative Uses for Advanced Materials in the Modern World (AM2), with support from Advantage West Midlands (AWM) and part funded by the European Regional Development Fund (ERDF). C.I.M. is funded by BBSRC Life Science Doctoral Training Partnership. M.I.G. acknowledges the ERC for a starter grant (CRYOMAT 638661).

REFERENCES

(1) Abbatt, J. P. D. *Chem. Rev.* **2003**, *103*, 4783−4800.
(2) John Morris, G.; Acton, E. *Cryobiology* **2013**, *66*, 85−92.
(3) Fowler, A.; Toner, M. *Ann. N. Y. Acad. Sci.* **2005**, *1066*, 119−135.
(4) Rubinsky, B. *Annu. Rev. Biomed. Eng.* **2000**, *2*, 157−187.
(5) Petzold, G.; Aguilera, J. *Food Biophys.* **2009**, *4*, 378−396.
(6) Wowk, B. *Cryobiology* **2010**, *60*, 11−22.
(7) Damodaran, S. *J. Agric. Food Chem.* **2007**, *55*, 10918−10923.
(8) Murray, B. J.; Broadley, S. L.; Wilson, T. W.; Atkinson, J. D.; Wills, R. H. *Atmos. Chem. Phys.* **2011**, *11*, 4191−4207.

DOI: 10.1021/acs.biomac.5b00774
Biomacromolecules XXXX, XXX, XXX−XXX

(9) Atkinson, J. D.; Murray, B. J.; Woodhouse, M. T.; Whale, T. F.; Baustian, K. J.; Carslaw, K. S.; Dobbie, S.; O'Sullivan, D.; Malkin, T. L. *Nature* **2013**, *498*, 355.
(10) Murray, B. J.; O'Sullivan, D.; Atkinson, J. D.; Webb, M. E. *Chem. Soc. Rev.* **2012**, *41*, 6519−6554.
(11) Duman, J. G. *Annu. Rev. Physiol.* **2001**, *63*, 327−357.
(12) Kawahara, H. *J. Biosci. Bioeng.* **2002**, *94*, 492−496.
(13) Cochet, N.; Widehem, P. *Appl. Microbiol. Biotechnol.* **2000**, *54*, 153−161.
(14) Wilson, P. W.; Leader, J. P. *Biophys. J.* **1995**, *68*, 2098−2107.
(15) Gurian-Sherman, D.; Lindow, S. E. *FASEB J.* **1993**, *7*, 1338−1343.
(16) Holt, C. B. *CryoLetters* **2003**, *24*, 323−330.
(17) Eto, T. K.; Rubinsky, B. *Biochem. Biophys. Res. Commun.* **1993**, *197*, 927−931.
(18) Wilson, P. W.; Osterday, K. E.; Heneghan, A. F.; Haymet, A. D. J. *J. Biol. Chem.* **2010**, *285*, 34741−34745.
(19) Zachariassen, K. E.; Kristiansen, E. *Cryobiology* **2000**, *41*, 257−279.
(20) Parody-Morreale, A.; Murphy, K. P.; Di Cera, E.; Fall, R.; DeVries, A. L.; Gill, S. J. *Nature* **1988**, *333*, 782−783.
(21) Wilkinson, B. L.; Stone, R. S.; Capicciotti, C. J.; Thaysen-Andersen, M.; Matthews, J. M.; Packer, N. H.; Ben, R. N.; Payne, R. J. *Angew. Chem., Int. Ed.* **2012**, *51*, 3606−3610.
(22) Trant, J. F.; Biggs, R. A.; Capicciotti, C. J.; Ben, R. N. *RSC Adv.* **2013**, *3*, 26005−26009.
(23) Gibson, M. I. *Polym. Chem.* **2010**, *1*, 1141−1152.
(24) Deller, R. C.; Congdon, T.; Sahid, M. A.; Morgan, M.; Vatish, M.; Mitchell, D. A.; Notman, R.; Gibson, M. I. *Biomater. Sci.* **2013**, *1*, 478−485.
(25) Congdon, T.; Notman, R.; Gibson, M. I. *Biomacromolecules* **2013**, *14*, 1578−1586.
(26) Wowk, B.; Fahy, G. M. *Cryobiology* **2002**, *44*, 14−23.
(27) Franks, F.; Darlington, J.; Schenz, T.; Mathias, S. F.; Slade, L.; Levine, H. *Nature* **1987**, *325*, 146−147.
(28) Inada, T.; Modak, P. R. *Chem. Eng. Sci.* **2006**, *61*, 3149.
(29) Wang, H.-Y.; Inada, T.; Funakoshi, K.; Lu, S.-S. *Cryobiology* **2009**, *59*, 83−89.
(30) Stan, C. A.; Schneider, G. F.; Shevkoplyas, S. S.; Hashimoto, M.; Ibanescu, M.; Wiley, B. J.; Whitesides, G. M. *Lab Chip* **2009**, *9*, 2293−2305.
(31) Butorin, G. T.; Skripov, V. P. *Kristallografiya* **1972**, *17*, 379.
(32) Krämer, B.; Hübner, O.; Vortisch, H.; Wöste, L.; Leisner, T.; Schwell, M.; Rühl, E.; Baumgärtel, H. *J. Chem. Phys.* **1999**, *111*, 6521−6527.
(33) Duft, D.; Leisner, T. *Atmos. Chem. Phys.* **2004**, *4*, 1997−2000.
(34) Murray, B. J.; Broadley, S. L.; Wilson, T. W.; Bull, S. J.; Wills, R. H.; Christenson, H. K.; Murray, E. J. *Phys. Chem. Chem. Phys.* **2010**, *12*, 10380−10387.
(35) Campbell, J. M.; Meldrum, F. C.; Christenson, H. K. *J. Phys. Chem. C* **2015**, *119*, 1164−1169.
(36) Ogawa, S.; Koga, M.; Osanai, S. *Chem. Phys. Lett.* **2009**, *480*, 86−89.
(37) Inada, T.; Koyama, T.; Goto, F.; Seto, T. *J. Phys. Chem. B* **2011**, *115*, 7914−7922.
(38) Skey, J.; O'Reilly, R. K. *Chem. Commun.* **2008**, 4183−4185.
(39) Wilkins, L. E.; Phillips, D. J.; Deller, R. C.; Davies, G.-L.; Gibson, M. I. *Carbohydr. Res.* **2015**, *405*, 47−54.
(40) Phillips, D. J.; Gibson, M. I. *Biomacromolecules* **2012**, *13*, 3200−3208.
(41) Congdon, T.; Shaw, P.; Gibson, M. I. *Polym. Chem.* **2015**, *6*, 4749−4757.
(42) Niedermeier, D.; Shaw, R. A.; Hartmann, S.; Wex, H.; Clauss, T.; Voigtländer, J.; Stratmann, F. *Atmos. Chem. Phys.* **2011**, *11*, 8767−8775.
(43) Inada, T.; Lu, S. S. *Cryst. Growth Des.* **2003**, *3*, 747−752.
(44) O'Sullivan, D.; Murray, B. J.; Ross, J. F.; Whale, T. F.; Price, H. C.; Atkinson, J. D.; Umo, N. S.; Webb, M. E. *Sci. Rep.* **2015**, *5*, 8082.
(45) O'Reilly, R.; Ieong, N. S.; Chua, P. C.; Kelland, M. A. *Energy Fuels* **2011**, *25*, 4595−4599.
(46) Storr, M. T.; Taylor, P. C.; Monfort, J.-P.; Rodger, P. M. *J. Am. Chem. Soc.* **2004**, *126*, 1569−1576.
(47) Kelland, M. A. *Energy Fuels* **2006**, *20*, 825−847.
(48) Koyama, T.; Inada, T.; Kuwabara, C.; Arakawa, K.; Fujikawa, S. *Cryobiology* **2014**, *69*, 223−228.
(49) Inada, T.; Koyama, T.; Goto, F.; Seto, T. *J. Phys. Chem. B* **2012**, *116*, 5364−5371.

DOI: 10.1021/acs.biomac.5b00774
Biomacromolecules XXXX, XXX, XXX−XXX

Multivalent Glycopolymer-coated Gold Nanoparticles

Sarah-Jane Richards, Caroline I. Biggs, and Matthew I. Gibson

To be published in Methods in Molecular Biology- Macro-Glycoligands

Publishing Date November 2015

eBook ISBN 978-1-4939-3130-9

Abstract

Glycosylated noble metal nanoparticles are a useful tool for probing biological binding events due to their aggregation-induced colour changes, particularly for lectins that have multiple binding sites. To overcome the challenges of colloidal instability, which leads to false positive results, it is essential to add polymeric coatings to these particles. Here we describe a versatile, and reliable, approach to enable coating of gold nanoparticles using well-defined polymers, with carbohydrate end-groups. This produces multivalent nanoparticles that are both colloidally stable, but still retain their rapid colorimetric responses to lectin binding.

Keywords: Gold nanoparticles, glycopolymers, RAFT polymerisation, lectins.

1 Introduction

Carbohydrate-functionalised AuNPs (glycoAuNPs) are emerging as important tools for the colourimetric determination of carbohydrate-protein interactions as they constitute a good biomimetic model of carbohydrates at the cell surface (glycocalyx). GlycoAuNPs are attractive biosensors due to the multivalent presentation of carbohydrates can compensate for the low affinity of individual protein-carbohydrate interactions and the inherent multivalency of lectins should lead to acolourimetricresponse, as a result of aggregation, if the correct lectin-carbohydrate paring is present, changing from red to blue (**Figure 1**). This therefore provides a promising platform for new sensors, without the need for expensive equipment and fluorescent- or radio-labelling of proteins.

The colourimetric change associated with the aggregation of AuNPs using protein-carbohydrate interactions has been exploited in the detection of lectins [1-4], bacteria [5,6] and different strains of influenza [7]. We have shown that mannosylatedglycoAuNPs can be used to distinguish between bacteria with and without type 1 fimbriae, but that the mode of presentation of the carbohydrates and their distance from the gold surface impacts greatly on the detection read-outs.Whilst AuNPs are appealing scaffolds, directly glycosylated nanoparticles have intrinsically low colloidal stability, which can result in either false-positive aggregation responses in biological media or can prevent high-throughput application due to large errors.Conversely, very slow responses (aggregation) are observed for particleswith polymer coatings, which therefore limits their application as point-of-care diagnostics [6]. Therefore *via* a screening study we demonstrated that through precision macromolecular engineering using RAFT (reversible addition-fragmentation chain transfer) polymerisation it is possible to both improve colloidal stability, whilst avoiding the problem of presenting a steric block to aggregation [4]. The key features of this are a polymer coating of just the right length, and by using the RAFT process, a latent thiol is installed on each

chain end, suitable for conjugation to the gold surface without any further chemical modification.

Herein, we describe a polymer-stabilised glycosylated gold nanoparticle platform for the high throughput, label-free screening of carbohydrate-lectin interactions and demonstrate the potential applications within a range of glycobiological assays (**Figure 1**). A mix-and-match synthetic strategy enables huge chemical space to be explored, with the outputs being read in a simple multi-well plate format by either a microplate reader, or simply using a digital camera.

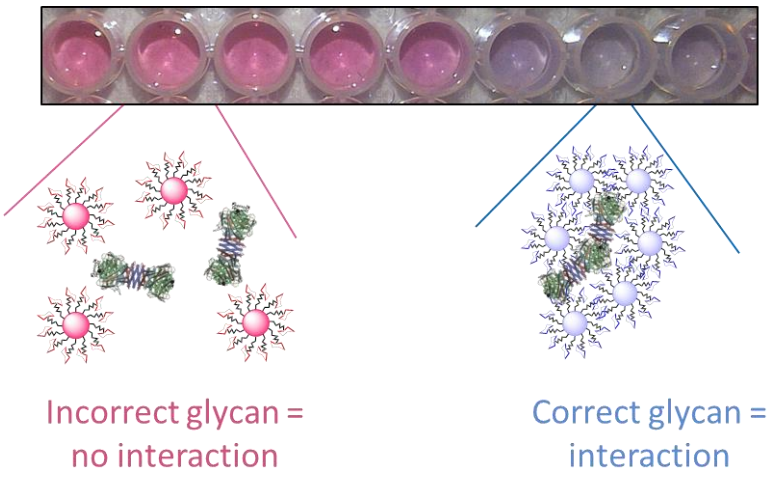

Figure 1. Overview of the approach used to allow direct measurement of carbohydrate-lectin interactions by monitoring a colourimetric change (red to blue) due to aggregation of glycoAuNPs bound to lectins.

2 Materials

2.1 Chemicals

1. Potassium phosphate tribasic (Sigma Aldrich)
2. 1-Dodecanethiol (Sigma Aldrich)
3. Carbon disulfide (Sigma Aldrich)
4. 2-Bromo-2-methyl propionic acid (Acros)
5. Pentafluorophenol (PFP) (Alfa Aeser)
6. *N*-hydroxyethyl acrylamide (HEA) (Sigma Aldrich)
7. 4,4'Azobis(4-cyanovaleric acid) (ACVA) (Sigma Aldrich)
8. 60 nm gold nanoparticles (BBI solutions)
9. Low bind, low volume clear 96-well plates (Greiner Bio-one)

2.2 Solvents

1. Acetone (Sigma Aldrich).
2. Dichloromethane (Sigma Aldrich)
3. Dimethylformamide (Sigma Aldrich)
4. Toluene (Fischer Scientific)
5. Methanol (Sigma Aldrich)

2.3 Buffer

1. HEPES buffer: 10 mM HEPES, 0.15 M 0.05 M NaCl, 0.1 mM $CaCl_2$ and 0.01 mM $MnCl_2$ (pH 7.5) (*See***Note 1**)
2. Acetate buffer:100 mM acetate buffer (0.09g acetic acid, 1.15g sodium acetate in 100 mL milli-Q water) containing 1 mM aniline (pH 5.5)

2.4 Lectins(*see***Note 2**)

1. Concanavalin A (Con A) (Vector Laboratories)
2. Peanut Agglutinin (PNA) (Vector Laboratories)
3. Soybean Agglutinin (SBA) (Vector Laboratories).
4. *Ricinus Communis* Agglutinin (RCA_{120}) (Vector Laboratories)
5. *Ulex Europeus* Agglutinin (UEA) (Vector Laboratories)
6. Wheat Germ Agglutinin (WGA) (Vector Laboratories)

3 Methods

GlycoAuNPs were prepared using an optimised polymer coating method that we developed recently,[4] which produces particles that are stable at physiological salt concentration and gives fast lectin detection/identification. We have suggested two methods for the carbohydrate functionalisation of RAFT-derived polymers (Figure2). RAFT polymerisation was used due to this technique producing telechelic polymers with, in this case, a conjugatable pentafluorophenyl ester at one end and masked thiol (trithiocarbonate) at the other, which is necessary for the gold immobilisation. Poly(*N*-hydroxyethyl acrylamide) (pHEA) is the optimal polymer for this as it has high water solubility, but also it does not display an LCST (lower critical solution temperature). Polymers with an LCST aggregate in water when heated, and this critical temperature decreases when on a particle surface [8,9]. Other commonly used, neutral, hydrophilic polymers such as oligoethyleneglycol methacrylate (OEGMA) and hydroxyethyl methacrylate (HEMA) are not suitable for this reason. Also, pOEGMAs do not graft in high density to the particles due to their comb-like shape. Commercial telechelic linear PEGs can be used, but the choice of degree of polymerisation (DP) is limited, which is important for ensuring fast colourimetric readouts and the choice of end group is limited, unlike here.

To enable control over the end-groups a pentafluorophenol (PFP) trithiocarbonate RAFT agent is employed, which is an excellent mediator for acrylamides such as HEA. The PFP group is stable in the polymerisation conditions but is readily converted into a range of other functionality, post-polymerisation *via* addition of amines. This approach ensures identical polymers, with different end groups can be obtained, essential for any structure-property studies.

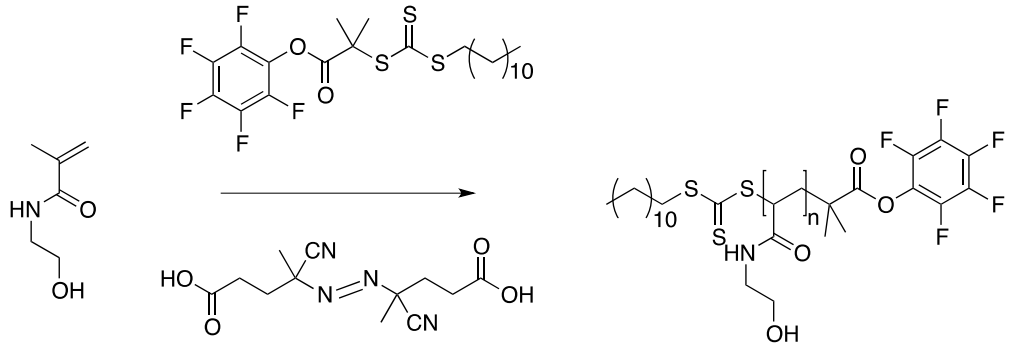

Figure 2. Polymerisation of *N*-hydroxyethyl acrylamide using 2-(Dodecylthiocarbonothioylthio)-2-methylpropionic acid as the RAFT agent for simple end group modification.

Two facile and versatile methods are available for the functionalisation of AuNPs using native, underivatised carbohydrates with proper ligand presentation using the method presented here. This also alleviates the inconvenience and limitations of carbohydrate pre-functionalisation, required for many carbohydrate conjugations, and offers rapid access to glycoAuNPs with a wide variety of glycans suitable for high-throughput microarray applications [10] as outlined in Figure 3.

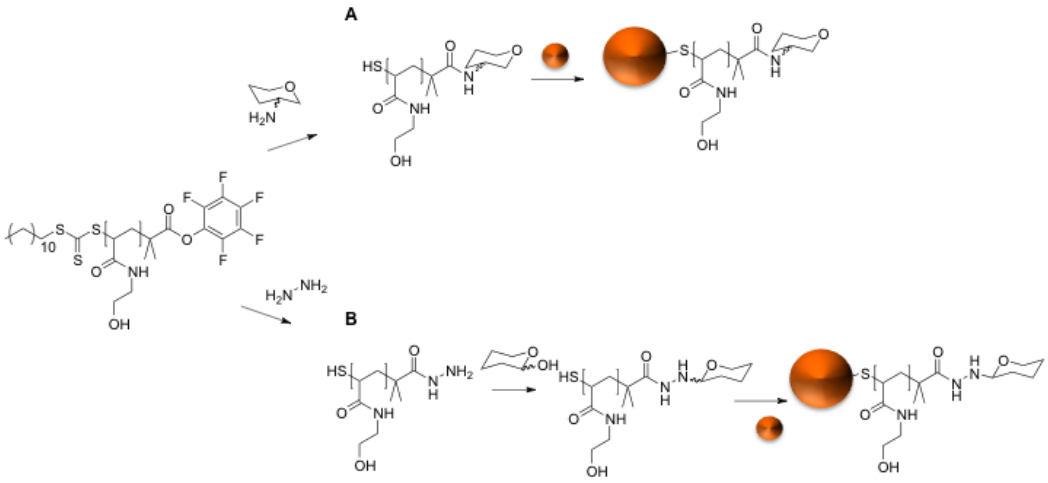

Figure 3.Preparation of carbohydrate functionalised gold nanoparticles. Synthetic approach resulting in polymer stabilised gold nanoparticles with terminal carbohydrate functionality. Two synthetic approaches are suggested, A) pentafluorophenol terminated polymers and amino-carbohydrates and B) using hydrazide terminated polymers with reducing sugars

Firstly, *N*-hydroxylethylacrylamide (HEA) is polymerised toDP20, as detailed studies have shown this is the optimum length for 60 nm particles for saline stability and a fast readout.[4] This polymerisation was carried out by RAFT using a pentafluorophenol ester α-terminated RAFT agent. This can then be functionalised directly using amino-2-deoxy-sugars (**Figure3A**) or hydrazide (**Figure 3B**). The hydrazide-terminated polymers can then be functionalised with reducing sugars. The stable *N*-glycoside end-terminated polymers are formed due to the intrinsic reactivity of reducing sugars toward hydrazides. The reaction occurs under mild conditions, with good conjugation efficiencies and stereoselectivity. The reducing sugars react with α-heteroatom nucleophiles (e.g. hydrazide or alkylaminooxy groups) to give cyclic pyranosides [11].

The ω-terminal thiol from the RAFT agent can then be used to conjugate thecarbohydrate-functionalised polymers, from either route, onto preformed 60 nm AuNPs. We have found that larger particles give greater responses [6]. However, the polymer coating has to be tailored to the AuNPs to be used. The post-polymerisation route means that all the

polymers have the same initial chain length distribution and therefore reduces the variability between particle types, but allows versatile end-group functionalisation to make libraries of a variety of particles. These glycoAuNPs can then be used to test carbohydrate-protein interactions in a multi-well plate format.

3.1 Preparation of 2-(dodecylthiocarbonothioylthio)-2-methylpropionic acid (DMP)

1. Add 4.0g (19.76mmol) of dodecanethiol dropwise over 25 minutes to a stirred suspension of 4.2 g of K_3PO_4 (19.76 mmol) in 60 mL of acetone.
2. Add 4.1 g CS_2 (53.85 mmol). Reaction mixture turns bright yellow.
3. After 10 minutes, add 3g of 2-bromo-2-methyl propionic acid (17.76 mmol. A KBr precipitate is noted.
4. Stir the reaction mixtureat room temperature for 16 h.
5. Remove KBr by filtration and remove the solvent under reduced pressure.
6. Extract in 2 x 200 mL of dichloromethane (DCM) from 1M HCl andwash with 200 mL of H_2O and 200 mL of Brine and dry over $MgSO_4$.
7. Concentrate under reduced pressure.
8. Purify by column chromatography using 24:75:1 ethyl acetate: petroleum ether: acetic acid ($R_{fproduct}$ = 0.25).
9. Characterize the product using IR, ^{1}H and ^{13}C NMR

3.2 Preparation of 2-(dodecylthiocarbonothioylthio)-2-methylpropionic acid pentafluorophenyl ester (DMP-PFP)

1. Add 0.5 g (1.37 mmol) of DMP (see **Step3.1** for preparation), 0.39g (2.05 mmol) of*N*′-(3-Dimethylaminopropyl)-*N*′-ethylcarbodiimide hydrochloride (EDC), and 0.25 g (2.05

mmol) of 4-(dimethylamino)pyridine (DMAP) in 40 mL of DCM and stirfor 20 minutes at room temperature under N_2.

2. Add 0.76 g (4.24 mmol) of pentafluorophenolin 5 mL DCM and stir rhe reaction mixture was overnight at room temperature.
3. Wash the reaction solution successively with 3 M HCl (100 mL), 1 M $NaHCO_3$(100 mL) and 0.5 M NaCl (100 mL).
4. Dry the reaction solution over $MgSO_4$, filter and then concentrateunder reduced pressure, to afford a yellow oil that crystallises.No further purification isrequired.
5. Characterize the product using IR, ^{1}H and ^{13}C NMR.

3.3 Polymerisation of *N*-hydroxyethyl acrylamide(HEA) (DP20) using DMP-PFP

1. Dissolve 0.5 g (4.34 mmol) of *N*-hydroxyethylacrylamide (HEA), 0.115 g (0.22 mmol) of PFP-DMP, 0.0122 g(0.043 mmol) of 4,4′-Azobis(4-cyanovaleric acid) (ACVA) in 50:50 Toluene:Methanol (4 mL).
2. Add mesitylene (150 μL) as an internal reference (*See***Note 3**).
3. Degas under N_2 for 30 mins then stir at 70 °C for 90 mins.
4. Rapidly cool in liquid nitrogen and precipitate into diethyl ether (35 mL). Reprecipitate into diethyl ether (35 mL) from methanol (5 mL) twice, to yield a yellow polymer product.Dry under vacuum.
5. Characterize the product using H^1 NMR, IR and size exclusion chromatography (SEC) (*See* **Note 4**).

3.4 Functionalisation of polymer end group

3.4.1 Method 1: Functionalisation with hexosamines

1. Dissolve 50 mg (0.018 mmol) of PFP-pHEA and hexosamine (15 mg, 0.088 mmol) in 5mL of DMF (with TEA (0.05 M).
2. Stir at 50 °C for 16 hrs.
3. Precipitate into diethyl ether (35 mL) from methanol (5 mL) three times and dry under vacuum.
4. IR analysis indicates loss of C=O stretch corresponding to the PFP ester (*See* **Note 5**).

3.4.2 Method 2: Functionalisation with reducing sugars

1. Dissolve 500 mg (0.18 mmol) of PFP-pHEA, 50 μL hydrazine (1.5 mmol) in 5 mL DMF.
2. Stir at 50 °C for 16 hrs.
3. Precipitate into diethyl ether (35 mL)from methanol (5 mL) three times and dried under vacuum.
4. IR indicates loss of C=O stretch corresponding to the PFP ester (*See***Note 5**).
5. Add 10 mg (0.0043 mmol) of hydrazide-pHEA and reducing hexose (3 mg) in 1 mL of 100 mM acetate containing 1 mM aniline.
6. Leave it at 50 °C overnight.
7. Employit immediately for goldnanoparticle functionalization.

3.5 Functionalisation of gold nanoparticles

1. Add 1 mg of polymer in 100 μL water to 1 mL of 60 nm particles (OD_{600} = 1, 0.288 mM Au) (*See* **Notes 6** and **7**).
2. Leave it for 30 minutes at room temperature.

3. Centrifuge the particles solution at 6000rpm,remove the supernatant along with any unattached polymer.
4. Resuspend the particles in water.
8. Characterize by DLS and NaCl titration (*See* **Notes 8** and **9**).

3.6 Lectin induced aggregation

1. A panel of six lectins (Con A, RCA_{120}, SBA, UEA, PNA and WGA) are used from Lectin Kit 1 obtained from Vector Laboratories.
2. Make a stock solution of each lectin (0.1 mg/mL) in HEPES buffer with 0.05 M NaCl, 0.1 mM $CaCl_2$ and 0.01 mM $MnCl_2$.
3. Make 25µL serial dilutions (from 0.1 mg/mLto 0 mg/mL)in the same HEPES buffer in a low volume 96-well micro-titre plate.
4. Add 25µLof glycoAuNP to each well.

3.7 Data collection and analysis

3.7.1 Method 1: UV/Vis Spectrometry

1. 96 well plates are prepared as above in Step **3.6**.
2. Measure absorbance at 450 nm and 700 nm every minute for 30 minutes at 37 °C using a BioTek Synergy HT microplate reader.
3. After 30 minutes, record an absorbance spectrum from 450 -700 nm with 10 nm intervals (1 nm intervals can be used for greater precision).
4. Normalize absorbance at 700 nm to that of reference wavelength 400 nm. Plot normalised 700 nm values on a logarithmic scale and fit to a Hill function. Determine $K_d$apparent value from this (**Figure 4**) (*See* **Note 10**).

3.7.2 Method 2: Pixel intensity using image analysis

1. An image of the 96-well plate prepared in **Step 3.6** is taken using a flatbed scanner.
2. A region of interest is drawn around every well using the open-source image analysis package Image J (version 1.46a).
3. The colour (RGB) image is then converted into a hue, saturation and brightness (HSB) stack of images and the saturation image used.
4. The regions of interest drawn on the original image are added to the saturation image using the ROI manager and average pixel intensity in each region of interest is measured using an inbuilt function in ImageJ.

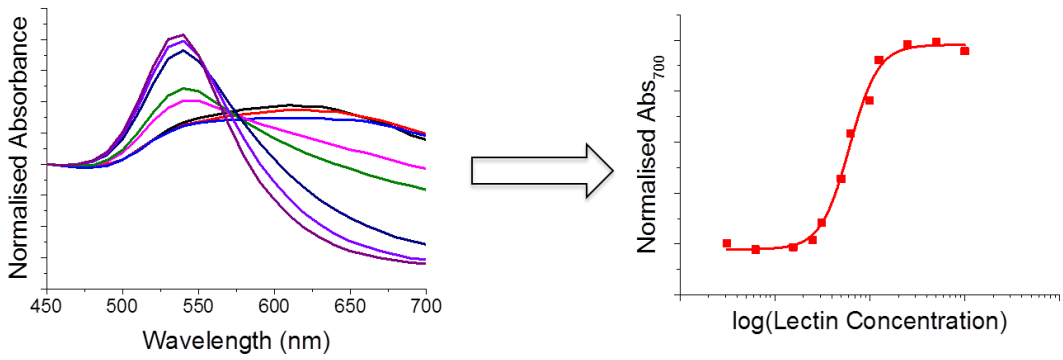

Figure 4.

Figure 4. Example data analysis: UV-Vis spectra of fucose-AuNP upon addition of increasing concentrations of UEA following 30 minutes of incubation. Binding isotherms (at 37 °C) of fucose-AuNPs with UEA from plotting normalised absorbance at 700 nm as a function of concentration.

4 Notes

1. Ca^{2+} and Mn^{2+} in HEPES buffer required for correct function of lectins. Do not use PBS as it binds Ca^{2+} and calcium phosphate precipitates.
2. Best results are obtained using fresh lectins. Lectins should be stored in buffer at 4-8 °C for no longer than 1 week.

3. ^{1}H NMR should be used obtain conversion. 25 μL of reaction mixture should be taken prior to reaction and ^{1}H NMR spectrum obtained, in $CDCl_3$. 25 μL of reaction mixture should be taken after reaction completion and ^{1}H NMR spectrum obtained in MeOD. Compare vinyl peaks of each sample to the internal standard mesitylene (δ = 6.8 ppm).
4. SEC was carried out in DMF. Note that the calibration standards do not give absolute M_n values. End group analysis by ^{1}H NMR should be used to get a good estimate of DP.
5. Conversion of PFP ester C=O to amide C=O can be seen by disappearance of peak at around 1750 cm^{-1} or by ^{19}F NMR.
6. Commercial AuNPs should be checked before use for size discrepancies and dispersity to ensure they are in fact 60 nm as it is important for stability and readout speed.[4] Size characterisation can be carried out using the SPR peak location,[12] DLS and transmission electron microscopy (TEM).
7. AuNPs can be synthesised by citrate reduction method of Turkevich*et al*.[13] however, commercial products will have lower dispersity.
8. Successful coating can be determined by a simple NaCl aggregation test. Coated particles will be stable beyond 0.1 M NaCl whereas uncoated citrate stabilised particles will aggregate.
9. DLS will confirm size increase due to coating and x-ray photoelectron spectroscopy (XPS) will give confirmation of surface functionalisation.TEM will not confirm coating.
10. To determine a comparable $K_d$apparent, the sigmoidal curves require an obvious start and end plateau as shown in **Figure 4**.

Acknowledgements

Equipment used was supported by the Innovative Uses for Advanced Materials in the Modern World (AM2), with support from Advantage West Midlands (AWM) and part funded by the European Regional Development Fund (ERDF). MIG was a Birmingham Science City Interdisciplinary Research Fellow funded by the Higher Education Funding Council for England (HEFCE). SJR acknowledges the EPSRC funded MOAC doctoral training centre for a studentship. CIB acknowledges the BBSRC for a studentship.

References

1. Schofield CL, Mukhopadhyay B, Hardy SM, McDonnell MB, Field RA, Russell DA (2008) Colorimetric detection of *Ricinus communis* Agglutinin 120 using optimally presented carbohydrate-stabilised gold nanoparticles. *Analyst* **133**:626-634.
2. Lin CC, Yeh YC, Yang CY, Chen GF, Chen YC, Wu YC, Chen CC (2003) Quantitative analysis of multivalent interactions of carbohydrate-encapsulated gold nanoparticles with concanavalin A. *Chem Commun* 2920-2921.
3. Jayawardena HSN, Wang X, Yan M (2013) Classification of lectins by pattern recognition using glyconanoparticles. *Anal Chem* **85**:10277-10281.
4. Richards S-J, Gibson MI (2014) Optimization of the polymer coating for glycosylated gold nanoparticle biosensors to ensure stability and rapid optical readouts. *ACS Macro Lett* **3**:1004-1008.
5. Lin CC, Yeh YC, Yang CY, Chen CL, Chen GF, Chen CC, Wu YC (2002) Selective binding of mannose-encapsulated gold nanoparticles to type 1 Pili in *Escherichia coli*. *J Am Chem Soc* **124**:3508-3509.

6. Richards S-J, Fullam E, Besra GS, Gibson MI (2014) Discrimination between bacterial phenotypes using glyco-nanoparticles and the impact of polymer coating on detection readouts . *J Mater Chem B* **2**:1490-1498.
7. Marin MJ, Rashid A, Rejzek M, Fairhurst SA, Wharton SA, Martin SR, McCauley JW, Wileman T, Field RA, Russell DA (2013) Glyconanoparticles for the plasmonic detection and discrimination between human and avian influenza virus. *Org Biomol Chem* **11**:7101-7107.
8. Gibson MI, Paripovic D, Klok H-A (2010) Size-dependent LCST transitions of polymer-coated gold nanoparticles: cooperative aggregation and surface assembly. *Adv Mater* **22**:4721-4725.
9. Ieong NS, Brebis K, Daniel LE, O'Reilly RK, Gibson MI (2011) The critical importance of size on thermoresponsive nanoparticle transition temperatures: gold and micelle-based polymer nanoparticles. *Chem Commun* **47**:11627-11629.
10. Biggs CI, Edmondson S, Gibson MI (2015) Thiol-ene immobilisation of carbohydrates onto glass slides as a simple alternative to gold-thiol monolayers, amines or lipid binding. *Biomater Sci* **3**:175-181.
11. Godula K, Bertozzi CR (2010) Synthesis of glycopolymers for microarray applications *via* ligation of reducing sugars to a poly(acryloyl hydrazide) scaffold. *J Am Chem Soc* **132**:9963-9965.
12. Haiss W, Thanh NTK, Aveyard J, Fernig DG (2007) Determination of size and concentration of gold nanoparticles from UV−vis spectra. *Anal Chem* **79**:4215-4221.
13. Turkevich J, Stevenson PC, Hillier J (1951) A study of the nucleation and growth processes in the synthesis of colloidal gold. *Discuss Faraday Soc* **11**:55-75.